Inaugural dissertation

for

obtaining the doctoral degree

of the

Combined Faculty of Mathematics, Engineering and Natural Sciences

of the

Ruprecht - Karls - University

Heidelberg

Presented by

Mgr. Tomáš Hofman

born in: Broumov, Czech Republic

Oral examination: April 23rd 2024

Defining innate immune checkpoints controlling Natural Killer cell recognition of melanoma cells

Referees:

Prof. Dr. Michael Boutros

Prof. Dr. Adelheid Cerwenka

1 TABLE OF CONTENTS

2 ZUSAMMENFASSUNG

Das Melanom ist selten, aber eine der tödlichsten Formen von Hautkrebs. Immun-Checkpoint-Inhibitoren, die auf hemmende Rezeptoren auf T-Zellen abzielen, stellen eine wirksame Therapie dar, die die klinische Reaktion auf Melanome bei einer Untergruppe von Krebspatienten erheblich verbessert hat. Da NK-Zellen die erste Verteidigungslinie gegen Tumore darstellen, habe ich ein genomweites (GW) CRISPR/Cas9 Knockout (KO) Screening eingesetzt, um Checkpoint-Kandidaten auf Melanomzellen zu identifizieren, die die Anti-Tumor-Reaktivität menschlicher NK-Zellen hemmen. Nach der Ko-Kultur mit primären NK-Zellen konnte ich beobachten, dass Melanomzellen, denen es an Genen für die Antigen-präsentierende Maschinerie mangelt, stark aus dem Pool der überlebenden Melanome dezimiert wurden. Ich stellte fest, dass IFNγ als NK-Abschaltmechanismus über NK-Untergruppen-spezifische klassische oder nicht-klassische MHC-I-abhängige Wege eine entscheidende Rolle spielt, was zu einer starken Induktion der Melanomresistenz führt. Ich grenzte die Wirkung von IFNγ weiter auf hemmende NKG2A- und KIR-Rezeptoren ein. Dementsprechend bestätigte ich, dass HLA-E allein NKG2A$^+$ KIR$^-$ NK-Zellen vollständig, NKG2A$^+$ KIR$^+$ NK-Zellen dagegen nur teilweise hemmt. Die klassischen MHC-I-Moleküle vermittelten die Hemmung der NKG2A$^-$ KIR$^+$ NK-Zelluntergruppe. Die Kombination von HLA-E und klassischem MHC-I war dann für die Hemmung von NKG2A$^+$ KIR+ NK-Zellen verantwortlich, wobei NKG2A eine dominante hemmende Rolle gegenüber den KIRs spielte. Die Verwendung von Monalizumab, einem NKG2A-blockierenden Antikörper, Lirilumab, einem KIR2-blockierenden Antikörper, und DX9, einem häufig verwendeten KIR3DL1-blockierenden Antikörper, erwies sich als ausreichend, um die beobachteten Effekte in Ko-Kulturen mit Melanom-HLA-KO-Zellen zu replizieren und die IFNγ-vermittelte Resistenz nicht nur in Melanomzellen, sondern auch in anderen Tumorentitäten vollständig aufzuheben und sie für die Abtötung durch NK-Zellen empfänglich zu machen.

Darüber hinaus führte ich einen GW CRISPR/Cas9 KO Screen in einer B2M-KO-Zelllinie durch, der die starke Rolle von MHC-I ausschloss und den Sialinsäure-Biosyntheseweg als weiteren inhibierenden Mechanismus der Melanomzellen aufzeigte. Durch den Verlust von SLC35A1 und TM9SF3 in Melanomzellen wurde die Expression von Liganden für hemmende Siglec-Rezeptoren aufgehoben und die Funktion von Siglec-9$^+$ NK-Zellen spezifisch wiederhergestellt.

Die Kombination beider Aspekte meiner Arbeit, die Erzeugung von NKG2A$^-$ KIR$^-$ Siglec-9$^-$ NK-Zellen oder die Verwendung einer Kombination aus Monalizumab/

Lirilumab/DX9-Antikörperbehandlung in Verbindung mit einer Blockade von Siglec-9 könnte also sowohl die IFNγ- als auch die Sialinsäure-vermittelte Tumorzellresistenz gegen die NK-Zellzytotoxizität überwinden.

3 SUMMARY

Melanoma, though rare, stands as one of the most lethal forms of skin cancer. Immune checkpoint inhibitors targeting inhibitory receptors on T cells represent an effective therapy that has greatly improved clinical responses against melanoma in a subset of cancer patients. Since NK cells represent the first line of defence against tumors, I used a genome-wide (GW) CRISPR/Cas9 knockout (KO) screen to identify checkpoint candidates on melanoma cells that inhibit human NK cell anti-tumor reactivity. After co-culture with primary NK cells, I observed that melanoma cells deficient in antigen-presenting machinery genes were strongly depleted from the surviving melanoma pool. I determined a crucial role of IFNγ acting as a NK shut off mechanism via NK subset-specific classical or non-classical MHC-I-dependent pathways, resulting in a strong induction of melanoma resistance. I further narrowed down the effect of IFNγ to inhibitory NKG2A and KIR receptors. Accordingly, I confirmed that HLA-E alone fully inhibited NKG2A$^+$ KIR$^-$ NK cells, while only partially NKG2A$^+$ KIR$^+$ NK cells. The classical MHC-I molecules mediated the inhibition of NKG2A$^-$ KIR$^+$ NK cell subset. The combination of both HLA-E and classical MHC-I were then responsible for the inhibition of NKG2A$^+$ KIR$^+$ NK cells where NKG2A showed dominant inhibitory role over the KIRs. The use of monalizumab, a NKG2A blocking antibody, lirilumab, a KIR2 blocking antibody, and DX9, a commonly used KIR3DL1 blocking antibody, proved sufficient to replicate the observed effects in co-cultures with melanoma HLA KO cells and completely abolished IFNγ-mediated resistance, not only in melanoma cells but also in other tumor entities, rendering them susceptible to NK cell killing.

I further performed a GW CRISPR/Cas9 KO screen in a B2M KO cell line, that excluded the potent role of MHC-I, and showed the sialic acid biosynthesis pathway as another melanoma cell resistant mechanism to NK cell cytotoxicity. The loss of *SLC35A1* or *TM9SF3* in melanoma cells abolished the expression of ligands for Siglec inhibitory receptors and specifically restored Siglec-9$^+$ NK cell function.

Thus, combining both aspects of my thesis, generating NKG2A$^-$ KIR$^-$ Siglec-9$^-$ NK cells or using a combination of monalizumab/lirilumab/DX9 antibody treatment combined with a blockade of Siglec-9 could overcome both IFNγ- and sialic acid-mediated tumor cell resistance to NK cell cytotoxicity.

4 INTRODUCTION

4.1 The Immune System

The immune system is the defence mechanism protecting the host body against a range of diseases. Its primary role is to recognise external pathogens such as macroscopic parasites, fungi, bacteria and viruses that could cause lethal damage to the host body. In addition to external pathogens, the immune system also detects damaged host cells that could undergo malignant transformation. Quick and correct immune responses limiting the spread of infection or cancer development is vital for host survival. The vertebrate immune system consists of two major arms, innate and adaptive immune system, cooperating together. The innate immune response is the first system triggered in a matter of min or hours by conserved pathogen patterns or stress/damage signals. Additionally to the innate system, that is present in some form in all organisms, vertebrates evolved to possess an adaptive immune system. This antigen-specific adaptive immune system is triggered within days or weeks after pathogen encounter and innate immunity activation. It requires an antigen-specific clonal expansion of effector cells resulting in pathogen clearance and formation of a long-lasting immunological memory allowing fast responses after second pathogen encounter.

4.2 Innate Immunity

The innate immune system can be divided into three distinct mechanisms of action. The first component is solely physical separation of external environment from host system by the epithelial barrier, protecting skin, respiratory, gastrointestinal, urinary and reproductive tract from pathogens entering host tissues or the blood stream. This physical cell barrier is often accompanied by chemical barriers such as secreted mucus, saliva enzymes, antimicrobial peptides, acidic pH, tears, urine or biological barriers in gastrointestinal tract where pathogenic bacteria compete with commensal bacteria[1].

4.2.1 Complement and immune cells

A second component is provided by the complement system that comes into play when barriers are breached and pathogens reach tissues. Complement is composed of approximately 30 different plasma proteins that work together when the initial cascade is triggered. Complement activation can be triggered on any membrane surface that lacks protective

proteins, or by binding to either pathogen carbohydrates or by an antibody binding a pathogen antigen thus contributing to both innate and adaptive immunity. Activation of complement then result in promoting inflammation, triggering of phagocytosis or formation of a membrane attack complex pore resulting in direct pathogen lysis[2] (Figure 4.1).

A third component of innate immunity consists of a dedicated immune cells, which become active when the physical barrier is compromised and pathogens enter a host system. Pathogens are then recognized by innate immune cells such as neutrophils, macrophages, basophils, eosinophils, natural killer (NK) cells, innate lymphoid cells (ILCs) and dendritic cells (DC) (Figure 4.1). Neutrophils, whose main function is the phagocytosis, migrate from blood to inflamed tissue and mediate short-lived but fast responses against pathogens. Macrophages, a long-lived, tissue-resident type of phagocytic cells are also able to directly phagocytose invaded pathogens and subsequently inactivate them by reactive oxygen species or digestion by lysosomal enzymes. They also play an important role in tissue homeostasis and remodelling by removing apoptotic cells after injury. Basophils and eosinophils are important defence arm to destroy parasites that are too big to be phagocytosed by macrophages or neutrophils by releasing toxic granules after contact. ILCs and NK cells possess the ability recognize stressed, tumor or virus infected cells and directly eliminate them (see chapter 4.4). DC are professional antigen-presenting cells (APC) bridging the innate and adaptive immunity. Conventional DCs phagocytose and digest pathogens and then present pathogen peptides on their cell surface to induce the activation of antigen-specific adaptive immunity (see chapter 4.3). Plasmacytoid DC are primarily specialized to detect viral infections. They have a broad range of pattern recognition receptors (PRR) that induce production of large amounts of antiviral type I interferons (IFN)[1].

4.2.2 Pathogen recognition

PRR are germ-line encoded receptors that bind conserved pathogen-associated molecular patterns (PAMPs) or damage-associated molecular patterns (DAMPs). Examples of PAMPs are bacterial carbohydrates, fungal cell wall components or viral nucleic acid. DAMPs are usually cytoplasmic host molecules that are released or exposed after tissue damage. Major PRRs are the toll-like receptors (TLR), a family of 9 members from which some are located at the cell surface and some in endosomal compartments of cells. Surface TLRs detect pathogen membrane molecules such as lipopeptides, lipopolysaccharide (LPS) or flagellin. Some

endosomal TLRs detect endocytosed viral DNA or RNA. Besides membrane bound nucleic acid sensing TLRs, intracellular receptors such as RIG-1, MDA-5 or cGAS are able to detect foreign nucleic acid present in the cytosol of an infected cell and trigger antiviral responses. Finally, intracellular bacterial peptidoglycan receptors such as NOD receptors are able to detect bacteria in cytosol since not only viruses but also bacteria can directly invade cells and persist in the cytosol of infected cells. Detection of PAMPs via PRRs induces production of inflammatory cytokines such interferons (IFN), tumor necrosis factor α (TNFα), interleukin (IL) 6, IL-1β, IL-12, IL-18 and chemokines. IFNs increase antiviral responses of neighbouring cells, limiting viral spread and together with other cytokines amplify the immune reaction and recruit more immune cells into inflamed tissue such as monocytes, neutrophils or NK cells[3]. Unfortunately, PRRs lack the ability to react to pathogen changes. Escape mutations or pattern modifications can protect a pathogen from elimination by innate immune responses.

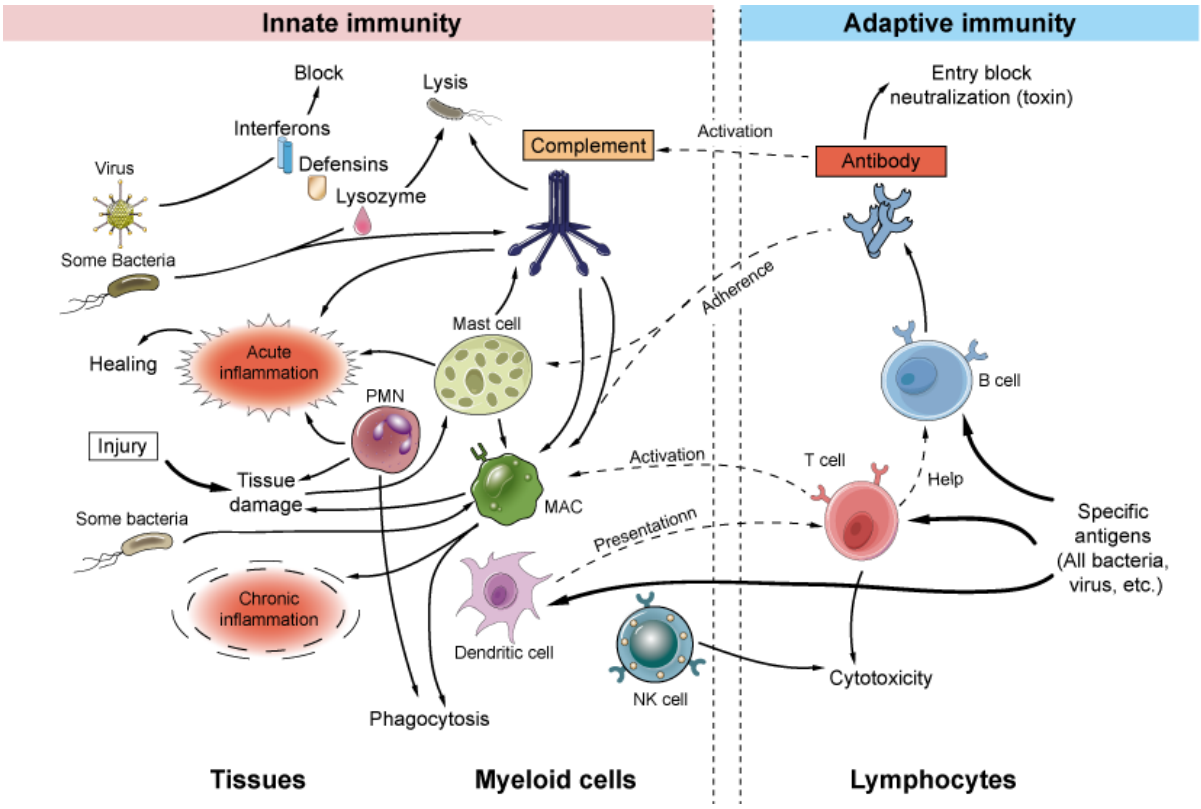

Figure 4.1 The axes and important players of the innate and adaptive immune systems.
Innate (left) and adaptive (right) immune players are composed from cellular (lower part) and humoral components (upper part). Adapted from[4]

4.3 Adaptive Immunity

The adaptive immune system becomes activated and highly effective after innate immune system detects a pathogen or a malignant cell. It involves a cellular component of antigen-specific T and B lymphocyte clonal expansion as well as a humoral response via the production of antigen-specific antibodies by these B cells (Figure 4.1). Besides effector functions of adaptive immune cells, some antigen-specific T- and B cell reactive clones remain present long after initial infection forming an immunological memory pool that can quickly expand upon rechallenge.

4.3.1 T and B cells

T and B cells are the main adaptive immune cells originating from the bone marrow and equipped with a single Ag-specific receptor. Their development is dependent on lymphoid organs where cell clones with functional but not autoreactive T-cell receptor (TCR) and B-cell receptor (BCR) mature. TCR and BCR single Ag-specificity is ensured by somatic recombination and unique assembly of V, D and J receptor regions. The combination of V, D and J chains theoretically generates a ~10^{11} BCR and ~10^{16} TCR[5]. However, such a high Ag binding diversity also includes cell clones that bind host body proteins. In case of TCRs, all T cell progenitors migrate into the thymus where all T cell clones in which genetic rearrangement in α- and β-chain TCR cause binding to a host protein Ag are eliminated by induced apoptosis. These proteins are presented in the form of short peptides bound on major histocompatibility complex (MHC) molecules. Besides TCRs, another round of selection involves correct engagement of co-receptors CD4 and CD8, which bind either MHC-II or MHC-I, respectively. First, T cell clones are controlled for their ability to bind MHC by co-receptors and then are further selected for their antigen specificity. The thymus has the ability to express and present all host proteins that are otherwise expressed only during host development or in a tissue-specific manner. Clones in which the TCR is not engaged become naïve CD4 or CD8 T cells migrating into the periphery, while the cells that recognize any self-antigens undergo programmed cell death. This selection process is called central tolerance. Despite this strict selection mechanism, it is not rare that some autoreactive T cells escape this selection. In contrast to αβ T cell receptors, γδ T cell TCRs have a more limited diversity and do not recognize peptides presented on MHC, but via butyrophilin molecules, which bind phosphorylated antigens, or by CD1 molecules presenting lipid antigens. Thus, γδ T cells display a more innate immune-like function. B cell development takes place in the bone marrow

and gives rise to immature B cells with functional heavy- and light-chains of the BCR. Similar to T cells, B cells in which V, D, J rearrangement in BCR results in binding to a self-antigen undergo cell death or become anergic to a self-Ag stimuli[1,6,7].

4.3.2 Adaptive immune response

Generating an adaptive immune response is an effective process of pathogen elimination. However, it requires an initial priming with help of the innate immune system and it fully develops after days of initial pathogen encounter. DCs migrate into secondary lymphoid organs such as the spleen or lymph nodes to prime T and B cells into an effector function state by presenting pathogen Ag peptides on MHC molecules. In addition to MHC-TCR signal, DC provide co-stimulatory signals required for T cell activation such as CD80 and CD86 binding to CD28 on T cells. Broad TCR and BCR diversity ensures a high chance of finding a T cell or B cell that recognizes a given foreign Ag. However, the number of reactive clones is limited. Thus, reactive T and B cells undergo several rounds of proliferation and TCR/BCR maturation. Receptor maturation is a process of increasing the affinity of TCR and BCR by introducing mutations in their variable regions. The higher affinity the higher proliferation of specific clones. The result of naïve T cell activation is the generation of effector cytotoxic CD8 T cells and stimulatory CD4 T cells. CD4 T cells can be further divided into regulatory T cells (Treg), which regulate immune response by secreting immunosuppressive IL-10 and transforming growth factor β (TGF-β), and helper T cells (Th) Th1, Th2 and Th17 cells. Th cells produce cytokines such as IFNγ (Th1), IL-4 (Th2) and IL-17 (Th17) to direct immune responses against various pathogens[8]. Interaction between Th cells and B cells is required for B cell activation and differentiation into antibody-producing plasma cells (PC). Antibodies are a soluble form of the BCR, referred to as immunoglobulin (Ig). They are formed by two heavy and two light chains connected together creating an Ag binding site (Fab) and a constant region (Fc) which can be divided into 5 isotypes. Isotypes differ in their function: IgE has a role in eosinophil activation against parasites, IgA has a role in the protection of mucous membranes such as respiratory and digestive tracts, IgM is an antibody produced by B cells at the initial state after infection and corresponds to initial BCR. After B cell activation and BCR affinity maturation the IgM isotype switch into more potent IgG isotype. However, the production of IgG usually takes 14 days after infection[9]. Antibodies are potent in pathogen neutralisation and opsonisation facilitating complement activation, antibody-dependent cell phagocytosis (ADCP) or antibody-dependent cell cytotoxicity (ADCC). The cytotoxic activity is mediated by the exposed Fc

region of the antibody which binds to an Fc receptors expressed by NK cells or CD8 T cells. When the pathogen is eliminated, the immune response subsides due to the lack of antigen stimulation. However, some cells survive and form long-lasting memory cells that can be quickly activated by Ag re-appearance in the host system[1,8,9].

4.4 Natural Killer (NK) cells

NK cells are a granular cytotoxic cells that together with innate lymphoid cells (ILC) are part of the innate lymphocytes. ILC can be further defined by surface markers into ILC1, ILC2, ILC3, and lymphoid tissue inducer (LTi) cells. NK cells percentage in the blood typically ranges between 5% and 15% of the total number of peripheral blood mononuclear cells (PBMC) in healthy individuals. Just like ILCs, NK cells can be divided into several subgroups or populations based on their marker expression. NK cells are mostly divided into 2 major subsets by the expression of CD56 and CD16 (FcγRIIIA). CD56 is a neural cell adhesion molecule (NCAM), which was originally described on brain cells, but later found to be expressed on NK cells[10]. CD56 divides NK cells into two main subtypes: CD56bright and CD56dim, that differs in their cytotoxic and regulatory functions[11]. CD16 is potent NK activating Fc receptor that mediates ADCC[12]. Similar to CD56, CD16 defines two NK subsets and together with CD56 forms two subsets. The major NK subset is identified as $CD56^{dim}CD16^{high}$ while a small subset of around 10-15 % of total NK cells is $CD56^{high}CD16^{low}$[11]. The cytotoxicity of NK cells is mediated by either a release of lytic granules, triggered by activating receptors, or by engagement with death receptors expressed on tumor cells (Figure 4.2). NK cells as well as cytotoxic T cells produce multiple granules that contain perforin, a pore-forming protein, and granzyme, an apoptosis inducing protease[13–16]. When the immunological synapse is established between NK cell and a target cell, the granules are mobilised towards the interface and fuse with the NK membrane causing a release of perforin and granzyme into the synaptic cleft. The release is not random but carefully directed within an immunological synapse reaching target cell membrane while the NK cells membrane is shielded from perforin by packed lipid membrane[17–19]. Besides granule release, NK cells express on their surface ligands such as CD95L or TNF-related apoptosis-inducing ligand (TRAIL) that bind to respective death receptors CD95/Fas and TRAIL-R1-R2 expressed on the surface of target cells. Activation of death receptors results in formation of death-inducing signalling complexes that initiate a caspase cascade and cell apoptosis[20–25]. NK cells which can kill not only one target cell but proceed to kill multiple targets are then referred as a serial killers. The first target cell killing

by serial killer NK cells is mediated by fast perforin/granzymeB release which reduces intracellular levels of cytotoxic granules and increased death receptor ligand expression on the NK cell surface. The subsequent target cell killing then gravitate towards death receptor–mediated killing. The death receptor–mediated killing marks the last killing event by serial killer NK cells[16].

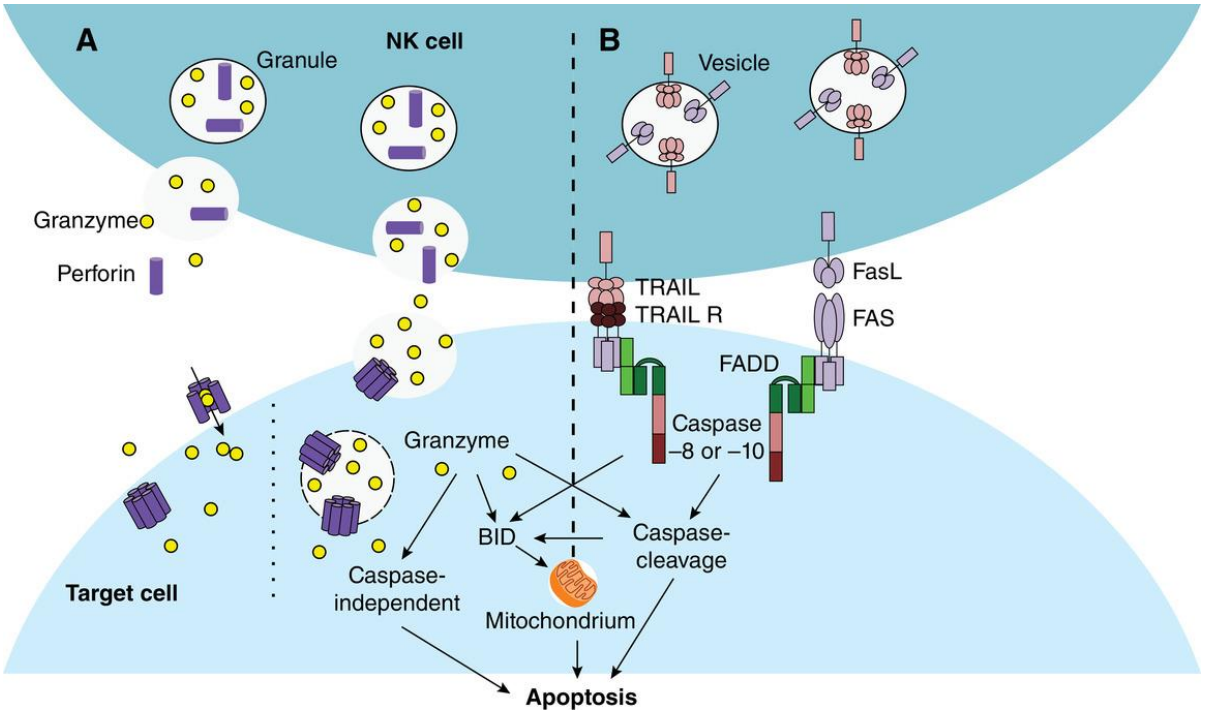

Figure 4.2 Two mechanisms of NK cell mediated killing of target cells.
A) Lytic granule release is triggered by activating receptor engagement causing perforin integration into the target cell membrane and transport of granzyme into its cytosol where apoptosis is triggered. B) Death receptor-mediated cytotoxicity is mediated by FasL or TRAIL, which bind and activate their respective receptors. This activation leads to the initiation of caspase activation, mitochondrial dysfunction, and ultimately, apoptosis. Adapted from Prager and Watzl, 2019[26]

NK cell activation is frequently accompanied by cytokine production. The major cytokine produced by NK cells is IFN gamma (IFNγ). IFNγ plays a crucial role in anti-tumor immunity by recruiting and activating other immune cells[27–30]. By itself but also in combination with TNFα, IFNγ induces senescence, apoptosis and tumor growth arrest [31–34]. It also changes the expression of multiple immune related molecules expressed by the tumor[35,36]. Besides IFNγ, NK cells secrete multiple chemokines and cytokines modulating tumor immune cell recruitment, activation and differentiation[30,37]. The functional properties differ in regards to NK cell subsets, but also in which stage of development and maturation the NK cells are.

4.4.1 NK cells development

The development of NK cells begins in the bone marrow (BM) from a common lymphoid progenitor cell (CLP) that gives rise to both T cells, B cells, ILCs and NK cells. NK cells then continue their development in the BM, after which they mature in the blood and lymphoid organs passing through a total of six distinct developmental stages[38]. The first developmental stage starts with a CD244 (2B4) expression that is sustained throughout all 6 following developmental processes (Figure 4.3). Stage 2 defines NK cell progenitors by CD117, CD127, CD7, CD122 and increasing interleukin (IL)-1R1 expression. The next stage producing immature NK cells (iNK) is characterized by high expression of IL-1R1 and by appearance of NKG2D, NKp46, NKp30, and CD161 expression. Stages 4a and 4b starts differentiating iNKs into mature NKs marked by high expression of NKG2A, NKG2D, NKp46, NKp30, CD161, CD56 and NKp80. The increase in CD16 and inhibitory killer immunoglobulin-like receptors (KIRs) expression is connected to stage 5 when CD56 expression is reduced and CD56 NK subsets are formed (Figure 4.3). In this stage NK cells acquire anti-tumor cytotoxicity characterized by the cytolytic function of the $CD56^{dim}$ population and inflammatory cytokine production by $CD56^{bright}$ NK cells. The majority of NK cells then present in circulation are of the $CD56^{dim}$ subset while less matured $CD56^{bright}$ NK cells reside primarily in secondary lymphoid tissue. The final stage of NK development also known as terminal differentiation is induced by interactions with other cells of the immune system or target cells, as well as different cytokines. It leads to generation of adaptive or memory-like NK cells[39–41].

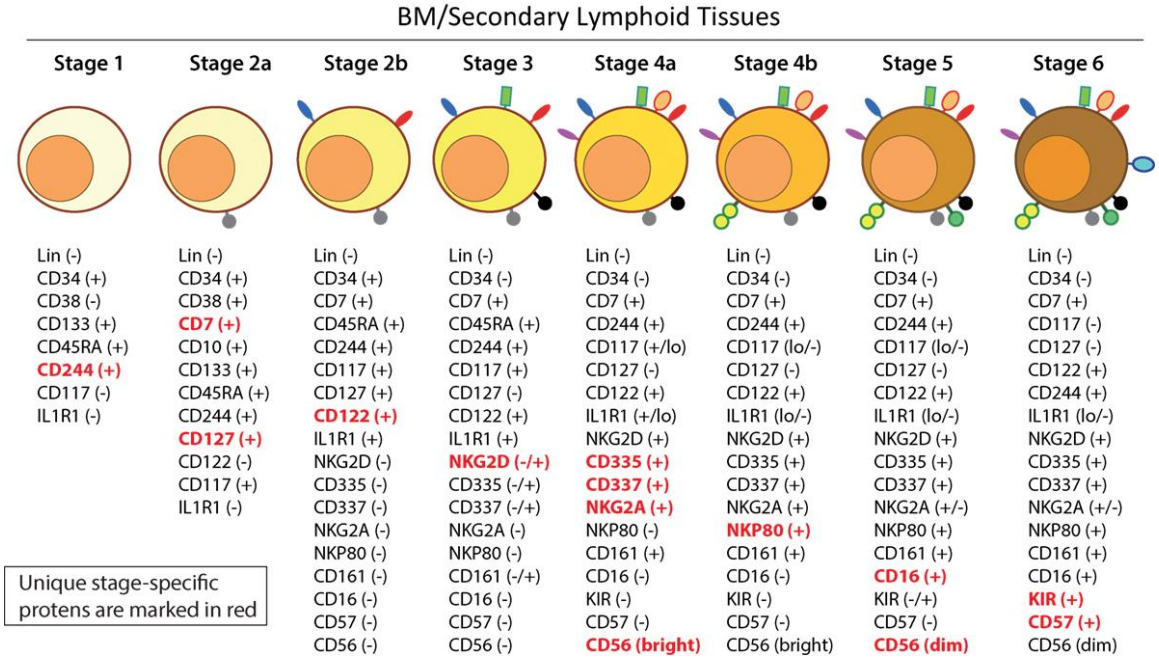

Figure 4.3 Developmental stages of NK cells.

Expression is designated as (-/+) (starting expression), (+) (high expression), (-) (no expression). Molecules marked in red are main markers for each stage. Image adapted from Abel et al. 2018 [39].

4.4.2 NK cell activating receptors

The ability of an NK cell to detect and eliminate target cells is not mediated by receptors that undergo somatic gene rearrangements like T or B cells. Instead, an NK cell expresses multiple germline-encoded inhibitory and activating surface receptors (Figure 4.4). The expression of these receptors vary in NK cells thus resulting in functional differences among NK subsets. The receptor potency and the balance between the amount of activating and inhibitory receptors engaged dictates whether an immunological synapse is formed and lytic granules are released by the NK cell. The most potent NK receptor and also the first identified is CD16[42,43]. CD16 is the low-affinity FcγRIII receptor that enables recognition of target cells coated with an antibody in a process called ADCC. CD16 associates with ITAM-bearing adaptor proteins FcεRIγ and CD3ζ that transmit the activation signal after CD16 binds to an Fc portion of IgG triggering strong NK cytotoxicity and cytokine production[44,45]. This process is used in the clinic by using therapeutic antibodies such as Rituximab, in patients with non-Hodgkin lymphoma and chronic lymphocytic leukemia to target CD20, thus inducing ADCC and clearance of transformed cells[46,47]. The activation of CD16 depends on the adaptive immune system recognizing foreign antigen and producing a specific antibody, which can be circumvented by directly administering high-affinity antibodies[48].

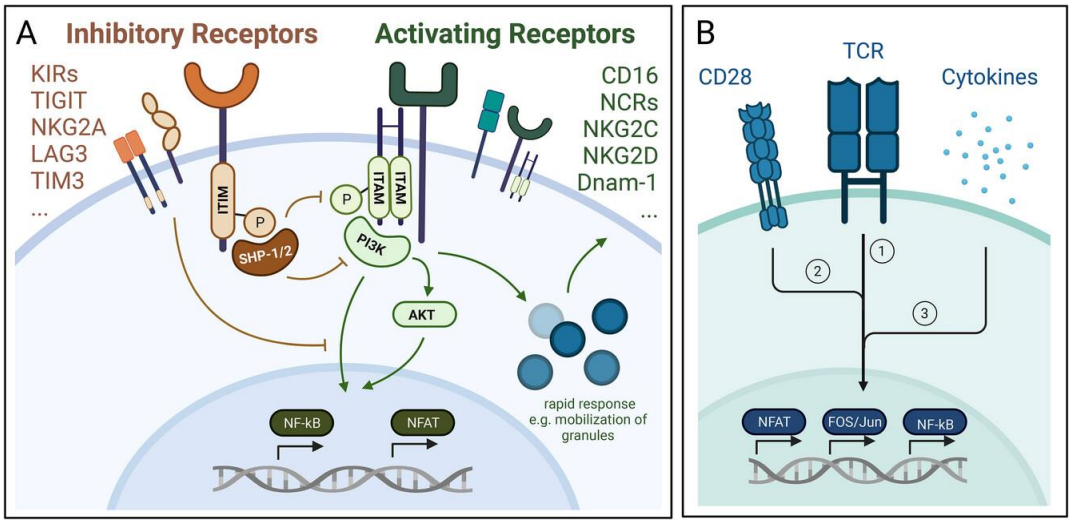

Figure 4.4 The differences in NK cell and T cell activation.

A) NK cells activation results from the balance between activating and inhibitory receptors. Activating receptors trigger a kinase signalling cascade starting with the phosphorylation of ITAM containing

adaptors, which are counterbalanced by inhibitory receptors phosphorylated in their immunoreceptor tyrosine-based inhibitory motif (ITIM) that recruit phosphatases (SHP-1/2) to dephosphorylate ITAM and activated kinases thus blocking NK cell activation. **B)** T cell activation strictly requires T-cell receptor (TCR) and co-receptor signalling that engage with specific antigen presented by MHC-I molecules, followed by activation via CD28 and cytokines. Adapted from Balzasch and Cerwenka, 2019[49].

NKG2D

The NKG2 family contains two activating receptors NKG2C and NKG2D and one inhibitory NKG2A receptor. Human NKG2D is a C-type lectin-like receptor and one of the most important activating receptors on NK cells. Its signalling capacity is mediated by the ITAM-containing DAP10 adaptor protein. The ligands for NKG2D are MHC-I chain-related molecule A (MICA) and MICB and six different UL16-binding proteins (ULBP). All NKG2D ligands are homologous to MHC class I molecules[50–54]. MICA and ULBP belong to the stress-induced NK ligands, since their expression is absent on healthy cells but increased on tumor cells that display multiple active stress pathways such as excessive cell proliferation, genotoxic stress, DNA damage response (DDR) or viral infection. The DDR, often connected to cell proliferation, induces the expression of NKG2D ligands and alerts the immune system to potentially malignant cells[55,56]. Overexpression of NKG2D ligands on healthy cells is sufficient to sensitize cells to NK cells[57]. Engagement of the NKG2D leads to rapid internalization of the receptor and impairment of NKG2D-dependent NK cell function[58]. Tumor cells, that frequently express ligands for NKG2D, develop tumor escape mechanisms to downregulate NKG2D expression on NK cells by proteolytic ULBP and MICA/B shedding. The soluble NKG2D ligands then interact with NKG2D expressed on NK and impair NKG2D ligand recognition on tumor cells [59–63]. Blocking of the shedding process is thus also a target for immunotherapy. Antibody-mediated blocking of the site for proteolytic shedding can prevent this loss of MICA and MICB from the tumor cell surface and lead to a fourfold reduction in the number of detected metastases in mice with melanoma xenografts in an NK-cell-dependent manner[64,65]. Another way how to increase MICA/B surface levels is direct blocking of sheddases a disintegrin and metalloprotease (ADAM)17 or ADAM10 or matrix metalloprotease 14 (MMP14) that cleave and shed MICAB[66–68]. The levels of soluble NKG2D ligands can be used as potential biomarkers for tumor progression[69–71]. However, not only stress, but also IFNγ, a cytokine produced by activated NK cells in large amounts, was shown to downregulate NKG2D ligand expression and impair NKG2D-mediated NK cytotoxicity[72].

NKG2C

NKG2C and NKG2A forms a disulphide-linked heterodimer with CD94[73–75]. CD94 has no intrinsic signalling capacity, thus the positive signal relies on the DAP12 adaptor that associates with NKG2C[76]. NKG2C is induced on adaptive NK cells and is well-characterized during a human cytomegalovirus (HCMV) infection where $NKG2C^+$ positive NK cells are preferentially expanded in response to HCMV infected cells [77,78]. NKG2A and NKG2C share the same ligands which is the non-classical MHC-I molecule HLA-E, yet transmit opposing signals[73–75]. HLA-E also presents peptides on the cell surface but differs from the classical MHC-I in terms of allele diversity. While the MHC-I gene cluster is the most polymorphic locus in humans, only three alleles have been described for HLA-E. The peptide binding groove in HLA-E presents peptides derived from the leader sequences of classical MHC-I molecules. Thus, the HLA-E expression and stability is primarily a reflection of proper expression of the classical MHC-I HLAs[79]. In the context of HCMV, HIV or EBV infection, HLA-E has been shown to also present viral peptides as an escape mechanism via inhibitory NKG2A axis[80–83].

Natural Cytotoxicity Receptors (NCRs)

NCRs are a group of receptors of the immunoglobulin (Ig) superfamily that play a critical role in the recognition and elimination of infected or transformed cells. The members of NCRs are NKp46/NCR1/CD335, NKp44/NCR2/CD336, and NKp30/NCR3/CD337[84–88]. NCRs recognise self-molecules expressed upon cellular stress or exogenous microbial molecules produced during infections[89].

NKp46

NKp46 has two extracellular C2-type Ig-like domains and a cytoplasmic domain, which lacks an ITAM motif. The transmembrane domain associates with CD3ζ or FcRγ ITAM signalling adaptors[89]. NKp46 was shown to activate NK cell cytotoxicity and cytokine production and blocking of NKp46 inhibits NK cell activation [84,85,90]. Its expression is stable in all NK cells not depending on their activation status. NKp46 is also expressed by ILC1, a subset of ILC3s and γδ T cells[89]. The first ligand described for NKp46 is a hemagglutinin (HA) which mediates enhanced killing of Influenza virus-infected cells that express HA, which can be reversed by blocking of HA or NKp46[91]. Vimentin, an intracellular filamentous cytoskeletal protein, is another ligand found by increased killing of monocytes infected with Mycobacterium tuberculosis where blocking of vimentin inhibited NK cell lysis of infected monocytes[92]. NKp46 ligands are not limited to infections. NKp46 was shown to recognize ligands expressed

on a several tumor cell lines including melanoma cell lines[93,94]. In human melanoma patients, tumor tissue stained strongly for NKp46 ligands while normal melanocytes displayed low NKp46 ligand expression. Several ligands for NKp46 have been described, with likely additional NKp46 ligand remaining to be identified[95,96].

NKp44

NKp44 is the second member of NCR, and usually absent on peripheral blood (PB) resting NK cells, but upregulated after IL-2, IL-15 or IL-1β stimulation particularly on the $CD56^{bright}$ subpopulation of NK cells. Even though the cytoplasmic domain contains an ITIM motif, NKp44 can also associate with the ITAM containing DAP12 adaptor protein inducing an activating signals[86,97,98]. The ligand for NKp44 was identified as an isoform of mixed-lineage leukaemia protein-5 (MLL5), a spliced variant 21spe-MLL5, which is originally a nuclear antigen regulating cell cycle progression. 21spe-MLL5 is barely expressed in healthy tissues but frequently expressed at high levels in the cytoplasm and at the cell surface of malignant cells where it induces NKp44-mediated cytotoxicity[99]. Similar to NKp46, NKp44 has a role in eliminating virus-infected cells since several HA and viral proteins were found to bind NKp44[100–104]. NKp44 also recognizes surface-associated heparan sulfate (HS) or heparin-type molecules which result in enhanced IFN-γ secretion[105,106]. Recently, two more ligands were described for NKp44, Nidogen 1 (NID1) and platelet-derived growth factor (PDGF)-DD. Secreted NID1 was shown to interfere with NKp44-mediated NK cell activation, potentially serves more as a decoy NKp44 ligand[107]. The interaction of PDGF-DD with NKp44 triggers cytokine and chemokine production by the NK cell and induce tumor growth arrest by downregulation of cell cycle genes[108]. Proliferating Cell Nuclear Antigen (PCNA) protein, involved in the regulation of cell cycle progression, DNA replication and repair, was also found to be a ligand for NKp44. PCNA can be overexpressed and detected on cell surface of tumor cells in complex with MHC-I or via exosomes [109,110]. In contrast to the above-mentioned activating ligands, NKp44 interaction with PCNA triggers inhibition of NK cell cytotoxicity and IFN-γ secretion mediated by the NKp44-1 isoform and its cytoplasmic ITIM motif[111]. PCNA has an important role in tumor survival itself since targeting of PCNA resulted in tumor growth arrest *in vivo* and apoptosis of tumor cell lines *in vitro*[112].

NKp30

The last NCR member is NKp30, an important activating receptor expressed by all NK cells. Similar to CD16, NKp30 associates with the ITAM adaptors, CD3ζ and/or FcRγ, to

transduce an activating signal[88]. NKp30 binds B7H6, a member of the B7 family of co-stimulatory ligands with minimal expression in healthy cells but frequent on the surface of tumor cells through either Myc-regulated transcription, TLR stimulation, stress responses or pro-inflammatory cytokine stimulation[113–116]. Thus, its tumor-restricted expression makes B7H6 a promising target for immunotherapy. However, similar to NKG2D ligands, tumors use metalloproteases to cleave and shed B7-H6 from their surface to escape NKp30-mediated recognition[117]. Additionally, histone deacetylases (HDACs) inhibitors were also shown to reduce B7H6 expression[118]. Another NKp30 ligand is nuclear factor HLA-B-associated transcript 3 (BAT3). BAT3 is not presented on the cell surface but released from cells via the exosomal pathway and interferes with NK cell activity as a part of tumor immune escape mechanisms[119,120]. Another ligand that is released by tumor cells as part of immune evasion is galectin-3. Soluble galectin-3 then interacts with NKp30 and thus interferes with NKp30-mediated cytotoxicity[121,122].

2B4

2B4 (SLAMF4, CD244) receptor is present on all human NK cells from the initial stage of NK cell development. The ligand for 2B4 is described to be CD48[123,124]. The 2B4:CD48 axis is activating in humans whereas in mice it induces inhibition and improves survival of CD48+ tumors[125,126].

DNAM-1

Another highly expressed activating receptor that triggers NK cell function is DNAX accessory molecule-1 (DNAM-1, CD226). DNAM-1 is an Ig-like domain-containing receptor that does not associate with any ITAM-containing adaptor. Nevertheless, its intracellular ITT-like motif gets phosphorylated upon ligand binding to deliver an activating signal[127] (Figure 4.5). Ligands for DNAM-1 are CD155 (polio virus receptor, PVR) and CD112 (nectin-2, PVRL2) and are frequently overexpressed in tumors[128–135]. CD112 and CD155 are closely related molecules and members of a larger Nectin family and are also ligands for inhibitory receptor TIGIT[136–138]. CD155 is also a ligand for CD96, which role remains unclear[139–141]. As CD112 and CD155 are also expressed on other tissues, the expression itself does not sensitize cells to be killed by NK cells.

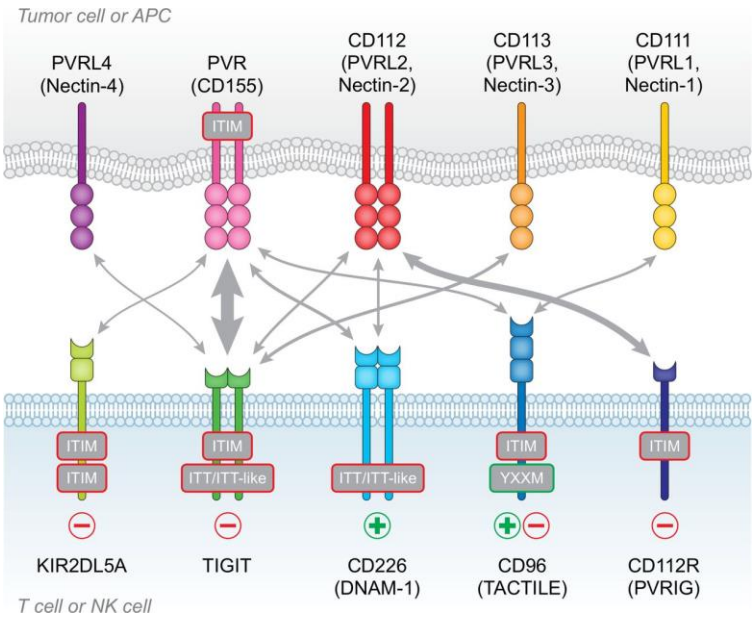

Figure 4.5 Nectin and Nectin-like pathway.

Protein interactions with NK receptors with different affinities and intracellular signalling motifs. Adapted and modified from Chiang and Mellman, 2022 [142].

LFA-1

DNAM-1 complexes with the β2-integrin LFA-1, a receptor for intercellular cell adhesion molecule (ICAM-1, CD54), which results in the phosphorylation of the cytoplasmic domain of DNAM-1[143,144]. ICAM-1 is a surface adhesion molecule induced on epithelial and immune cells during inflammation, which regulates the recruitment of leukocytes from the circulation to the sites of inflammation by increased adhesion[145,146]. ICAM-1 is also frequently expressed on tumor cells in a membrane-bound or soluble form[147–149]. ICAM-1:LFA-1 co-stimulation causes an increase in NK cell cytotoxicity and reduced tumor survival[150–154] LFA-1 triggering alone by ICAM-1-decorated beads causes transient NK cell granule polarization, but fails to induce cytolytic granule release in the absence of other receptor stimulation.[154,155].

Some of the NK activating ligands are not exclusively expressed by tumor or infected cells. However, the protection of healthy cells from NK cell–mediated killing is controlled by expression of inhibitory ligands such as, MHC-I which are the main ligands for the inhibitory KIR or NKG2A receptors. The outcome of NK cell activation then relies on the balance of signalling by activating vs inhibitory receptors (Figure 4.6).

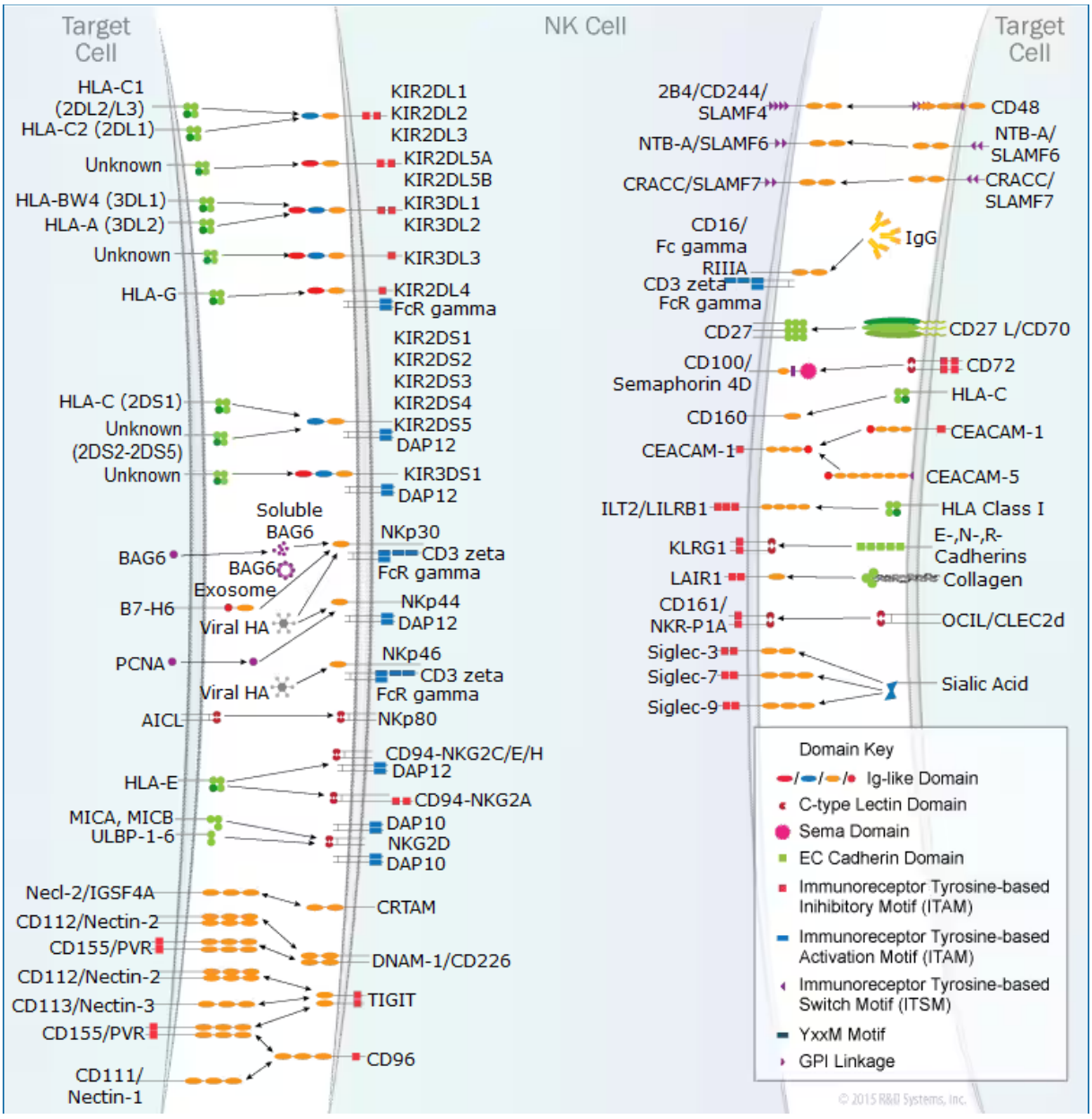

Figure 4.6 Summary of activating and inhibitory NK cell receptors and cognate ligands. Image adapted from RNDsystems[156].

4.4.3 NK cell inhibitory receptors

NK cells function is counterbalanced by multiple inhibitory receptors. Interaction with inhibitory receptors results in phosphorylation of intracellular inhibitory motifs triggering downstream signalling. Phosphorylated motifs attract phosphatases that dephosphorylate substrates triggered by engagement with activating receptors (Figure 4.5). NK inhibitory receptors play a crucial role in immune homeostasis and prevent excessive immune reaction against healthy cells, but are therefore also often involved in tumor escape.

MHC molecules and KIRs

One family of the major inhibitory receptors are involved in NK cell education, a process in which iNK cells acquire the ability to distinguish between normal and healthy "self" cells and virus-infected or cancerous "non-self" cells. This process of NK cell education is mediated by interactions with Human Leukocyte Antigens (HLA) that signal to NK cells enhancing their functional abilities. These educated NK cells are then able to recognize “self” inhibitory ligands expressed on all nucleated healthy cells, and do not attack normal healthy cells while eliminating abnormal cells that have lost or downregulated HLA molecules (Figure 4.7)[1].

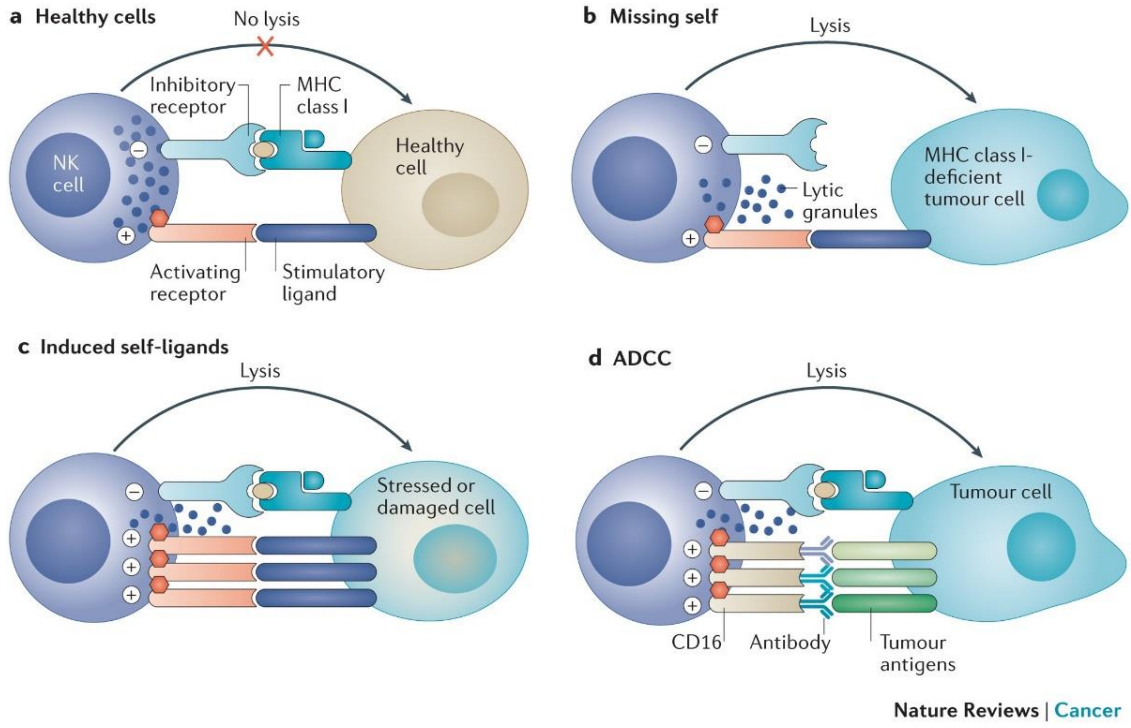

Figure 4.7 Schematic representation of healthy and tumor cell recognition by NK cells.
A) Balanced activating and inhibitory receptors signals delivered from healthy cells to NK cells. **B)** Tumour cells detected as 'missing self' due to loss of MHC-I are lysed by NK cells. **C)** Overexpressed stress ligands prevail the inhibitory signals causing tumor cells to be recognized and lyses by NK cells. **D)** ADCC mediated by CD16 binding to an antigen-specific antibody triggering tumor lysis by NK cell. Adapted from Morvan and Lanier, 2016[157].

HLA molecules interact with receptors such as the killer immunoglobulin-like receptors (KIRs) encoded by one of the most variable regions in the human genome enabling diverse NK cell responses with a limited number of genes[158]. HLA molecules can be divided into two categories: classical and non-classical. The classical HLA genes consist of HLA-A, HLA-B,

HLA-C, HLA-DR, HLA-DP and HLA-DQ. The non-classical HLA genes are HLA-E, HLA-F, HLA-G, HLA-DM, and HLA-DO. Besides the classical and non-classical subdivision, HLA genes are also divided into two major histocompatibility complex (MHC) classes. MHC class I (MHC-I) consists of HLA-A, -B, -C, -E, -F and –G genes and require formation of a heterodimer with β2-microglobulin (B2M) to be expressed on the cell surface. MHC class II (MHC-II) includes B2M-independent HLA-DR, -DP, -DQ, -DM and –DO. Each HLA gene is present in two alleles in the human genome[1]. Due to high polymorphism, up to March 2023 a total count reached over 25 000 alleles of MHC-I and over 10 000 MHC-II alleles[159]. MHC-I presents short peptides (8-10 amino acids) of endogenous proteins produced inside of the cells[160,161]. Intracellular proteins are cleaved by proteasome units and peptides transported via channels (TAP1, TAP2) into the endoplasmic reticulum (ER)/ Golgi intermediate compartment where they are loaded into an empty MHC-I peptide groove and together transported to the cell surface (Figure 4.8). MHC-II is expressed as a heterodimer of α and β chain and presents peptides of endocytosed antigens originating outside of the cells. Loading of peptides into MHC-II occurs in endosomal compartments[1]. Dendritic cells, especially plasmacytoid dendritic cells, bypass this exclusivity of MHC-I presenting intracellular antigens and MHC-II presenting outside antigens by so-called cross-presentation, where exogenous antigens are loaded and presented by MHC-I to initiate cytotoxic $CD8^+$ T cell responses[162].

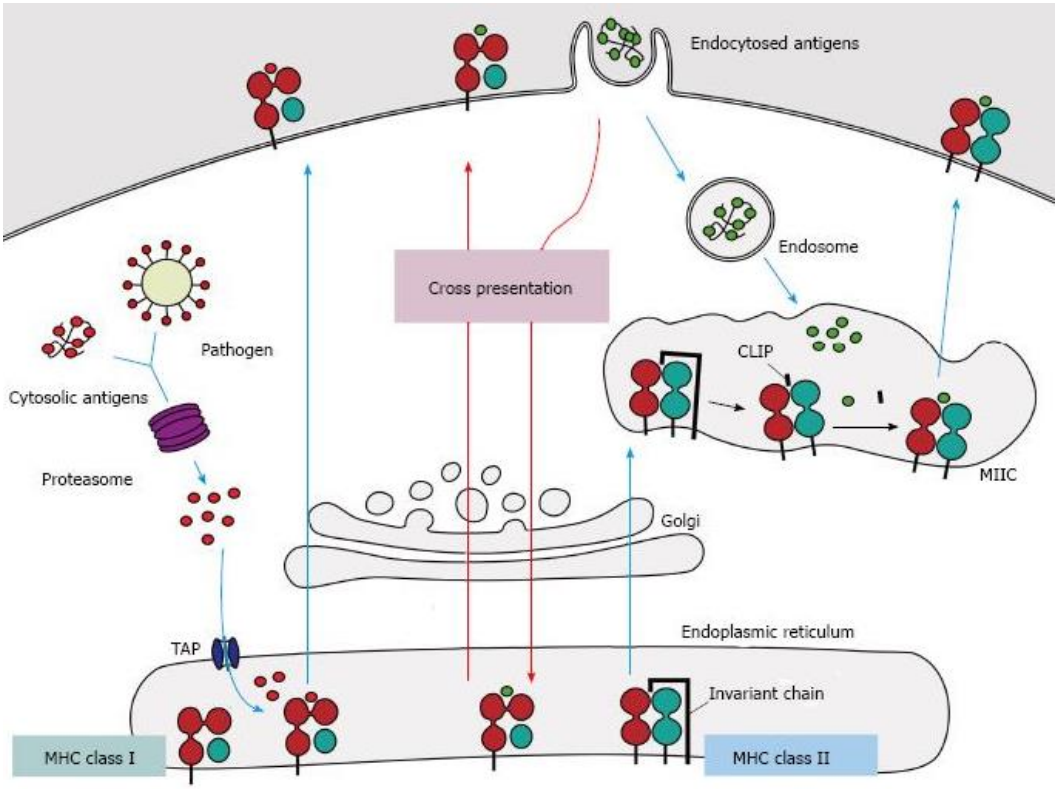

Figure 4.8 MHC-I and –II peptide loading pathways.

MHC-I molecules present peptides derived from endogenous proteins cleaved by the proteasome into short peptides. Cytosolic peptides are then translocated by the TAP transporter into the ER to be loaded into the peptide groove of MHC-I molecules. MHC-I molecules in ER are stabilized by chaperones such as tapasin or calreticulin[163,164] and replaced if peptides with sufficient affinity appear. MHC-I/peptide complexes are then transported to the cell surface for antigen presentation. MHC-II molecules present endocytosed exogenous peptides. A so-called invariant-chain protects α and β chains assembled in the ER from binding endogenous peptides, which is partially degraded into class II-associated invariant chain (CLIP) within endosomal compartments and exchanges with exogenous peptides and to be transported to cell surface. Cross-presentation occurs in pDCs where MHC-I is loaded with exogenous peptides transported from endosomes to the cytosol. Adapted from da Silva et al. 2017[165].

Besides serving antigen presentation to T cells, HLAs act as potent inhibitory ligands of NK cells. Each HLA allele differs in its ability to bind corresponding KIRs (Figure 4.9). KIRs are the dominant NK inhibitory receptors due to their ability to distinguish self vs non-self HLAs and counterbalance the activating signals. Inhibitory KIRs are characterized by a long cytoplasmic tail with ITIM that upon phosphorylation of tyrosine residues recruits phosphatases that blocks activating signals[166]. Activating KIRs contain a short cytoplasmic tail and associate with the ITAM containing DAP12 adaptor protein. KIRs can be divided into two groups based on the number of Ig domains they contain: KIR2D and KIR3D. KIR2DL group contain 5 inhibitory members (KIR2DL1, KIR2DL2, KIR2DL3, KIR2DL4 and KIR2DL5) and KIR3D contain 3 inhibitory members (KIR3DL1, KIR3DL2 and KIR3DL1). The binding of KIRs to HLA is dependent on the peptide presented and on epitopes specific for that HLA molecule (Figure 4.9, Table 4.1) [167,168] . Most KIR2DL recognize HLA-C-specific epitopes C1 or C2, while KIR2DL4 recognizes HLA-G, a non-classical HLA[169,170]. KIR3DL2 recognizes HLA-A Aw3 and Aw11 epitopes, and KIR3DL1 recognizes the broadly distributed HLA-B Bw4 epitope but also HLA-A epitopes[170]. Recently, CD155 was described to bind KIR2DL5 and transmit an inhibitory signal responsible for KIR2DL5-mediated NK cell immune evasion[171,172].

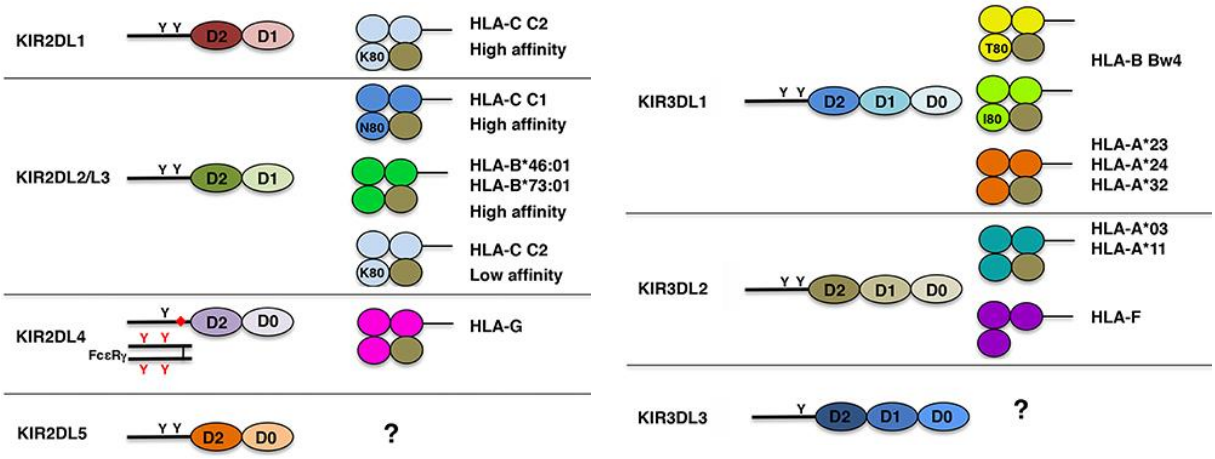

Figure 4.9 Schematic representation of the inhibitory KIR and their corresponding HLA class I ligands. Structure of inhibitory KIRs and their Ig domains represented as D0, D1, and D2. Black and red Y indicates ITIM motifs. HLA domains are represented as a circles with β2m as a brown circle. Image adapted from Pende et al 2019[173].

C2-epitope^{lys80}	HLA-Cw02, Cw04, Cw05, Cw06, Cw15, CW1602, Cw17, Cw18
C1-epitope^{Asn80}	HLA-Cw01, Cw03, Cw07, Cw08, Cw12, Cw14, Cw16 (not Cw1602)
HLA-Bw4 epitope	B4, B5102, B5103, B13, B17, B27, B37, B38(16), B44(12), B47, B49(21), B51(5), B52(5), B53, B57(17), B58(17), B59, B63(15), B77(15), A9, A23(9), A24(9), A2403, A25(10), A32(19).

Table 4.1 HLA-alleles that contain the same epitope detected by KIR receptors. Adapted from Epling-Burnette et al. 2010[168].

NKG2A

NKG2A, another potent inhibitory receptor expressed by NK cells, is a C-type lectin-like receptor that forms a heterodimer with CD94 and binds non-classical MHC-I HLA-E. It shares this ligand with the activating NKG2C[74,174,175]. Similar to KIRs, NKG2A is important for NK cell education[176]. HLA-E does not display high polymorphism and is usually expressed at low levels on the cell surface which can be greatly induced by inflammatory cytokines such as IFNγ[177]. HLA-E presents peptides derived from the leader sequences of the classical MHC – I[178]. HLA-E is frequently expressed on tumors as a part of immune escape mechanisms and blocking the NKG2A/HLA-E axis increases NK and T cell reactivity against tumor[179,180].

LILR

Besides KIRs, classical HLA molecules are ligands for inhibitory receptors from leukocyte immunoglobulin-like receptors (LILR) family, also known as also known as CD85, ILTs and LIR. The LILR family comprises 6 activating receptors (LILRA1-6) and 5 inhibitory receptors (LILRB1-5) that are structurally related to the KIRs and FcαR and are located in the same region of chromosome 19 [181]. LILRs are expressed on a broad range of immune cells such as NK cells, T cells, B cells, DC, macrophages and monocytes, however, their expression was also detected on cells outside of immune cell compartment. LILRB1 and LILRB2 are the two most well studied members of LILR family with known ligands. High expression of LILRB1 in cancer correlates with poor patient outcomes, enhanced tumor growth and a decrease in NK cell functions [182,183]. Among LILRBs, LILRB1 (ILT2) is most frequently expressed. LILRB1 binds UL18, a CMV HLA class I homologue, and HLA class I molecules with the highest affinity to HLA-G[184–186]. LILRB1 interacts with the α3 domain and β2-microglobulin of MHC-I, making its recognition peptide independent (Figure 4.10) [187]. Activation of LILRB1 inhibits NK cell function which can be reversed by LILRB1 blocking [188–190]. LILRB2 (ILT4) binds to several ligands such as CD1d, Angptls, β-amyloid and HLA class I [191–194]. The last member of LILR inhibitory receptors reported to bind HLA molecules is LILRB5 (ILT3), which binds HLA-B7 and HLA-B27 heavy chains, [195]. LILRB5 expression seems to be restricted to NK cells but no studies focus on its impact on NK cell function[196].

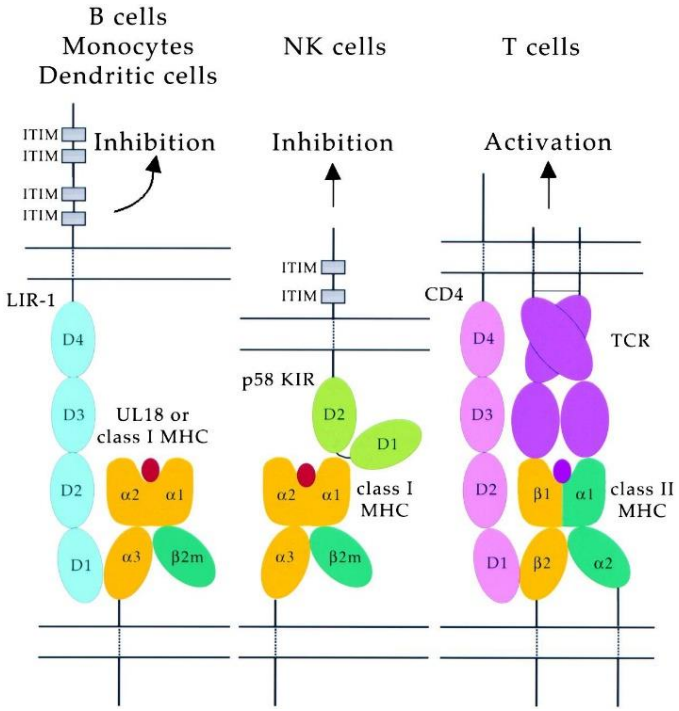

Figure 4.10 Schematic comparison of LILRB1, KIR and TCR binding site of MHC.

LILRB1 (LIR1) binds α3 domain/β2m region analogous to the interaction of CD4 with MHC-II β2 domain. KIRs bind α1 domain that for a peptide groove with α2 domain. Adapted and modified from Chapman et.al 1999 [187].

TIGIT

T cell immunoreceptor with Ig and ITIM domains (TIGIT) is a member of the PVR/nectin family and inhibitory receptor with the highest affinity to CD155 and much lower to CD112, CD113 and Nectin-4 (PVRL4)[136,197,198]. The functional interactions among competing PVR/nectin ligand and receptors will likely result in dominant TIGIT-CD155 inhibitory engagement, due to higher CD155 affinity towards TIGIT than DNAM-1. TIGIT is expressed on T-cells as well as NK cells and is one of the molecules responsible for T and NK cell dysfunction [199–202]. Its expression is mostly low in naive cells, but is upregulated upon activation[197]. High TIGIT expression on tumor infiltrating lymphocytes (TILs) or in peripheral blood of tumor patients has been associated with poor survival and development of metastases[137,203,204]. TIGIT is a promising target for immune checkpoint therapy since TIGIT blockade enhanced antitumor immunity by T and NK cells[137,205–207].

CD112R

CD112R (PVRIG) is an inhibitory receptor expressed by NK cells and T cells. CD112R is highly expressed on effector/memory T cells but not on naïve T cells[208]. CD112R is part of the PVR/nectin pathway and the only known ligand for CD112R is CD112[209]. Even though CD112R competes with TIGIT and DNAM-1 for interaction with CD112, the CD112R/CD112 axis seems to prevail due to higher affinity[209,210]. CD112R is also expressed on exhausted T and NK cells together with other exhaustion markers[211–213]. Due to its inhibitory role and a single ligand, CD112R is a promising target for immune checkpoint blockade. In support of anti-tumor potential of such an approach, CD112R-deficient mice display tumor growth arrest in context of melanoma and colon cancer [214]. Blocking of CD112R also showed increased NK and T cells function in vitro [208,211,214,215].

CD96

CD96 (TACTILE) is the last receptor of complexed PVR/nectin network expressed by T and NK cells. CD96 binds CD155 and CD111, but not CD112. The outcome of these interactions varies depending on the study with differences observed between mouse and human experiments, leaving its potential inhibitory function still incompletely understood [139,140,216,217].

KLRG1

Killer Cell Lectin-like Receptor G1 (KLRG1) is a C-type lectin-like inhibitory receptor expressed on a subset of mature $CD56^{dim}$ NK cells and terminally differentiated T cells[218–221].

KLRG1 binds to cell adhesion molecules such as E-, N- and R-Cadherins. Expression of E-cadherin protected target cells against lysis in KLRG1-dependent manner[221,222]. Moreover, high KLRG1 expression also impaired IFNγ expression, proliferation and increased NK cell apoptosis[223,224]. High E-cadherin expression is connected to epithelial-mesenchymal transition (EMT), which is a process of transcriptional reprogramming of epithelial cells, resulting in reduced adhesion and enhanced migration and invasiveness[225]. E-cadherin expressed on tumor cells increases the ability of metastasis formation[226].

Siglecs

Sialic acid-binding immunoglobulin-type lectins (Siglecs) are members of the immunoglobulin-like protein superfamily with affinity towards glycans with sialic acid residues. Siglecs are predominantly expressed by hematopoietic cells and consist of 16 members that can be divided into two groups. Conventional (Siglecs 1, 2, 4 and 15), that are structurally conserved between vertebrates and Siglec 3/CD33 and CD33-related Siglecs (e.g. Siglecs -3, -5, -6, -7, -8, -9, -10, -11, -12, -14 and -16) that display 50–85% extracellular domain homology to CD33[227]. Most siglecs possess an ITIM or ITIM-like motif in their cytoplasmic domain transmitting inhibitory signals. However, some contain an ITAM motif or no motif. The function of siglecs thus varies from inhibition, activation to adhesion depending on the member engaged (Figure 4.11). Siglecs display unique specificity to sialylated stuctures containing the N-acetylneuraminic acid (Neu5 Ac) α2–6 and α2–3 linkages (Figure 4.11)[228]. Tumor cells are frequently hypersialylated as protection from immune cell attack [229,230]. NK cells were shown to express Siglec-7, -9 and -10[231–233]. Siglec 10 interacts with CD24 and represses tissue damage-caused immune responses[234]. It is also highly expressed on NK cells from hepatocellular carcinoma (HCC) in comparison to surrounding non-tumor tissues. Siglec-10-positive NK cells show impaired effector function compared to counterparts lacking Siglec-10,which was associated with decreased patient survival[235]. In addition to CD24, Siglec-10 also binds CD52 and VAP-1[236,237]. Siglec7 and Siglec-9 show high similarity in amino acid sequences, but differ in ligand affinity. Siglec7 shows highest affinity to α2,8-sialyl residues, lower affinity to α2,6-sialyl residues and lowest affinity to α2,3-sialyl residues. On the other hand, α2,6-sialyl and α2,3-sialyl residues are preferentially bound by Siglec9[233,238,239]. Siglec-7 was reported to be preferentially expressed on mature NK cells and proposed as a marker of more cytotoxic NK cells since more activating receptors than inhibitory receptors are expressed by Siglec7^{+} NK cells[240]. Recently, a Genome-wide CRISPR screen revealed CD43 as a ligand for Siglec-7 protecting leukemia cells from immune cell responses[241]. Siglec-9 interacts with

heavily glycosylated proteins such as MUC1 and MUC16, which are normally produced by epithelial tissues but frequently overexpressed by tumors[230,242–248]. LGALS3BP is the last ligand of Siglec-9 described[249]. In line with the potent inhibition of immune cells mediated by Siglec ligands, blocking of Siglec-7 and Siglec-9 increases antitumor immunity suggesting suitability for use as novel immune checkpoint therapy approach[250,251].

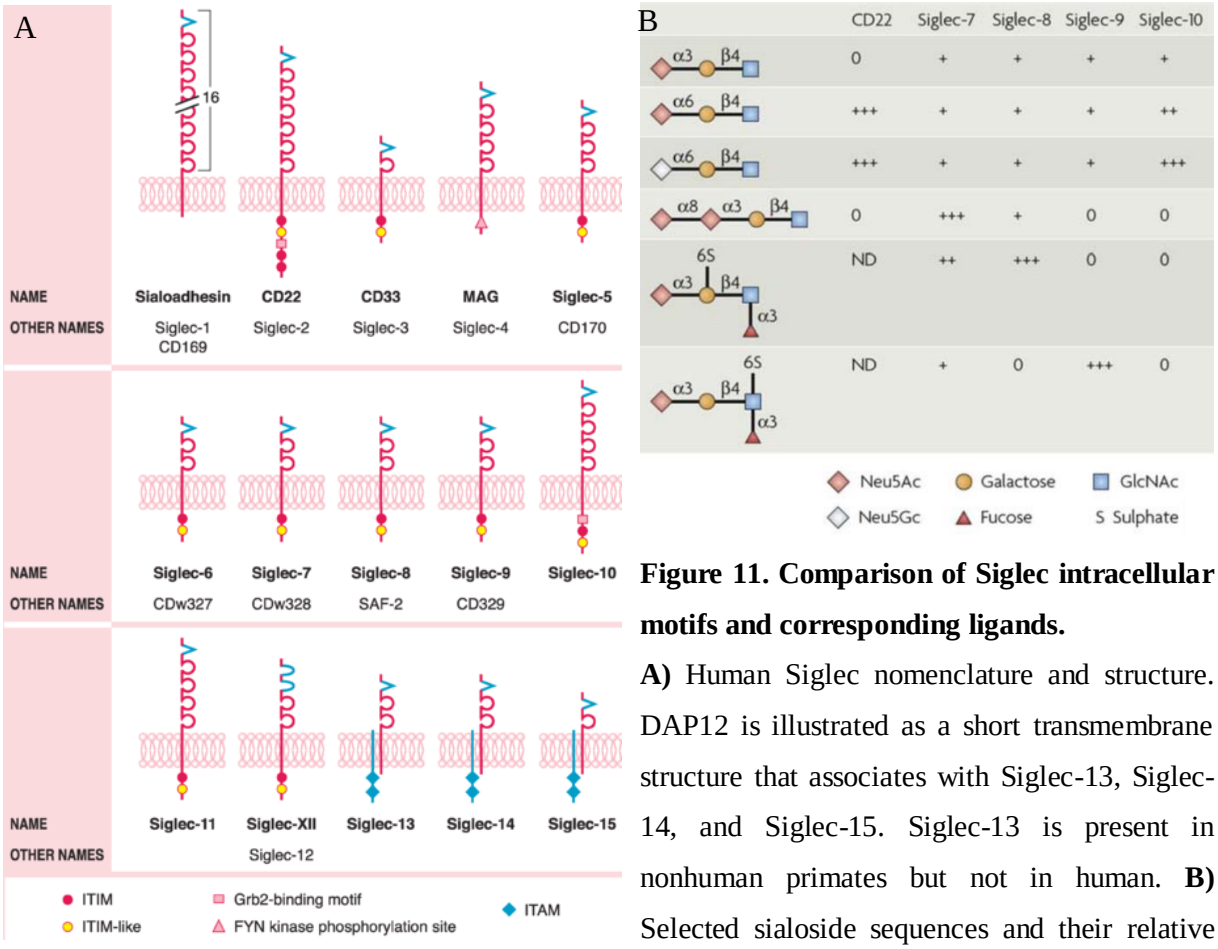

Figure 11. Comparison of Siglec intracellular motifs and corresponding ligands.

A) Human Siglec nomenclature and structure. DAP12 is illustrated as a short transmembrane structure that associates with Siglec-13, Siglec-14, and Siglec-15. Siglec-13 is present in nonhuman primates but not in human. **B)** Selected sialoside sequences and their relative affinity towards selected Siglecs depicted as a stars. High affinity (+++); moderate affinity (++); low affinity (+); detectable affinity (±); no detectable affinity (0); not determined (ND). Adapted and modified from von Gunten & Bochner, 2008 [228].

LAG-3

Lymphocyte-activation gene 3 (LAG-3) is an immune checkpoint receptor predominantly affecting T cell responsiveness via binding to MHC-II[252,253]. Other ligands such as Galectin-3, LSECtin and FGL1 were also shown to mediate T-cell inhibition[254–256]. While LAG3 appears to be expressed by activated NK cells, both negative as well as no effect on NK cell cytotoxic activity has been observed [252,257,258]. LAG-3 can be induced by IL-15 or by a chronic exposure to NKG2C ligands, however the effect of this induced LAG-3 on NK cell function has not

beenexamined[259]. LAG-3 is not expressed on naive T cells, but induced after antigen recognition together with CTLA-4 and PD-1 where it contributes to overall T cell dysfuction and reduced antitumor imunity[260].

4.5 Tumor immunology

Tumor immunology investigates the complex crosstalk between cancer cells and various immune cells such as T cells, NK cells, dendritic cells and macrophages forming a complex tumor microenvironment (TME). The field of tumor immunology dramatically changed over the past decades by understanding tumor escape mechanisms and the development of immune checkpoint blockade unleashing antitumor functions of immune cells.

4.5.1 Tumor escape mechanisms

Tumor surveillance tightly depends on the balance between activation and inhibition of immune responses. Transformation from healthy cells towards a malignancy is frequently accompanied by a disbalance in cell surface composition, signalling capabilities and generation of neoantigens. These non-self antigens can be a recognized by the adaptive immune system, while changes in surface molecules such as expression of stress molecules are often recognized by innate immune system. Properly orchestrated immune responses ensure tumor cell recognition and successful elimination of transformed cells. However, proper tumor elimination requires 100% immune system accuracy on multiple levels of tumor surveillance. Unfortunately, tumor cells either proliferate faster than the immune system can deal with, or adopt many escapes mechanisms that block immune system reactivity and tumor cell apoptosis. In this context, a tumor cell can be viewed as a single-cell organism such as *E. coli* challenged either by natural environmental factors or manmade antibiotics to stop its dissemination. Even a small survival advantage or antibiotics resistance is passed on to the next generation and results in a wide spread of resistant clones, constituting a problem for elimination (Figure 4.12). In principle, a single resistant tumor cell that acquired some tumor escape mechanism, can proliferate to generate an uncontrolled tumor outburst. These escape mechanisms can be divided into many categories, such as production of soluble inhibitory molecules, recruitment of immunosuppressive cells, reduction of immune cell infiltration, downregulation of tumor antigens or upregulation of inhibitory ligands for immune cells. Together, these mechanisms form a complex tumor microenvironment between healthy tissue, tumor cells and immune cells where the balance towards tumor elimination is increasingly counterbalanced [1,261].

A

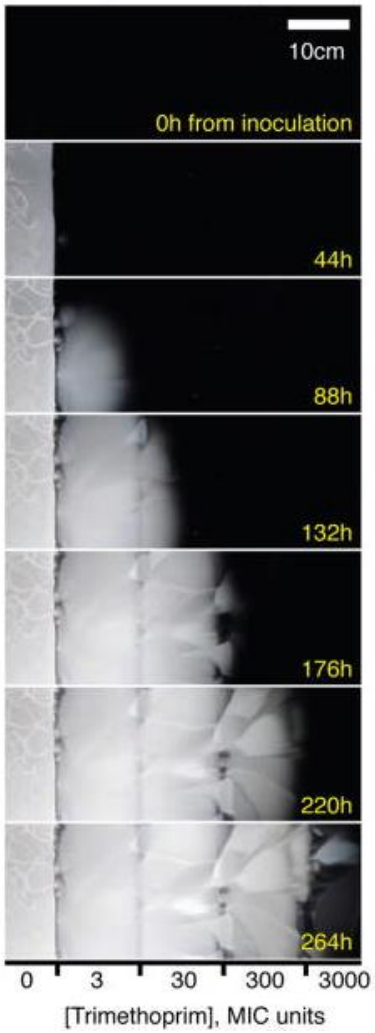

B

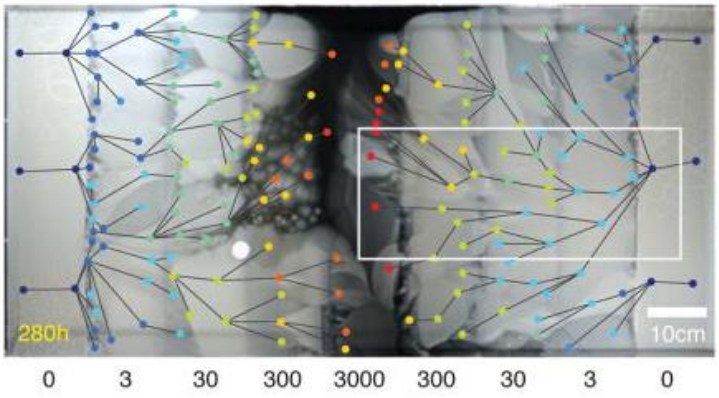

Figure 4.12 Evolution of an antibiotic resisitance as an analogy to tumor cell immune escape.

A) Setup of the four-step gradient of antibiotics. Exponentially increasing antibiotic concentrations in agar sections. In first section *E. coli*, appearing as white on the black background grows without limitations until section with low antibiotic concentration. Eventually an escape mutation occurs that gives rise to a new colony in each section with higher concentration. **B)** Mapping of antibiotic resistance evolution of *E. coli* on a clonal level. Adapted from Baym et al., 2016[262].

4.5.2 Immunosuppressive cytokines

One of the tumor escape mechanisms is the release of inhibitory molecules suppressing immune cells. Transforming growth factor-beta (TGF-β) is an immunosuppressive cytokine frequently produced by tumor cells, which reduces proliferation and downregulates the expression of activating receptors or cytotoxic gene products, thus inhibiting the cytotoxic activity or function of T-cells, NK and DC[263–273]. Blocking of TGF-β can effectively increase immune-mediated tumor eradication[274]. Another well-known immunosuppressive cytokine produced by tumor and immune cells within the TME is IL-10[275–278]. The immunosuppressive function on NK cells and T cells is caused indirectly via inhibition of APC-mediated production of proinflammatory cytokines or expression of antigen presentation and lymphocyte activation molecules[279]. IL-10 and TGF-β are also important for Treg differentiation, thus further supporting the establishment of an immunosuppressive environment [280–282]. In addition to IL-

10, tumors also produce vascular endothelial growth factor A (VEGF-A) and prostaglandin E_2 (PGE_2), which together induce FasL expression in endothelial cells to trigger apoptosis of effector $CD8^+$ T cells[283]. VEGF is a potent angiogenic factor promoting blood vessel growth access to nutrients and oxygen. However, VEGF alters the tumor vasculature resulting in reduced immune cell infiltration and functionality[284–286]. PGE_2 is a homeostatic factor involved in the immunopathology of chronic infections and cancer. It suppresses the effector functions of cytotoxic T cells, NK cells, macrophages and neutrophils and promotes regulatory T cell responses[287–296]. Indoleamine 2,3-dioxygenase (IDO) is an immunosuppressive enzyme processing tryptophan into kynurenine, which strongly supresses cytotoxic T cell function and promotes the generation and function of Tregs and Myeloid-derived suppressor cells (MDSC) [297–300]. The production of kynurenine, a ligand for aryl hydrocarbon receptor (AHR), also inhibits cytotoxic immune function and induces tolerogenesis[301–308]. In addition to the direct production of immunosuppressive molecules, solid tumors often develop a hypoxic environment that drives metabolic changes affecting immune cells and prevents efficient antitumor reactions[309–313].

4.5.3 Immunosuppressive cells

Another mechanism that is partially facilitated by above-mentioned soluble molecules produced in the TME is the recruitment of immunosuppressive cells and reduction in effector immune cells tumor infiltration. High tumor infiltration of immune cells with lower presence of immunosuppressive cells correlates with longer survival in cancer patients[314,315]. As may be expected from their central role in regulating the migratory behaviour of immune cells, a reduction of chemokine expression in tumors correlates with low immune cell infiltration. Reduced expression of CXCR3 ligands such as CXCL9, CXCL10, and CXCL11 results in reduced immune cell migration [316,317]. The examples of cell types with immunosuppressive properties are Tregs, MDSCs, tumor-associated macrophages (TAMs) and tumor-associated neutrophils (TANs). Tregs play a critical role in immune regulation by limiting excessive or autoreactive responses of other immune cells. However, their function can be hijacked by tumors to suppress anti-tumor immune responses[318]. Tregs directly inhibit CD8+ T and NK cells and produce immunosuppressive cytokines[319,320]. MDSCs are a heterogeneous population of immature myeloid cells often found in the spleen, lymph nodes and within the tumor microenvironment. Similar to Tregs, MDSCs secrete IL-10 and TGF-β, which directly inhibit T and NK cell function. MDSC suppressive activity is also associated with L-arginine

metabolism via Arginase 1 and inducible nitric oxide synthase generating nitric oxide, urea and L-ornithine associated with T-cell inhibition [321–323]. The importance of MDSC ROS production, another potent suppressive factor, is evidenced by the complete abrogation of MDSC suppressive effects upon the inhibition of ROS production[324]. MDSCs are also able to suppress T-cell proliferation and induce anergic and suppressive Treg development[325]. Within the TME, TAMs are one of the most abundant immune cells present, and they are recruited via VEGF, chemokines and inflammatory cytokines. In the early stages of tumor expansion, TAMs display M1-like pro-inflammatory phenotype and participate in anti-tumor immune response. Macrophages produce IFNγ which is crucial for recruitment of T and NK cells [326]. However, with tumor progression, TAMs functionally change towards an M2-like phenotype and instead support tumor growth and immunosuppression[327]. The transition from M1-like to M2-like is tightly connected to tumor hypoxic conditions and factors produced within the TME such as VEGF, TGF-β, IL-4, CSF-1, Eotaxin and Oncostatin M[328–332]. Whereas neutrophils are classically considered to defend against invading microorganisms and participating in wound healing, they are also important players in anti-tumor immunity. TANs make up a significant portion of infiltrated immune cells, as many cells within the TME produce neutrophil chemoattractant molecules such as IL-8. Blocking of IL-8 or IL-8 receptors reduces TAN infiltration and inhibits tumor growth[333–336]. Polarization of neutrophils towards immunosuppressive TANs is induced by TGFβ or IFNβ during tumor progression[337–339]. TAN immunosuppressive function, in turn, is mediated via secretion of TNFα, NO and ROS, recruitment of Tregs or direct contact with T cells via the PD-L1 immune checkpoint molecule [340,341].

4.5.4 Alterations in cell surface antigens

The last most prominent tumor immune escape mechanism prevents recognition by immune cells either by reduction of immune activation ligand expression or by direct cell-to-cell contact inhibition of immune cells via expression of inhibitory ligands. One of the mechanisms of tumor antigen downregulation is shedding of those antigens from the tumor cell surface creating a soluble version of the ligand that still binds the corresponding receptor, thus blocking immune cell activation and tumor cell recognition. Shedding is often mediated by matrix metalloproteases (MMP) or as "a disintegrin and metalloproteinase" (ADAM). A perfect example of immune evasion via ligand shedding is the well-described cleavage of NKG2D ligands by MMPs, ADAM10 and ADAM17 induced by intratumor genotoxic stress and the

TME[60,63,68,342–345]. Soluble NKG2D ligands then interfere with NKG2D-mediated anti-immune cell cytotoxicity [62,70,346–349]. The serum levels of soluble NKG2D ligands correlates with tumor progression and poor prognosis[346,350–352]. Targeting the shedding process of NKG2D ligands can increase NKG2D ligand expression and improve the anti-tumor immune response in various preclinical model systems[64–67,353]. In addition to NKG2D ligands, the cleavage of the NKp30 receptor ligands B7H6 and BAG6 has also been reported to reduce NKp30-mediated NK cell cytotoxicity[117,354.] Tumor-derived soluble CD155 was shown to be elevated in cancer patients and inhibit DNAM-1 dependent anti-tumor cytotoxicity of NK cells[355–357]. Not only activating ligands are cleaved but also inhibitory ligands can be cleaved and mediate immunosuppression. One of the examples is E-cadherin, an adhesion molecule and ligand for the inhibitory KLRG1 receptor. E-cadherin can be cleaved into a soluble version that engages T-cell-expressed KLRG1 to inhibit of T-cell activation [358,359]. Soluble versions of tumor-derived classical HLA molecules have also been observed and described to induce NK and T-cell inhibition and even T-cell apoptosis[360–363]. MHC-I molecules are not just cleaved but frequently downregulated or not expressed on tumor cell surfaces to avoid recognition by cytotoxic T cells[364,365]. Tumors initially originate from MHC-I positive cells and acquire heterogeneity in MHC-I expression with tumor progression[366]. The intratumoral diversity in MHC-I expression is caused by epigenetic modification, posttranscriptional regulation by microRNAs either preventing translation or inducing mRNA degradation, or by mutations in the HLA locus and genes regulating MHC expression [367–379]. The strong selection process toward MHC-I negativity is mediated by the ability of CD8+ T-cells to recognize and kill MHC-I-expressing tumor cells (Figure 4.13). Early tumor stage MHC-I heterogeneity is immunoedited into a homogeneous MHC-I-deficient tumor resistant to CD8+ T-cell cytotoxicity [380–382]. Without MHC-I tumor cells escape recognition by T-cells, but not NK cells. MHC-I is a crucial tolerance signal that prevents host cells from attack by NK cells. In general, MHC-I-deficientcells are efficiently killed by NK cells. However, higher NK cell infiltration of MHC-I-deficient tumors compared to tumors that retain MHC-I expression is not evident[383]. Also MHC-I deficiency itself is not sufficient to induce NK cell cytotoxicity, as tumor cell may develop other MHC-I-independent mechanisms to avoid recognition by NK cells[62,117,266,310,358,384,385]. Tumors with low classical MHC-I expression may, for instance, still express non-classical MHC-I molecules such as HLA-E and HLA-G[386,387]. Nevertheless, the crosstalk between T and NK cells with their opposite dependency on MHC-I expression is crucial for tumor elimination. NK cells are often considered as the first line of defence to deal with transformed cells before a tumor is fully established, requiring further involvement of antigen-specific T cells [388–392]. An ensuing

efficient T-cell response then also depends on initial NK cell recognition of the tumor cells and priming of T cells via DCs and tumor-specific antigens[388–392393–400]. The timing of individual immune cell responses is also a reason that MHC-I-deficient tumors develop, since NK cells may act only in the early stages of tumor progression, when the tumor still expresses MHC-I as a protection from NK cells. If the tumor loses MHC-I expression in the beginning, it is quickly eliminated by NK cells. At later stages of tumor progression as mutations accumulate that create neoantigens, tumor elimination is predominantly controlled by T cells and the loss of MHC-I becomes advantageous to the tumor[389,399].

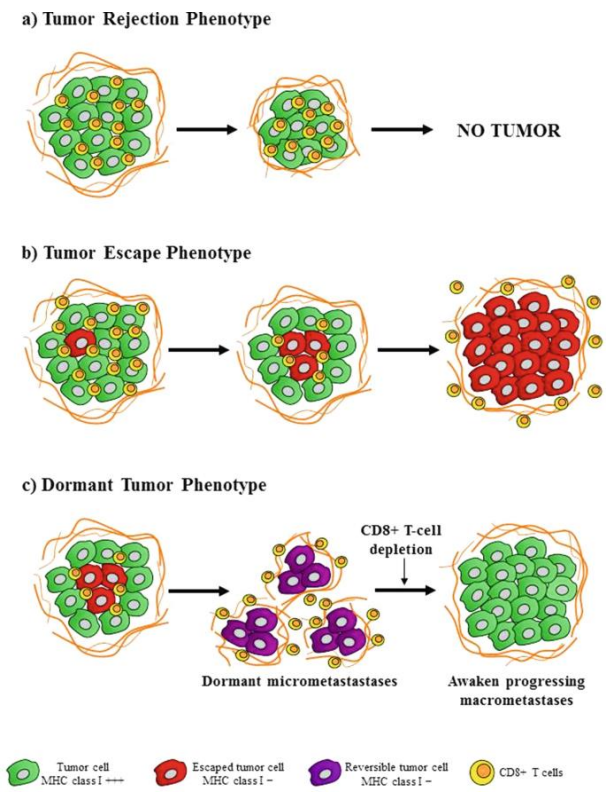

Figure 4.13. Schematic representation of the progression of different tumor phenotypes. **A)** Tumor rejection - tumor cells without heterogeneity in MHC-I and are all eliminated by TILs. Tumor rejection occurs with no clinical evidence in majority of the cases. **B)** Tumor escape - appearance of MHC-I heterogeneous cells within tumor. $CD8^+$ TILs eliminate $MHC\text{-}I^+$ cells, while $MHC\text{-}I^-$ cells (red) escape the recognition by $CD8^+$ T-cell and continue to proliferate. **C)** Tumor dormacy - $MHC\text{-}I^-$ cells form an unnoticed micrometastases maintained in an immuno-logical equilibrium. Dormant cells survive for long periods of time and progress by the depletion $CD8^+$ T cell. Newly formed macrometastases regain $MHC\text{-}I$[401]. Adapted from Garrido, 2019[365].

4.5.5 Immune checkpoints

Loss of MHC-I also negatively affects the efficacy of ICB that depends on unleashing the cytotoxicity of T-cells[402–406] . Alterations in MHC-I or activation ligand expression are not the only immune escape mechanisms mediated by changes in cell surface. Tumor cells may also escape immune surveillance by expressing ligands that interfere with immune cell activation or by impairing their co-stimulation. These inhibitory axes are classified as immune checkpoints and are the main interest for the development of therapeutic antibodies used for immune checkpoint blockade (ICB), which restores the function of immune cells. The concept of immune therapy, where the use of modified cells from the tumor is a promising approach for

cancer immunotherapy, was first discussed in 1975 by James Allison and colleagues[407]. 20 years later a new era of cancer immunotherapy started by discovering the first immune checkpoint molecule, the cytotoxic T lymphocyte antigen (CTLA4) [408]. CTLA-4 is a high-affinity homolog of CD28, yet with an opposite function that dampens T-cell antitumor immunity[409]. CTLA-4 is upregulated on T cells upon activation and competes with the co-stimulatory receptor CD28 for B7 family ligands such as CD80 and CD86 that are expressed by APCs but also tumor cells[409–411]. In 2011, the first successful ICB therapy for advanced melanoma cancer was approved by using ipilimumab, an anti-CTLA4 antibody (Figure 4.14, 4.15). Ipilimumab therapy improved antitumor response and prolonged patient survival across multiple cancer types [412–417]. The second most well-known immune checkpoint target is Programmed cell death protein 1 (PD-1). PD-1 is an inhibitory cell surface receptor that is upregulated on T cells upon activation discovered in 1992 by Tasuku Honjo [418,419]. PD-1 interacts with PD-L1 and PD-L2, which also belong to B7 family, and transmits an inhibitory signal downregulating T cell activity[420,421]. PD-L1 and PD-L2 are often expressed on tumor cells and suppress antitumor immune cell responses[421,422]. PD-1 expression is higher on exhausted and tumor infiltrating T and NK cells resulting in weaker anti-tumor reactivity[423–428]. The discovery of this PD-1 inhibitory axis led to the development of nivolumab, an anti-PD-1 antibody, approved in 2014 for a clinical use. Pembrolizumab, humanized anti-PD-1 antibody, and atezolizumab, an anti-PD-L1 antibody, have been approved in 2014 and 2016, respectively (Figure 4.14, 4.15). Nivolumab, pembrolizumab and atezolizumab are currently used as a standard treatment of multiple cancer types and dramatically improved patient survival [429–438]. Combined blockade of CTLA-4 and PD-1/PD-L1 axis significantly improved immune responses and overall patient survival in various cancers and are currently the best examples of ICB therapy [413,439–444]. In 2018, James Allison and Tasuku Honjo were awarded with a Nobel Prize in Physiology or Medicine for "the discovery of cancer therapy by inhibition of negative immune regulation"[445]. Even though, ICB shows remarkable successes, a subset of cancer patients fail to respond or acquire resistance to this therapy. Thus, it is crucial to continue to identify novel immune checkpoint pathways that can improve efficacy of a current treatment and increase patient survival. The most recent new ICB is relatlimab, an anti-LAG-3 antibody, which was approved in 2022 for an advanced melanoma treatment in combination with nivolumab [258,446,447]. More inhibitory ligands such as TIM-3 or TIGIT are now targeted in clinical trials and showing preliminary signs of increased anti-tumor activity with the potential to be an additional class of ICB [448–450].

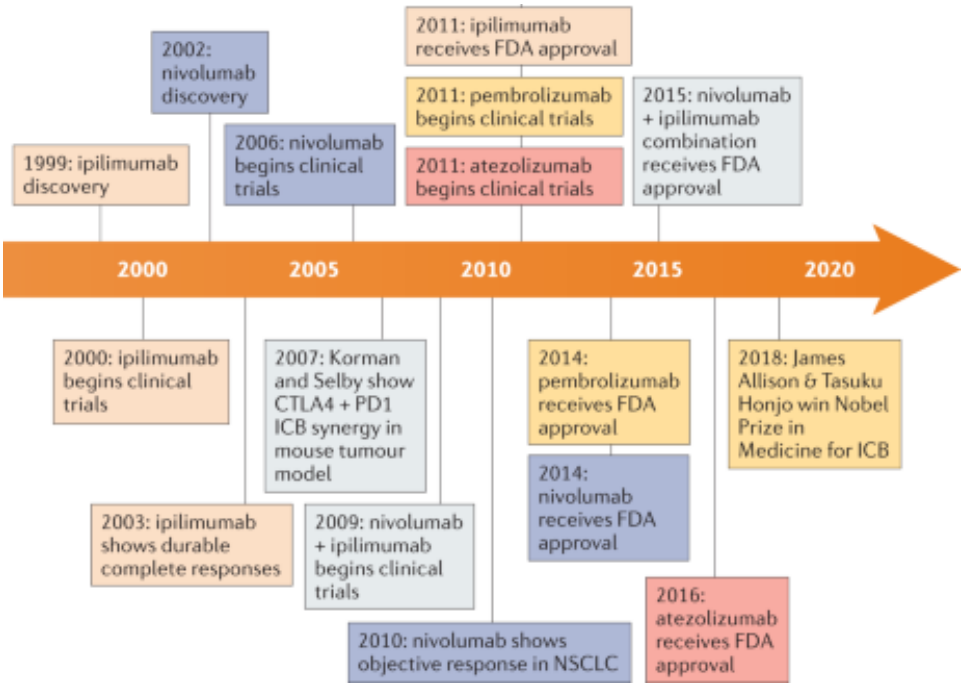

Figure 4.14 Key milestones of ICB.

The discovery and development of the first FDA-approved ICB drugs - ipilimumab, nivolumab, pembrolizumab and atezolizumab. Adapted and modified from Korman et.al 2022 [439].

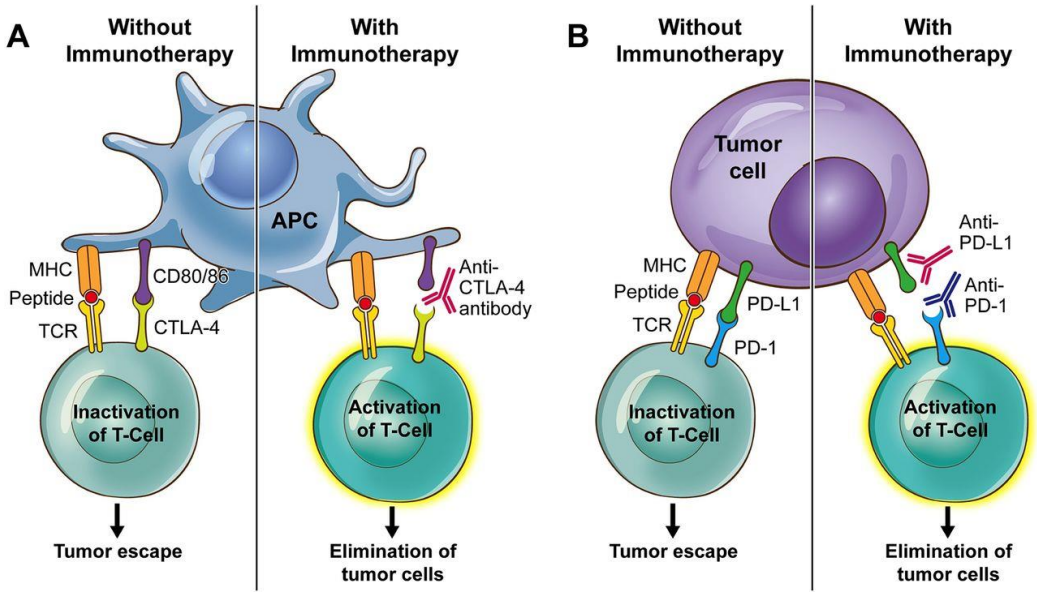

Figure 4.15 Scheme of CTLA-4 and PD-1/PD-L1 blockade.

A) T-cell activation via interaction of MHC with TCR abolished by CD80 and CD86 interaction with CTLA-4 instead of costimulatory CD28 receptor on the T cells. Anti-CTLA-4 blockade abolishes interaction with CD80 and CD86, favouring CD28 engagement and T-cell activation. **B)** PD-1 expressed on T cells interacts with PD-L1 resulting in T cell inactivation. Blockade of PD-1 and PD-L1 interaction result in T cell activation. Adapted from Soularue et al., 2018[451].

4.6 Skin cancer

Skin is divided into the epidermis, dermis, and subcutaneous fat (Figure 4.16). The basal layer, the deepest layer of epidermis, consists of keratinocytes, which proliferate into a more superficial layer while losing their nuclei and becoming fully keratinized cells forming a top mechanical layer, the stratum corneum. Melanocytes reside in the basal layer and produce ultraviolet (UV) radiation protective pigment melanin. Both of these cell types can develop into skin cancer. Skin cancer is the most commonly diagnosed type of cancer. It is divided into two groups: melanoma and non-melanoma skin cancer (NMSC)[452].

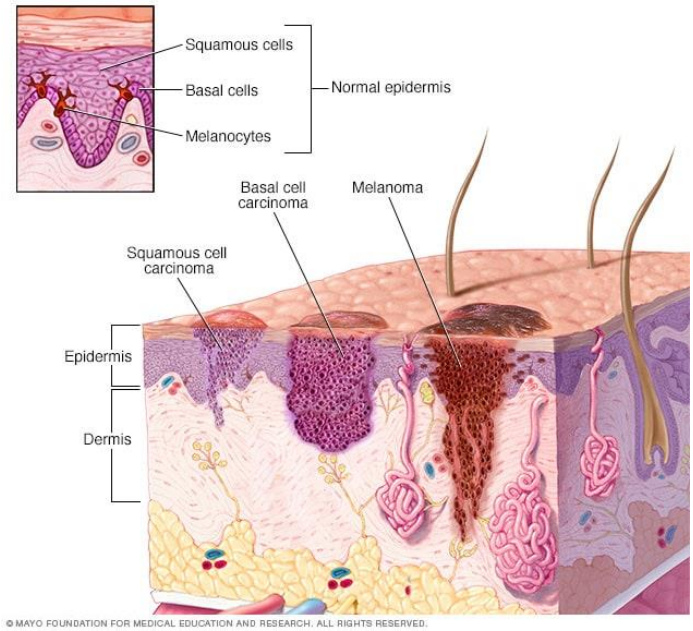

Figure 4.16 Anatomy of skin and different types of skin cancer.
Skin cancer originates from keratinocytes (basal and squamous) and melanocytes present in the epidermis. BCC develop from basal cells that continuously grow and push older cells upwards. Ascending cells become flattened squamous cells, where SCC occurs. Melanoma develops from pigment cells (melanocytes) in the basal layer. Adapted from MayoClinic[453].

4.6.1 Non-melanoma skin cancer

NMSC originates from keratinocytes and includes basal cell carcinoma (BCC) and squamous cell carcinoma (SCC). In comparison to other types of cancer, NMSC are the most common type of cancer in humans. However, the exact incidence is not known, since the cases are not required to be reported to cancer registries and are therefore excluded from cancer statistics. The estimated incidence increases each year, which can be either attributed to improved registration or higher sun/UV exposure, which is the main risk factor [454]. BCC is approximately 80% of NMSC and originates from keratinocytes in the basal layer[452]. The majority of BCC occurs in head and neck, where the sun exposure is the highest[455]. For patients, BCC is often difficult to distinguish from benign growths. BCC rarely forms metastases, but

the lesions can be highly destructive, with others presenting as non-aggressive and often left unnoticed[456]. Approximately 16 % of skin cancer cases are SCC and as in BCC the main risk factor is UV exposure. Compared to BCC, SCC presents as a malignant tumor that invades the dermis and can spread into metastases in advanced stages (Figure 4.16). The main therapy is surgical removal for BCC and primary SCC lesion with excellent overall prognosis[452].

4.6.2 Melanoma

The incidence of melanoma accounts only for about 1% of all skin cancer cases, yet the majority of skin cancer deaths is attributed to melanoma. Compared to BCC and SCC, melanoma can be highly aggressive due to its invasiveness in the dermis and metastases formation (Figure 16) [457]. The main risk factor is UV radiation from the sun causing about 86 % of melanomas[458]. Having more than five sunburns is on average associated with double the risk of developing melanoma, while having just one blistering sunburn in childhood or adolescence is associated with more than double the risk[459,460]. Overall, one in 28 white men and one in 41 white women will develop melanoma in their lifetime[457]. The number of new melanoma cases diagnosed annually increased by 27 % in the past decade. In contrast to incidence, the mortality of melanoma patients declined rapidly over the past decade, mainly because of the advances in treatment[457]. The success in melanoma treatment highly depends on the stage of melanoma progression. The earliest form of melanoma is stage 0 (melanoma in situ) which then progresses into stages I up to stage 4. In stage 0-2, the tumor is localized within the epidermis and has not metastasized to neighbouring lymph nodes or distant organs. The differences between stage 0, 1 and 2 is determined by the thickness (up to 4 mm) and ulceration. The surgical removal of localized melanoma has a 5-year survival rate around 99%. Stage 3 of melanoma is further categorized into substages 3A, 3B, 3C, or 3D depending on the size, depth, ulceration and lymph node infiltration. Stage 3 melanoma has usually spread to 1 to 3 adjacent lymph nodes, where metastases remain microscopically small, and has not spread into distant organs. Stage 4 tumor can have any thickness and have spread to nearby lymph nodes, distant lymph nodes and organs such as the lungs, liver or brain. The survival rate drops dramatically in stage 3 to 71% and in stage 4 to 32%. The overall 5-year relative survival rate for all stages of melanoma is 94%. However, immunotherapy and targeted therapy of melanoma significantly improved and the survival rates only start to reflect this revolution[457,461].

4.6.3 Role of NK cells in melanoma

The relationship between NK cells and melanoma cells were studied as far as in the 1970s[462,463]. Years later the importance of NK cells in melanoma was shown in in vivo experiments by depletion of mouse NK. Early-infiltrating NK cells play a significant role in the initial recognition and anti-tumor response. The depletion of NK cells markedly increased the melanoma cells localization and growth. Moreover, in the absence of NK cells CD8+ tumour-specific CTL did not develop[27,464]. Tumor cells killed by NK cells are usually engulfed by DCs, which present tumor peptides on MHC molecules and stimulate the generation of tumor ag-specific T cells[465]. NK cells are one of the main producers of IFNγ, which is also an important cytokine in the anti-tumor response. IFNγ induces the expression of MHC, which is crucial for T-cell mediated recognition and tumor elimination[1,35]. It was shown that IFN-γ-insensitive mice developed tumors more rapidly than wild-type mice and that certain tumors may lose IFN-γ sensitivity as a mechanism to evade immune detection[29]. The loss of IFN-*γ* pathway genes in tumor cells is also a mechanism of resistance to ICB therapy[466]. Melanoma cells express a broad range of NK ligands that together control melanoma cell killing[467]. High ICAM-1 expression mediates melanoma recognition and killing by NK cells, while simultaneously contributing to metastasis formation as an adhesion molecule[150,468,469]. The majority of melanomas express ligands for DNAM-1, which also play an important role in their elimination[128,470,471]. Melanoma cell lines also frequently express ligands for the NK-activating receptor NKG2D that can also be shed to avoid killing by NK cells as a tumor escape mechanism [64,72,471]. Another ligand shed from melanoma and detected in melanoma patient serum is B7H6, a ligand for the activating NKp30 receptor[117,470,472]. Not only activating ligands but also inhibitory ones are frequently expressed by melanoma. Melanoma cells display high sialylation that help facilitate adhesion and tumor metastasis formation[473,474]. Sialic acid residues are ligands for inhibitory Siglec receptors that mediate immunosuppression and blocking of interaction with Siglec receptors can restore immune function[230,250,475]. MHC-I is also one of the major inhibitory molecules present on melanoma. Melanomas differ in HLA variability and expression. The expression of MHC-I by melanoma prevents immune recognition by NK cells due to inhibitory signalling via KIRs, NKG2A or LIRBs[74,363,476,477] (discussed in Tumor escape mechanism chapter). Irrespective of the expression of activating ligands, melanomas frequently become resistant to NK cells, suggesting additional mechanisms to be at play. Even in in vitro settings, melanoma cells acquire resistance to NK-cell-mediated killing when exposed to NK cell numbers that reflects NK cell infiltration in the tumor [478]. In support of inhibitory effects originating from

the melanoma cells, NK cells found in melanoma appear to have decreased expression of activating receptors and effector molecules[479]. On the other hand, higher NK cell numbers in patients with melanoma were found to correlate with higher overall survival and patient responsiveness to immunotherapy[480], suggesting that NK cells can have key contributions to an effective immune response.

4.6.4 Melanoma therapy

The treatment of melanoma depends on the stage and location of the tumor. Stage 0-1 is usually treated by surgical removal of the melanoma with a margin of surrounding tissue. In the majority of cases, additional treatment is unnecessary. Stage 2 is also treated by wide excision and a potential sentinel lymph node biopsy to determine if the melanoma has spread into nearby lymph nodes. If melanoma is detected in the sentinel node (stage 3), the lymph nodes in the area are dissected and adjuvant treatment with immune checkpoint inhibitors, targeted drug therapy or radiotherapy is started to lower the chance of melanoma progression. In addition to standard treatment options, other therapeutic approaches such as novel drugs or potential vaccine treatments may be considered in the context of a clinical trial. Stage 4 melanomas have already metastasized to distant lymph nodes or other organs and require more comprehensive treatment. Primary tumor, lymph nodes and metastases that cause symptoms can be surgically removed or treated with radiation therapy. Radiation, immunotherapy, targeted therapy, or chemotherapy are the current options for advanced melanoma treatment. The first drugs administered are typically ICB[481]. ICB biologicals used for melanoma treatment are pembrolizumab, nivolumab or ipilimumab and combinations such as nivolumab + relatlimab (anti-LAG-3), nivolumab + ipilimumab and pembrolizumab + ipilimumab[413,436,442,444,447,482–484]. Combined ICB dramatically increases progression-free survival of patients with untreated metastatic or unresectable melanoma compared to a single ICB agent that also individually have a substantial positive impact on patient survival. Melanoma is one of the most mutated cancers due to chronic UV exposure. The mutations in melanoma are both “driver” and “passenger” genes that present an opportunity for targeted therapy. Approximately 50% of invasive melanoma harbour *BRAF* V600 mutations as a driver for their malignancy. Treatment with the BRAF kinase inhibitor Vemurafenib improves overall and progression-free survival rates in patients with the BRAF V600E melanoma mutation[485]. NRAS is the second most frequently mutated (20%) gene in melanoma, which currently lacks specific therapy options and can be targeted by multiple MEK kinase inhibitors with 15-30%

efficiency of improved survival[486–489]. The gene encoding receptor tyrosine kinase C-KIT is another gene frequently mutated in melanoma that enables targeted therapy by multiple inhibitors showing improved overall survival [490–492]. Such personalized chemotherapy drugs are usually the last option for advanced melanoma treatment. While most of these targeted small-molecule inhibitors of mutated driver pathways reduce tumor growth, the cancer usually relapses within several months[493]. Over the past years, chimeric antigen receptor (CAR) T cell therapy has emerged as a promising and efficient cancer treatment option which is not restricted to HLA. Initial success in treatment of hematologic malignancies has promoted examining its application against solid tumors and hopefully will lead to novel melanoma treatment options improving patients survival[494–498].

Despite the natural anti-tumor immune response against melanoma as well as existing therapies, resistant melanoma clones typically arise and overall survival of disseminated melanoma remains low. Thus, finding novel therapeutic approaches that improve immune reactions and tumor control are needed. CRISPR-Cas9 technology enables large-scale studies to assess the role of individual genes on tumor progression and immune sensitivity and could yield multiple novel treatment options that can expand the repertoire of available therapy options for melanoma patients.

4.7 Gene silencing and editing

Initially, the study of individual gene function depended on naturally occurring or induced mutations and observing a phenotypic changes. Later, direct manipulation of DNA gene sequence by random mutagenesis, homologous recombination or chemical mutagens were used to study gene effects. Introduction of exogenous gene sequences causing gene overexpression complemented these gene manipulation approaches to study the effect of individual genes on particular biological functions. In the past two decades, gene studies have commonly been conducted using gene silencing via RNA-specific degradation or by direct disruption of gene sequences using RNA-guided bacterial Cas9 endonucleases.

4.7.1 RNA interference

RNA interference (RNAi) is a process of gene silencing by introduction of small RNAs that sequence-specifically bind a mRNA and either target that mRNA for degradation or block its translation into protein. RNAi was initially discovered by observations in *Caenorhabditis elegans,* where introduction of double-stranded RNA (dsRNA) caused a reduction of target

protein expression[499]. These observations were further engineered into short interfering RNAs (siRNA) or short hairpin RNAs (shRNA) that specifically bind gene transcripts and target it for degradation or retention, causing reduction of protein levels[500–505]. ShRNA relies on the enzyme Dicer that cleaves long dsRNA into 21–23 bp siRNA, which is then utilized by RNA-induced silencing complex (RISC) to guide its sequence-specific cleavage of the mRNA (Figure 4.17). As an alternative to dsRNA, direct transfection of synthesized siRNA into cells can be used for gene silencing, producing a so-called gene knockdown[506]. Libraries combining multiple siRNAs that target nearly all known genes in the human genome were used to perform the first large-scale Genome-wide (GW) screens [507]. Genome-wide screens were subsequently used as powerful tools to study various biological functions, critical genes in diseases, receptor ligands, signalling pathways, cancer vulnerabilities to drugs or immune cells and many others [508–515].

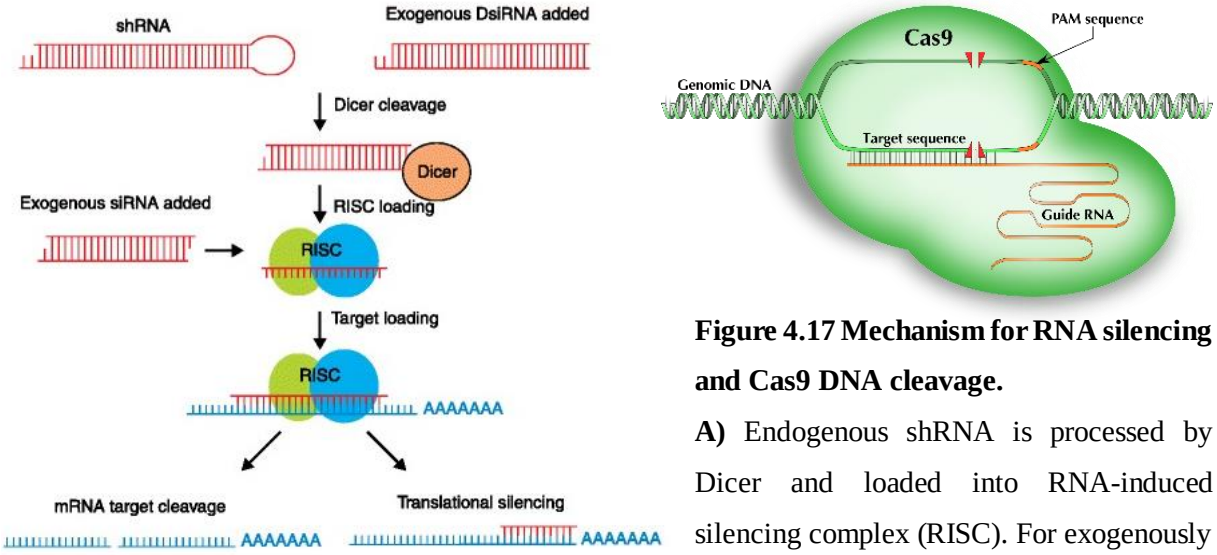

Figure 4.17 Mechanism for RNA silencing and Cas9 DNA cleavage.

A) Endogenous shRNA is processed by Dicer and loaded into RNA-induced silencing complex (RISC). For exogenously delivered siRNA, the passenger strand is removed from the guide RNA and RISC/guideRNA complex bind to its complementary mRNA target and targets the mRNA for degradation. **B)** Cas9 protein complexes with a sgRNA, binds to a complementary DNA that contains a Protospacer Adjacent Motif (PAM) sequence after the target sequence and cleaves the DNA. Adapted and modified from Bobbin et al., 2015 and Origene[516,517].

4.7.2 CRISPR/Cas9

The evolution of the CRISPR (Clustered Regularly Interspaced Short Palindromic Repeats)/Cas9 system as a tool for gene disruption started with the discovery that homologous DNA sequence repetitions separated by a few nucleotide spacer sequences were found in bacteria and archaea genomes[518,519]. Cas proteins were later found to associate with these

CRISPR sequences[520]. The CRISPR/Cas system functions as a type of prokaryotic adaptive defence mechanism based on endogenous small RNA that drives the cleavage of viral DNA. Subsequently, the CRISPR/Cas9 system was exploited as a gene editing tool for eukaryotic cells. The Cas9 protein forms a ribonucleoprotein (RNP) with a 20-bp single guide RNA (sgRNA) that is designed to bind the DNA sequence of gene of interest (Figure 4.17). Cas9/sgRNA RNP specifically cleaves the target genomic DNA and non-conservative repair introduces frameshift insertions/deletions that may result in disrupted gene transcription[521]. The CRISPR/Cas9 system outperforms RNAi screens due to the generation of complete genetic gene knockouts (KO) and abolishing gene expression compared to siRNA that often only reduce mRNA/protein levels[522]. Similar to siRNA, a library of multiple sgRNA are commonly used to perform GW CRISPR/Cas9 KO screens[523]. A potential disadvantage of the CRISPR/Cas9 KO is that targeting of essential genes does not produce viable mutants that can be further studied. Moreover, genes that are not expressed in the cells cannot be studied. To overcome these problems, a modified version of Cas9 (dCas9-VP64) that lacks endonuclease function but contains a transcriptional activator domain was developed. This Cas9 version enables targeted gene activation and induced expression[524]. GW CRISPR/Cas9 activation screens possess the power to identify effects of genes that are normally expressed at low levels or restricted to certain cell types or specific stimulations[524,525]. CRISPR/Cas9 screens are commonly used to generate comprehensive analyses of immune evasion mechanisms, for new ligand/drug discovery or to identify key molecules in the regulation of various biological pathways [241,523,526–533].

Such genome-wide screens in tumor co-cultures with immune cells can not only confirm the role of known molecules, but also indentify new candidates that have potential to be drug-targeted to curb tumor growth itself or unleash immune cell reactivity.

5 AIMS OF THE STUDY

Despite constituting the rarest type of skin cancer, melanoma accounts for the majority of skin cancer mortalities. Melanoma is known for its aggressive nature and metastatic potential if not detected and treated early. In recent years, immune checkpoint blockade has emerged as a novel treatment option for advanced melanoma, showing remarkable success in many melanoma patients. Unfortunately, a subset of patients experiences only limited benefits or does not respond to current treatment options.

NK cells are often referred to as the first tumor responders. Moreover, the recognition of early-stage tumors by NK cells directly influences subsequent steps of adaptive immune cell activation and elimination of tumor cells that escaped the initial NK cell encounter. Improvement of NK cell cytotoxicity towards tumor in an early stage in combination with current ICB could greatly improve patient survival.

In this project, I use a CRISPR/Cas9-based library screen in order to identify key resistance mechanisms protecting melanoma cells from NK cell cytotoxicity.

I address the following aims:

- Establish and optimize a GW CRISPR/Cas9 KO screen co-culture system of NK and melanoma cells.
- Examine known and novel candidate genes that reduce alters the resistance of melanoma cell to NK cell cytotoxicity.

The relative contribution of candidate genes and new molecules discovered in our project will be highly relevant for the development of novel immunotherapeutic strategies based on innate immune recognition of melanoma cells or other solid tumors.

6 MATERIALS AND METHODS

6.1 Materials

6.1.1 Laboratory Equipment

Product	Company
Analytical scale ME2002	Mettler Toledo
Azure c200 Gel Documentation Platform	Azure Biosystems
Bioruptor Plus Sonicator	Diagenode
Blue Light LED Illuminator BLstar 16	Biometra
Cell culture incubator NU-5820E	Ibs Tecnomara
Cell culture incubator NU-5841E	Ibs Tecnomara
Centrifuge Heraeus Multifuge X3R	Thermo Scientific
Centrifuge Heraeus Presco 17	Thermo Scientific
Centrifuge Heraeus Pico 17	Thermo Scientific
Counting Chamber (Neubauer)	Glaswarenfabrik, Karl Hecht GmbH & CoKG
Duomax 1030	Heidolph
FACSAria Fusion cell sorter	BD Bioscience
Flow Cytometer, FACS Calibur	BD Bioscience
Flow Cytometer, LSRFortessa	BD Bioscience
Flow Hood NU-543-400E	Ibs Tecnomara
Flow Hood NU-S481-400E	Ibs Tecnomara
Freezer -20°C Mediline	Liebherr
Freezer -80°C U410	New Brunswick
Fridge Mediline	Liebherr
Ice Maschine AF100	Scotsman
Incubation-shaking cabinet CERTOMAT	Sartorius
Vacusafe aspiration system	Integra Biosciences
Microcentrifuge MiniStar	VWR
Microscope Primovert	Zeiss
Minicentrifuge SU1550	SunLab

N2 tank Biosafe 220	Biosafe
QuantStudio 5 Real-Time PCR System	ThermoFischer Scientific
Qubit 5	Invitrogen
Sub-Cell GT Electrophoresis	Bio-Rad
Spark Multimode Microplate Reader	Tecan
Thermal Cycler C1000 Touch	Bio-Rad
Thermo Shaker Incubator TS Basic	Cell Media
Trans-Blot Turbo Transfer System	Bio-Rad
Vortex D-6012	neoLab
Vortex SU1900	SunLab
Water Bath 1083	Thermolab, GFL

Table 6.1: Laboratory equipment used for experiments.

6.1.2 Cells

Cell name	Type of cell line	Medium	Source
A375	Human melanoma	RPMI	Prof. Michael Boutros
A421	Human epidermoid carcinoma	RPMI	Dr. Michaela Arndt
HEK293T	Human epithelial kidney	DMEM	Prof. Carsten Watzl
HeLa	Human cervical carcinoma	RPMI	Dr. Gerd Moldenhauer
HepG2	Human hepatocellular carcinoma	DMEM	Prof. Thomas Hofmann
MaMel-86b	Human melanoma	RPMI	Prof. Stefan Eichmüller
MCF7	Human breast cancer	DMEM	ATCC
K562	Human chronic myeloid leukemia	RPMI	Prof. Carsten Watzl
SKMel-28	Human melanoma	RPMI	ATCC
SKMel-37	Human melanoma	DMEM	Prof. Helga Bernhard
UKRV-Mel02	Human melanoma	RPMI	Prof. Stefan Eichmüller
NK	Primary NK cells from healthy donors	MACS/ SCGM	Blutspende - DRK-KV Mannheim

Table 6.2: Cell lines used in experiments.

6.1.3 Cell culture consumables

Product	Company	Catalogue

6-well CellStar Suspension culture plate	Greiner	657185
6-well Tissue culture plate	Sarstedt	83.3920.005
12-well Tissue culture plate	Sarstedt	83.3921.300
12-well Suspension culture plate	Sarstedt	83.3922.500
24-well Tissue culture plate	TPP	92024
48-well Tissue culture plate	Sarstedt	83.3923.300
96-well microplate, flat-bottom	TPP	92096
96-well microplate, round-bottom	Sarstedt, TPP	83.3926, 92097
Amicon™ 15ml Ultra Centrifugal Filter Units 100kDa	Merck	UFC910008
CellStar Falcon tubes (15 ml, 50 ml)	Greiner	188271N, 227261,
Culture flask T25	Sarstedt	83.3910.302
Culture flask T75	Sarstedt	83.391.002
Culture flask T175	Sarstedt	83.3912.002
Culture flask T225 CytoOne	Starlab	CC7682-4225
MACS LS columns	Miltenyi	130-042-401
Serological pipets (5 ml)	Sarstedt	86.1253.001
Serological pipets (10 ml)	Sarstedt	86.1254.001
Serological pipets (25 ml)	Thermo Scientific	170357
Pipette filter tips (10 µl)	BioZym, Sarstedt	770005, 701130.215
Pipette filter tips (20 µl) SafeSeal	BioZym	770050
Pipette filter tips (200 µl) SafeSeal SurPhob	BioZym	VT0240
Pipette tips (200 µl)	Sarstedt	70.3031
Pipette filter tips (1000 µl)	Sarstedt	70.3050
Reservoirs 50mL	VWR	89094-676

Table 6.3: Cell culture consumables used in experiments.

6.1.4 Cell culture reagents and kits

Reagent product	Company	Catalogue
Biocoll seperating solution	Biochrom, Berlin, Germany	L6115
Cell Dissociation Solution Non-enzymatic (1x)	Sigma-Aldrich	C5914

CellGenix® GMP SCGM	Cell Genix	20802-0500
Dimethylsulphoxide Hybri Max® (DMSO)	Sigma-Aldrich	D2650
Dulbecco's Modeified Eagle's Medium (DMEM	Sigma-Aldrich	D6459
Dulbecco's phosphate buffered saline	Gibco	1490144
Fetal calf serum	Sigma	F7524
Gibco™ RPMI 1640 Medium	Fisher Scientific	11530586
Gibco™ Opti-MEM™ I Reduced Serum Medium	Fisher Scientific	11524456
Human Serum, sterile filtered	PAN Biotech	P30-2401
L-Glutamine 200 mM (100x), 29.2 mg/mL	GIBCO-Invitrogen	25030
NK MACS® Medium	Miltenyi	130-114-429
Pancoll human	PAN-Biotech	P04-60500
Penicillin/Streptomycin-Solution 10000 U/mL penicillin, 10000 µg/mL streptomycin	GIBCO-Invitrogen	15140
Trypan Blue	Thermo Fisher	15250-061
Trypsin-EDTA (1x)	GIBCO-Invitrogen	25300
Kit product	Company	Catalogue
Annexin V FITC Apoptosis Detection Kit with PI	Biolegend	640914
anti-Biotin MicroBeads	Miltenyi	130-090-485
Blood & Cell Culture DNA Maxi Kit (10)	QIAGEN	13362
CytoTox-Glo™ Cytotoxicity Assay	Promega	G9292
DNA Clean & Concentrator-100	Zymoresearch	D4030
eBioscienceTM FoxP3 transcription factor staining buffer set	eBioscience	00-5523-00
Genomic DNA Buffer Set + QIAGEN Genomic-tip 500/G	QIAGEN	19060, 10262
jetOptimus	Polyplus	117-07
Lipofectamine™ 2000	Invitrogen	11668019
Mirus Bio™ TransIT™ Lentivirus System	Mirusbio	MIR6655
NEBNext® Ultra™ II Q5® Master Mix	NEB	M0544S
NextSeq 500/550 High Output Kit v2.5	Illumina	20024906

(75 Cycles)		
NK cell isolation kit	Miltenyi	130-092-657
Plus reagent	Invitrogen	11514015
PureLink™ HiPure Plasmid Filter Maxiprep Kit	Invitrogen	K210016
Trans-Blot Turbo Midi 0.2 µm PVDF Transfer Packs	BioRad	1704157
Trans-Blot Turbo Midi 0.2 µm Nitrocellulose Transfer Packs	BioRad	1704159
QIAprep Spin Miniprep Kit	QIAGEN	27104
QIAquick Gel Extraction Kit	QIAGEN	28704
Qubit™ dsDNA BR- Assay-Kit	Invitrogen™	Q32850
Qubit™ dsDNA HS- Assay-Kit	Invitrogen	Q32851
Qubit™ Protein and Protein Broad Range (BR) Assay Kits	Invitrogen™	Q33212
WesternBright Chemilumineszenz Substrat Sirius	Advansta	541021

Table 6.4: Cell culture reagents and kits used in experiments.

6.1.5 Antibodies for flow cytometry

Target	Flourophore	Clone	Isotype	Company
AHR	PE	FF3399	Mouse IgG2b	Invitrogen
B7-H3	PE	DCN.70	Mouse IgG1	Biolegend
B7-H6	PE	875001	Mouse IgG1	R&D Systems
B7-H6	PE	5.51.18	Mouse IgG1	D080 / G. Moldenhauer
CD1a	APC	SK9	Mouse IgG2b	BioLegend
CD1b	SN13	SN13	Mouse IgG1	BioLegend
CD1c	APC	L161	Mouse IgG1	BioLegend
CD1d	PE	51.1	Mouse IgG2b	BioLegend
CD107a	FITC, BV785	H4A3	Mouse IgG1	BioLegend
CD112	APC	TX31	Mouse IgG1	Biolegend
CD155	APC, PE	SKII.4	Mouse IgG1	BioLegend
CD16	APC, FITC, PE	3G8	Mouse IgG1	BioLegend

CD160	PE-Cy7	By55	Mouse IgM	BioLegend
CD25	APC, FITC	BC96	Mouse IgG1	Biolegend
CD3	BV510, FITC	OKT3	Mouse IgG2a	Biolegend
CD45	APC, PE, FITC, PE-Cy7, APC Cy7, Pacific Blue, BV421, BV605	HI30	Mouse IgG1	BioLegend
CD56	APC, PE, BV785, PE-Cy7, BV605	HCD56	Mouse IgG1	BioLegend
CD57	Pacific Blue	HCD57	Mouse IgM	BioLegend
CD69	APC, BV421,	FN50	Mouse IgG1	BioLegend
DNAM-1	PE-Cy7	11A8	Mouse IgG1	BioLegend
DNAM-1	PE, FITC	TX25	Mouse IgG1	BioLegend
EGFR	APC	AY13	Mouse IgG1	BioLegend
Fc	APC	HP6017	Mouse IgG1	Biolegend
Fc	biotin	M1310G05	Rat IgG2a	Biolegend
FasL	BV421	NOK-1	Mouse IgG1	Biolegend
Galectin-3	APC	M3/38	Rat IgG2a	BioLegend
Galectin-9	PE	9M1-3	Mouse IgG1	Biolegend
HLA-A,B,C	APC, FITC	W6/32	Mouse IgG2a	Biolegend
HLA-A1	pure	MAb90	Mouse IgG1	Antibodies-online
HLA-A2	APC	BB7.2	Mouse IgG2b	Biolegend
HLA-Bw4	APC	REA274	rhIgG1	Miltenyi
HLA-C	biotin	DT9	Mouse IgG2b	Biolegend
HLA-DR	APC, BV605	L243	Mouse IgG2a	Biolegend
HLA-E	APC, PE	3D12	Mouse IgG1	Biolegend
HLA-F	PE	3D11	Mouse IgG1	Biolegend
HLA-G	PE	87G	Mouse IgG2a	Biolegend
ICAM-1	APC, PE	HCD54	Mouse IgG1	Biolegend
IFNγ	APC, PE	4S.B3	Mouse IgG1	Biolegend
IFNγ	APC, PE	B27	Mouse IgG1	Biolegend

ILT2	APC	GHI/75	Mouse IgG2b	BioLegend
ILT4	APC	42D1	rat IgG2a	BioLegend
KIR2DL1	FITC	HP-MA4	Mouse IgG2b	BioLegend
KIR2DL2/L3	FITC	DX27	Mouse IgG2a	BioLegend
KIR2DL4	PE	mAb 33	Mouse IgG1	BioLegend
KIR2DL5	PE	UP-R1	Mouse IgG1	Biolegend
KIR3DL1	PE	DX9	Mouse IgG1	Biolegend
KIR3DL2	PE	539304	Mouse IgG1	R&D Systems
KIR3DL2	PE	1136B	Mouse IgG1	R&D Systems
KLRG1	PE/C7	SA231A2	Mouse IgG2a,k	Biolegend
LAG-3	APC	7H2C65	Mouse IgG1	BioLegend
LAG-3	FITC	11C3C65	Mouse IgG1	BioLegend
LSECtin	APC	845404	Mouse IgG2a	R&D Systems
MICA	pure	AMO-1	Mouse IgG1	Acris Antibodies
MIC-A/B	PE	6D4	Mouse IgG2a	BioLegend
MICB	pure	BMO-1	Mouse IgG1	Acris Antibodies
NKG2A	APC, PE, biotin	REA110	rh IgG1	Miltenyi
NKG2C	APC	REA205	rh IgG1	Miltenyi
NKG2D	APC	1D11	Mouse IgG1	Biolegend
NKp30	APC, PE,	P30-15	Mouse IgG1	BioLegend
NKp44	APC, PE	P44-8	Mouse IgG1	Biolegend
NKp46	APC	9E2	Mouse IgG1	BD
NKp80	APC	5D12	Mouse IgG1	BioLegend
OX40	PE	ACT35	Mouse IgG1	Biolegend
PD-1	APC, FITC	MIH43	Mouse IgG1	ebioscience
PD-L1	PE, BV421	MIH1	Mouse IgG1	BD
PD-L2	PE	MIH18	Mouse IgG1	BioLegend
Siglec7	pure	6-434	Mouse IgG1	Biolegend
Siglec9	PE	K8	Mouse IgG1	Biolegend
TIGIT	APC, FITC	MBSA43	Mouse IgG1	eBioscience
TNFa	PE, PE-Cy7	Mab11	Mouse IgG1	BD
TRAIL	PE	RIK-2	Mouse IgG1	Biolegend
TRAIL-R1	APC	DJR1	Mouse IgG1	Biolegend

TRAIL-R1	PE	69036	Mouse IgG1	R&D Systems
TRAIL-R2	APC	DJR2-4	Mouse IgG1	Biolegend
TRAIL-R2	PE	71908	Mouse IgG2b	R&D Systems
mIgM isotype	PE-Cy7,PE	MM-30	Mouse IgGM	Biolegend
mIgG2a isotype	all	MOPC-173	Mouse IgG1	Biolegend
mIgG2b isotype	all	MG2b-57	Mouse IgG2b	Biolegend
mIgG1 isotype	all	MOPC-21	Mouse IgG1	Biolegend
rIgG2a isotype	all	MRG2a-83	Rat IgG2a	Biolegend

Table 6.5: Primary antibodies used for flow cytometry.

6.1.6 Secondary antibodies

Secondary antibody	Flourophore	Company
Anti-Biotin	FITC	Miltenyi
Goat anti Mouse	PE, APC	BD
Goat anti-Rabbit	APC	invotrogen
Goat anti-Rabbit	PE	Santa Cruz
Rat anti Mouse	FITC	Biolegend
Streptavidin	APC, PE, FITC, BV605	Biolegend

Table 6.6: Secondary antibodies used for flow cytometry.

6.1.7 Pure antibodies used for blocking/ADCC

Target/Name	Clone	Company	Species	Final conc.
Cetuximab		Invivogen	hIgG1	5ug/ml
CD160	By55	Biolegend	Mouse IgM	5ug/ml
DNAM-1	11A8	Biolegend	Mouse IgG1	5ug/ml
HLA-ABC	W6/32	Biolegend	Mouse IgG2a	5ug/ml
ICAM-1	HCD54	Biolegend	Mouse IgG1	5ug/ml
IFNΓR1	GIR-208	Biolegend	Mouse IgG1	5ug/ml
IFNγ	B27	Biolegend	Mouse IgG1	10ug/ml
ILT2	GHI/75	Biolegend	Mouse Igg2b	5ug/ml
ILT2	HP-F1	eBioscience	Mouse IgG1	5ug/ml
ILT4	42D1	Biolegend	Rat igg2a	5ug/ml

Monalizumab	IPH5201	Innate Pharma	Mouse IgG1	
NKG2D	1D11	Biolegend	Mouse IgG1	5ug/ml
NKp30	P30-15	Biolegend	Mouse IgG1	5ug/ml
NKp44	P44-8	Biolegend	Mouse IgG1	5ug/ml
NKp46	9E2	Biolegend	Mouse IgG1	5ug/ml
Lirilumab	IPH2102	Innate Pharma	Mouse IgG1	5ug/ml
TIGIT	MBSA43	eBioscience	Mouse IgG1	5ug/ml
hIgG1 isotype	QA16A12	Biolegend	Mouse IgG1	As primary
mIgG2a isotype	MOPC-173	Biolegend	Mouse IgG1	As primary
mIgG2b isotype	MG2b-57	Biolegend	Mouse IgG2b	As primary
mIgG1 isotype	MOPC-21	Biolegend	Mouse IgG1	As primary
rIgG2a isotype	MRG2a-83	Biolegend	Rat IgG2a	As primary

Table 6.7: Blocking antibodies and control isotypes used in functional assays.

6.1.8 Recombinant human proteins

Name	Company	Catalog n.
Siglec-7-Fc	RND	1138-SL
Siglec-9-Fc	RND	1139-SL
NKp30-Fc	RND	1849-NK
NKp44-Fc	RND	2249-NK
NKp46-Fc	RND	1850-NK
DNAM-1-Fc	RND	666-DN
NKG2D-Fc	RND	1299-NK

Table 6.8: Recombinant FC fusion proteins used to detect cognate ligands.

6.1.9 Chemical reagents and biological compounds

Product	Company	Catalog n.
7-AAD	Biolegend	420404
Ampicilin	Sigma-Aldrich	A9393
Aqua zombieTM	Biolegend	423102
BfuA1	NEB	R0701S
Cell Lysis Buffer (10X)	Cell Signaling Technology	9803

Cell Trace Violet	Invitrogen	C34557
Crystal Violet	Sigma-Aldrich	C0775
Golgi plug™	BD Bioscience	555029
Golgi stop™	BD Bioscience	554724
Ionomycin	Sigma-Aldrich	I3909
Nuclease-Free Water	Ambion	AM9937
MIDORI Green Advance	Nippongenetics	MG04
PMA	Sigma-Aldrich	P1585
Puromycin	Sigma-Aldrich	P9620
Recombinant IL-2	Roche	Ro 23-6019
Recombinant TNF-α	Peprotech	300-01A
Recombinant IFN-γ	Peprotech	300-02
Retro-Concentin	Systembio	RV100A-1
Sambucus Nigra Lectin FITC	Invitrogen™	L32479
One Shot™ Stbl3™ Chemically Competent E.coli	Invitrogen	C737303
T4 Ligase	NEB	M0202L
T4 DNA Ligase Buffer	NEB	B0202S
T4 PNK	NEB	M0201L
Quick CIP	NEB	M0525L

Table 6.9: Chemical reagents and biological compounds used in experiments.

6.1.10 Cell culture media, buffers and gels

Buffer	Composition
DMEM medium	DMEM + 10 % FCS + 1% Pen/Strep + 1% L-Glut
Freezing medium	90% FCS + 10% DMSO
MACS Buffer	PBS + 1 % FCS + 2 mM EDTA
MACS NK medium	MACS + 10 % Human serum + 1% Pen/Strep + 1% L-Glut
PBS	137 mM NaCl, 2.7 mM KCL, 12 mM H2PO4, pH 7.4
RPMI 1640 medium	RPMI 1640 + 10 % FCS + 1% Pen/Strep + 1% L-Glut
SCGM NK medium	SCGM + 10 % Human serum + 1% Pen/Strep + 1% L-Glut
Sorting Buffer	PBS + 2 mM EDTA

Agarose gel 1-2%	1-2 % agarose, Midori Green (1:50), 1x TAE buffer
FACS Buffer	PBS + 1 % FCS + 2 mM EDTA + 0.1 % sodium azide
LB medium (1l)	10 g tryptone, 10 g NaCl, 5 g yeast extract
SDS sample buffer (2X)	0.15 M Tris-HCl pH 6.8, 10 % β-Mercaptoethanol, 1.2 % SDS, 30 % Glycerol, 0.04 % Bromphenol blue
12 % Resolving gel	3.4 ml H_2O, 4 ml acrylamide (30 %), 2.5 ml 1.5 M tris (pH 8.8), 50 µl SDS (20%), 100 µl APS (10%), 10 µl TEMED
5 % Stacking gel	2.7 ml H_2O, 0.8 ml acrylamide (30 %), 0.5 ml 1 M tris (pH 6.8), 20 µl SDS (20%), 40 µl APS (10%), 4 µl TEMED
SDS running buffer	6.04g Tris, 28.8g glycine, 0.1 % SDS
Blocking solution	1X TBS, 0.1% Tween 20, 5% nonfat dry milk
TAE buffer	40mM Tris, 20mM Acetate and 1mM EDTA
TBS	50 mM Tris, 150 mM NaCl, pH 7.5
PBST	PBS + 0.05 % Tween 20
TBST	TBS + 0.05 % Tween 20

Table 6.10: Media, buffers and gels used in experiments.

6.1.11 Plasmids

Name	Origin	Catalog n.
lentiCas9-EGFP	Addgene	#63592
lentiCas9-Blast	Addgene	#52962
psPAX2	Addgene	#12260
pMD2.G	Addgene	#12259
pLenti-HDCRISPR_sgRNA_Target Ctr	Prof. Michael Boutros - DKFZ	
pLenti-HDCRISPR-eGFP_empty sgRNA	Prof. Michael Boutros - DKFZ	
pLenti-HDCRISPR – GW library	Prof. Michael Boutros - DKFZ	

Table 6.11: Plasmids used in experiments.

6.1.12 Sequences of sgRNAs

Gene	Number	Guide seq 5‘ ---- 3‘
AHR	1	CACCG CGGTCTCTATGCCGCTTGGA

AHR	2	CACCG GTAAAGCCAATCCCAGCTGA
B2M	1	CACCG CAGTAAGTCAACTTCAATGT
B2M	2	CACCG AGTCACATGGTTCACACGGC
B2M	3	CACCG CACAGCCCAAGATAGTTAAG
HLA-ABC	1	CACCG GGGTCCGGAGTATTGGGACG
HLA-A	1	CACCG CAGACTGACCGAGTGGACCT
HLA-A	2	CACCG TACCGGCAGGACGCCTACGA
HLA-A	3	CACCG ACGGCCATCCTCGGCGTCTG
HLA-B	1	CACCG GCTGTCGAACCTCACGAACT
HLA-B	2	CACCG CGCTGTCGAACCTCACGAAC
HLA-B	3	CACCG GCGCGGTGCGCAGGTTCTCT
HLA-B	4	CACCG GTAAGTCTGTGTGTTGGTCT
HLA-C	1	CACCG GATCTGAGCCGCCGTGTCCG
HLA-C	2	CACCG GAGACCAGGCCAGCAGGAGA
HLA-C	3	CACCG GAAGTACAAGCGCCAGGCAC
HLA-C	4	CACCG GAGTCCGAGAGGGGAGCCCC
HLA-E	1	CACCG GTTGTCGAAGCGCACGAACT
HLA-E	2	CACCG GTGAATCTGCGGACGCTGCG
HLA-E	3	CACCG GAAAATCTGTGCGGTGTCCC
ICAM1	1	CACCG CCTGCCTGGGAACAACCGGA
SLC35A1	1	CACCG GGTATAGACTGCAGCCATCA
SLC35A1	2	CACCG CTGGAGTTACGCTTGTACAG
SLC35A1	3	CACCG TGAACAGCATACACTAACGA
TAP2	1	CACCG GACCCGCGGGTCTCGTACAA
TAP2	2	CACCG CTGACGTTTACCCTACGTCC
TAP2	3	CACCG CTGGGGACTTTGCTTCCTCA
TM9SF3	1	CACCG GTCTTATGGATGAATACTGT
TM9SF3	2	CACCG ACATCCAGAACCAATCAGAG
TM9SF3	3	CACCG GATGTTAATCTAACTAGTGA
WWTR1	1	CACCG TGGAGGTTCATATGATTCAG
WWTR1	2	CACCG GATACTGCCATGGACCTCTG
WWTR1	3	CACCG AGGCTTACCGAGATTTGGCT

Table 6.12: Sequences of sgRNAs used to generate KO cells.

6.1.13 Indexing + sequencing primers

Gene	Primer seq 5‘ ---- 3‘
F_TrueSq_HDCR_lib	AATGATACGGCGACCACCGAGATCTACACTCTTTCC CTACACGACGCTCTTCCGATCT TCTTGTGGAAAGGACGAAACACCG
Index primer template without index (NNNNNN)	CAAGCAGAAGACGGCATACGAGAT **NNNNNN** GTGACTGGAGTTCAGACGTGTGCTCTTCCGATC TCTTTTAAAATTGTGGATGAATACTGCCATTT
R1_Sq_HDCR_lib	template + **CGTGAT**
R2_Sq_HDCR_lib	template + **ACATCG**
R3_Sq_HDCR_lib	template + **GCCTAA**
R4_Sq_HDCR_lib	template + **TGGTCA**
R6_Sq_HDCR_lib	template + **ATTGGC**
R7_Sq_HDCR_lib	template + **GATCTG**
R8_Sq_HDCR_lib	template + **TCAAGT**
R9_Sq_HDCR_lib	template + **CTGATC**
R12_Sq_HDCR_lib	template + **TACAAG**
R13_Sq_HDCR_lib	template + **TTGACT**
SeqPrimer_HDCRISPR	CCGATCTTCTTGTGGAAAGGACGAAACACCG

Table 6.13: Sequences of primers used to amplify and sequence sgRNA cassette.

6.2 Methods

6.2.1 Cell culture methods

6.2.1.1 Thawing of cells

Frozen cryovials with cells were taken out from liquid nitrogen tank and briefly thawed in a waterbath at 37 ℃ until the solution was half thawed. The cryovial was disinfected with ethanol and let thaw in RT. Vial content was then transferred to 15 ml falcon tube with 10 ml of PBS and centrifuged for 10 minutes (min) at 1500 rpm for 10 min. Pelleted cells were resuspended in pre-warmed medium and transferred to a cell culture flasks in the incubator (37 °C, 5 % CO2).

6.2.1.2 Passaging of cells

Melanoma cells were grown in T75 culture flasks for 2-3 days (d). When cells reached 80-90% confluency, medium was discarded and cells washed with RT PBS. For detaching of cells 3 ml of Trypsin/EDTA solution was used per 75 cm2 flask for 5 min at 37℃. When cells fully detached from the flask, 7 ml of RPMI was added to neutralize Trypsin and pipetted to fully resuspend the cells. After resuspending, 1 or 2 ml of cell suspension was left in a flask to reach 1:5 or 1:10 dilution. Cell were then cultured in 10-15 ml of fresh medium for 2-3 d until another round of passaging. When cell line exceeded 1 month of culture, the cells were discarded and a new fresh batch was thawed.

6.2.1.3 Counting of cells

After harvesting the cells and washing by centrifugation, cell pellet was resuspended in 1-10 ml of medium. For high amounts of cells expected, 10 µl of cells suspension was diluted in 90 µl of Trypan Blue reaching 10x dilution. For small amounts of cells 2x dilution was used. Diluted cells were loaded into the Neubauer chamber and the amount cells was counted excluding dead cells stained by Trypan Blue. Cell number was then determined by Neubauer chamber formula:

cell number in 1ml = (cells counted/squares counted)(dilution*10^4)*

6.2.1.4 Storage of cells

The early passage of the cell line culture was expanded into a large amounts, frozen and stored in a liquid nitrogen tank. In brief, cells were detached using trypsin, counted and centrifuged for 10 min 1500 rpm for 10 min. Cell pellet was resuspended in FCS containing

10% DMSO to achieve a concentration of 1-2 million cells per ml and transferred to a cryovial. The cryovials containing the cell suspension were placed in an isopropanol freezing box and frozen at -80°C for 2 d. After freezing, the cryovials were transferred to a liquid nitrogen tank for long-term storage.

6.2.1.5 Culture of cell lines

A375, A431, HeLa, MaMel-86b, K562, SKMel-28 and UKRV-Mel02 cell lines were cultured in RPMI 1640 supplemented with 10 % FCS, 2 mM L-glutamine, and 1 % Penicillin/Streptomycin. HEK293T, HepG2 and SKMel-37 cell lines were cultured in DMEM supplemented with 10 % FCS, 2 mM L-glutamine, and 1 % Penicillin/Streptomycin.

6.2.1.6 Isolation of peripheral blood mononuclear cells (PBMCs)

PBMCs were isolated from buffy coats obtained from healthy donors. Content of a buffy coat was transferred to a T75 flask and diluted with PBS to a total volume of 140 ml. The suspension was then carefully loaded on top of 15 ml Ficoll/Bicoll in 50 ml falcon tube and centrifuged at 2000rpm for 25 min in RT without brakes. After centrifugation a white layer separating plasma and Ficoll is carefully transferred into new 50 ml falcon tube and washed with PBS at 1500 rpm for 15 min in RT. Supernatant is then discarded and cell pellet is resuspended in 50 ml PBS and centrifuged at 800 rpm for 15 min at RT to remove thrombocytes. Cell pellet is then resuspended in 15 ml of RCL buffer and incubated in a water bath at 37 °C to remove residual erythrocytes. Cells are then washed with PBS by centrifugation at 800 rpm followed by another centrifugation in fresh PBS at 1500 rpm for 15 min at RT. All supernatants were discarded and isolated PBMCs resuspended in PBS for counting.

6.2.1.7 Isolation an culture of primary NK cells

Isolation of primary NK cells was performed using Miltenyi NK isolation Kit. Freshly isolated PBMCs were counted and 200 million of PBMCs were centrifuged at 1500 rpm for 15 min at RT. Supernatant was discarded and cell pellet was resuspended in 600 µl of MACS buffer. Cell were then stained by adding 150 µl of NK Biotin Antibody Cocktail and incubated 5 min at 4 °C. Subsequently, 450 µl of MACS buffer and 300 µl of Microbeads was added and incubated 10 min at 4 °C. After incubation, 30 ml of MACS buffer was added to cell suspension and centrifuged at 1500 rpm for 15 min at RT. Supernatant was then discarded and cell pellet resuspended in 2 ml of MACS buffer to a concentration of 100 million PBMCs/ml. Meanwhile LS columns were placed into a magnetic separating rack and washed with 3 ml of MACS buffer

to equilibrate to columns. After washing, 15 ml falcon tube was placed under the column and 1 ml of stained PBMCs suspension was loaded into the column and the suspension was let flow through. 3 ml of MACS buffer was then added to wash the column. Collected flow through cells were counted centrifuged at 1500 rpm, 15 min, RT. Isolated NK cell pellet was then resuspended in MACS or SCGM medium with 10% human AB serum, 1% Penicilin/Strptavidin, 2nm L-Glutamine and 400U/ml of IL-2 to a final concentration of 2 million NK cells/ml. NK cells were cultured at least 2 d in the incubator at 37 °C before any assay. For isolation of NKG2A$^-$ NK cells, 10 million of isolated NK cells were stained with 20 µl of biotinylated NKG2A mAb for 5 min and for 10 min with 80 µl of anti-Biotin MicroBeads (130-090-485). Stained NK cells were then washed with PBS by centrifugation, resuspended in 1 ml of MACS buffer and loaded onto LS column for magnetic separation. Column was then washed with 5 ml of MACS buffer and flow through cells collected, counted, resuspended in NK cell medium containing 400U/ml of IL-2 and cultured at 37 °C.

Using 200 million of PBMCs should yield approximately 10-20 million NK cells. For higher NK numbers needed the amount of PBMC and reagents was up-scaled accordingly.

6.2.2 Lentivirus generation methods

6.2.2.1 Lentivirus production

HEK293T cells were in culture at least 1 week before transfection with a target vector and lentivirus packaging plasmids. Day before the transfection, 5 million HEK293T cells were seeded per T75 flask in a fresh DMEM medium in biosafety S2 laboratory to reach 80-90% cell confluence at the day of transfection. Plasmid vectors were mixed in a 15 ml falcon tube combining 1.5 ml of serum free OptiMEM, 5 µg of target plasmid, 5 µg of psPAX2 and 2.5 µg of pMD2.G lentivirus packaging plasmids. DNA solution was mixed and 15 µl of Plus Reagent was added. In another falcon 60 µl of Lipofectamine^{TM} 2000 was added to 1.5 ml of serum free OptiMEM and mixed. Content of both falcons were mixed together and let sit for 20 min at RT to form lipid-DNA conjugates. After 20 min, the solution with lipid-DNA conjugates was added directly to HEK293T cells together with 10 ml of serum free DMEM medium and placed into incubator at 37°C. After 6 h, 1 ml of FCS was added to HEK293T cells and cultured overnight (o/n). The next day medium was replaced with 15 ml of fresh complete DMEM and cultured for 2 d. Medium was then collected and centrifuged at 1500 rpm for 10 min to pellet detached cell. Supernatant was then filtered through 0.45 low protein binding membrane (Milipore Sterilflip HV/PVDF) and stored at -80°C in cryovials.

In addition to above mention lentivirus production, MirusBio™ TransIT lentivirus system reagent was used to generate high titer of lentivirus for the GW lentiviral sgRNA library. In brief, HEK293T cell were seeded in T75 flask in a fresh DMEM medium in S2 laboratory reaching 80-90% of cell confluence at the day of transfection. The next day, 75 µl of Lentivirus Packaging Mix and 7,5 µg of GW library was combined, mixed thoroughly and diluted in 1.5 ml of Opti-MEM® I Reduced-Serum medium. Next, 45 µl of TransIT®-Lenti Reagent was added to the diluted DNA mixture and let the transfection complexes to form by incubating at RT for 10 min. The TransIT®-Lenti Reagent:DNA complex was drop-wise added to T75 flask with HEK293T cells in fresh DMEM medium to a different areas of the flask and gently rocked to evenly distribute. Cell were then incubate at 37°C in 5% CO2 for 2 d without replacing the medium. Medium containing lentivirus was then collected as described above.

6.2.2.2 Lentivirus concentration

For some virus, the supernatant was concentrated by adding 2.5 ml of Retro-Concentin™ to 10 ml of supernatant and let sit at 4°C for 24 h. Next day the solution was centrifuged at 2000 rpm for 15 min to pellet concentrated virus particles. Supernatant was discarded and viral pellet was resuspended in 500 µl of PBS and stored in 50 µl aliquots at -80°C. Other method used for the concentration of lentivirus was the centrifugation of HEK293T supernatant through size separating filter tubes. Supernatant was first filtered through 0.45 low protein binding membrane and then applied into the Amicon™ 15ml Ultra Centrifugal Filter Units 100kDa followed by centrifugation at 2000 rpm for 20 min at 4°C. High sized virus particles were left concentrated in a reservoir and frozen in cryovials at -80°C.

6.2.2.3 Lentivirus titration by colony formation method

Lentivirus containing the antibiotic resistance as the only selection marker was titrated using a colony formation assay. Lentivirus was diluted in a series of 10 fold dilutions and used for infecting melanoma cells seeded in a 6-well plate, T25 of T75 flasks. To increase infection, 8 µg/ml of Polybrene was added to medium during the infection. Medium was replaced after 1 day of infection and cells cultured at least 2 d without cell passaging. After 2 d, cells were cultured in a fresh medium containing selection antibiotic for another 2 d. Medium with dead cells was replaced for fresh medium with selection antibiotic and cultured again for 2 d without cell passaging. By this time cells formed an isolated small colonies of infected resistant cells. When cell colonies were visible by eye, the medium was discarded and wells or flask washed with PBS. To count cell colonies, a crystal violet dye solution was added onto dish surface and

let stain attached cells for 15 min. Cells were then carefully washed with PBS and dyed colonies counted. Lentivirus titer was then determined using following equation:

*Titer (TU/ml) = (number of colonies /total volume) * dilution factor*

6.2.2.4 Lentivirus titration by EGFP expression

Titration of lentivirus containing GFP was performed by infecting melanoma cells with several dilutions of lentivirus stock. Defined number of melanoma cells were seeded in a 6-well plate and each well infected with dilutions of 10 fold decreasing amount of lentivirus. Cell were then incubated for 1 d in the presence of 8 µg/ml of Polybrene. Medium was replaced and cells cultured at least 2 d. Cells were then harvested and the expression of GFP was measured by flow cytometry. The concentration of lentivirus stock was then determined by the percentage of GFP^+ cells and the initial number of melanoma cells infected using following equation:
*Titer (TU/ml) = (Initial cell number infected * percentage) / (Virus volume * dilution fold)*

To correctly determine the lentivirus titer, only conditions with 10-20% GFP^+ cells were used to exclude multiple infection.

6.2.2.5 Stable Cas9 overexpression in melanoma cell lines

Plasmids containing Cas9 protein together with either GFP or resistance to Blasticidin were used for lentivirus production. Cultured melanoma cells were seeded in several T25 flask and cultured o/n. Next day Cas9-EGFP or Cas9-Blast lentivirus was thawed and diluted in fresh RPMI. Each T25 flask with melanoma cells received a dilution with decreasing amounts of lentivirus. Cells were incubated o/n, transferred to a bigger T75 flask and cultured for 2 d. Cells infected with Cas9-Blasticidin lentivirus were cultured in the presence of 10 µg/ml of Blasticidin for 1 week. Cells infected with Cas9-eGFP were sorted for high GFP expression by BD FACS Aria.

6.2.2.6 Single cell colony cell line generation

A375 Cas9 expressing cell line was harvested using Trypsin and washed by centrifugation at 1500 rpm for 10 min at 4°C. Cell were resuspended in cold RPMI medium and counted. The cell concentration was adjusted to obtain 30 cells in 10 ml of RPMI followed by adding 100 µl of cell suspension each well of 96 well plate. Each well containing only a single cell was marked and cultured to expand the cell for 4 d. Wells containing a single cell

obtained additional 100 µl of conditioned medium. Cell colonies grown from a single cell were detached and expanded to a larger amounts for further testing.

6.2.3 Flow cytometry methods

6.2.3.1 Surface staining

NK or tumor cells were harvested and seeded in a 96 well round-bottom plate in a concentration 50 – 100 000 cells per well followed by centrifugation at 2100 rpm for 3 min at 4°C. Pelleted cells were resuspended in 50 µl of PBS containing diluted fluorochrome-conjugated antibodies and Zombie Aqua™ viability dye (1:150) and incubated 20 min at RT in dark. Cells were then washed with 200 µl of cold FACS buffer, resuspended in 100-150 µl of cold FACS buffer and measured by BD LSR Fortessa™ cytometer.

6.2.3.2 Intracellular staining

For intracellular staining, cells were stained with Zombie Aqua™ viability dye together with surface staining mix in PBS and incubated 20 min at RT in dark. 200 µl of FACS buffer was then added to each well containing cells and centrifuged at 2100 rpm for 3 min. Cell pellet was then resuspended in 150 µl of Fixation Buffer (eBioscience™ Foxp3/Transcription Factor Staining Buffer Set) and incubated for 30 min at 4°C. Afterwards, 100 µl of permeabilisation buffer was added to each well and centrifuged at 2100 rpm for 3 min. Cell pellet was then incubated in dark with 50 µl of permeabilisation buffer with diluted fluorochrome-conjugated antibodies for 30 min at RT. Cell were then washed with 200 µl of FACS Buffer, resuspended in 100-150 µl of FACS Buffer and measured by BD LSR Fortessa™ cytometer.

6.2.3.3 Proliferation staining of NK cells

Cell proliferation was determined by staining of freshly isolated NK cells with Cell Trace Violet dye resuspended in PBS in 1:1000 and incubated at 37°C for 20 min. NK cells were then washed two times with FCS containing RPMI medium, resuspended in the NK cell medium containing 400U/ml of IL-2 and cultured at 37 °C for 6-9 d. NK cells were then collected, stained with fluorochrome-conjugated mAbs for surface markers and measured by BD LSR Fortessa™ for cell proliferation determined by the reduction in Cell Trace Violet staining.

6.2.3.4 Fluorescence-activated cell sorting (FACS)

Altered melanoma cells were detached using Accutase™, counted and washed with PBS by centrifugation at 1500 rpm for 10 min at 4°C. For Cas9-EGFP positivity sorting, cells were diluted in EDTA-containing PBS to a concentration of $1*10^6$/ml and filtered through a cell strainer to remove clumps that could clog the machine. For sorting of specific KO cell populations, cells were stained with fluorochrome-conjugated mAbs mix for 15 min in the dark. Cells were then washed by PBS, diluted to a concentration of $1*10^6$ cells/ml and sorted using BD FACS Aria™ Fusion flow cytometer. For sorting of NK cells, cells were collected, washed with PBS by centrifugation and counted. NK cell pellet was then resuspended in fluorochrome-conjugated mAbs mix and incubated for 15 min in the dark. NK cells were then washed with PBS by centrifugation, resuspended in EDTA-containing PBS to a concentration of $2*10^6$/ml, filtered through a cell strainer and FACs sorted using BD FACS Aria™ Fusion flow cytometer.

6.2.4 sgRNA cloning and gene KO methods

6.2.4.1 Digestion of sgRNA vector plasmid

Vector plasmid Heidelberg (HD) CRISPR library sub-library A[534] obtained from Prof. Boutros lab was used for cloning of 20 nucleotide (nt) sgRNA was first cleaved using BfuA1 restriction enzyme for 30 min at 37°C in a following reaction:

1 µg	pLenti_HDCRISPR plasmid
1 µl	BfuA1
5 µl	NEB 3.1 Buffer
43 µl	ddH_2O

Cleaved vector was then dephosphorylated by adding 2.6 units of Calf Intestine Phosphatase per 1 µg of cleaved vector and incubated for 30 min at 37°C.

6.2.4.2 DNA purification by gel electrophoresis

To obtain a pure PCR product or cleaved sgRNA vector without other DNA fragments, DNA was subjected to purification by gel electrophoresis through a 2% agarose gel, prepared by resuspending of 4 g of agarose in TAE buffer. Mixture was then heated in the microwave until agarose dissolved completely. For visualization of the DNA, 4 µl of Midori Green nucleic acid stain was added to agarose solution and mixed. Solution was then poured into the electrophoresis block and let solidify. DNA was then loaded on gel and let run at 90V for 1h in 1x TAE buffer. Separated DNA was then visualized under UV light and DNA band excised from the gel. DNA was then extracted using QIAquick Gel Extraction Kit by following manufacturer's protocol.

6.2.4.3 Cloning of sgRNA into cleaved vector plasmid

sgRNAs targeting genes of interest were designed using online tool design.synthego.com. Target gene sgRNAs were selected using lowest off-target ratio and highest on-target ratio. In order to clone 20 nt oligonucleotide, an additional reverse complementary oligonucleotide to sgRNA was needed. Both oligonucleotides contained complementary overhangs designed to bind to the cleaved vector in the correct orientation.

oligo 1 5' - CACCG NNNNNNNNNNNNNNNNNNNN - 3'

3' - C NNNNNNNNNNNNNNNNNNNN CAAA - 5' oligo 2

Each pair of oligonucleotides was phosphorylated and annealed in thermocycler to create a stable oligonucleotide duplex in a following reaction:

1 µl	oligo 1 (100uM)
1 µl	oligo 2 (100uM)
1 µl	10x T4 Ligation Buffer (NEB)
6.5 µl	ddH_2O
0.5 µl	T4 PNK (NEB)

The phosphorylation reaction lasted for 30 min at 37°C, followed by annealing, which began at 95°C for 5 min and then gradually cooled to 25°C at a rate of 5°C per minute. Oligonucleotide duplex was then diluted 1:200 in dH_2O and used for cloning and ligation in a following reaction:

x µl	50 ng cleaved pLenti_HDCRISPR vector
1 µl	Oligo duplex (1:200)
1 µl	10x T4 Ligation Buffer (NEB)
x µl	ddH_2O
1 µl	T4 Ligase (NEB)
11 µl	total reaction

Reaction was let run for 30 min at 37°C and directly used for bacterial transformation to amplify the plasmid.

6.2.4.4 Heat-shock transformation

One Shot™ Stbl3™ chemically competent E-coli cells were thawed on ice. The solution with finished ligation reaction was added to one vial of Stbl3 cells and let sit on ice for 10 min. Cells were then incubated 45 s at 42° C and then 2 min on ice. Subsequently, 1 ml of SOCS medium was added to cells and incubated for 1 h at 37° C. Cell suspension was then poured onto agar plates containing selection antibiotic (Ampicilin) and cultivated 16 - 24 h at 37°C.

6.2.4.5 Plasmid isolation

Individual bacterial colonies growing on agar plates were inoculated into 5-10 ml of LB medium containing selection antibiotic and cultivated 16 - 24 h at 37°C on shaker. DNA from transformed cells was isolated using QIAprep Spin Miniprep Kit or PureLink™ HiPure Plasmid Filter Maxiprep Kit following manufacturer's protocol. DNA concentration was then measured by TECAN Spark.

6.2.4.6 Generation of KO cell lines

Cas9 expressing melanoma cell lines were seeded in 6-well plate to reach 60-70% confluence in the day of transfection or infection. For lentiviral infection with sgRNA expressing vector cells were infected in a low multiplicity for 1 d. Transduced cells were then transferred to a bigger dish and cultured for 2 d. Medium was then replaced with fresh medium containing 2.5 µg/ml of puromycin and cultured for 2 d. Survived cells were then expanded in a puromycin containing medium and the expression of target gene was measured by flow cytometry to determine the percentage of cell KO population. Cells were then FACS-sorted for gene KO cell population. Sorted KO cells were expanded a stored in liquid nitrogen tank. For transfection method, Cas9 expressing melanoma cell lines were transiently transfected with plasmid containing sgRNA against target gene using Lipofectamine™ 2000 or jetOPTIMUS reagent. Cell were cultured for 1 d and medium was then replaced with fresh medium containing 2.5 µg/ml of puromycin followed by culture for 2 d. Cells were then expanded, sorted for KO cell population and stored in liquid nitrogen tank.

6.2.5 Western blot

6.2.5.1 Sample preparation

For sample preparation, Cas9 melanoma cells were seeded at the same concentration and cultured for 1-2 d in a 6-well plate at 37°C. Cells were then harvested using trypsin, washed by PBS and resuspended in 100 µl of cell lysis buffer (Cell Signaling Technology) with 1mM PMSF or Protease and Phosphatase Inhibitor Cocktail while kept on ice. Lysates were sonicated 15 s for 5 cycles to reduce viscosity and centrifuged 13,000g for 10 min to remove insoluble clumps. Supernatant was collected and protein concentration measured using Qubit™ Protein and Protein Broad Range (BR) Assay Kit. Samples containing 20 µg of protein were diluted 1:1 with SDS-PAGE loading buffer and incubated for 10 min at 95°C. Denatured samples were then frozen or analysed by SDS-PAGE.

6.2.5.2 SDS-PAGE and semi-dry blotting

Prepared samples were loaded on a 5% stacking polyacrylamide gel followed by 10% separating polyacrylamide gel in a SDS-PAGE running buffer. Gel was let run at 100V until sample bands hit the separating gel. Voltage was then increased to 120V and let run for 2-4 h. Gel with separated proteins were then transferred onto membrane using Trans-Blot Turbo 0.2 µm PVDF or Nitrocelulose Transfer Packs and blotted using Trans-Blot Turbo Transfer System. Membrane was then incubated in blocking buffer (5% milk in TBST) with agitation for 1 h at RT. Membrane was then cut accordingly to a target protein size and incubated with different mAbs. Primary Ab were diluted in a blocking buffer and incubated with membrane o/n at 4 ℃ with agitation in dark. Afterward, membrane was washed 3 times with 15 ml of TBS-T buffer and incubated for 1 h at RT with HRP conjugated secondary antibody diluted in blocking buffer. Membrane was then washed 5 times with 15 ml of TBS-T buffer. HRP substrate WesternBright Sirius was mixed and loaded on top of the membrane and covered with transparent foil for even substrate distribution. After 1 minute excess amount of substrate was removed and membrane developed in a BioRad ChemiDoc MP Imaging System. Signals were then quantified using Image Lab software.

6.2.6 Functional assays

6.2.6.1 Degranulation assay

Tumor cells were harvested using Accutase and washed in RPMI by centrifugation at 1500 rpm for 5 min at RT. Cell pellet was resuspended in cold RPMI medium and the amount of cells counted. Cell suspension was kept on ice to prevent adhesion of cells. Meanwhile, NK cells were harvested, washed by centrifugation at 1500 rpm for 10 min at RT and resuspended in fresh RPMI for counting. NK and tumor cell concentration was adjusted to 60 000 cells/ 40 µl ($1.5x10^6$/ml). Fluorochrome-conjugated Ab against CD107a was added into each wells of 96-well plate. As positive control for CD107a or IFNγ detection, NK cells without tumor cells were stimulated with PMA/ionomycin or IL-12 (1 ng/well) and IL-18 (10 ng/well). Subsequently, NK cells and melanoma cells were added to corresponding wells in 1:1 E:T ratios mixing 40 µl of NK and 40 µl of melanoma cells. For NK cell only conditions, 40 µl of medium was added instead of tumor cells. Whole plate was then centrifuged at low speed (300 rpm) for 30 s and incubated at 37℃ for at least 30 min. Meanwhile, a Golgi Stop reagent was diluted 1:100 in RPMI medium. After 30 min, plate was taken out of the incubator and 10 µl of Golgi Stop dilution was carefully added into each well and mixed by pipette without disrupting sedimented cells.

Optionally, receptor or ligand blocking mAbs were added to each well in the beginning of co-culture to a final concentration of 5 µg/ml. For triggering ADCC, a Cetuximab antibody was added to a melanoma cells to a final concentration 2 µg/ml and let sit for 10 min before adding NK cell.

6.2.6.2 Confluency assay

Melanoma cells were cultured at the same cell number at least a week prior seeding for confluency assay. Melanoma cells were then harvested using Accutase, counted and diluted to a defined concentration in fresh RPMI medium. NK cells were collected, counted and resuspended in a fresh RPMI medium to a defined concentration. The same amount of melanoma cells was added per well (24-well plate) through all conditions. NK cells were then added to melanoma cells in a decreasing amounts to reach desired E:T ratio (2:1 - 0.25:1). Whole plate was shaken to mix cells to evenly distribute in wells and incubated at 37°C for 24 h. After the co-culture, plate was shaken and medium with NK cells and detached dead melanoma cells was carefully removed. Each well was washed gently with warm RPMI and new fresh warm RPMI was added to each well. The plate was then placed into a TECAN Spark reader and the cell confluency in each well was determined.

6.2.6.3 WT/ KO cell ratio co-culture

WT and KO cells were harvested, counted and diluted to the same concentration. WT and KO cells were pooled together in a 1:1 ratio and seeded in a tissue culture plate. Primary NK cells were added to each well in a different ratios, mixed and cultured for 24 h as described previously in confluency assay. NK cells were washed from remaining attached melanoma cells and the confluency of remained attached melanoma cells was determined by TECAN Spark reader. Melanoma cells were then detached and stained with fluorochrome-conjugated mAb against target gene KO to separate WT from KO melanoma cells and determining the changes in the ratio of WT/KO cells. For separation of HLA-E KO and WT cells, melanoma cells were detached after co-culture, seeded in a new culture dish and cultured for 1 day in a fresh medium. Cells were then treated with IFNγ for 12 h and stained for HLA-E expression. Preferential killing or resistance of WT or KO cells was then determined based on the decrease in KO cell population from the bulk population of mixed WT/KO cells. Optionally, blocking mAbs were used to pre-treat NK cells for 10 min at concentration of 5 µg/ml before the co-culture.

6.2.6.4 Cytotoxicity assay

NK cell cytotoxicity assay was performed in a multiple E:T ratios (starting at 16:1 down to 0.5:1) following 6 h co-culture with tumor cells in total volume of 50 ul. First, NK cell were harvested, counted and diluted to a concentration $1,6*10^6$ cells/mL resulting in 40 000 NK cells in 25 µl. Melanoma cells were detached using Accutase, washes with PBS during centrifugation, counted and diluted to a concentration of $1*10^5$ cells/ml resulting in 1250 cells per 12.5 µl. Diluted NK cells were then transferred to 384-well plate performing 2-fold serial dilution (12.5 µl + 12.5 µl medium), resulting in 12.5 µl cell suspension per well. 12.5 µl of melanoma cells were then added to the wells with NK cells. Controls well consisted of NK cells only, tumor cells only and tumor cells incubated with lysis buffer to obtain a maximum release of proteases. NK cells were carefully mixed with melanoma cells and incubated at 37°C for 5.5 h. 12.5 µl of Lysis-Solution (from CytoTox Glo Assay) was then added to a wells containing tumor cells only and incubated for 30 min at 37°C. Meanwhile a 2-fold concentrated CytoTox Fluor reagent was prepared. Next, 25 µl of CytoTox Fluor reagent was added to each well, plate was shaked 700-900 rpm for 1 min and incubated for 30 min at RT in the dark. The fluorescence was the measured at 485-500nm ex/520-530nm em using TECAN Spark.

The percentage of cytotoxicity against melanoma was then calculated by following formula:

*[(NK+melanoma) – (melanoma spontaneous release) - (NK spontaneous release)]*100 / [(melanoma maximum release) – (melanoma spontaneous release)]*

6.2.7 Screen assays

6.2.7.1 Transduction of A375 cells with GW lentivirus library

Selected three single-clone lines were expanded to a large quantities, detached, washed and then placed into separate T175 flasks, resulting in a total of 150 million cells suspended in 300 ml of RPMI medium. Cells treated with 8 µg/ml of Polybrene were then infected in suspension with lentiviral sgRNA library targeting 18 000 genes, where each gene is covered by 3-4 individual sgRNAs. Non-targeting and sgRNAs targeting essential genes are included in the library as negative and positive control. The target MOI was set to a maximum of 0.3 to ensure that at least 500 cells would contain the same sgRNA. Cells were distributed and cultured in 10 T175 flasks for 24 h and medium changed for fresh RPMI containing 2.5 µg/ml of puromycin. After 1 d, medium with dead cells was discarded, cells detached, washed and cultured again in 10 T175 with fresh RPMI containing 2.5 µg/ml of puromycin for 1 d. Selected transduced cells were harvested, washed and aliquoted into cryovials for storage in liquid nitrogen. Before the screen co-culture, three single-clone lines were pooled together at 1:1:1

ratio and used for co-culture with NK cells. For B2M KO screen only bulk A375 cells were used for library lentivirus transduction.

6.2.7.2 NK/A375 screen co-culture

NK cells were cultured and expanded in complete SCGM medium containing 400U/ml of IL-2 in a concentration of 2 million cells/ml. NK cells were cultured for 6 d at 37 °C and used in a 24-h co-culture with transduced and pooled A375 single-clone cells to determine the E:T ratios in which 25%, 50% and 75% killing of A375 cells is achieved. Next day, when the desired E:T ratio was determined, NK cells from 1 donor were harvested, washed and diluted in fresh RPMI. Meanwhile, library infected and pooled A375 single-clone cells were detached, washed and diluted in a fresh RPMI. NK and melanoma cells were mixed together to reach desired E:T ratio and cultured for 24 h. Each condition consisted of 50 million melanoma cells to ensure that each sgRNA is represented by at least 500 cells. Cells were co-cultured in 3x T175 flasks in a 50 ml of RPMI. Afterward, supernatants from co-cultured conditions were collected, centrifuged a filtered for further use. NK cells from co-cultured conditions were washed out by PBS and remaining attached melanoma cells were harvested and counted. Remained melanoma cells were seeded for 1 d to recover and frozen next day for DNA isolation. Melanoma cells in control conditions without NK cells were treated for one day with NK/A375 supernatant or cultured in fresh medium and frozen for DNA isolation.

For B2M KO screen, transduced B2M KO A375 cells were cultured with 7-d expanded NK cells isolated from 3 healthy donors, in two consecutive rounds of co-culture. Prior to the first round of co-culture, B2M KO cells were co-cultured with NK cell donors for 24 h to determine the E:T ratios resulting in 50% killing of B2M KO A375 cells. Next day, the desired E:T ratio was determined for each NK cell donor and used for 24-h screen co-culture. Each condition consisted of more than 50 million B2M KO A375 cells to ensure a coverage of at least 500 cells/sgRNA. Subsequently, NK cells from the co-culture conditions were washed away and the remaining attached melanoma cells were harvested, counted, and expanded to obtain a sufficient quantity for the second round of screen co-culture. Prior to the second round of the screen co-culture, the expanded remaining B2M KO cells were once again co-cultured with the corresponding NK cell donors for 24 h to determine the E:T ratios resulting in 50% killing of B2M KO cells. New E:T ratios were then applied for the second round of 24-h screen co-culture. After the second round of co-culture, NK cells were washed away and remained B2M KO cells were cultured for 2-3 d to recover and used for the isolation of genomic DNA once the cell population reached 50 million cells

6.2.7.3 DNA isolation and PCR amplification

Genomic DNA from remained melanoma cells after screen co-culture was isolated using QIAGEN Blood & Cell Culture DNA Maxi Kit (10) or Genomic DNA Buffer Set with Genomic-tip 500/G according to manufacturer's protocol. DNA concentration was measured using TECAN Spark or Qubit dsDNA HS and BR Assay Kits. For PCR amplification of sgRNA cassette 100 µg of Genomic DNA was used with unique indexing primer for each sample. Indexing of the samples was performed in thermocycler a following reaction:

25 µl	NEB Next Ultra II Q5
2.5 µl	reverse indexing primer (10uM)
2.5 µl	forward primer (10uM)
2.5 ug	genomic DNA
x µl	ddH_2O
50 µl	total volume

PCR Cycles

98° C	30 s	
98° C	10 s	30x
66° C	30 s	
72° C	15 s	
72° C	2 min	
10° C	30 s	

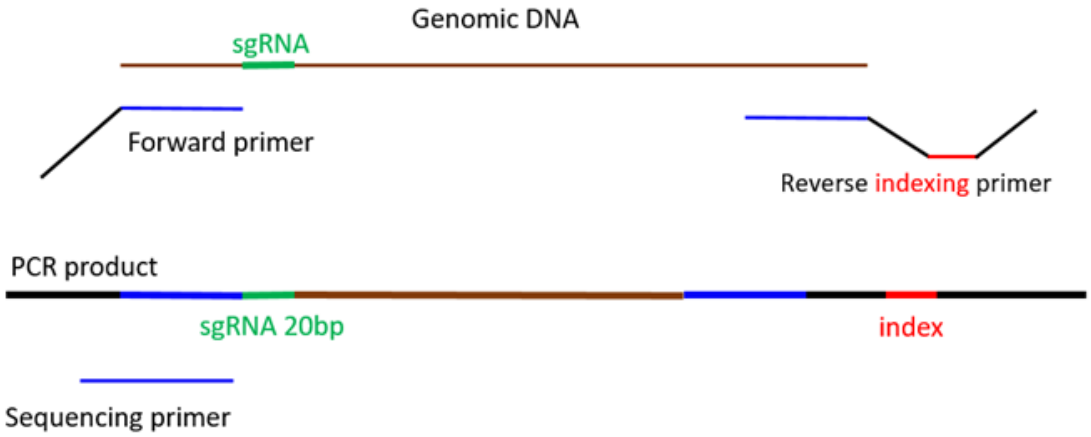

Figure 6.1: Schematic representation of the indexing of the sgRNA cassette.

PCR product was then let run on middle size 1.5% agarose gel at 120 V for 1 h. DNA size matching the PCR product was then excised and DNA isolated. DNA Clean & Concentrator-100 was then used for the purification of DNA after the gel extraction and the concentration of purified DNA was then measured using TECAN Spark or Qubit dsDNA HS and BR Assay Kits.

6.2.7.4 Sequencing and analysis

The DNA quality and quantity was determined using Agilent 2100 Bioanalyzer. DNA concentration was adjusted and pooled in 1:1 ratio. Sequencing was performed using Illumina NextSeq 500/550 High Output Kit v2.5 (75 Cycles) with a custom primer with a binding site directly in front of 20 nt sgRNA sequence. Reaction was terminated after 20 cycles excluding thus the sequencing of identical sequences. Conditions were then demultiplexed using MAGeCK package[535] based on the index reading and the absolute number of sgRNA reads was were first normalized and log-transformed. Log-normalized read-counts from the corresponding control samples were used to determine fold-changes between conditions. The average sgRNA fold-change of a gene and the non-targeting controls was used to determine the statistical significance using Wilcoxon rank sum test. Replicates were combined by arithmetic mean for each sgRNA and a corresponding gene. Multiple testing by Benjamini Hochberg correction was used to correct p-values. For a hit selection, a false discovery rate (fdr) of 0.05 was applied. A375 "core-essential genes", defined as genes in which gene inactivation altered cell proliferation or viability, were marked and excluded from analysis. These genes were identified in a separate sgRNA dropout screen performed on A375 cell line in Prof. Boutros Lab in DKFZ. The analysis of was performed in collaboration with Siu Wang Ng from Prof. Boutros Lab in DKFZ.

6.2.8 Data visualisation and statistical analysis

Data visualisation was performed using GraphPad Prism 8 and data presented as mean with SD. Statistical analysis was performed by one-way ANOVA (multiple comparisons) test; two-way ANOVA (multiple comparisons) test and two-tailed Student's *t* test (B, D), p-value *<0.05, **<0.01, ***<0.001, ****<0.0001.

7 RESULTS

7.1 WT GW CRISPR/Cas9 KO screen

7.1.1 Characterization and generation of Cas9$^+$ melanoma cell line

To select a suitable melanoma cell line for co-culture with allogenic healthy donor-derived NK cells, I first assessed the expression of surface NK cell ligands on human melanoma cell lines. All melanoma cell lines expressed ligands for activating receptors NKp30, DNAM-1, and NKG2D, but differed primarily in the expression of MHC class I (MHC-I). Specifically, A375, SKMel-28, and SKMel-37 cell lines displayed prominent expression of MHC-I, while MaMel-86b and UKRV-Mel02 exhibited a complete lack of MHC-I surface expression determined by flow cytometry (Figure 7.1 A). Since the GW library is introduced by lentiviral transduction of a sgRNA-expressing vector, the transduction efficiency of melanoma cell lines was evaluated. Cells were counted, transduced with serial dilution of the GFP-expressing vector and cultured for 2 days (d) before measuring the expression of GFP by flow cytometry. All melanoma cell lines exhibited high expression of GFP (>75% cells GFP$^+$), except for the SKMel-37 cell line, which demonstrated relatively low transduction efficiency of less than 30%. UKRV-Mel02 showed the highest expression of GFP (Figure 7.1 B-C). Using forward/side scatter (FSC/SSC) in a flow cytometry, A375 cells were found the smallest in size while SKMel-37 cells the largest in size (Figure 7.1 D). Additionally, A375 displayed the most rapid growth rate (Figure 7.1 E).

The most crucial parameter for melanoma cell line suitability for screen co-culture is the cell susceptibility to NK cell-mediated cytotoxicity. The degranulation of NK cells, gated as CD45$^+$ CD56$^+$ population, was measured by the expression of surface CD107a exposed after cytotoxic granule release during 4 hours (h) of co-culture with target cells (Figure 7.2 A). In these co-culture experiments, primary NK cells activated for 2 d with 400 U/ml of IL-2 were used, as unactivated NK cells displayed low degranulation capacity, which can be potently enhanced by ADCC (Figure 7.2 B). NK cells co-cultured with A375, SKMel-37 and UKRV-Mel02 cells exhibited higher NK cell degranulation compared to the MaMel-86b and SKMel-28 cells (Figure 7. 2 C). Similar results were obtained during 6-h co-culture (Figure 7.2 D). Since the cytotoxic mechanisms of NK cells exhibit varying kinetics, I extended the duration co-culture to 24 h to also engage NK cell cytotoxic mechanisms that occur during the later stages of target cell recognition (Figure 7.2 E). Up to 90% of melanoma cells were killed at 4:1 effector

to target (E:T) ratio, and the relative resistance of melanoma cell lines aligned with NK cell degranulation observed before. MaMel-86b and SKMel-28 cells showed higher resistance compared to A375, SKMel-37 and UKRV-Mel02 cells (Figure 7.2 E). Based on the parameters tested, I selected A375 cells as a target cell line for GW CRISPR/Cas9 KO screen co-culture. High susceptibility of A375 cells to NK cell-mediated killing combined with a fast growth can ensure a significant differences between individual depleted and enriched sgRNA counts after screen co-culture, while the full range of expressed NK cell ligands potentially enables detection of all relevant target recognition pathways.

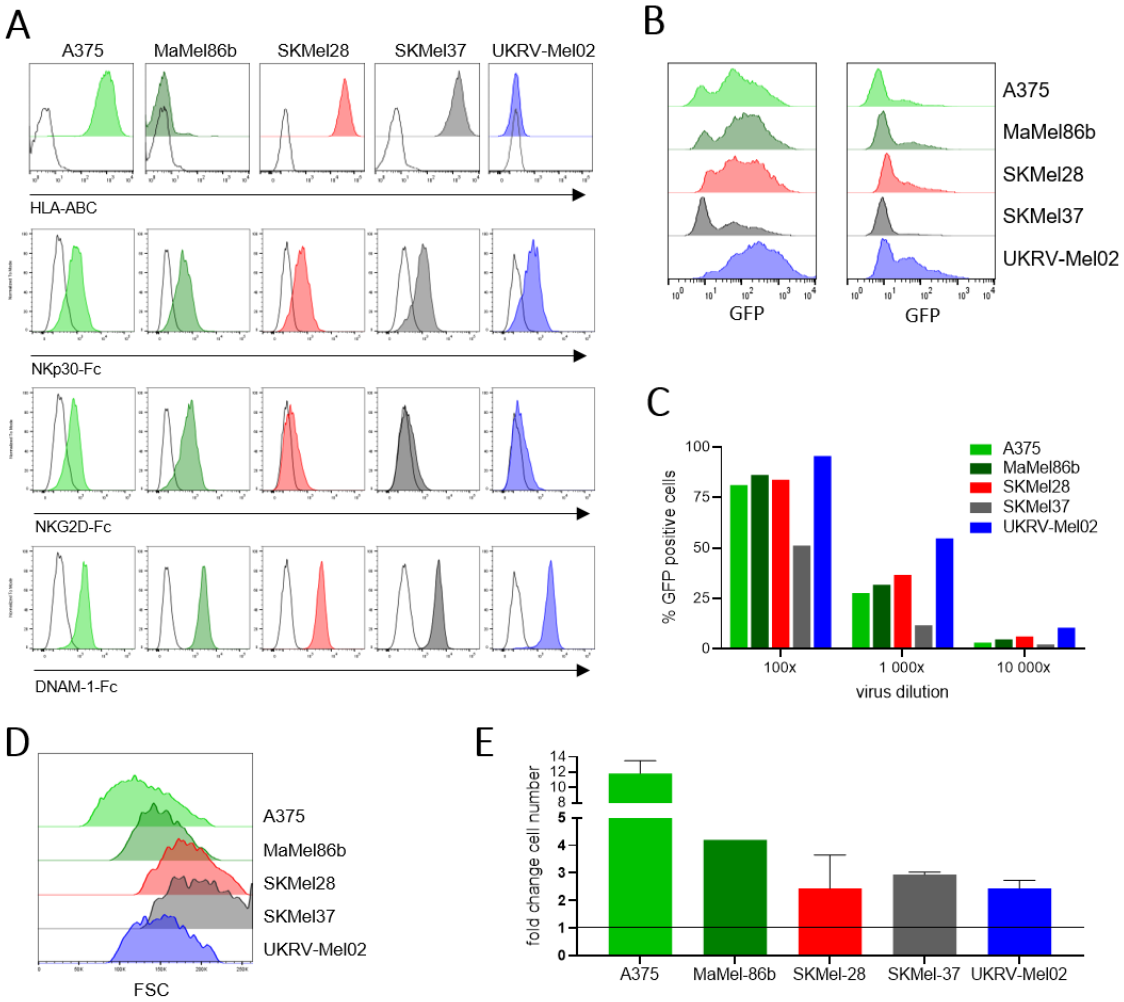

Figure 7.1 The comparison of melanoma cell lines.

A) Histograms showing the expression of HLA-ABC and ligands for NK cells activating receptors on melanoma cell lines. Cells were stained with recombinant receptor Fc fusion proteins together followed by anti-Fc mAb. **B)** Histograms showing transduction efficiency of melanoma cell lines measured by the expression GFP. Cells were infected with GFP-expressing lentiviral vector and measured after 2 d. **C)** Percentage of GFP-expressing cells after infection with different dilutions of lentivirus. **D)** Size comparison of melanoma cell lines determined by FSC flow cytometry. **E)** Comparison of melanoma cells lines proliferation rate. Cell were seeded at equal cell numbers and counted after 2.5 d of culture.

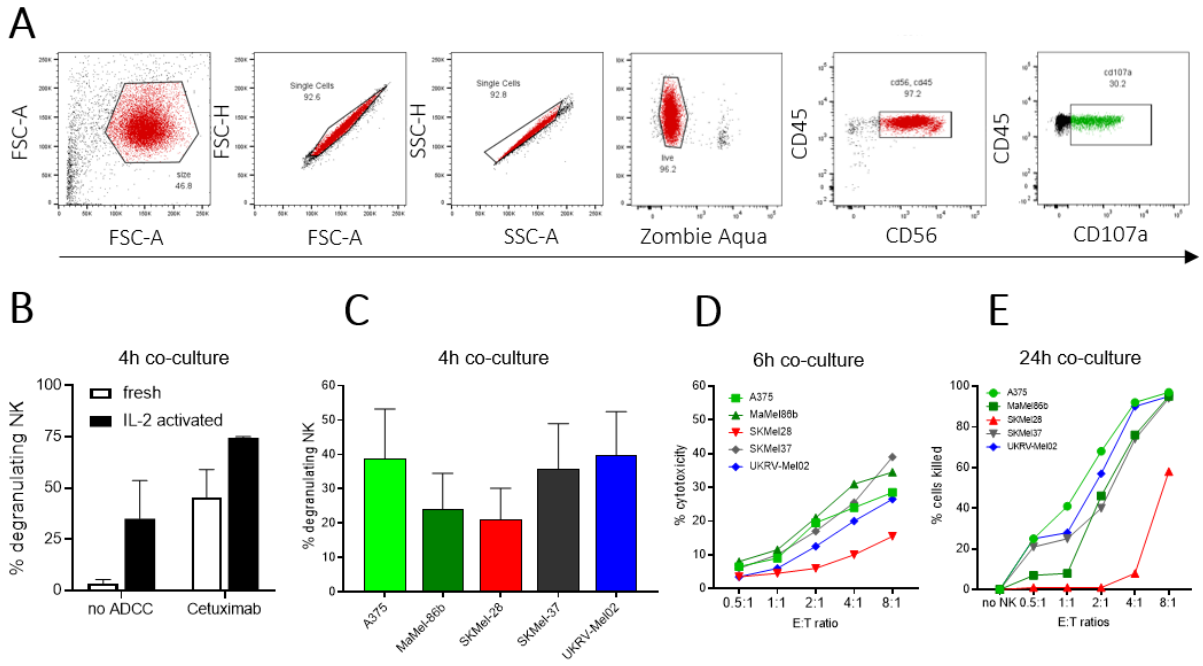

Figure 7.2 Sensitivity of melanoma cell lines to NK cell killing in functional assays.

A) Gating strategy for detection of NK cell degranulation after 4-h co-culture with melanoma cells. **B)** Degranulation of freshly isolated (fresh) vs 2-d IL-2-activated primary NK cells after 4-h co-culture with A375 cells at 1:1 E:T ratio. Cells were co-cultured in the presence of hIgG1 or Cetuximab mAb inducing ADCC. n=3 **C)** NK cell degranulation after 4-h co-culture with melanoma cell lines. n=3 **D)** NK cell cytotoxicity against melanoma cell lines during 6-h co-culture measured by a fluorescent substrate cleaved by proteases released from dead melanoma cells. n=1 **E)** Resistance/sensitivity of melanoma cell lines after 24-h co-culture with NK cells. n=2

I further characterized which known receptors are responsible for high cytotoxicity of NK cells against the A375 cells. I used blocking monoclonal antibodies (mAbs) against the prominent activating receptors NKp30, NKp46, DNAM-1 and NKG2D during co-culture. Blocking of all above mentioned receptors resulted in a reduction of NK cell degranulation (Figure 7.3 A). For a CRISPR/Cas9 KO screen and future KO cell line generation, parental A375 cells were transduced with lentiviral vector, encoding Cas9 transgene fused to an enhanced green fluorescent protein (GFP), at low multiplicity of infection, followed by a fluorescence-activated cell sorting (FACS) of cells showing high expression of GFP and Cas9 (Figure 7.3 B, C). The editing efficiency of Cas9 is pivotal for a successful generation of KO cell line. Thus, I selected CD155, a highly expressed surface molecule, as a target gene to evaluate Cas9 function. The CD155-targeting single-guide RNA (sgRNA) was cloned into a lentiviral vector and transduced into the A375-Cas9 cells. Cells were then subjected to a selection in a puromycin containing media for 3 d to enrich successfully transduced cells, in

which the surface expression of CD155 was subsequently evaluated (Figure 7.3 D). Puromycin-enriched cells contained more than 75% cells negative for surface expression of CD155, which confirmed both the editing efficiency of Cas9 within the A375 cells and the functionality of the sgRNA vector in generating KO cell lines. To further increase the Cas9 editing efficiency, I proceeded to generate A375-Cas9 single-clone lines and select clones that display higher Cas9 editing efficiency. Each single-clone line was transduced with CD155 sgRNA. Despite the expansion of FACS-sorted Cas9 expressing cells, certain clones demonstrated retained expression of CD155 after transduction with CD155 sgRNA (Figure 7.3 E). All A375-Cas9 single-clones, that produced high percentages of CD155 KO cells, induced comparable NK cells degranulation displaying only minor variability among the clones (Figure 7.3 F).

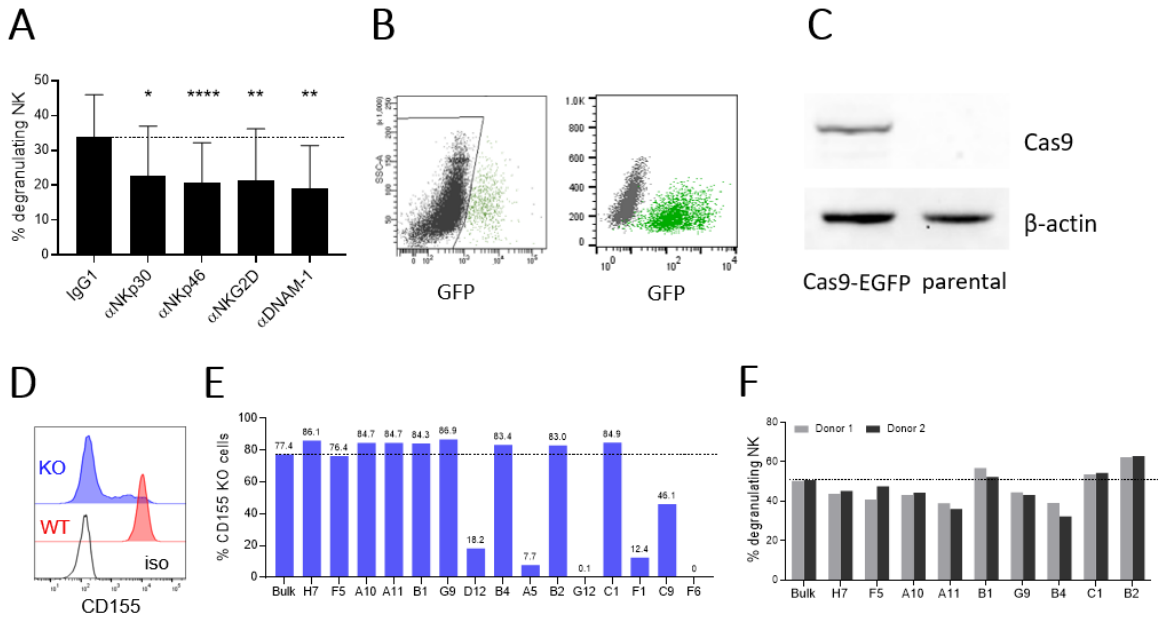

Figure 7.3 Generation and comparison of the A375-Cas9 single-clone lines.

A) NK cell degranulation after 4-h co-culture with parental A375 cells in the presence of mAbs blocking activating NK cell receptors. n=6 **B)** Dot plots showing expression of GFP before and after FACS sorting of A375 cells transduced with Cas9-EGFP vector. **C)** Western blot detection of the Cas9 protein on parental A375 and the A375-Cas9 cells. **D)** Surface expression of CD155 on wild-type (WT) and on CD155 sgRNA transduced A375 cells. CD155 sgRNA-expressing vector was transduced into the A375-Cas9 cells and cultured in puromycin containing media for 2 d before surface CD155 staining. **E)** Cas9 efficiency in bulk A375-Cas9 and single-clones transduced with CD155 sgRNA. **F)** NK cell degranulation after 4-h co-culture with bulk A375-Cas9 and single-clones. Statistical analysis was performed by one-way ANOVA (multiple comparisons) test (A), p-value *<0.05, **<0.01, ***<0.001, ****<0.0001.

Given the observed variability in NK cell degranulation in response to A375 clones, the surface expression of various NK cell-related molecules on each A375 clone was evaluated in comparison to the bulk A375 cells (Figure 7.4 A-C, E). While the differences in percentage expression across the clones were not prominent, significant variations were evident when examining the Mean Fluorescence Intensity (MFI) values, particularly for MICA/B, ICAM-1 and EGFR (Figure 7.4 A-C, E). Since the pooling of multiple clones, from which one clone possesses an accelerated growth rate, could introduce a bias and skew the outcomes of the sgRNA representation during a co-culture screen, I evaluated the growth rate of individual A375 single-clones that did not show marked differences in the surface protein expression (Figure 7.4 D). Clones A11, B1, G9, and C1 exhibited altered growth rate and were thus excluded (Figure 7.4 D). In summary, I successfully generated Cas9 overexpressing A375 cells and selected 3 clones H7, F5, and A10 line for the GW CRISPR/Cas9 KO screen co-culture, as they showed high Cas9-edditing efficiency, similar growth rate, comparable surface expression of NK cell ligands and similar sensitivity to NK cells (Figure 7.4 E).

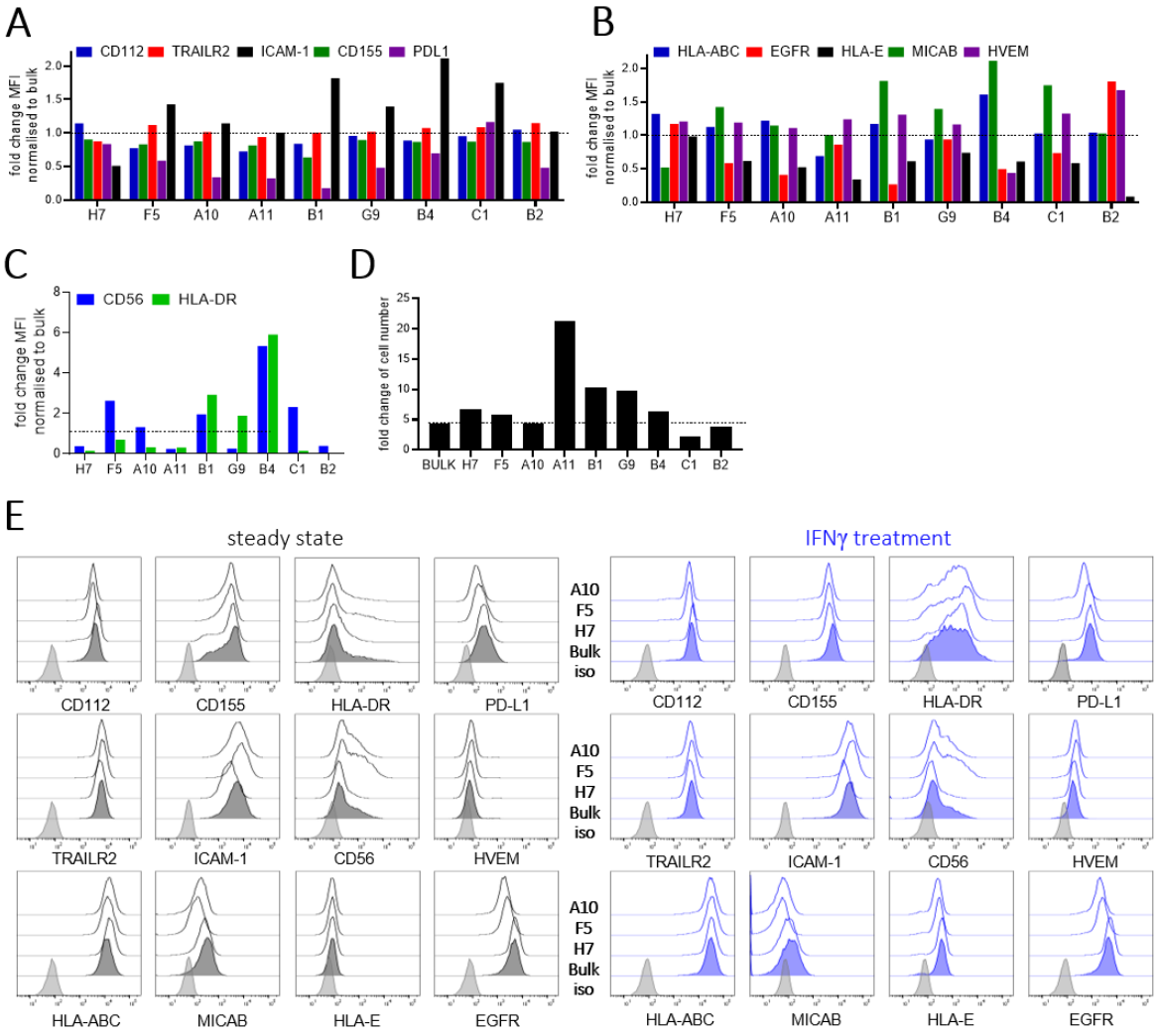

(Figure legend on the next page)

Figure 7.4 Comparison of cell surface molecules on A375 single-clones.
A-C) MFI of selected surface molecules normalized to the expression in bulk A375. **D)** Growth rate of selected single-clones compared to bulk A375. Cells were synchronized in serum free media and plated in complete medium. Cell number was determined after 72 h. **E)** Histograms showing expression of surface molecules on A10, F5, H7 clones and bulk A375 cells at the steady state or after pre-treatment with 1000U/ml of IFNγ 24 h before staining.

7.1.2 Initial validation of top scoring candidates from GW CRISPR/Cas9 KO screen

The GW CRISPR/Cas9 KO screen started with a transduction of A10, F5, and H7 A375 single clone lines with the sgRNA library, subsequent expansion of cells under selection media and pooling them at an equimolar ratio. The initial amount of transduced A375 cells corresponded to a coverage of at least 500 cells being targeted by each individual sgRNA. NK cells were isolated from healthy blood donors and expanded in IL-2-containing media to obtain a sufficient amount of NK cells. These expanded NK cells were then used for a 24-h co-culture with A375 cells, which enabled engaging all NK cell cytotoxic mechanisms. For a comparison, the A375 cells are cultured alone to determine a baseline sgRNA representation (Figure 7.5 A). Before the screen co-culture experiment, pooled A375 clones were co-cultured for 24 h with IL-2-activated NK cells at different E:T ratios to determine the amount of NK cells required to achieve high (80%), moderate (50%), or low killing (20%) (Figure 7.5 B). After the 24-h co-culture at selected E:T ratios, NK cells are washed away from the remaining attached melanoma cells. Subsequently, melanoma cells were harvested for the isolation of genomic DNA (gDNA) and PCR amplification of the sgRNA cassette in the presence of indexing primers specific to each condition (Figure 7.5 C). Amplified and cleaned PCR products were then pooled together at equimolar concentrations and subjected to sequencing. For analysis, conditions involving moderate and high killing were used, as low cytotoxicity conditions yielded sgRNA profiles with low alterations suitable for analysis (Figure 7.5 D). Since some gene deletions have the potential to independently induce changes in cell viability and proliferation, which can alter sgRNA representation, these genes were identified by a separate sgRNA dropout screen and excluded from analysis (Figure 7.5 E). sgRNAs targeting genes in the antigen presentation pathway (*TAPBP, TAP2, B2M, TAP1, CALR*), as well as genes involved in the IFNγ signalling pathway (*IRF1, IRF2, STAT1*), showed a substantial reduced sgRNA counts, indicating their role in A375 cell resistance to NK cell cytotoxicity. As expected, sgRNAs targeting *NCRL3LG1* (B7H6) and *ICAM-1,* the ligands for activating NK cell receptors, were significantly enriched

following NK cell co-culture (Figure 7.5 D-E). In summary, I successfully performed the GW CRISPR/Cas9 KO screen in A375 melanoma cells co-cultured with primary human NK cells that resulted in significantly altered sgRNA counts. Gene ontology analysis of these significantly altered sgRNAs underscores the prominent contribution of the antigen presentation machinery to melanoma cell resistance to NK cell killing (Figure 7.5 F).

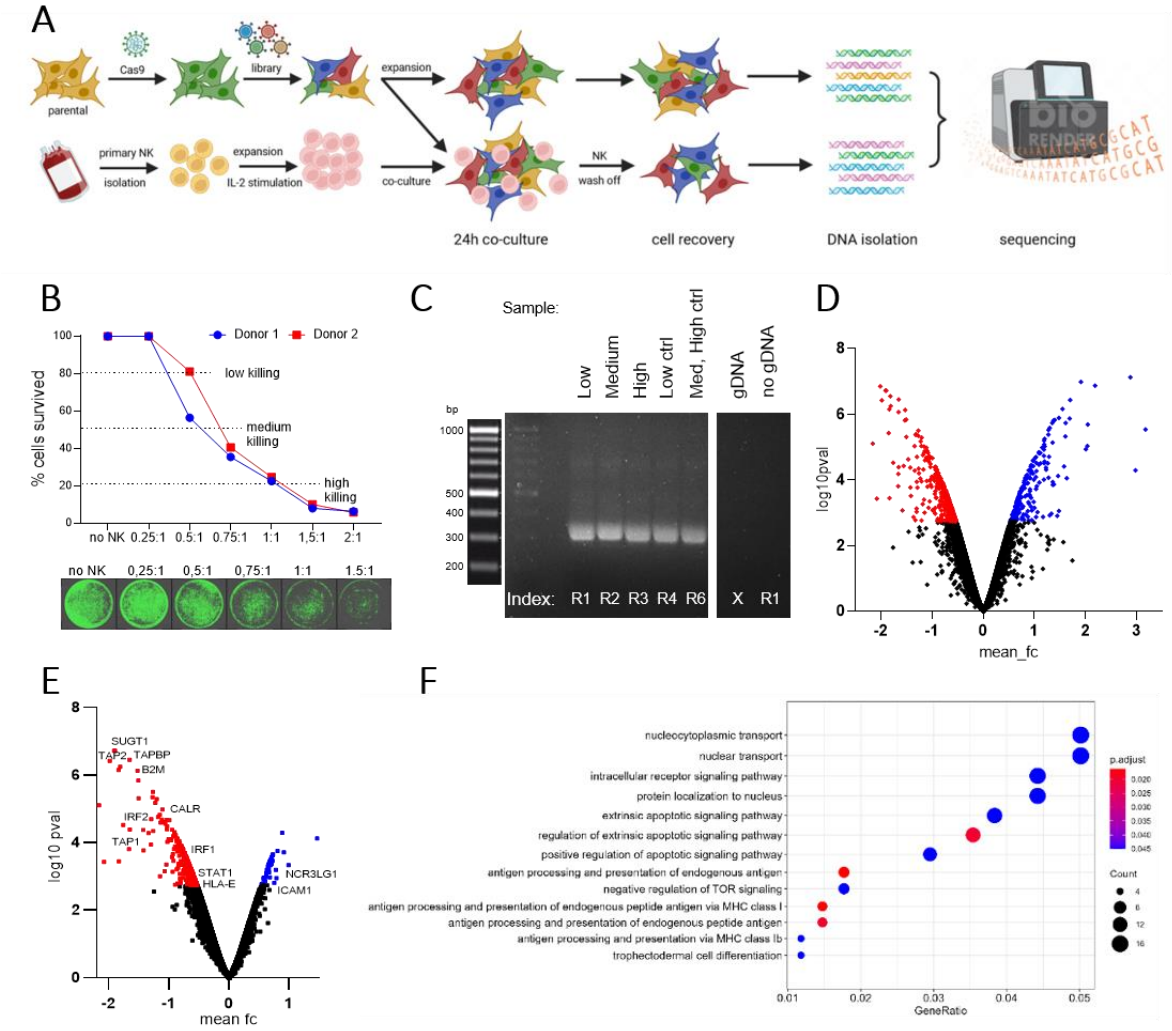

Figure 7.5 GW CRISPR/Cas9 KO screen co-culture.

A) A schematic representation of a GW CRISPR/Cas9 KO screen co-culture. Image created using Biorender. **B)** Survival curve of A375 cells after 24-h co-culture with primary NK cells at different E:T ratios measured by remaining cell confluency by TECAN Spark. **C)** Electrophoresis of PCR amplified and indexed sgRNA cassettes from gDNA isolated from A375 cells that remained the screen co-culture. **D)** Volcano plot showing sensitive KO cells (depleted sgRNA) vs resistant KO cells (enriched sgRNA). Significantly altered sgRNA counts bellow false discovery rate (fdr) 0.05 are marked as red (depleted sgRNA) and blue (enriched sgRNA). **E)** Volcano plot showing sensitive KO cells (depleted sgRNA) vs resistant KO cells (enriched sgRNA) without sgRNAs independently affecting cell proliferation and viability. **F)** Gene ontology analysis of genes with significantly altered sgRNAs.

To confirm the accuracy of the GW CRISPR/Cas9 KO screen, I used neutralizing mAbs to block ligands that showed enriched sgRNA counts. B7H6 is the primary ligand for the activating receptor NKp30 inducing NK cell degranulation and IFNγ production[536]. Despite low expression of B7H6 on A375 cells (Figure 7.6 A), blocking of NKp30 with mAb reduced NK cell degranulation and IFNγ production (Figure 7.6 B-C). Another significantly enriched

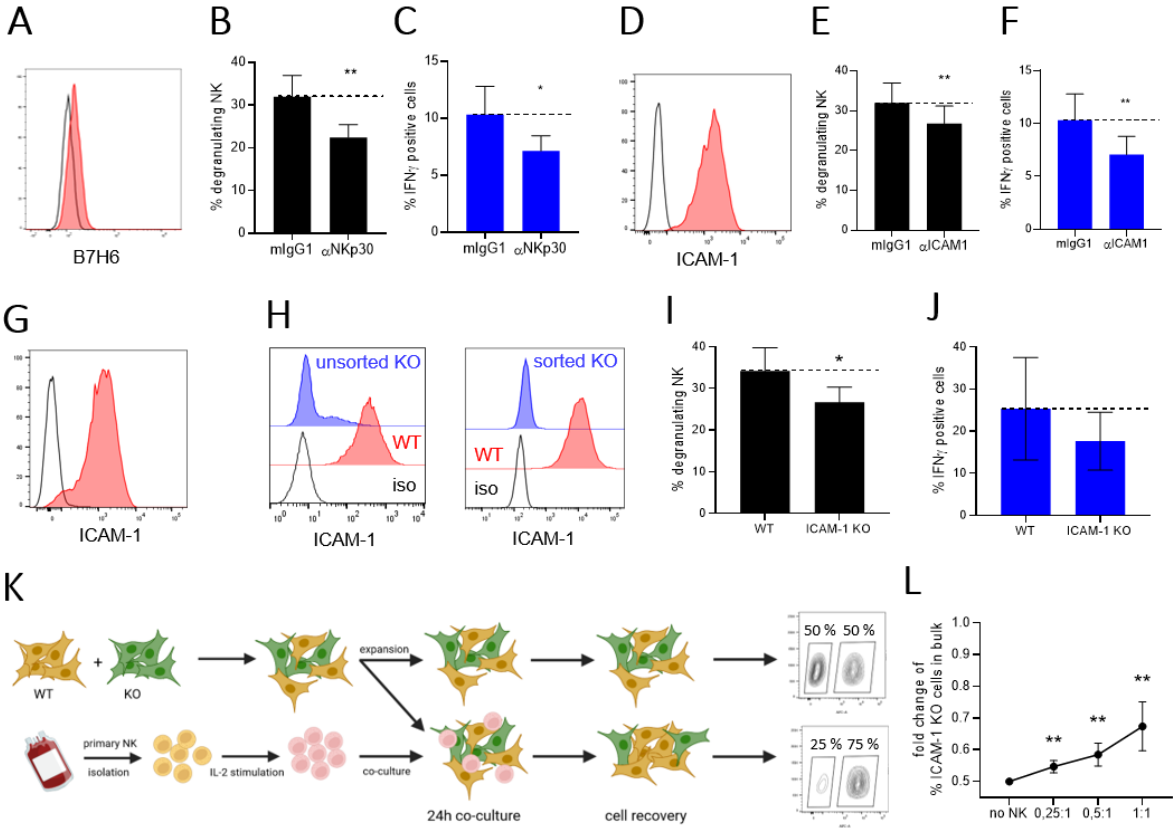

Figure 7.6 Validation of B7H6 and ICAM-1 as NK cell activating ligands.

A) Histogram showing the expression of B7H6 on the A375 cells. **B-C)** NK cell degranulation and IFNγ production after 4-h co-culture with A375 cells in the presence of NKp30 blocking mAb. n=5 **D)** Histogram showing the expression of ICAM-1 on the A375 cells. **E-F)** NK cell degranulation and IFNγ production after 4-h co-culture with A375 cells in the presence of ICAM-1 blocking mAb. n=5 **G)** Histogram showing the expression of ICAM-1 on NK cells. **H)** Histogram showing the expression of ICAM-1 on the A375 cells transduced with ICAM-1 sgRNA before and after FACS sorting. **I-J)** NK cell degranulation and IFNγ production during 4-h co-culture with WT or ICAM-1 KO A375 cells. n=5 **K)** Schematic representation of screen-like setup assay determining the resistance of WT or KO A375 cells to NK cell killing. WT and KO cells were mixed together (1:1) and cultured either alone or with NK cells for 24 h. Remained A375 cells were then stained for ICAM-1 to determine changes in WT:KO ratio. **L)** Resistance of ICAM-1 KO cells reflected in changes in WT:KO ratio after 24-h co-culture with NK cells at different E:T ratios. n=6 Statistical analysis was performed by one-way ANOVA (multiple comparisons) test (L) and two-tailed Student's *t* test (B, C, E, F, I), p-value *<0.05, **<0.01.

sgRNA targeted *ICAM-1*, highly expressed molecule involved in cell adhesion via interaction with LFA-1 molecules expressed on leukocytes[150] (Figure 7.5 D). Blocking of ICAM-1 by mAb during the co-culture reduced NK cell degranulation and IFNγ production (Figure 7.5 E-F). Since ICAM-1 is also expressed on NK cells (Figure 7.5 G), I generated ICAM-1 KO A375 cell line to avoid using blocking mAb that could potentially bind NK cells and directly impair their degranulation (Figure 7.5 H). NK cell co-culture with WT or ICAM-1 KO cells showed a similar effect as ICAM-1 blocking mAb in reducing NK cell degranulation and IFNγ production (Figure 7.5 I-J). In addition to evaluating NK cell degranulation, a co-culture assay resembling the screen co-culture conditions was set up to assess the resistance advantage of either WT or KO melanoma cells. WT and ICAM-1 KO A375 cells were mixed together at 1:1 ratio and cultured either alone or in co-culture with NK cells for 24 h at different E:T ratios. Subsequently, NK cells were removed, and the expression of ICAM-1 on remaining melanoma cells was determined. High expression of ICAM-1 allowed a clear separation of WT from ICAM-1 KO cell in order to determine changes at WT:KO ratio (Figure 7.6 K). The percentage representation of ICAM-1 KO cells within the mixed bulk population increased after NK cell co-culture at E:T ratio-dependent manner, suggesting a preferential killing of WT cells and a partial resistance of ICAM-1 KO cells to NK cell killing (Figure 7.6 L).

Even though the NK cells and A375 cells were HLA-mismatched, sgRNAs targeting antigen presenting machinery genes were strongly depleted from the sgRNA pool in A375 cells after the co-culture with NK cell. To investigate and quantify the effect of MHC-I on the resistance of melanoma cells to NK cell cytotoxicity, I generated A375 cell line deficient in *B2M* gene (B2M KO) and confirmed the absence of surface expression of MHC-I in B2M KO cells by flow cytometry (Figure 7.7 A). WT and B2M KO A375 cells were then separately co-cultured with NK cells for 24 h and the number of remained melanoma cells was quantified. B2M KO cells showed reduced resistance to NK cell killing in comparison to WT cells (Figure 7.7 B). I next compared the resistance of B2M KO cells in comparison to WT cells in a mixed (1:1) 24-h co-culture assay with increasing number of NK cells. The overall killing increased with higher E:T ratios (Figure 7.7 C) which also corresponded to a higher preferential killing of B2M KO cells or a higher resistance of WT cells (Figure 7.7 D). Importantly, these changes in B2M KO/WT ratio were caused by NK cell-mediated killing rather than cytokines produced by NK cells, as neither the exogenous treatment with conditioned medium from such co-cultures nor addition of recombinant IFNγ or TNFα caused changes in WT:B2M KO ratio (Figure 7.7 E). Taken together, accordingly to the GW CRISPR/Cas9 KO screen results, I validated B7H6 and ICAM-1 as molecules responsible for melanoma cells susceptibility to NK

cell killing and B2M, crucial for the expression of MHC-I, as a molecule responsible for the resistance of melanoma cells to NK cell cytotoxicity.

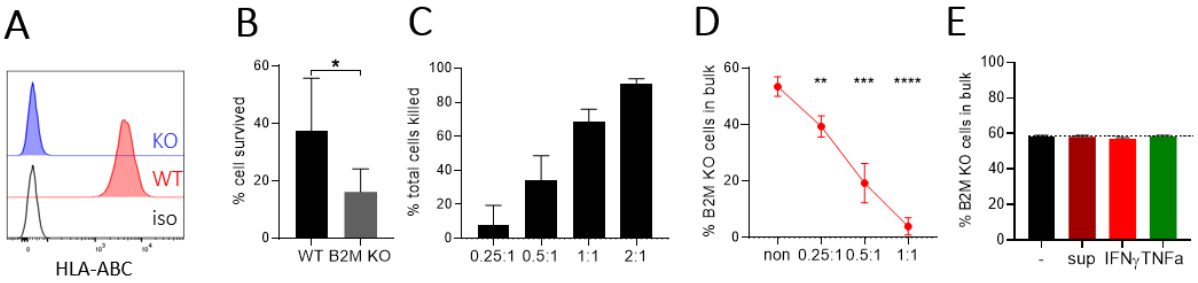

Figure 7.7 The resistance of B2M KO cells to NK cell killing

A) Histogram showing the expression of HLA-ABC on FACS-sorted B2M KO and WT A375 cells. **B)** Remaining confluency of WT and B2M KO cells after separate 24-h co-culture with NK cells. n=5 **C)** Overall killing of mixed WT/B2M KO cells after 24-h co-culture with NK cells. n=6 **D)** Resistance of B2M KO cells after 24-h co-culture of mixed WT/B2M KO cells with NK cells. n=6 **E)** Changes in WT/B2M KO cell ratio after treatment with NK/A375 24-h co-culture supernatant, IFNγ or TNFα (50 ng/ml). WT/B2M KO cells were mixed, pre-treated with cytokines for 24 h and stained for HLA-ABC to determine changes in B2M KO/WT ratio. n=3-6 Statistical analysis was performed by one-way ANOVA (multiple comparisons) test (D) and two-tailed Student's *t* test (B), p-value *<0.05, **<0.01, ***<0.001, ****<0.0001.

7.1.3 IFNγ protects MHC-I sufficient melanoma cells from NK cell cytotoxicity

In addition to addressing the resistance of B2M KO cells to NK cell killing, a direct effect of on NK cell activity was investigated. WT and B2M KO cells were co-cultured with IL-2-activated NK cells a higher degranulation against B2M KO cells was observed. However, this 5% (1.2 fold) increase in was not of a magnitude that would correspond to a high preferential killing of B2M KO cells observed in a 24-h co-culture (Figure 7.8 A). Since the degranulation can only be measured few hours after the co-culture, I decided to mimic a tumor microenvironment present during 24-h co-culture. I collected the supernatant after 24-h co-culture of NK cells with A375 cells and used it for overnight (o/n) pre-treatment of A375 cells. Supernatant pre-treated A375 cells were then co-cultured with NK cells for 4 h. The NK cell degranulation against B2M KO cells was 3 times higher as compared to WT cells (Figure 7.8 B). However, supernatant pre-treatment of WT cells caused more than 70% reduction in NK cell degranulation Figure 7.8 A-B). Given that NK cells produce a substantial amounts of IFNγ (Figure 7.8 C), melanoma cells were pre-treated with recombinant IFNγ or co-culture supernatant and compared in respect to their impact on NK cell degranulation. O/n

pre-treatment of melanoma cells with 500 U/ml of IFNγ also reduced NK cell degranulation to a similar extent as supernatant pre-treatment (Figure 7.8 D). This IFNγ-mediated resistance of WT cells to NK cells was also absent in B2M KO cells, which induced comparable NK cell degranulation and IFNγ production to untreated conditions (Figure 7.8 E, F).

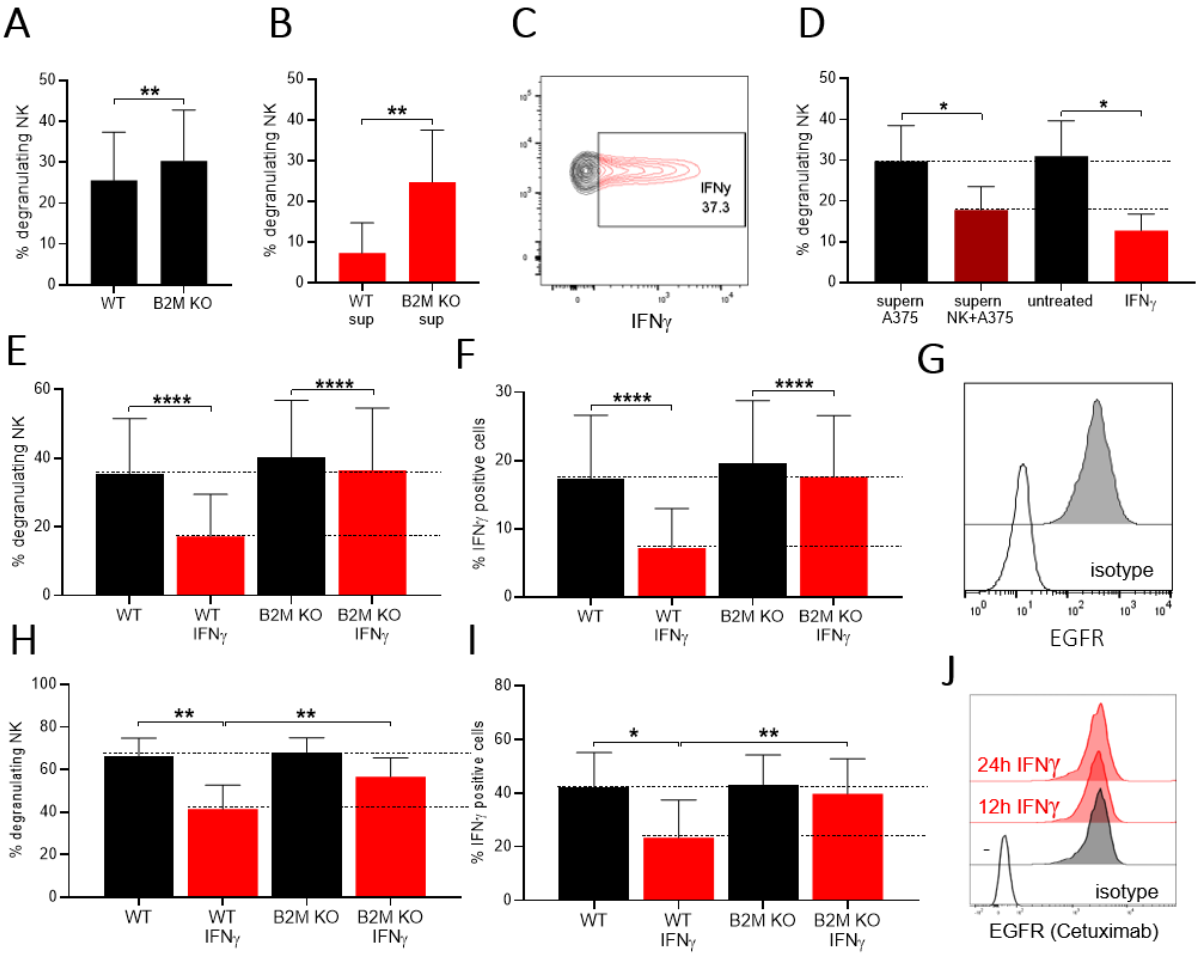

Figure 7.8 NK cell degranulation and IFNγ production against B2M KO A375 cells.

A) Degranulation of NK cells after 4-h co-culture with WT or B2M KO A375 cells. n=6 **B)** Degranulation of NK cells after 4-h co-culture with WT or B2M KO A375 cells o/n pre-treated with supernatant from 24-h NK/A375 co-culture. n=6 **C)** Intracellular staining of IFNγ production in NK cells after 4-h co-culture with A375 cells. **D)** Comparison of NK cell degranulation against A375 cells o/n pre-treated with co-culture supernatant (NK+A375) and recombinant IFNγ. n=3 **E-F)** NK cell degranulation and IFNγ production after 4-h co-culture with o/n IFNγ-pre-treated WT and B2M KO cells. n=17 **I)** Histograms showing the expression of EGFR on A375 cells. **H-I)** ADCC-mediated NK cell degranulation and IFNγ production after 4-h co-culture with o/n IFNγ-pre-treated WT and B2M KO cells. n=6 **J)** Histograms showing the staining of A375 cells with Cetuximab mAb. A375 cells were pre-treated o/n (red) or not (grey) with IFNγ and stained with Cetuximab and anti-Fc IgG mAb. Statistical analysis was performed by one-way ANOVA (multiple comparisons) test (D, E, F, H, I) and two-tailed Student's *t* test (A, B), p-value *<0.05, **<0.01, ****<0.0001.

Next, I assessed the effect of IFNγ pre-treatment of melanoma cells on ADCC-mediated NK cell activity. I first confirmed the expression of the Epidermal Growth Factor Receptor (EGFR) on the melanoma cells in order to use Cetuximab, an EGFR therapeutic mAb (Figure 7.8 G). The absence of *B2M* in melanoma cells also increased ADCC-mediated NK cell degranulation and IFNγ production after co-culture with IFNγ-pre-treated melanoma cells (Figure 7.8 H-I). The reduction in ADCC-mediated NK cell activity against IFNγ-pre-treated melanoma cells was not caused by the downregulation of EGFR or by reduced binding of Cetuximab to melanoma cell surface after IFNγ pre-treatment (Figure 7.8 I). Together, these data show a minor effect of MHC-I on the resistance of melanoma cells to NK cell killing during 4-h co-culture unless IFNγ is present in the system. Moreover, decreased IFNγ signaling resulted in reduced resistance of WT melanoma cells to NK cell killing during 24-h co-culture. Since the previous experiments were performed with short 12 h or o/n IFNγ pre-treatment of A375 cells before the co-culture, I next used a longer IFNγ pre-treatment to explore if the A375 cell resistance to NK cell killing is transient or persistent. I pre-treated melanoma cells with IFNγ for 48, 24, 12 h or left untreated and measured the expression of HLA-ABC, which gradually increased with the duration of IFNγ treatment (Figure 7.9 A). When the cells were subsequently co-cultured with NK cells, the degranulation of NK cells was consistently reduced across all time points of IFNγ pre-treatment, whereas the degranulation of NK cells against B2M KO cells remained high, particularly after 12 h of IFNγ pre-treatment of melanoma cells (Figure 7.9 B). Similar results were observed in ADCC conditions (Figure 7.9 C). The reduction in NK cell degranulation after IFNγ pre-treatment of melanoma cells occurred despite

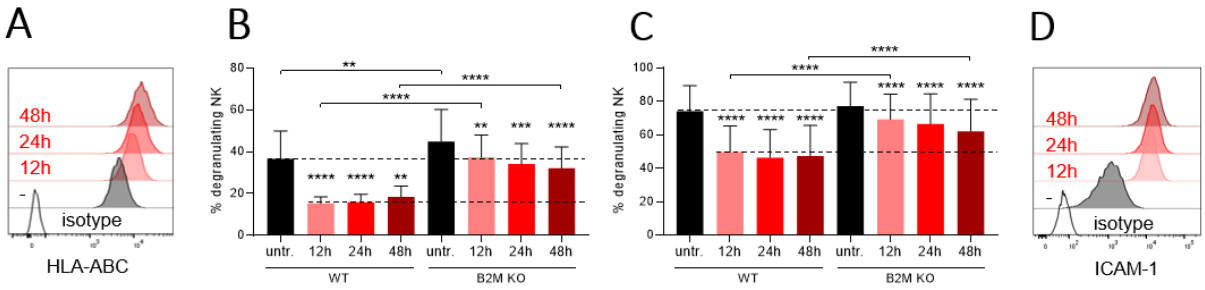

Figure 7.9 The effect of longer IFNγ pre-treatment of melanoma cells on NK cell degranulation. **A)** Histogram showing the expression of HLA-ABC on untreated vs 12, 24 and 48 h IFNγ-pre-treated A375 cells. **B-C)** NK cell degranulation after 4-h co-culture with WT or B2M KO A375 cells pre-treated or not with IFNγ 12, 24 and 48h before the co-culture in the presence of B) hIgG1 or C) Cetuximab mAb. n=6 **D)** Histogram showing the expression of ICAM-1 on untreated vs 12, 24 and 48 h IFNγ-pre-treated A375 cells. Statistical analysis was performed two-way ANOVA (multiple comparisons) test (B, C), p-value **<0.01, ***<0.001, ****<0.0001.

a marked upregulation of ICAM-1, a molecule known to sensitize A375 cells to NK cell killing (Figure 7.9 D). Together, these data show that across 48 h of IFNγ pre-treatment of A375 cells, which gradually increased the expression of MHC-I and ICAM-1, the degranulation of NK cells is reduced after co-culture with WT cells particularly at 12 h of IFNγ pre-treatment.

Since only a minor increase of NK cell degranulation after co-culture B2M KO cells was observed in the absence of IFNγ, I next investigated if during this 4-h co-culture, also a lower preferential killing of B2M KO cells is observed. I used mixed WT/B2M KO cell co-culture assay and monitored the resistance of WT and B2M KO cells. During a 4-h co-culture, only a slight decrease in the B2M KO cell population was observed. However, the killing of B2M KO cells was significantly enhanced when mixed WT/B2M KO cells were pre-treated with IFNγ 12 h before the co-culture (Figure 7.10 A). Notably, the extent of diminished B2M KO cell population after 24-h co-culture resembled the effect observed after 4-h co-culture in IFNγ-pre-treated condition (Figure 7.10 B). The overall killing of mixed WT/B2M KO cells remained relatively unchanged across tested conditions. IFNγ pre-treatment of melanoma cells resulted in a modest reduction in overall killing by NK cells but still led to substantial reduction in the B2M KO cell population (Figure 7.10 C). I next tried to reduce the resistance of melanoma cells to NK cell killing by blocking of IFNγ receptor (IFNGR1) expressed on the surface of melanoma cells (Figure 7.10 D) combined with neutralizing of IFNγ released during the 24-h co-culture. Blocking of IFNGR1 and IFNγ neutralization resulted in an increase of B2M KO cell population suggesting a reduction of IFNγ-induced resistance of WT cells to NK cell killing (Figure 7.10 E). However, the use of blocking mAb might not be sufficient enough to neutralize all IFNγ released by NK cells, which could still induce IFNγ signaling in melanoma cells. To reduce IFNγ released by NK cells, primary NK cells were electroporated with sgRNA targeting *IFNG* and Cas9 RNP generating IFNG KO NK cells (Figure 7.10 F). Since I used unsorted IFNG KO NK cells, I combined it with mAbs blocking IFNγ and IFNGR1, to neutralize IFNγ produced by residual WT NK cells. IFNG KO NK cells failed to efficiently eliminate B2M KO cell population during 24-h co-culture suggesting a low induction of WT melanoma cell resistance by IFNγ (Figure 7.10 G).

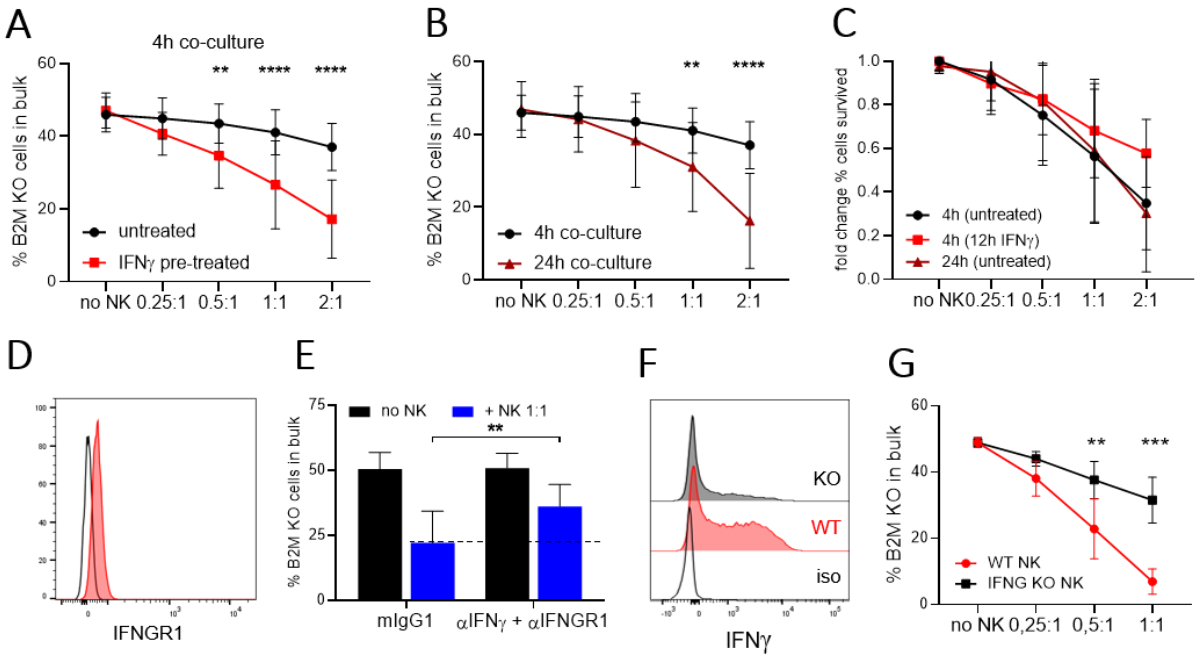

Figure 7.10 Resistance of WT and B2M KO cells during 4- and 24-h co-culture with NK cells. **A-B)** Reduction in B2M KO cell population after A) 4-h or B) 24-h co-culture with NK cells. Mixed WT:B2M KO cells (1:1) were pre-treated or not with IFNγ o/n before the co-culture with NK cells at different E:T ratios. n=6 **C)** Overall killing of mixed WT:B2M KO cells after 4-h and 24-h co-culture with NK cells. **D)** Histogram showing the expression of IFNGR1 on A375 cells. **E)** Reduction in B2M KO cell population after 24-h co-culture with NK cells in the presence of IFNγ and IFNGR1 blocking mAbs. Mixed WT:B2M KO cells (1:1) were co-cultured with NK cells at 1:1 E:T ratio. n=5 **F)** Representative histogram of intracellular staining of IFNγ production after 4-h treatment of WT vs IFNG KO NK cells with IL-12/18. IFNG KO NK cells were produced jointly with Irene Garcés Lázaro **G)** Reduction in B2M KO cell population after 24-h co-culture of mixed WT:B2M KO cells (1:1) with either WT or IFNG KO NK cells at different E:T ratios. n=3 Statistical analysis was performed by one-way ANOVA (multiple comparisons) test (E) and two-way ANOVA (multiple comparisons) test (A, B, G), p-value **<0.01, ***<0.001, ****<0.0001.

To investigate whether the effect of IFNγ on the resistance of melanoma cells to NK cell killing is not only A375 cell-specific, I also tested other melanoma cell lines. A substantial reduction in NK cell degranulation after co-culture with IFNγ-pre-treated MHC-I^{+} cell lines (A375, SKMel-28, SKMel-37) was observed, while the co-culture with IFNγ-pre-treated MHC-I^{-} cell lines (MaMel-86b, UKRV-Mel02) had only a minor impact on NK cell degranulation (Figure 7.11 A). This slight reduction in NK cell degranulation against MHC-I^{-} cells could potentially be attributed to a decrease in the surface expression of MICA/B after IFNγ pre-treatment (Figure 7.11 B). MICA/B, a ligand for NKG2D activating receptor, is

involved in NK cell degranulation since the blocking of NKG2D with mAb during co-culture with melanoma cells reduced NK cell degranulation (Figure 7.11 C). I next generated SKMel-28 B2M KO cell line, which also showed reduced resistance after 24-h co-culture with NK cells (Figure 7.11 D, E). and increased NK cells degranulation after IFNγ pre-treatment (Figure 7.11 F). The loss of *B2M* in SKMel-28 or in another MHC-I^{+} cell line SKMel-37 also increased NK cell degranulation after IFNγ pre-treatment of melanoma cells (Figure 7.11 F-H). I further confirmed that the reduction in NK cell degranulation during 4-h co-culture was mediated by cell-cell contact and not by the release of soluble factors from IFNγ-pre-treated melanoma cells, indicating that the inhibitory effect following IFNγ pre-treatment of melanoma cells is contact-dependent (Figure 7.11 I, J). In summary, these data collectively show that IFNγ pre-treatment induces melanoma cell resistance to NK cells, a phenomenon that is dependent on the expression of B2M/MHC-I and which can be partially reduced by mAbs blocking IFNγ and IFNGR1. Moreover, I showed that MHC-I alone does not play a prominent role in determining the immediate NK cell responses against melanoma cells, unless IFNγ is introduced into the system.

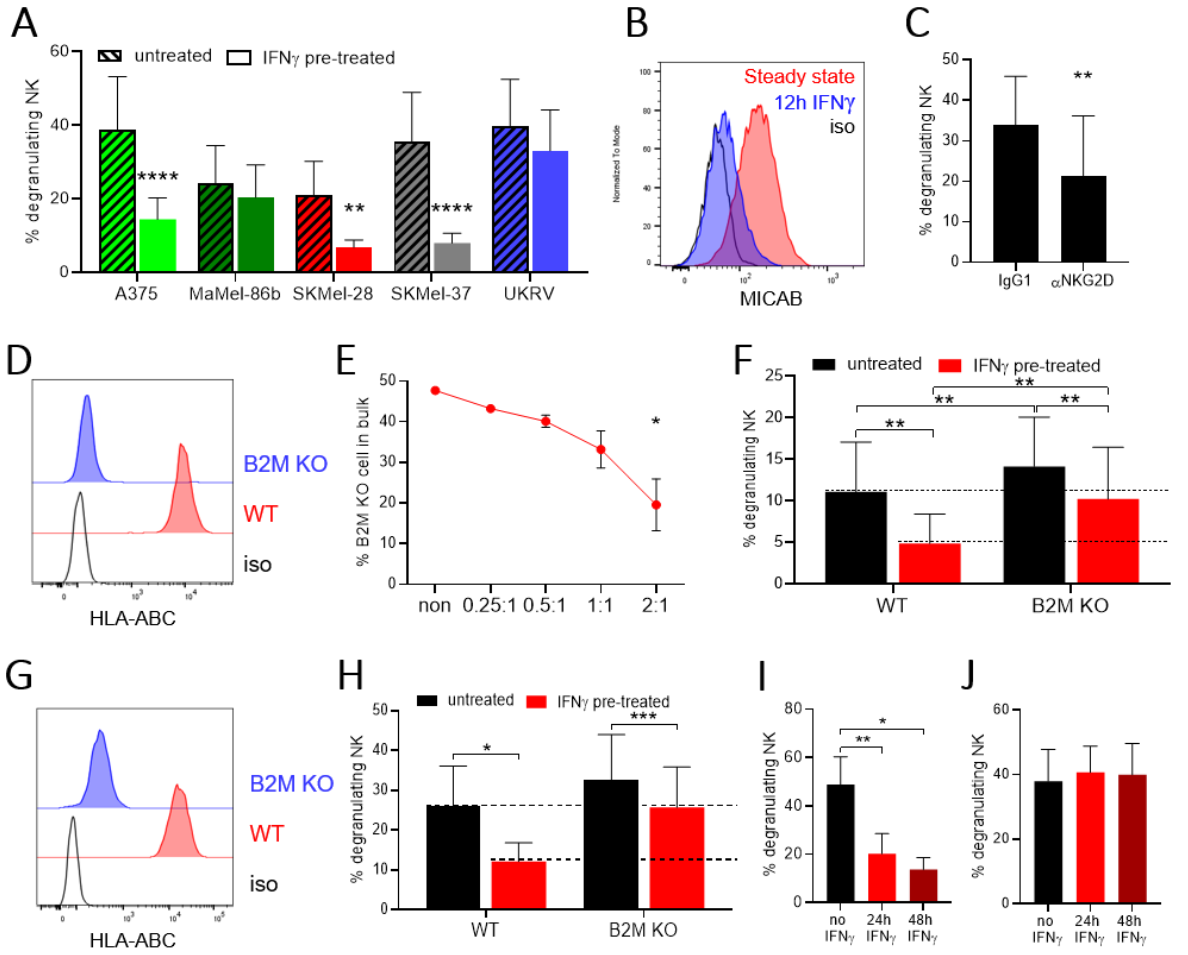

(Figure legend on the next page)

Figure 7.11 Effect of IFNγ pre-treatment of melanoma cell lines on NK cell function.
A) Degranulation of NK cells after 4-h co-culture with melanoma cell lines pre-treated or not with IFNγ 12 h before the co-culture. n=3 **B)** Histogram showing the expression of MICAB on A375 before and after 12 h IFNγ pre-treatment. **C)** Degranulation of NK cells after 4-h co-culture with A375 cells in the presence of mIgG1 or NKG2D blocking mAb. n=3 **D)** Histogram showing the expression of HLA-ABC on FACS-sorted B2M KO SKMel-28 cells. **E)** Reduction in SKMel-28 B2M KO cell population after 24-h co-culture of mixed WT:B2M KO cells (1:1) with NK cells at different E:T ratios. n=3 **F)** Degranulation of NK cells after 4-h co-culture with WT and B2M KO SKMel-28 cells pre-treated or not with IFNγ 12 h before the co-culture. n=9 **G)** Histogram showing the expression of HLA-ABC on FACS sorted B2M KO and WT SKMel-37 cells. **H)** Degranulation of NK cells after 4-h co-culture with WT and B2M KO SKMel-37 cells pre-treated or not with IFNγ 12 h before the co-culture. n=9 **I)** Degranulation of NK cells after 4-h co-culture with WT and B2M KO SKMel-37 cells pre-treated or not with IFNγ 48 h and 24 h before the co-culture. n=6 **J)** Degranulation of NK cells in presence of supernatant collected from IFNγ-pre-treated SKMel-37 cells. Cells were pre-treated with IFNγ for 24 and 48 h or left untreated, washed from the media containing IFNγ and cultured for 4 h in a fresh media. Media was then collected and used for the co-culture of NK cell with untreated SKMel-37 cells. Statistical analysis was performed by one-way ANOVA (multiple comparisons) test (A, E, F, H, I) and two-tailed Student's *t* test (C), p-value *<0.05, **<0.01, ***<0.001, ****<0.0001.

7.1.4 Role of HLA-E in melanoma cell resistance to NK cell cytotoxicity

I next compared the expression of classical and non-classical MHC-I on A375 cells after IFNγ pre-treatment. Besides HLA-ABC, only HLA-E and HLA-DR were partially expressed, but highly upregulated after 12 h of IFNγ pre-treatment (Figure 7.12 A). Since the expression of HLA-DR is independent of B2M, I focused on HLA-E, one of the candidates that significantly scored in GW CRISPR/Cas9 KO screen (Figure 7.12 B). HLA-E is a ligand for the inhibitory NKG2A and activating NKG2C receptor[174,175]. The expression of NKG2C was low/not detectable on NK cells, but the expression of NKG2A defined two NK cell subsets of $CD56^{dim}$ NK cells, while only one $CD56^{bright}$ $NKG2A^{+}$ NK cell subset (Figure 7.12 C, D). The degranulation of both $CD56^{dim}$ and $CD56^{bright}$ NK cells was reduced after IFNγ pre-treatment of melanoma cells (Figure 7.12 E, F). $NKG2A^{+}$ NK cells overall showed higher degranulation capacity in comparison to $NKG2A^{-}$ NK cells, but were both equally inhibited after co-culture with IFNγ-pre-treated melanoma cells (Figure 7.12 F).

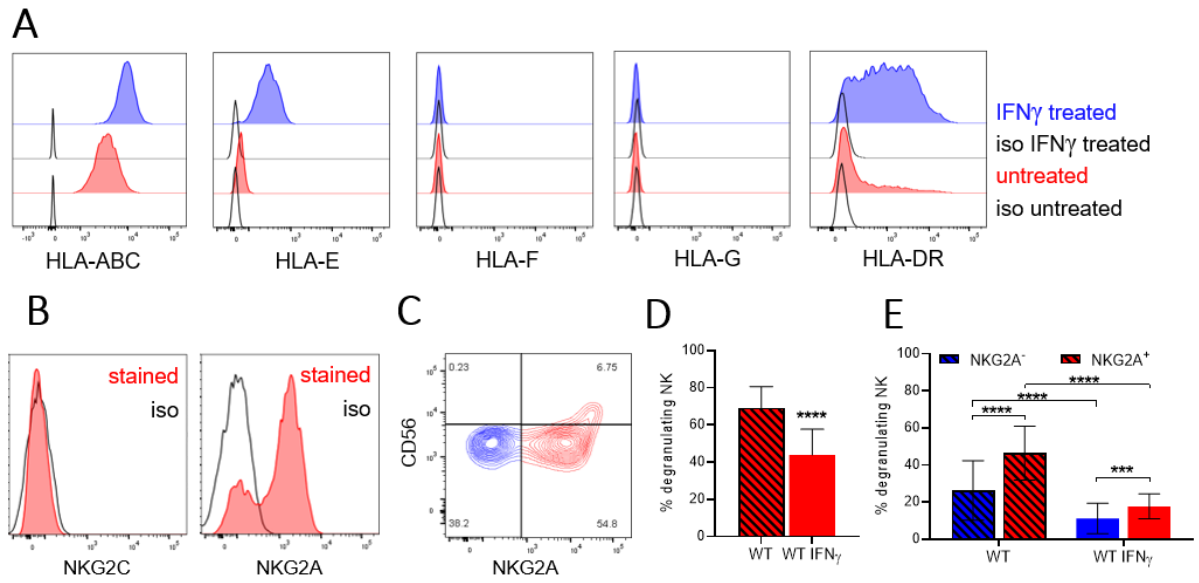

Figure 7.12 Effect IFNγ on the expression of MHC molecules.

A) Histogram showing the expression of MHC molecules before and after o/n IFNγ pre-treatment of A375 cells. **B)** Representative histograms showing the expression of NKG2C and NKG2A on NK cells. **C)** Histogram showing the expression of NKG2A on CD56 subsets of NK cells. **D, E)** Degranulation of D) $CD56^{bright}$ and E) $CD56^{dim}$ NKG2A NK cell subsets after 4-h co-culture with A375 cells pre-treated or not o/n with IFNγ before the co-culture. n=12 Statistical analysis was performed by one-way ANOVA (multiple comparisons) test (F) and two-tailed Student's *t* test (E), p-value ***<0.001, ****<0.0001.

I next focused on HLA-E, a potential candidate responsible for the IFNγ-mediated resistance of melanoma cells to NK cell killing. I pre-treated melanoma cells with IFNγ for 12, 24 and 48 h or left untreated and observed a rapid increase in surface HLA-E peaking at 12 h of IFNγ pre-treatment and rapid decline as the duration of IFNγ treatment increased, ultimately reaching a steady-state level after 48 h of IFNγ pre-treatment (Figure 7.13 A). To rule out the shedding of HLA-E as well as confirming the transcriptional or translational regulation of HLA-E as the underlying cause of its reduced surface expression, I determined the intracellular expression of HLA-E after IFNγ pre-treatment. The expression of intracellular HLA-E at the steady state was higher compared to the expression of HLA-E on cell surface, but displayed similar increased expression pattern and subsequent reduction in the expression of HLA-E upon > 12 h of IFNγ pre-treatment (Figure 7.13 B). When IFNγ-pre-treated melanoma cell were co-cultured with NK cells, the degranulation of $NKG2A^{+}$ NK cells was reduced at all timepoints of IFNγ pre-treatment with an increase of NK cell degranulation observed at later timepoints of IFNγ treatment alligning with the reduction of surface expression of HLA-E (Figure 7.13 C).

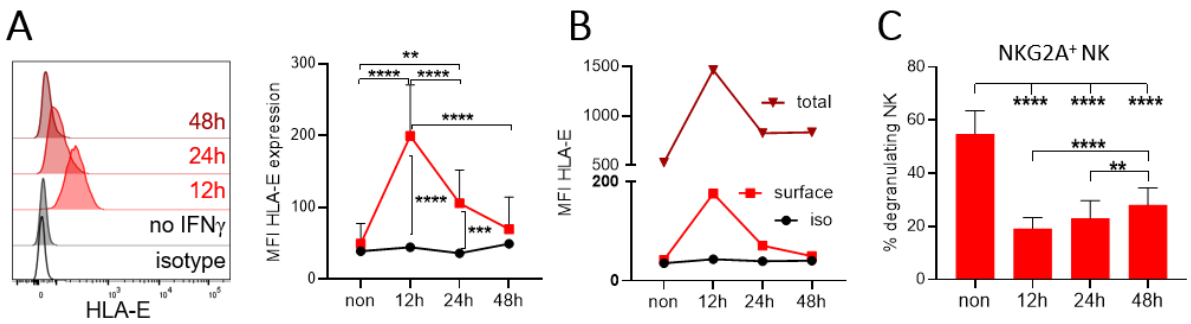

Figure 7.13 IFNγ induced transient expression of HLA-E on A375 cells.

A-B) The expression kinetics of HLA-E on A) surface + B) intracellular on untreated vs 12, 24 and 48 h IFNγ-pre-treated A375 cells. **C)** Degranulation of NKG2A$^+$ NK cells after 4-h co-culture with A375 cells pre-treated or not with IFNγ 12, 24 and 48 h before the co-culture. n=9 Statistical analysis was performed by one-way ANOVA (multiple comparisons) test (A, C) and two-tailed Student's *t* test (B, D), p-value **<0.01, ***<0.001, ****<0.0001.

To investigate whether the IFNγ-induced expression of HLA-E is responsible for the inhibition of NKG2A$^+$ NK cells, I generated the HLA-E KO A375 cell line (Figure 7.14 A). Similar to B2M KO cells, HLA-E KO cells displayed reduced resistance to NK cell killing after 24-h co-culture (Figure 7.14 B). The loss of *HLA-E* in IFNγ-pre-treated A375 cells also fully restored CD56^{bright} NK cells degranulation (Figure 7.14 C). However, the overall degranulation and IFNγ production of all (bulk) NK cells, was still partially inhibited after co-culture with HLA-E KO cells (Figure 7.14 D, E). As NKG2A is not uniformly expressed on all NK cells, I divided NK cell into NKG2A$^+$ and NKG2A$^+$ NK cell subsets. A minor inhibition of NKG2A$^+$ NK cell function was observed during co-culture with IFNγ-pre-treated HLA-E KO cells, while the strong inhibition of NKG2A$^-$ NK cells still remained (Figure 7.14 F). Together, these data show that IFNγ-mediated resistance of melanoma cells to NK cell cytotoxicity, is partially mediated by a transiently induced expression of HLA-E by IFNγ treatment resulting in the inhibition of NKG2A$^+$ NK cell subset. However, the sustained inhibition of NKG2A$^-$ NK cell function suggest the presence of an additional IFNγ-dependent mechanism contributing to NK cell inhibition.

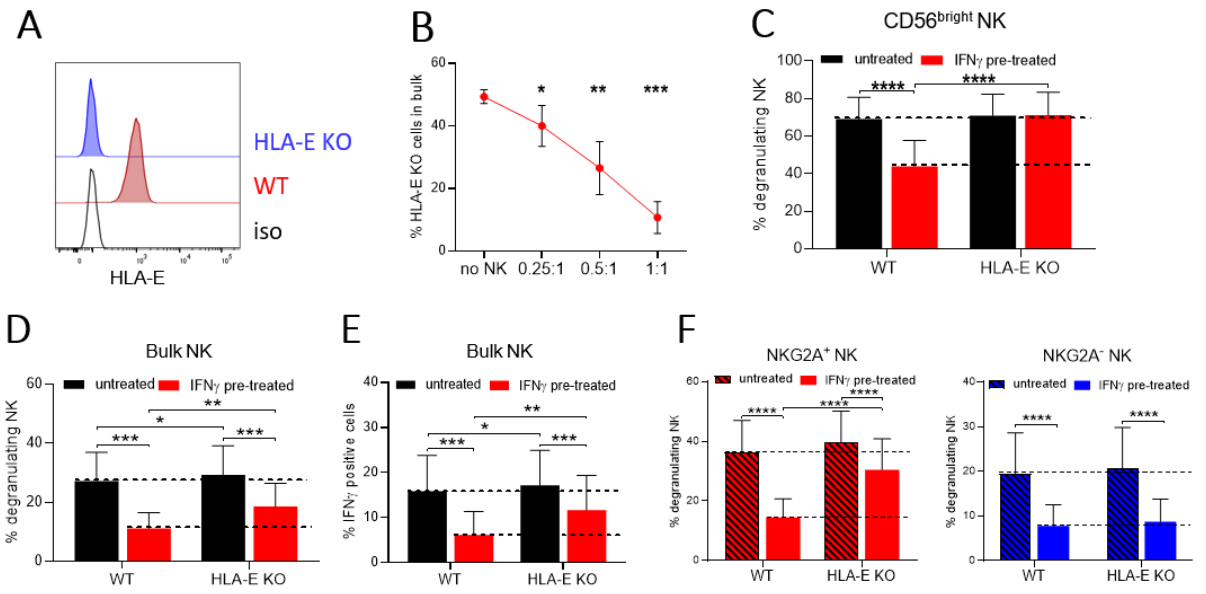

Figure 7.14 Effect of HLA-E on melanoma cell resistance to NK cell cytotoxicity

A) Histogram showing the expression of HLA-E on WT and HLA-E KO A375 cells pre-treated o/n with IFNγ. **B)** Reduction in HLA-E KO cell population after 24-h co-culture of NK cells with mixed WT:HLA-E KO cells (1:1) at different E:T ratios. n=6 **C-F)** Degranulation of C) $CD56^{bright}$ NK cells, D-E) degranulation and IFNγ production of bulk NK cells and F) degranulation of $NKG2A^+$ (red) and $NKG2A^-$ (blue) NK cell subsets after 4-h co-culture with WT or HLA-E KO A375 cells o/n pre-treated or not with IFNγ. n=11-14 Statistical analysis was performed by one-way ANOVA (multiple comparisons) test (B-F), p-value *<0.05, **<0.01, ***<0.001, ****<0.0001.

7.1.5 B2M-dependent inhibition of both NKG2A NK cell subsets

Previous findings have demonstrated that NK cells co-cultured with B2M KO cells display a nearly complete absence of inhibition after IFNγ pre-treatment of melanoma cells. Thus, I investigated the response both NKG2A NK cell subsets after co-culture with IFNγ-pre-treated WT and B2M KO cells. The absence of *B2M* from melanoma cells almost completely restored the function $NKG2A^+$ and $NKG2A^+$ NK cell subsets (Figure 7.15 A-B). I generated SKMel-37 HLA-E KO cell line to reproduce the effect of HLA-E on $NKG2A^+$ NK cell subset (Figure 7.15 C). The loss of *HLA-E* in the SKMel-37 cells similarly led to an increased degranulation of the $NKG2A^+$ NK cell subset, while no inhibition of both NKG2A NK cell subsets was observed after co-culture with B2M KO cells pre-treated with IFNγ (Figure 7.15 D). In summary, these data demonstrate that the inhibition of $NKG2A^+$ NK cells is primarily mediated by HLA-E, while the inhibition of both $NKG2A^+$ and $NKG2A^-$ NK cells after IFNγ pre-treatment of melanoma cell is dependent on expression of B2M by melanoma cells.

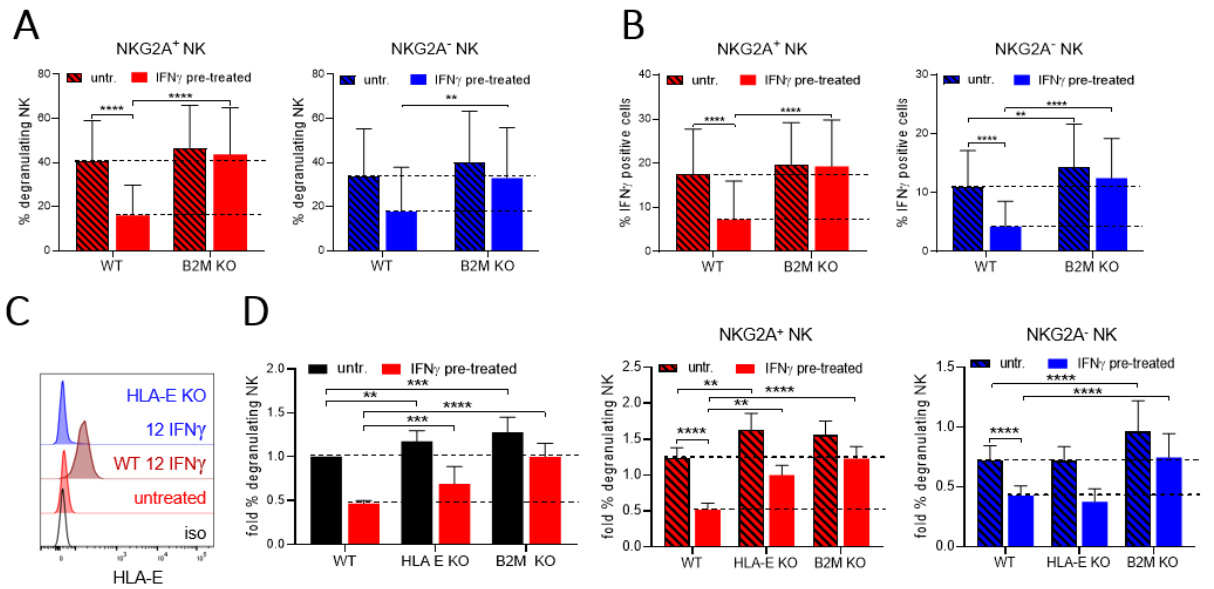

Figure 7.15 Inhibition of both NKG2A NK cell subsets by MHC-I.

A-B) Degranulation and IFNγ production of NKG2A$^+$ and NKG2A$^-$ NK cells after 4-h co-culture with WT and B2M KO A375 cells pre-treated or not with IFNγ for 12 h. n=9 **C)** Histogram showing the expression of HLA-E on WT and HLA-E KO SKMel-37 cells. **D)** Degranulation of Bulk (left), NKG2A$^+$ (red) and NKG2A$^-$ (blue) NK cells after 4-h co-culture with WT, HLA-E KO and B2M KO SKMel-37 cells pre-treated or not with IFNγ 12 h before the co-culture. Statistical analysis was performed by one-way ANOVA (multiple comparisons) test (A, B, D), p-value **<0.01, ***<0.001, ****<0.0001.

7.1.6 Inhibition of NKG2A$^-$ NK cells subsets.

Since in my previous experiments I used only NK cells that have been activated with IL-2 for 2 d, I compared unactivated (fresh) and 2-d IL-2-activated NK cells to observe if the IFNγ-mediated inhibition of NKG2A$^-$ NK cells is dependent on IL-2. Despite very low degranulation of unactivated NK cells, the inhibition of NKG2A$^-$ NK cells after co-culture with IFNγ-pre-treated melanoma cells was still apparent (Figure 7.16 A). To circumvent low degranulation of unactivated NK cells, I used the Cetuximab, mAb that induced high ADCC NK cell degranulation. However, IFNγ-pre-treated melanoma cells were still able to reduce ADCC-mediated degranulation of unactivated and IL-2-activated NKG2A$^-$ NK cells (Figure 7.16 A). I next focused on KIRs, the main inhibitory receptors for classical MHC-I. The expression of several members of KIR family is higher on NKG2A$^-$ NK cells compared to NKG2A$^+$ NK cells and also divides NK cells into two subsets, KIR$^-$ and KIR$^+$ NK cells (Figure 7.16 B). Regardless, the IFNγ pre-treatment of melanoma cells caused a reduction of NK cell degranulation across all NK cell subsets. The absence of B2M restored degranulation of both KIR$^-$ and KIR$^+$ NK cells across both NKG2A NK cell subsets (Figure 7.16 C).

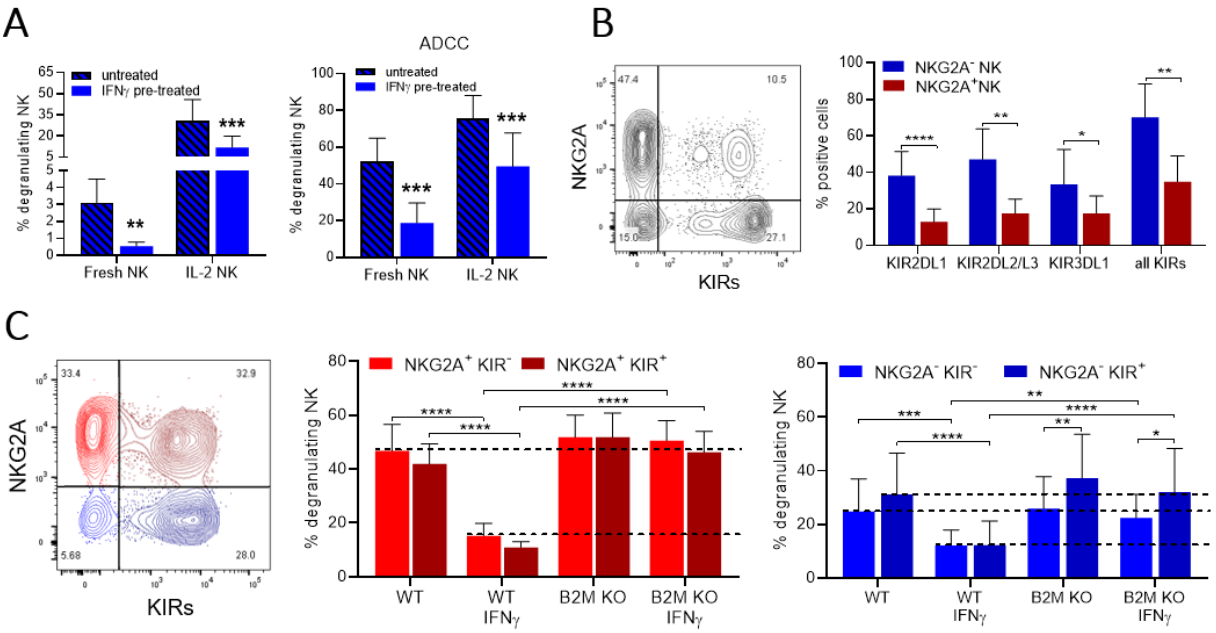

Figure 7.16 The expression of KIRs on NK cells.

A) Degranulation of unactivated (fresh) or 2-d IL-2-activated NKG2A$^-$ NK cells after 4-h co-culture with A375 cell pre-treated or not with IFNγ 12 h before the co-culture in the presence of hIgG1 (left) or Cetuximab mAb. n=6 **B)** Contour plot showing the expression of KIRs on 2-d IL-2-activated NKG2A$^-$ or NKG2A$^+$ NK cells. Ab against KIR2DL1/L2/L3/L4/L5 + KIR3DL1/L2/L3 were used for simultaneous staining of all KIRs. n=5-9 **C)** Representative contour plot showing 4 NK cell subsets based on the expression of NKG2A and KIRs and the corresponding degranulation of KIR$^+$ and KIR$^-$ NK cells in NKG2A NK cell subsets after 4-h co-culture with WT and B2M KO A375 cells pre-treated or not with IFNγ 12 h before the co-culture. n=6 Statistical analysis was performed by one-way ANOVA (multiple comparisons) test (A); two-way ANOVA (multiple comparisons) test (C) and two-tailed Student's *t* test (B), p-value *<0.05, **<0.01, ***<0.001, ****<0.0001.

In addition to KIRs, other MHC-I receptors have been identified on NK cells, such as ILT4 or ILT2. ILT4 is highly expressed on NK cells; however, blocking of ILT4 with mAb did not increase the degranulation of NKG2A$^-$ NK cells after IFNγ pre-treatment of melanoma cells (Figure 7.17 A, B). ILT2 defines two NK cell populations, ILT2$^+$ and ILT2$^-$ NK cells, with a higher expression observed on NKG2A$^-$ NK cells (Figure 7.17 C, D). The degranulation of all NK cell subsets, characterized by the expression of NKG2A and ILT2, was consistently suppressed after IFNγ pre-treatment of melanoma cells and was equally high after co-culture with B2M KO cells (Figure 7.17 E). Furthermore, blocking of ILT2 with two different blocking mAbs did not resulted in an increased NKG2A$^-$ NK cells degranulation after co-culture with IFNγ-pre-treated melanoma cells (Figure 7.17 F). Together, this data shows that the inhibition

of NKG2A$^-$ NK cells caused by IFNγ pre-treatment of melanoma cells occurs in both KIR$^-$ and KIR$^+$ NK cell subsets, regardless of the expression of NKG2A, and is absent during co-culture with B2M KO cells, suggesting a KIR-independent inhibitory pathway. Moreover, the blockade of other MHC-I receptors ILT2 and ILT4, expressed on NK cells, did not increase the degranulation of NKG2A$^-$ NK cells.

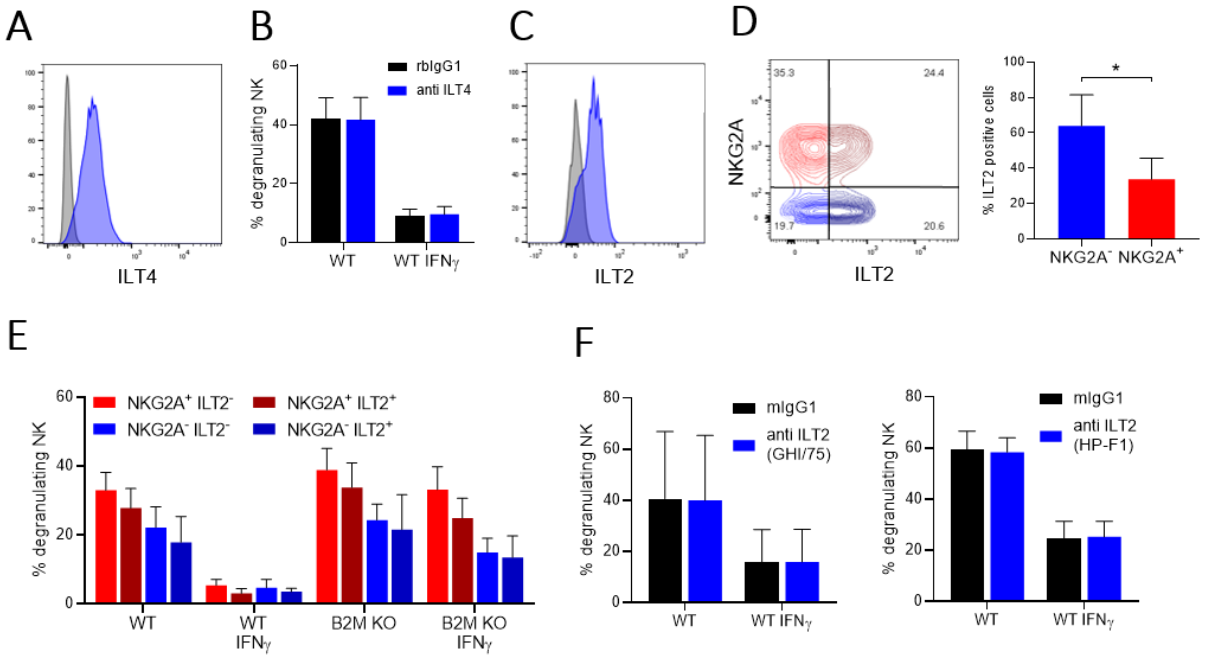

Figure 7.17 Role of ILT4 and ILT2 in the inhibition of NKG2A$^-$ NK cells.

A) Histogram showing the expression of ILT4 on 2-d IL-2-activated NK cells. **B)** Degranulation od NK cells after 4-h co-culture with A375 cells pre-treated or not with IFNγ 12 h before the co-culture in the presence of ILT4 blocking mAb. n=3 **C)** Histogram showing the expression of ILT2 on 2-d IL-2-activated NK cells. **D)** Representative contour plot and quantification of the expression of ILT2 on NKG2A$^+$ and NKG2A$^-$ NK cell subsets. n=5 **E)** Degranulation of ILT2/NKG2A NK cell subsets after 4-h co-culture with WT and B2M KO A375 cells pre-treated or not with IFNγ 12 h before the co-culture. n=3 **F)** Degranulation of NKG2A$^-$ NK cells 4-h co-culture with A375 cells pre-treated or not with IFNγ 12 h before the co-culture in the presence of two different ILT2 blocking mAb. n=3-6 Statistical analysis was performed by two-tailed Student's *t* test, p-value *<0.05.

7.1.7 Role of classical MHC-I in melanoma cells resistance to NK cell cytotoxicity

Since the results investigating the receptors responsible for the inhibition of NKG2A$^-$ NK cells remained unclear, I focused on individual classical MHC-I molecules expressed by A375 cells. According to A375 HLA genotype, I stained HLA molecules with corresponding allele specific antibodies (Figure 7.18 A-B). Surprisingly, only HLA-A molecules were

constitutively expressed, while HLA-B and HLA-C molecules were not expressed at the steady state. However, upon IFNγ treatment, all HLA molecules displayed upregulation, where HLA-A and HLA-B demonstrated a gradual increase in expression correlating with the duration of IFNγ pre-treatment. HLA-C displayed a transient expression similar as HLA-E with a peak of expression at 12 h post IFNγ treatment and a subsequent decline to low levels (Figure 7.18 B, C).

A

	Alleles	
HLA-A	01:01	02:01
HLA-B	57:01	44:03
HLA-C	16:02	06:02

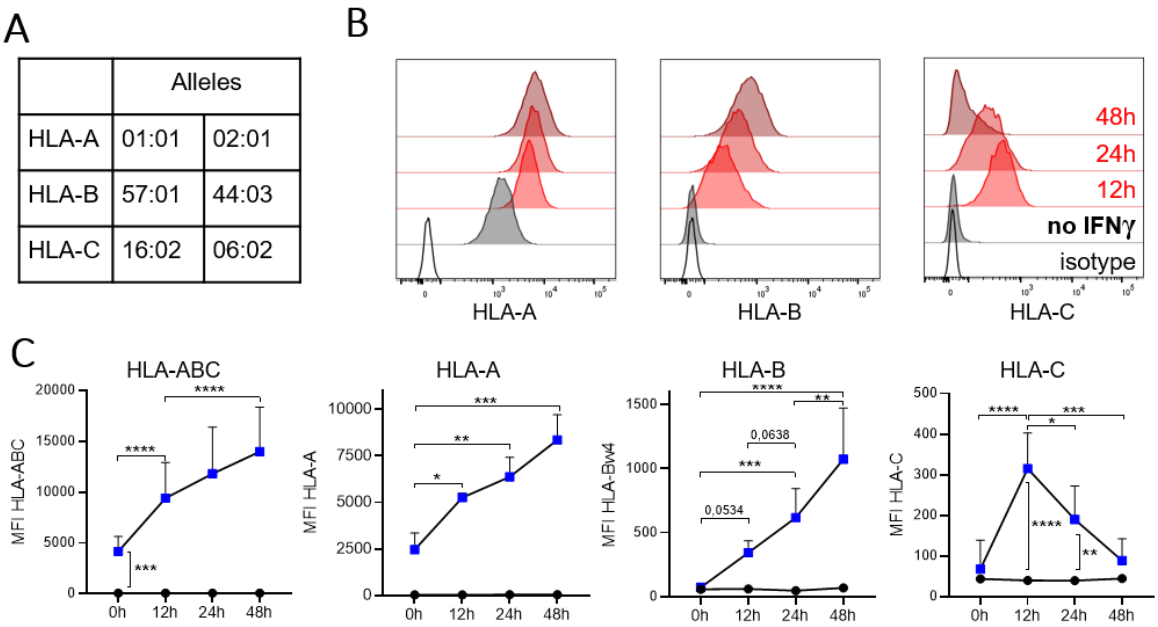

Figure 7.18 The expression of individual HLA molecules after IFNγ treatment

A) HLA alleles expressed by A375 cells. **B-C)** Histograms and MFI expression of HLA-A, HLA-B and HLA-C on A375 cells pre-treated or not with IFNγ for 12, 24 or 48 h before the co-culture. Statistical analysis was performed by one-way ANOVA (multiple comparisons) test (C) and two-tailed Student's *t* test (B, D), p-value *<0.05, **<0.01, ***<0.001, ****<0.0001.

To eliminate the potential influence of other molecules dependent on the expression of B2M, while confirming the role of classical MHC-I in mediating the inhibition of NKG2A$^-$ NK cells, I designed sgRNA targeting classical MHC-I molecules (Figure 7.19 A). The transfection HLA-ABC sgRNA into A375 cells resulted in nearly complete restoration of NKG2A$^-$ NK cells degranulation after IFNγ pre-treatment of melanoma cells (Figure 7.19 B). However, the loss of HLA-A, -B and -C also resulted in downregulation of HLA-E, since the peptides derived from the signal sequence of classical MHC-I are crucial for the expression of HLA-E[79,178]. Thus, the reduction of HLA-E in HLA-ABC KO cells also reduced the inhibition of NKG2A$^+$ NK cell subset degranulation.

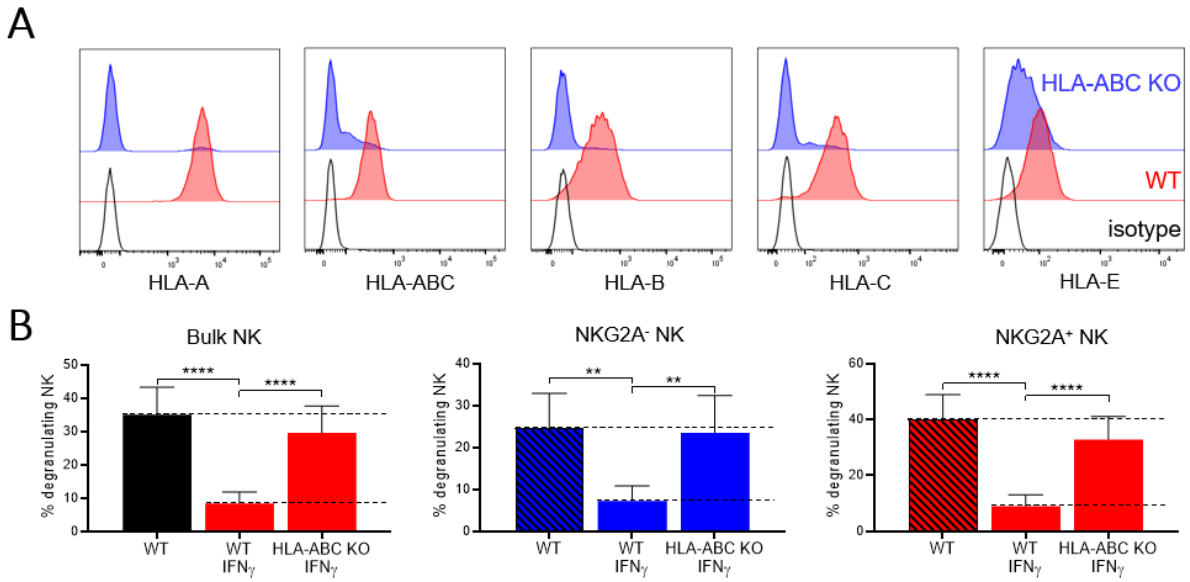

Figure 7.19 The effect of classical MHC-I on NK cell function

A) Histograms showing the expression of individual classical MHC-I molecules on WT and HLA-ABC KO A375 cells pre-treated o/n with IFNγ. **B)** Degranulation of bulk and NKG2A NK cell subsets after 4-h co-culture with WT and HLA-ABC KO A375 cells pre-treated or not with IFNγ 12 h before the co-culture. Statistical analysis was performed by one-way ANOVA (multiple comparisons) test (B), p-value **<0.01, ****<0.0001.

In parallel to HLA-ABC KO, I generated a TAP2 KO cell line, as TAP2 targeting sgRNAs were highly depleted in the GW CRISPR/Cas9 KO screen co-culture. Melanoma cells transfected with TAP2 sgRNA showed a reduced expression of HLA-ABC (Figure 7.20 A). During 24-h co-culture TAP2 KO cells showed reduced resisitance to NK cell killing in comparison to WT cells (Figure 7.20 B). Co-culture of A375 cells transfected with TAP2 sgRNA showed almost a no inhibition of degranulation in both NKG2A NK cell subsets after IFNγ pre-treatment of melanoma cells (Figure 7.20 C). Deletion of TAP2 reduced, but not abolished the expression of HLA-ABC at the steady state, when only HLA-A molecules are expressed (Figure 7.20 D). When individual HLA molecules were tested after 12 h of IFNγ pre-treatment, a mild reduction in the expression of HLA-A, abolished expression of HLA-B and HLA-C and reduced expression of HLA-E was observed in TAP2 KO cells (Figure 7.20 D). In summary, these findings collectively show the absence of IFNγ-mediated resistance of HLA-ABC KO and TAP2 KO melanoma cells to both NKG2A NK cell subsets. Moreover, A375 cells showed a robust expression of HLA-A, but absence of HLA-B and HLA-C at the steady-state conditions, which can be potently induced by IFNγ treatment.

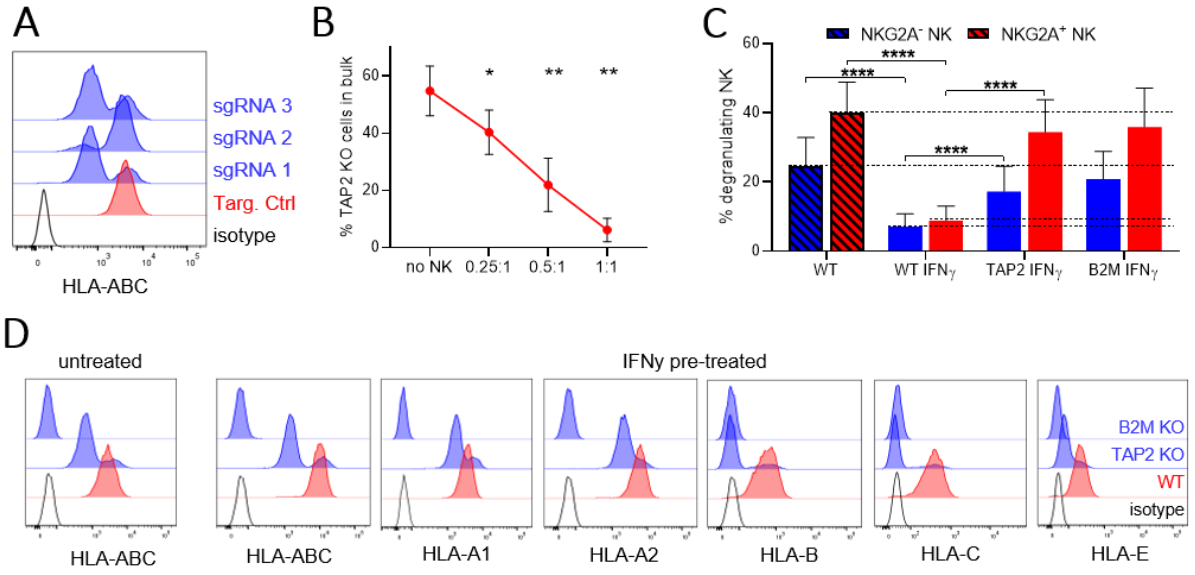

Figure 7.20 Deletion of TAP2 affects the expression of HLA molecules on melanoma cells and therefore the inhibition of NK cells.

A) Histogram showing the expression of HLA-ABC on A375 cells after transfection of 3 sgRNAs against the TAP2 gene. **B)** Resistance of TAP2 KO cells after 24-h co-culture of mixed WT/TAP2 KO cells (1:1) with NK cells at different E.T ratios. n=4-6 **C)** Degranulation of NKG2A NK cell subsets after 4-h co-culture with A375 cells transfected with TAP2 sgRNA #1 pre-treated or not with IFNγ 12 h before the co-culture. n=6 **D)** Histogram showing the expression of individual HLA molecules on WT and TAP2 sgRNA transfected A375 cells pre-treated or not with IFNγ 12 h before. Statistical analysis was performed by one-way ANOVA (multiple comparisons) test (B, C), p-value *<0.05, **<0.01, ****<0.0001.

The absence of IFNγ-mediated resistance of TAP2 KO cells to NK cells, which maintained relatively high expression of HLA-A, suggested a potentially low involvement of HLA-A in mediating the inhibition of NKG2A$^-$ NK cell subset. To exclude HLA-A as the mediator of IFNγ-mediated resistance of melanoma cells to NK cell killing, I transfected sgRNAs targeting HLA-A molecules into melanoma cells. SgRNA transfection resulted in the loss of expression of HLA-A2 in approximately 70% of melanoma cells. The subsequent IFNγ pre-treatment of HLA-A sgRNA transfected cells still induced potent inhibition of both NKG2A NK cell subsets (Figure 7.21 A, B). Unfortunately, the attempts for specific deletion of the other allele, HLA-A1, were unsuccessful (data not shown).

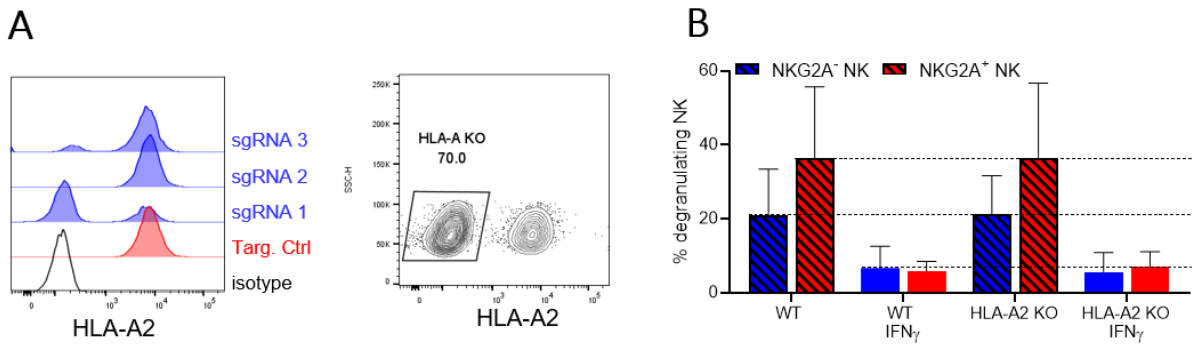

Figure 7.21 Degranulation of NKG2A NK cell subsets against the HLA-A2 KO A375 cells.
A) Histogram and dot plot showing the expression of HLA-A2 on A375 cells after transfection with HLA-A2 sgRNAs. **B)** Degranulation of NKG2A NK cell subsets after 4-h co-culture with A375 cells transfected with HLA-A2 sgRNA pre-treated or not with IFNγ 12 h before the co-culture. n=3

Next, I investigated the role of HLA-B and HLA-C molecules, given their abolished expression after *TAP2* deletion and their expression dependent on IFNγ. I transfected 4 sgRNAs targeting HLA-B into melanoma cells resulting in nearly complete depletion and a partial reduction in the expression of HLA-B depending on sgRNA (Figure 7.22 A). Subsequently, the co-culture of IFNγ-pre-treated HLA-B KO cells with NK cells showed in a slight reduction in the inhibition of the degranulation of NKG2A$^-$ NK cells, while the inhibition of NKG2A$^+$ NK cells was unchanged (Figure 7.22 B). Furthermore, no off-target activity of the sgRNAs used for generating HLA-B KO cells were observed, as the expression of other HLA molecules remained unchanged (Figure 7.22 B). The same steps were then repeated to generate HLA-C KO cells. Out of the four sgRNAs used, only two demonstrated a reduction in HLA-C expression (Figure 7.23 A). The loss of HLA-C induced more than 2 fold increase in the degranulation of NKG2A$^-$ NK cell against IFNγ-pre-treated melanoma cells (Figure 7.23 B). HLA-C KO cells also showed no changes in the expression other HLA molecules (Figure 7.23 C). To investigate the effect of HLA-B and HLA-C on the degranulation of NKG2A$^-$ NK cells, I generated HLA-BC double KO (dKO) cell line (Figure 7.23 D, E). The combined loss of HLA-B and HLA-C specifically increased the degranulation of NKG2A$^-$ NK cells against IFNγ-pre-treated melanoma cells, while having no effect on the degranulation of NKG2A$^+$ NK cells (Figure 7.23 F). Together, these data depicts HLA-C as the major contributor and HLA-B as a minor contributor to resistance of melanoma cells to NKG2A$^-$ NK cell cytotoxicity.

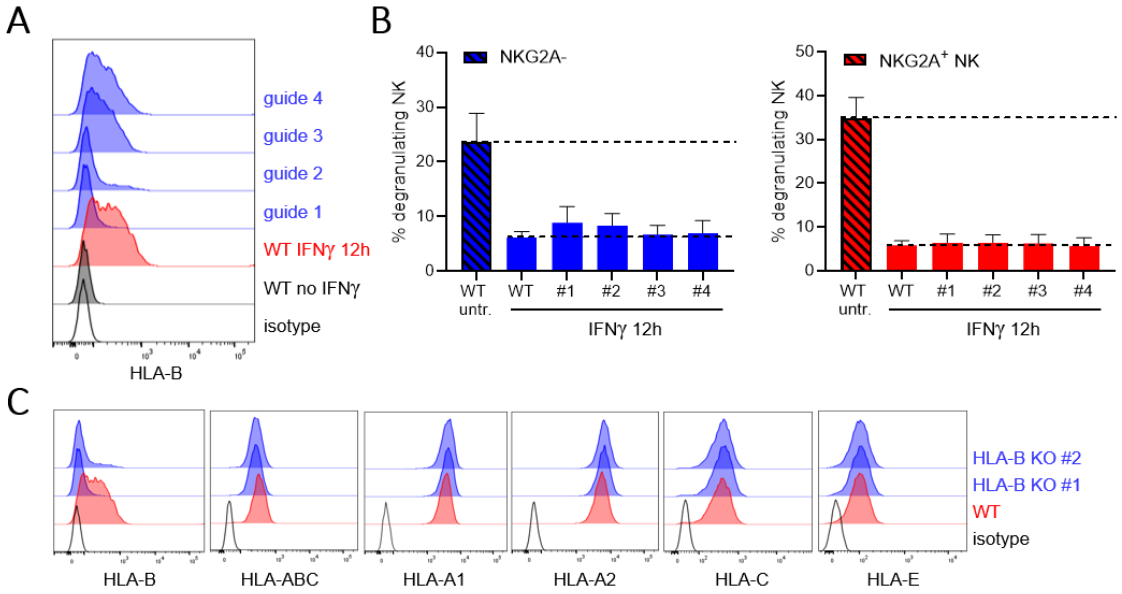

Figure 7.22 Degranulation of NKG2A NK cell subsets against the HLA-B KO A375 cells.

A) Histogram showing the expression of HLA-B on A375 cells transfected with HLA-B sgRNAs. **B)** Degranulation of NKG2A NK cell subsets after 4-h co-culture with A375 cells transfected with HLA-B sgRNAs pre-treated or not with IFNγ 12 h before the co-culture. n=3 **C)** Histogram showing the expression of individual HLA molecules on IFNγ pre-treated WT and HLA-B KO A375 cells for 12 h.

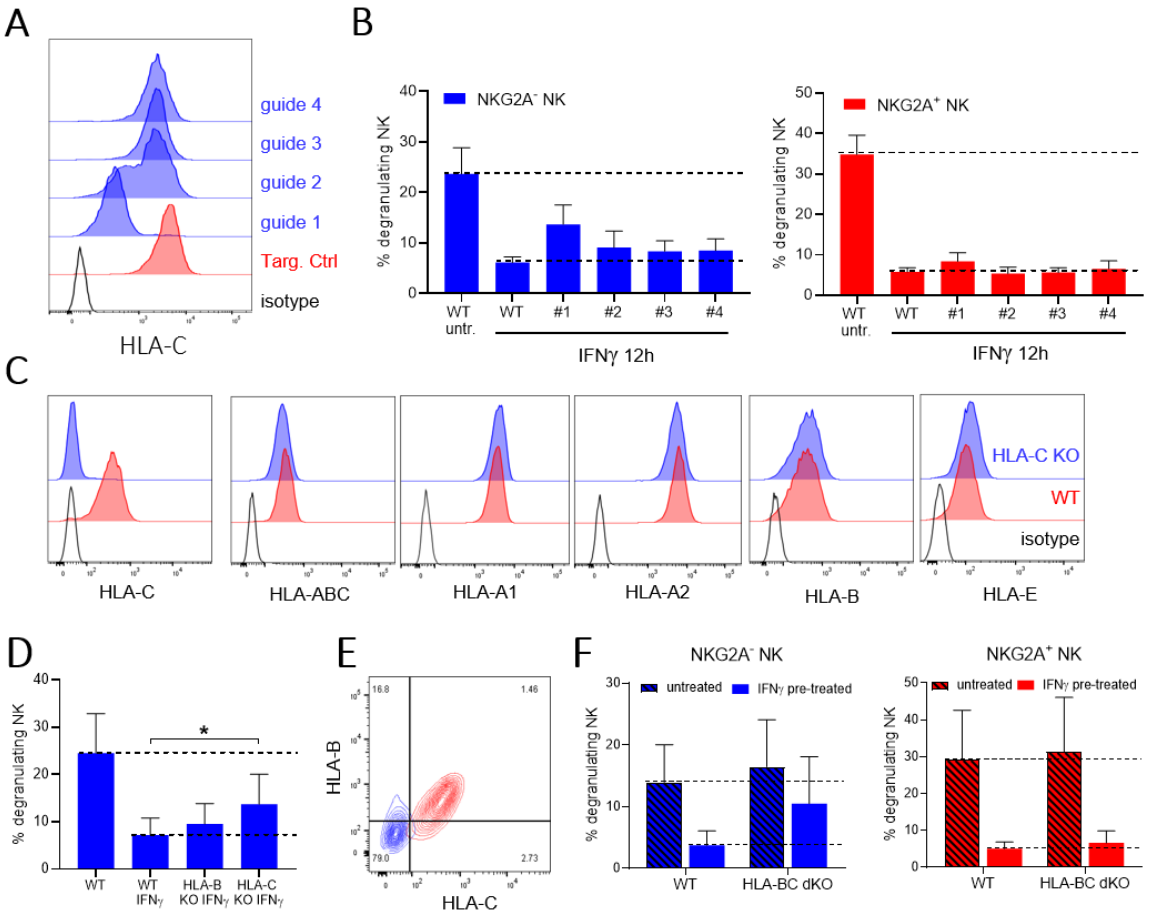

(Figure legend on the next page)

Figure 7.23 Degranulation of NK cells against the HLA-C KO and HLA-BC dKO A375 cells.
A) Histogram showing the expression of HLA-C on A375 cells transfected with sgRNAs targeting HLA-C. **B)** Degranulation of NKG2A NK cell subsets after 4-h co-culture with A375 cells transfected with HLA-C sgRNAs pre-treated or not with IFNγ 12 h before the co-culture. n=3 **C)** Histogram showing the expression of individual HLA molecules on WT and HLA-C KO A375 cells after 12 h of IFNγ pre-treatment. **D)** Degranulation of $NKG2A^-$ NK cells after 4-h co-culture with WT, HLA-B KO and HLA-C KO A375 cells pre-treated or not with IFNγ 12 h before the co-culture. n=3 **E)** Contour plot showing the expression of HLA-B and HLA-C on WT and HLA-BC dKO cells after 12 h of IFNγ pre-treatment. **F)** Degranulation of NKG2A NK cell subsets after 4-h co-culture with HLA-BC dKO A375 cells pre-treated or not with IFNγ 12 h before the co-culture. n=3 Statistical analysis was performed by two-tailed Student's *t* test (D), p-value *<0.05.

Given that the major receptors for HLA-B and HLA-C are KIRs, I co-stained all KIRs together with NKG2A to focus on 4 well-defined individual NK cell subsets. To directly compare the effect of individual MHC-I molecules on NK cell function, I used WT, HLA-E KO, HLA-BC dKO and B2M KO cells in one assay. All NKG2A/KIRs NK cell subsets showed potent reduction in degranulation after IFNγ pre-treatment of melanoma cells (Figure 7.24 A). Within these NK cell subsets, the degranulation of $NKG2A^+$ KIR^- NK cells demonstrated no inhibition after co-culture with HLA-E KO and B2M KO cells. However, $NKG2A^+$ KIR^+ NK cells still exhibited a partial inhibition of degranulation after the co-culture with HLA-E KO cells but no inhibition after co-culture with B2M KO cells. The degranulation of $NKG2A^-$ KIR^+ NK cells showed only partial inhibition after co-culture with HLA-BC dKO and B2M KO cells in comparison to high inhibition observed against IFNγ-pre-treated WT cells. The degranulation $NKG2A^-$ KIR^- NK cells remained inhibited by IFNγ pre-treatment of melanoma cells, except in B2M KO cell condition, where only a partial inhibition remained present. Surprisingly, $NKG2A^+$ KIR^+ cells still remained highly inhibited after co-culture with IFNγ-pre-treated HLA-BC dKO cells, despite the expression of KIRs (Figure 7.24 A). Collectively, these data show a different regulation of NK cell degranulation by classical and non-classical MHC-I molecules depending on the expression of NKG2A and KIRs.

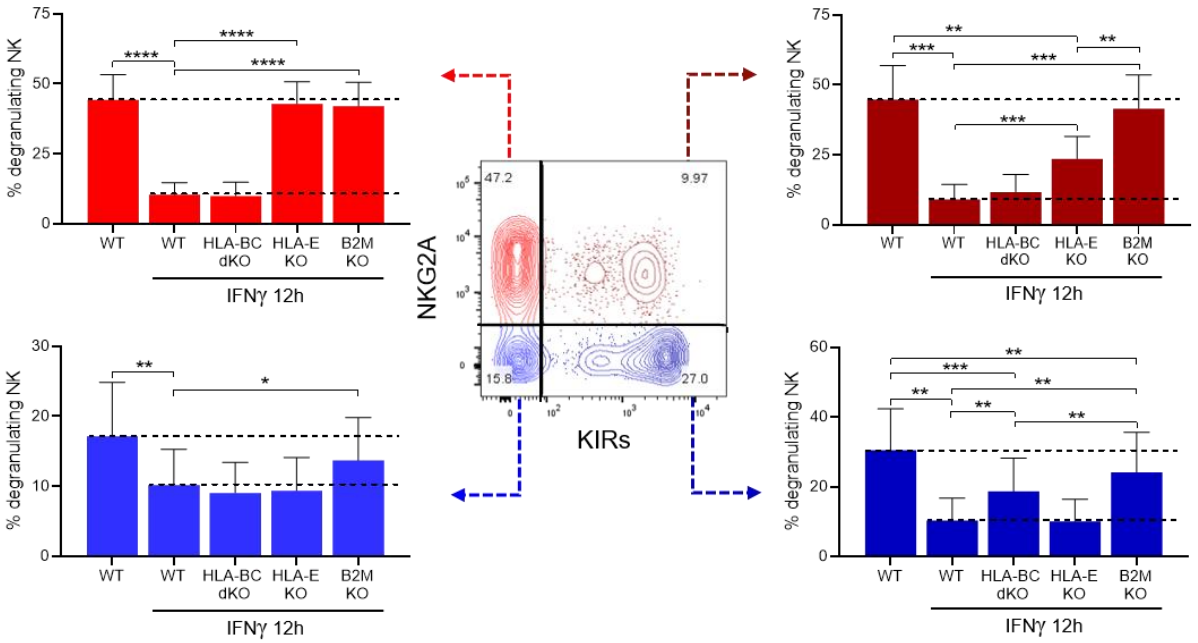

Figure 7.24 Degranulation of NKG2A/KIRs NK cell subsets against the HLA-E KO, HLA-BC dKO and B2M KO A375 cells.

Degranulation of NKG2A/KIRs NK cell subsets after 4-h co-culture with WT, HLA-E KO, HLA-BC dKO and B2M KO cells pre-treated or not for 12 h with IFNγ. n=4 Statistical analysis was performed by one-way ANOVA (multiple comparisons) test, p-value *<0.05, **<0.01, ***<0.001, ****<0.0001.

I next focused on regulation of NKG2A$^+$ KIR$^+$ NK cell function due to the different effect of HLA-BC on the degranulation of NKG2A$^-$ KIR$^+$ and NKG2A$^+$ KIR$^+$ NK cells. I first investigated the origin of NKG2A$^+$ KIR$^+$ NK cells. The expression of KIRs on freshly isolated and 2-d IL-2-activated NK cells is lower on NKG2A$^+$ NK cells compared to high expression on NKG2A$^-$ NK cells (Figure 7.16 B, 7.25 A). However, during NK cell expansion in IL-2-containing media, the expression of NKG2A increases on NK cells, reaching >90% NKG2A$^+$ NK cells at d9 of expansion (Figure 7.25 A). The reduction of NKG2A$^-$ KIR$^+$ NK cell population is accompanied with an increased population of NKG2A$^+$ KIR$^+$ NK cells (Figure 7.25 A). To confirm that NKG2A$^+$ KIR$^+$ NK cells originate from NKG2A$^-$ KIR$^+$ NK cells by upregulating the NKG2A, I isolated NKG2A$^-$ NK cells and subsequently expanded in IL-2-containing media. After 6 d of expansion, NKG2A$^-$ NK cells that have proliferated showed upregulation of NKG2A (Figure 7.25 B, C). The upregulation of NKG2A occurred in both KIR$^-$ and KIR$^+$ NK cells and resulted in a higher degranulation capacity in comparison to NKG2A$^-$ NK cells (Figure 7.25 D, E). Taken together, these data confirm that NKG2A is upregulated during NK cell proliferation, thus, during the NK cell expansion, NKG2A$^+$ KIR$^+$ NK cells originate from NKG2A$^-$ KIR$^+$ NK cells.

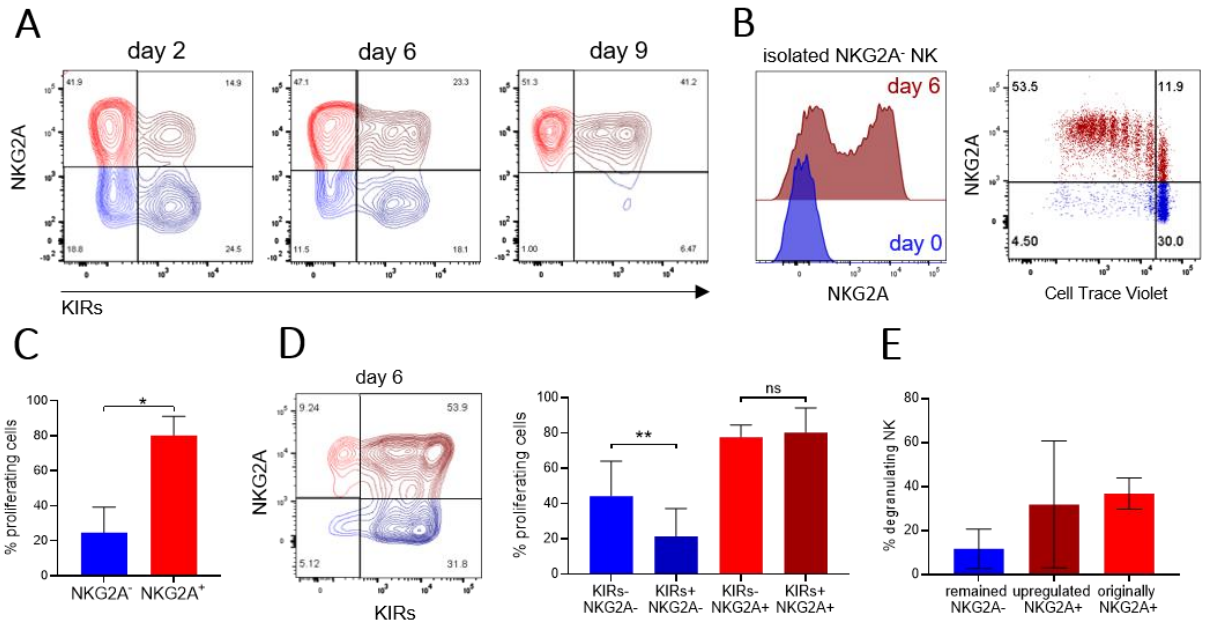

Figure 7.25 NKG2A$^-$ NK cells upregulate NKG2A during proliferation.

A) Representative contour plots showing the composition of NKG2A/KIRs NK cell subsets at day 0, 6 and 9 during the course of expansion in IL-2 containing media. **B)** Histogram showing the expression of NKG2A on isolated NKG2A$^-$ NK cells at d0 and d6 of culture in IL-2-containing media (left). Dot plot showing the expression of NKG2A and Cell Trace Violet proliferation staining on 6-d expanded NKG2A$^-$ NK cells. **C)** Proliferation of NKG2A NK cell subsets after 6 d of NKG2A$^-$ NK cells expansion. n=3 **D)** Contour plot showing the expression of NKG2A and KIRs on 6-d expanded NKG2A$^-$ NK cells. **E)** Degranulation of isolated NKG2A$^-$ NK cells that did or did not upregulated NKG2A and originally NKG2A$^+$ NK cells after 4-h co-culture with A375 cells. NKG2A$^-$ and NKG2A$^+$ NK cell were isolated and expanded for 6 d. n=2 Statistical analysis was performed by one-way ANOVA (multiple comparisons) test (D) and two-tailed Student's *t* test (C), p-value *<0.05, **<0.01.

Having confirmed that NKG2A$^+$ KIR$^+$ NK cells originate from NKG2A$^-$ KIR$^+$ NK cells, I next investigated why the loss of *HLA-BC* was insufficient to enhance the degranulation of NKG2A$^+$ KIR$^+$ NK cells. To test whether the potency of NKG2A might override the inhibitory signaling from KIRs, I transfected HLA-BC dKO cells with HLA-E sgRNA, which resulted in a high percentage of HLA-BCE triple KO (tKO) cells (Figure 7.26 A). Focusing primarily on the NKG2A$^+$ KIR$^+$ NK cell subset, I expanded NK cells for 9 d, ensuring that the majority of NKG2A$^-$ NK cells underwent proliferation and upregulated NKG2A (Figure 7.26 B). Subsequently, I co-cultured expanded NK cells with IFNγ-pre-treated melanoma cells harbouring deletions in MHC-I genes. The degranulation of NKG2A$^+$ KIR$^+$ NK cell was still highly inhibited after co-culture with HLA-BC dKO cells, despite no inhibition of

degranulation observed in residual NKG2A$^-$ KIR$^+$ NK cells against IFNγ-pre-treated HLA-BC dKO cells (Figure 7.26 B). However, the degranulation of NKG2A$^+$ KIR$^+$ NK cells against unsorted HLA-BCE tKO cells displayed much smaller inhibition in comparison to HLA-E KO cells. In summary, HLA-E and HLA-BC act synergistically in inhibiting the degranulation of NKG2A$^+$ KIR$^+$ NK cells, in which the potency of inhibitory signaling coming from NKG2A prevail over the signaling from KIRs.

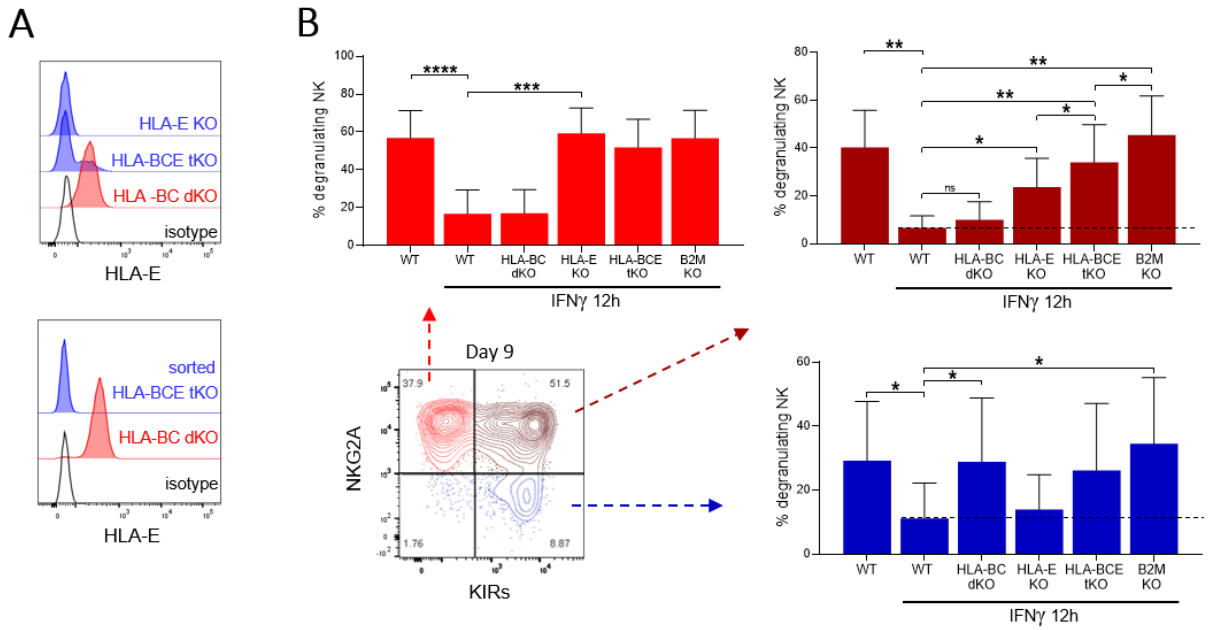

Figure 7.26 The degranulation of expanded NK cells against A375 KO cells.

A) Histograms showing the expression of HLA-E on WT, HLA-BC dKO, unsorted/sorted HLA-BCE tKO and HLA-E KO A375 cells. **B)** Degranulation of 9-d IL-2-activated NKG2A/KIRs NK cell subsets after 4-h co-culture with WT, HLA-BC dKO, HLA-E KO, unsorted HLA-BCE tKO and B2M KO A375 cells. n=8 Statistical analysis was performed by one-way ANOVA (multiple comparisons) test, p-value *<0.05, **<0.01, ***<0.001, ****<0.0001.

7.1.8 Blockade of NKG2A and KIRs by therapeutic mAb

Next step was to put data into a context of a potential therapy. I used monalizumab, a therapeutic anti-NKG2A mAb used in clinical trials[180,537–539]. Monalizumab effectively blocked NKG2A and prevented the separation into NKG2A subsets by flow cytometry (Figure 7.27 A). Nevertheless, monalizumab treatment increased the overall NK cell degranulation after co-culture with IFNγ-pre-treated melanoma cells to similar extend observed in co-culture with HLA-E KO cells (Figure 7.27 B). To investigate its effect on NKG2A$^+$ KIR$^+$ NK cells, 9 d expanded NK cells were co-cultured with melanoma cells in the presence of monalizumab

mAb. In line with the data obtained during NK cell co-culture with HLA-E KO cells, monalizumab treatment partially restored the degranulation of NKG2A$^+$ KIR$^+$ NK cells, while completely restoring the degranulation of NKG2A$^+$ KIR$^-$ NK cells against IFNγ-pre-treated melanoma cells (Figure 7.27 B). Monalizumab treatment in combination with HLA-BC dKO cells almost completely restored the degranulation of NKG2A$^+$ KIR$^+$ NK cells.

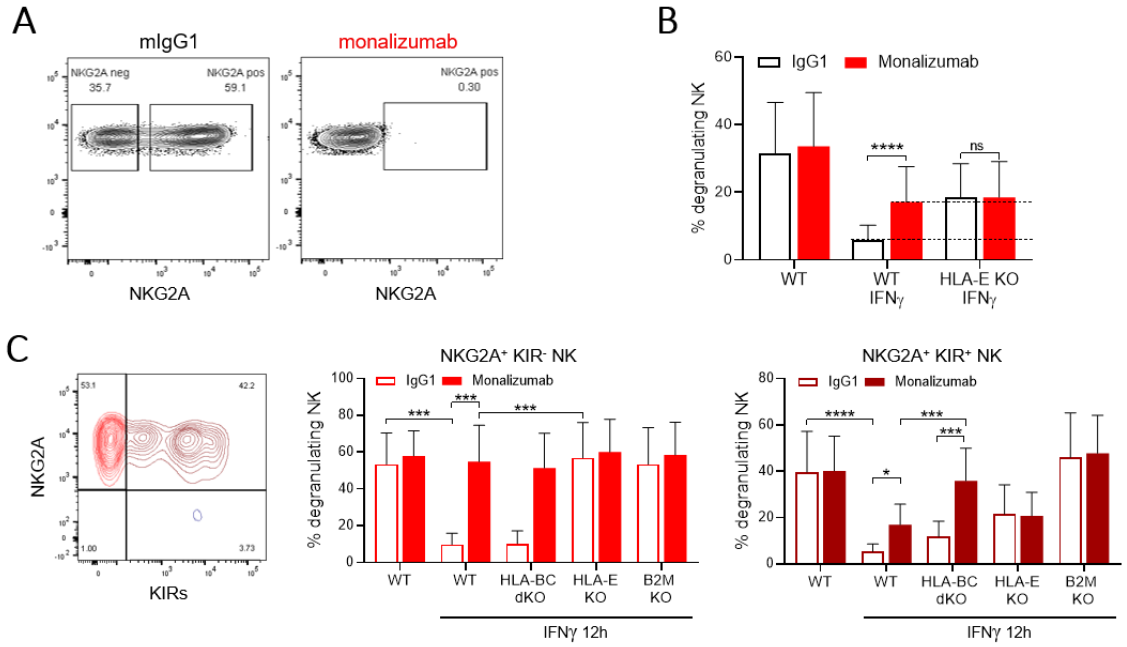

Figure 7.27 Blocking of NKG2A by therapeutic monalizumab mAb.

A) Representative contour plot showing the detection of NKG2A on NK cells treated with monalizumab or mIgG1 (5ug/ml) mAbs and stained with flourochrome-conjugated mAbs to detect the expression of NKG2A by flow cytometry. **B)** Degranulation of 9-d expanded NK cells after 4-h co-culture with WT and HLA-E KO A375 cells pre-treated or not with IFNγ 12 h before the co-culture in the presence of mIgG1 or monalizumab mAb. n=5 **C)** Representative contour plot showing the expression of NKG2A and KIRs on 9-d expanded NK cells and a corresponding degranulation after 4-h co-culture with WT, HLA-BC dKO, HLA-E KO and B2M KO A375 cells pre-treated or not with IFNγ 12 h before 4-h co-culture in the presence of mIgG1 or monalizumab mAb. n=3 Statistical analysis was performed by one-way ANOVA (multiple comparisons) test, p-value *<0.05, **<0.01, ****<0.0001.

As the previous data did not definitively confirm or exclude the involvement of KIRs in mediating the inhibition of NK cells, I used lirilumab, a therapeutic anti-KIR2DL1/L2/L3 mAb. The detection of all KIRs on NK cells following lirilumab treatment was not entirely abolished but rather reduced, as lirilumab specifically blocked only KIR2DL1, KIR2DL2, and KIR2DL3 (Figure 7.28 A). Lirilumab treatment increased the degranulation of NKG2A$^-$ NK cells after co-culture with IFNγ-pre-treated WT melanoma cells but not with HLA-BC dKO cells (Figure

7.28 B). The degranulation of NKG2A$^+$ KIR$^+$ NK cells was increased only in conditions where lirilumab together with HLA-E KO cells was used, thus confirming the involvement of KIRs in the inhibition of KIR$^+$ NK cells via classical MHC-I molecules (Figure 7.28 C).

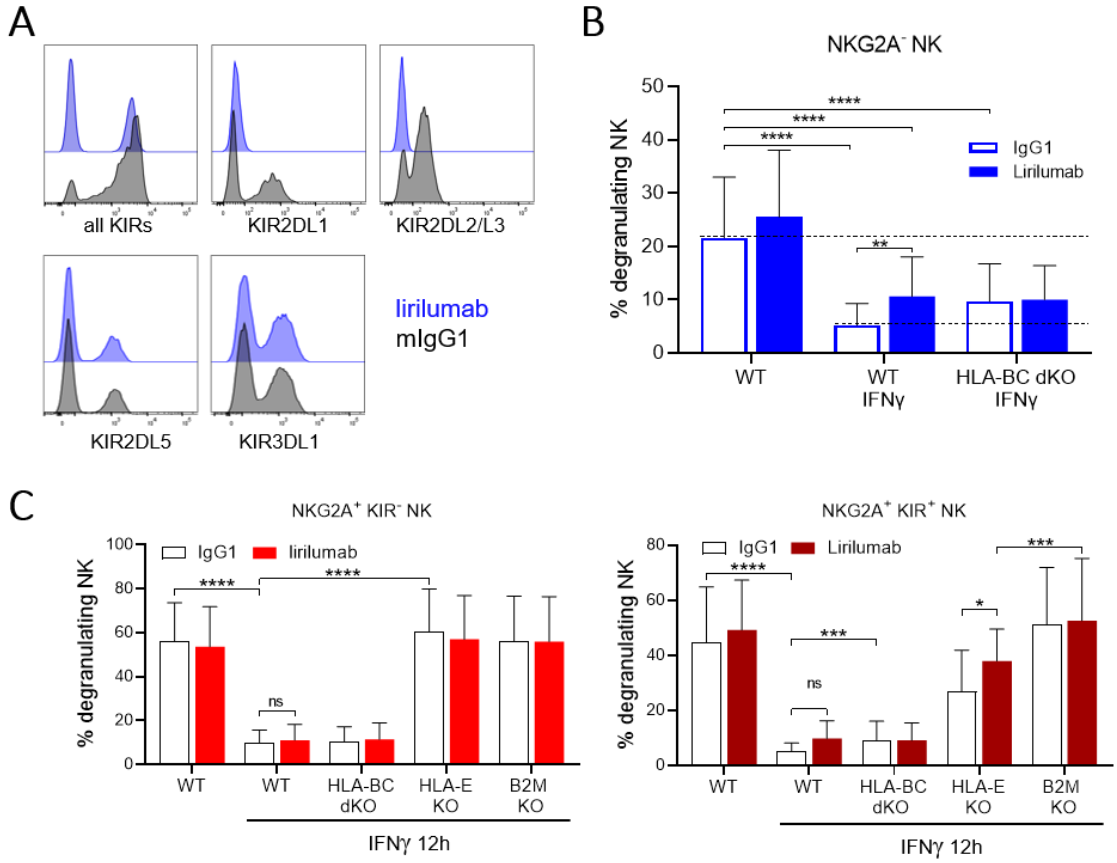

Figure 7.28 Blocking of KIRs by therapeutic lirilumab mAb.

A) Histograms showing the blocking effect lirilumab mAb on KIRs expressed on NK cells. **B)** Degranulation of bulk NK cells after 4-h co-culture with WT and HLA-BC dKO A375 cells pre-treated or not with IFNγ before the co-culture in the presence of mIgG1 or lirilumab mAb. n=6 **C)** Degranulation of 9-d expanded NKG2A/KIRs NK cell subsets after 4-h co-culture with WT, HLA-BC dKO, HLA-E KO and B2M KO A375 cells pre-treated or not with IFNγ before the co-culture in the presence of mIgG1 or lirilumab mAb. n=3 Statistical analysis was performed by one-way ANOVA (multiple comparisons) test, p-value *<0.05, **<0.01, ***<0.001, ****<0.0001.

Next, I combined monalizumab and lirilumab treatment to investigate their effect in restoring the degranulation of NK cells. As expected, simultaneous blocking of NKG2A and KIRs with monalizumab and lirilumab mAbs did not increase the degranulation of NK cells after co-culture with IFNγ untreated melanoma cells. However, it enhanced the degranulation of NK cells after co-culture with IFNγ-pre-treated melanoma cells, reaching a level comparable to that seen in B2M KO cells conditions (Figure 7.29 A). The monalizumab treatment had the

highest impact on restoring the overall degranulation of NK cells, since it restored highly cytotoxic CD56^{bright} and NKG2A^{+} CD56^{dim} NK cell subsets (Figure 7.29 A, B). Combined monalizumab and lirilumab treatment also highly restored the degranulation of NKG2A^{+} KIR^{+} NK cells to comparable levels as observed after co-culture with HLA-BCE tKO cells (Figure 7.29 C). However, monalizumab and lirilumab treatment did not completely abolished the inhibition of NKG2A^{+} KIR^{+} NK cells after IFNγ pre-treatment of melanoma cells (Figure 7.29 C). In conclusion, these data show that NKG2A and KIRs can be efficiently blocked by treatment with monalizumab and lirilumab mAbs and restore NK cell degranulation against IFNγ-pre-treated melanoma cells.

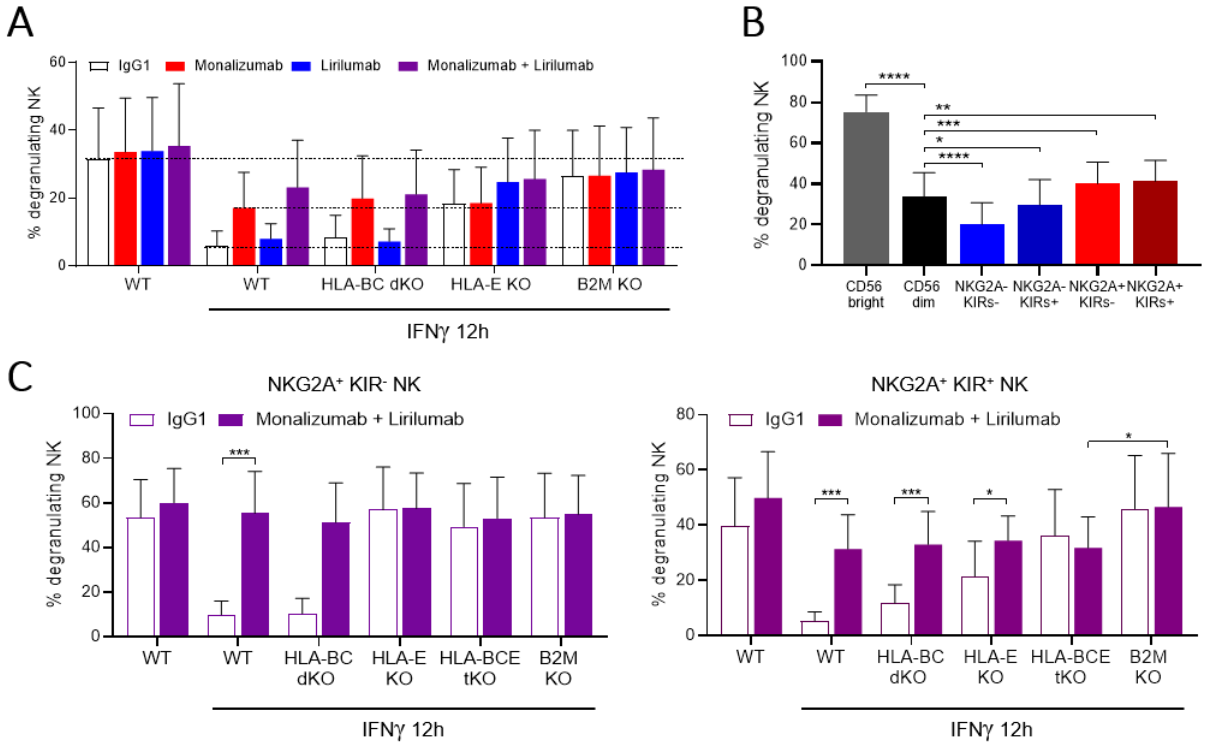

Figure 7.29 Combined blockade of NKG2A and KIRs by monalizumab and lirilumab mAbs.

A) Degranulation of NK cell after 4-h co-culture with WT, HLA-BC dKO, HLA-E KO and B2M KO A375 cells pre-treated or not with IFNγ 12 h before the co-culture in the presence of mIgG1, monalizumab, lirilumab or combined monalizumab and lirilumab mAbs. n=5 **B)** Degranulation of NK cell subsets defined by the expression of CD56, NKG2A and KIRs after 4-h co-culture with WT A375 cells. n=15 **C)** Degranulation of 9-d expanded NKG2A^{+} KIR^{-} and NKG2A^{+} KIR^{+} NK cell subsets after 4-h co-culture with WT, HLA-BC dKO, HLA-E KO, HLA-BCE tKO and B2M KO A375 cells pre-treated or not with IFNγ 12 h before the co-culture in the presence of mIgG1 or combined monalizumab and lirilumab blocking mAbs. n=3 Statistical analysis was performed by one-way ANOVA (multiple comparisons) test, p-value *<0.05, **<0.01, ***<0.001, ****<0.0001.

In line with a previous data, I investigated the effect of monalizumab and lirilumab on the resisitance of melanoma cells to NK cell killing during 24-h co-culture. I FACS sorted NKG2A$^+$ KIR$^+$ NK cells from expanded NK cells that were subsequently used for 24-h co-culture with mixed WT:B2M KO cells in the presence of mIgG1, monalizumab, lirilumab or monalizumab with lirilumab (Figure 7.30 A). Single treatment of NK cells with mAb only slightly increased the proportions of B2M KO cell population, but combined treatment highly reduced the resisitance of WT cells and the preferential killing of B2M KO cells (Figure 7.30 B). However, a substantial reduction in B2M KO cell population was still apparent after combined monalizumab/lirilumab treatment (Figure 7.30 B). The low efficiency of a single mAb treatment was also confirmed during 4-h co-culture, where only a minor increase in the degranulation of NKG2A$^+$ KIR$^+$ NK cells against IFNγ-pre-treated melanoma cells was observed (Figure 7.30 B). Accordingly, only combined monalizumab or lirilumab treatment highly increased NKG2A$^+$ KIR$^+$ NK cells degranulation, however not to the levels observed in co-culture with B2M KO cells (Figure 7.30 C).

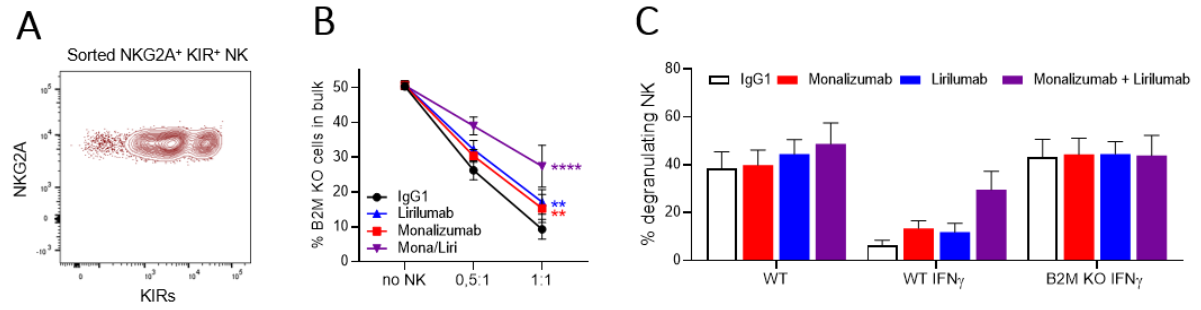

Figure 7.30 Effect of monalizumab/lirilumab treatment on NKG2A$^+$ KIR$^+$ NK cell activity.

A) Representative contour plot showing the expression of KIRs on FACS sorted NKG2A$^+$ KIR$^+$ NK cells used for subsequent assays. **B)** Reduction in B2M KO cell population after 24-h co-culture of mixed WT:B2M KO cells (1:1) with FACS sorted NKG2A$^+$ KIR$^+$ NK cells at different E:T ratios in the presence of mIgG1, monalizumab, lirilumab or monalizumab and lirilumab mAb. n=6 **C)** Degranulation of NKG2A$^+$ KIR$^+$ NK cells after 4-h co-culture with WT and B2M KO A375 cells pre-treated or not with IFNγ 12 h before the co-culture in the presence of mIgG1, monalizumab, lirilumab or monalizumab and lirilumab mAb. n=3 Statistical analysis was performed by one-way ANOVA (multiple comparisons) test, p-value **<0.01, ****<0.0001.

The partial inhibition of NKG2A$^+$ KIRs$^+$ NK cells that remained present in co-culture with HLA-BCE tKO or after combined monalizumab/lirilumab treatment led me further investigate the potential HLA-A/KIR3DL1 inhibitory axis. KIR3DL1 is highly expressed inhibitory receptor which is not blocked by lirilumab mAb (Figure 7.28 A). I used a DX9, a KIR3DL1mAb, in order to block KIR3DL1 during the co-culture with IFNγ-pre-treated

melanoma cells (Figure 7.31 A). DX9 treatment itself showed only minor increase in the degranulation of NKG2A$^-$ KIR$^+$ NK cells, in comparison to lirilumab treatment, which highly increased but not fully restored the degranulation of NKG2A$^-$ KIR$^+$ NK cells (Figure 7.31 B). However, the combination of DX9 with lirilumab treatment fully restored the degranulation of NKG2A$^-$ KIR$^+$ NK cells against IFNγ-pre-treated melanoma cells (Figure 7.31 B). The combination of monalizumab/lirilumab/DX9 also nearly completely restored the degranulation of NKG2A$^+$ KIRs$^+$ NK cell subset against IFNγ-pre-treated melanoma cells (Figure 7.31 C). When the DX9 mAb was used together with the combination of monalizumab/lirilumab treatment, the resistance of WT melanoma was highly reduced leading to higher proportions of B2M KO cells present in bulk after the 24-h co-culture (Figure 7.31 D). The overall killing of WT/B2M KO cells was not changed across the treatments (Figure 7.31 E). Together, these data show that the combination of monalizumab, lirilumab and DX9 treatment abolished the IFNγ-mediated resistance of melanoma cells to NK cell cytotoxicity.

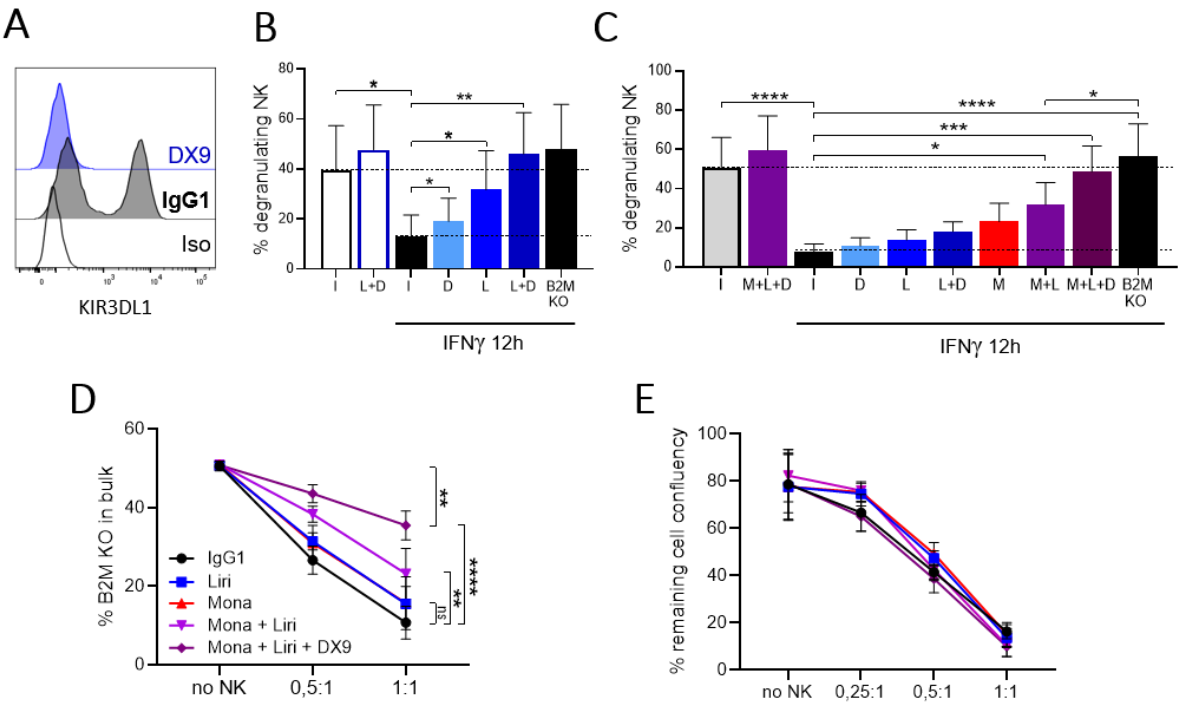

Figure 7.31 Effect of combined monalizumab/lirilumab/DX9 treatment on NK cell cytotoxicity.

A) Representative histograms showing the detection of KIR3DL1 on NK cells after DX9 treatment. **B)** Degranulation of NKG2A$^-$ KIR$^+$ NK cell subset after 4-h co-culture with WT and B2M KO A375 cells pre-treated or not with IFNγ 12 h before the co-culture in the presence of 5 µg/ml mIgG1, DX9, lirilumab or combined lirilumab/DX9 antibody. I=mIgG1, D=DX9, L=lirilumab. n=6 **C)** Degranulation of NKG2A$^+$ KIR$^+$ NK cell subset after 4-h co-culture with WT and B2M KO A375 cells pre-treated or not with IFNγ 12 h before the co-culture in the presence of 5 µg/ml of mAbs (single or a combination). I=mIgG1, D=DX9, L=lirilumab, M=monalizumab. n=6 **D)** Reduction in B2M KO cell population after

24-h co-culture of mixed WT:B2M KO cells (1:1) with FACS sorted NKG2A$^+$ KIR$^+$ NK cells at different E:T ratios in the presence of of 5 µg/ml of mAbs (single or a combination). n=3 **E)** Overall confluency of remaining WT/B2M KO (1:1) cells after 24-h co-culture with NKG2A$^+$ KIR$^+$ NK cells in the presence of presence of of 5 µg/ml of mAbs (single or a combination). n=3 Statistical analysis was performed by one-way ANOVA (multiple comparisons) test, p-value *<0.05, **<0.01, ***<0.001, ****<0.0001.

To exclude the A375 cell-specific effect of IFNγ, I used other MHC-I$^+$ cell lines such as epidermal carcinoma A431, SKMel-37 melanoma, cervical cancer HeLa cells, hepatoblastoma HepG2, breast cancer cell line MCF7 and lymphoblast K562 cells. All cell lines showed the expression of HLA-ABC and HLA-E either before or after IFNγ pre-treatment (Figure 7.32 A). IFNγ pre-treatment of all cell lines reduced the degranulation of NK cells, which was completely restored by combined monalizumab/lirilumab/DX9 treatment (Figure 7.32 B). In summary, these data show that IFNγ-mediated cell resistance to NK cell cytotoxicity occurred not only in melanoma cells but also in other tumor entities, and was potently abolished by treatment with a combination of monalizumab/lirilumab/DX9 mAbs.

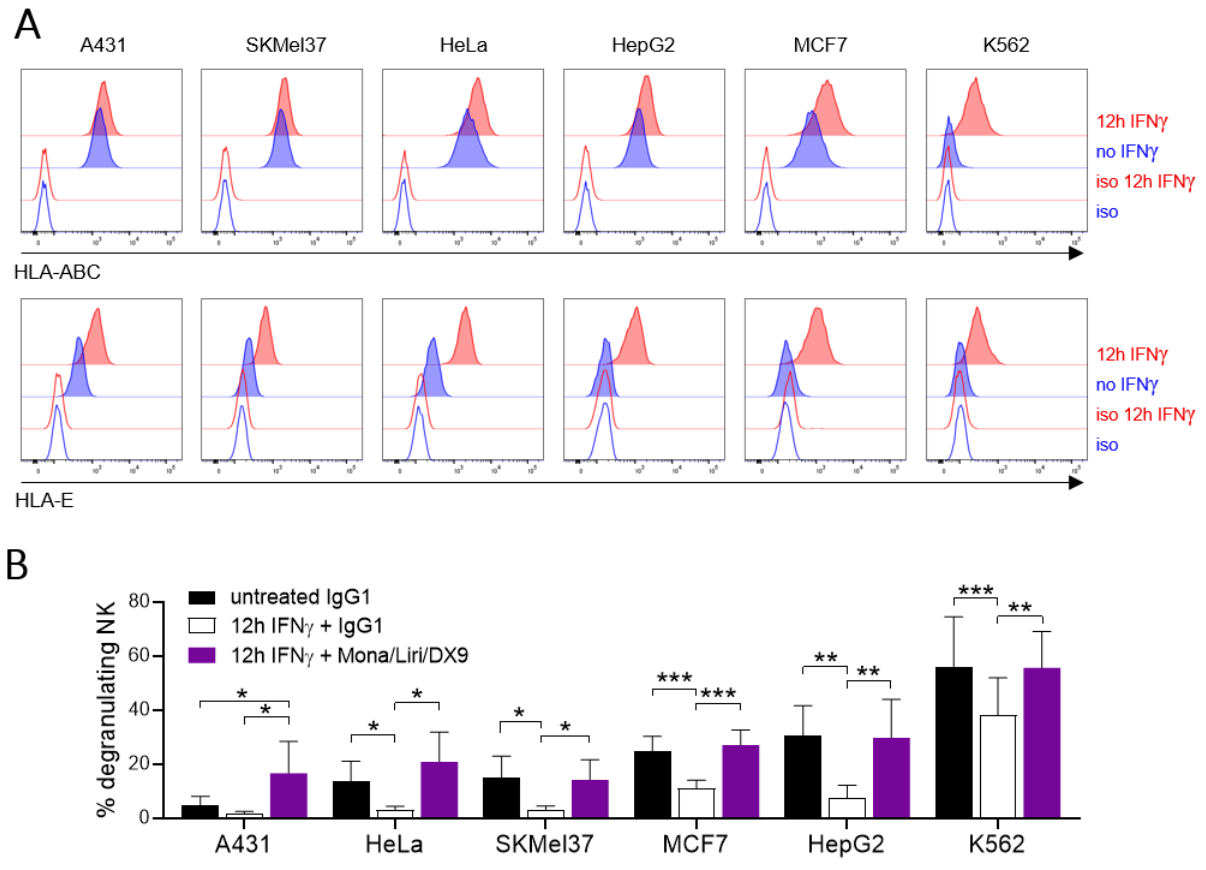

(Figure legend on the next page)

Figure 7.32 Effect of monalizumab/lirilumab/DX9 treatment on NK cells cytotoxicity against other tumor cell lines.

A) Histograms showing the expression of HLA-ABC and HLA-E on different tumor cell lines before and after 12 h IFNγ pre-treatment. **B)** Degranulation of bulk 9-d expanded NK cells after 4-h co-culture with MHC-I^+ tumor cells pre-treated or not with IFNγ 12 h before the co-culture in the presence of 5 µg/ml mIgG1or monalizumab/lirilumab/DX9. n=6 Statistical analysis was performed by one-way ANOVA (multiple comparisons) test, p-value *<0.05, **<0.01, ***<0.001.

7.2 B2M KO GW CRISPR/Cas9 KO screen

7.2.1 GW CRISPR/Cas9 KO screen on B2M KO A375 cells

The antigen presentation genes were identified as the major contributor to the resistance of melanoma cells to NK cell killing. To circumvent MHC-I-mediated inhibition of NK cell cytotoxicity during co-culture and to uncover other or less potent inhibitory ligands, I conducted a GW CRISPR/Cas9 KO screen on the B2M KO A375 cell line. To enhance the selection, the co-culture was performed in two consecutive rounds and in a biological triplicate using primary NK cells expanded for one week in IL-2-containing media (Figure 7.33 A). Day before the co-culture, the E:T ratio for achieving 50% killing of melanoma cells during 24-h co-culture was assessed by co-culturing B2M KO A375 cells with NK cells at various E:T ratios. The following day, the confluency of remaining melanoma cells was measured and the E:T ratio for each donor in the first round of co-culture was selected (Figure 7.33 B). After the first round of the screen co-culture, NK cells were removed and remaining attached melanoma cells cultured for 3 d to recover and expand. Before the second round screen of co-culture, the same process of determining the E:T ratio for achieving approximately 50% melanoma cell killing was repeated (Figure 7.33 C). After the second round of the screen co-culture, remaining attached melanoma cells were processed for sgRNA cassette amplification and sequencing followed by the analysis identifying significantly enriched and depleted sgRNAs (Figure 7.33 D). Gene ontology analysis of genes associated with significantly depleted sgRNAs revealed their involvement in the Hippo pathway (*NF2*, *LATS2*, *SAV1*) and pathways related to amino and nucleotide sugar metabolism, galactose metabolism, and biosynthesis of nucleotide sugars (*SLC35A1*, *SLC35A2*, *CMAS* and *GNE*). (Figure 7.33 E). Gene ontology analysis of genes associated with significantly enriched sgRNAs indicated their involvement in various mitochondrial genes related to gene expression and translation (Figure 7.33 F).

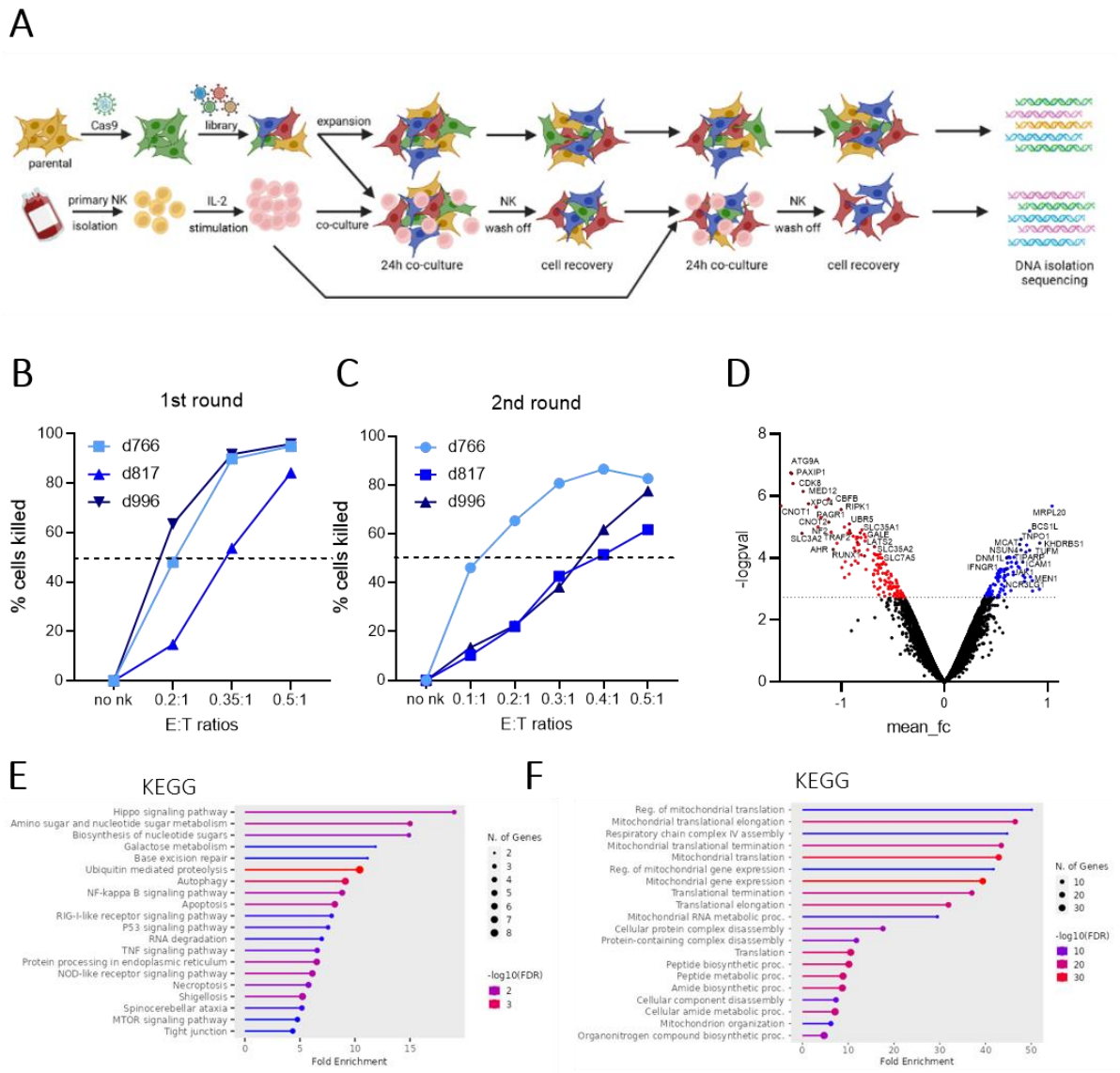

Figure 7.33 GW CRISPR/Cas9 KO screen setup on B2M KO A375 cells.

A) A schematic representation of a GW CRISPR/Cas9 KO screen on A375 B2M KO cells co-cultured with one week expanded IL-2-activated NK cells. Image created using Biorender. **B-C)** Survival curve of A375 B2M KO cells after 24-h co-culture with NK cells at different ratios before the 1st (left) and 2nd (right) round of the screen co-culture to determine optimal ratios for 50% killing. **D)** Volcano plot showing sensitive KO cells (depleted sgRNA) vs resistant KO cells (enriched sgRNA). Significantly altered sgRNA counts bellow fdr 0.05 are marked as red (depleted sgRNA) and blue (enriched sgRNA). **E)** KEGG pathway gene ontology analysis of significantly depleted genes > fdr 0.05 **F)** Biological processes gene ontology analysis of significantly enriched genes > fdr 0.05

As both screens were performed in the A375 cell line, I compared the datasets from WT and B2M KO cells screen co-culture. Antigen presentation and IFNγ signaling pathway genes, that showed highly depleted sgRNA counts WT screen, did not show alterations in B2M KO screen (Figure 7.34 A). Additionally, this dataset comparison allowed a separation of genes that scored in both screens and genes that scored more in the B2M KO screen than in the WT. Gene ontology analysis of genes that showed reduced sgRNA counts in both screens revealed a role of Hippo pathway, NFκB pathway or genes involved ubiquitin-mediated proteolysis. Gene ontology analysis of genes that showed more reduced sgRNA counts in B2M KO screen than in WT screen revealed a role in peptidyl modifications as well as UDP-galactose transmembrane transport (Figure 7.34 B). However, only a few candidates with predicted membrane localization scored in both or only one screen. Those candidates were involved in autophagy (*ATG9A*, *TMEM41B*), transport of sialic acid (*SLC35A1*, *SLC35A2*), glycosylation (*TMEM165*), tryptophan transport (*SLC7A5*) and *TM9SF3* with unclear function. In summary, I successfully performed a GW CRISPR/Cas9 KO screen in the A375 B2M KO cells which revealed the involvement of the AHR, Hippo pathway and biosynthesis of nucleotide sugars in the resistance of melanoma cells to NK cell cytotoxicity.

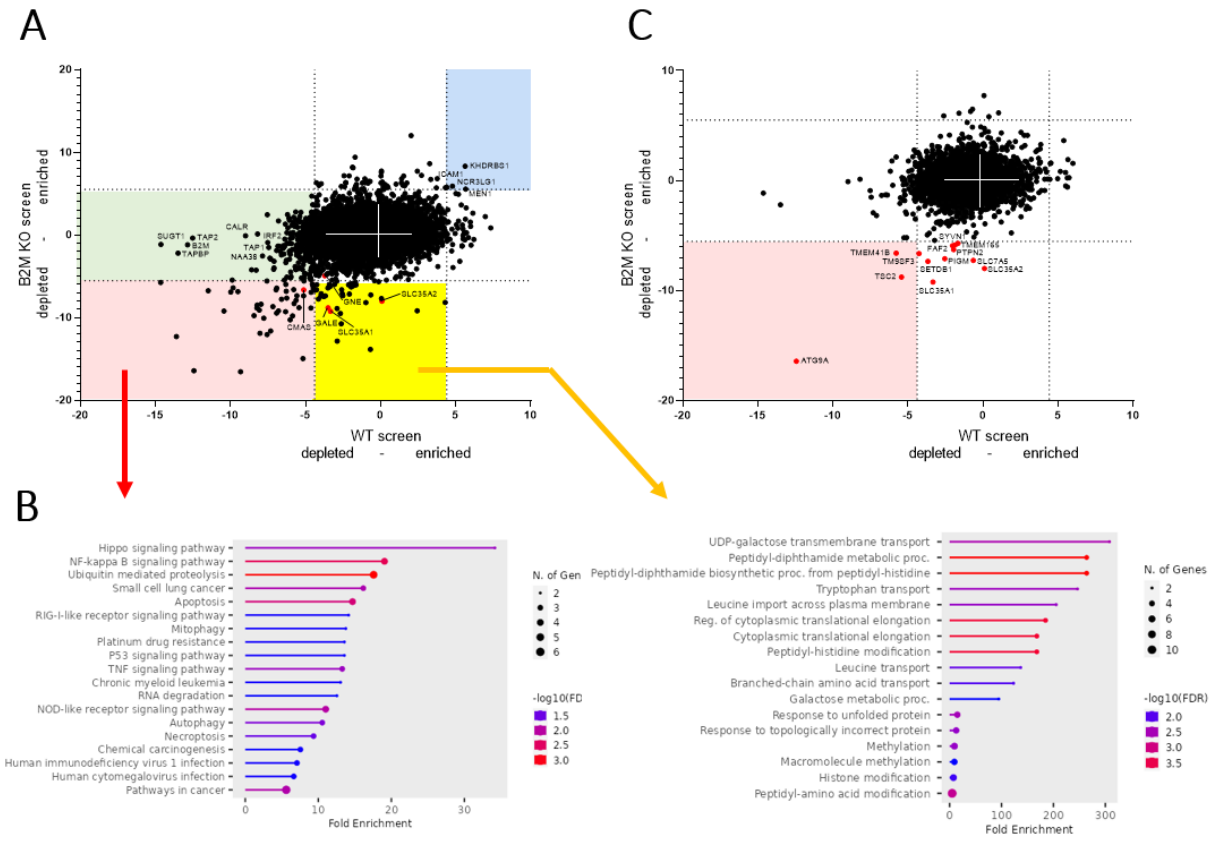

(Figure legend on the next page)

Figure 7.34 Comparison of WT and B2M KO screen datasets.

A) Comparison of depleted sgRNAs vs enriched sgRNAs from WT screen (x axis) and B2M KO screen (y axis) without genes that affect cell proliferation. **B)** Gene ontology analysis of candidate genes from corresponding gene segments. **C)** Comparison of depleted sgRNAs vs enriched sgRNAs from WT screen (x axis) and B2M KO screen (y axis) displaying genes with predicted membrane localization.

7.2.2 Role of SLC35A in melanoma cell resistance to NK cell cytotoxicity

SLC35A1 emerged as one of the top hits in the B2M KO screen. SLC35A1 gene encodes a membrane CMP-sialic acid transporter located in the Golgi network[540]. Deficiency in the expression of SLC35A1 leads to a reduction in sialylation of surface proteins, detectable through lectin staining[541]. Thus, I transfected melanoma cells with SLC35A1 sgRNAs followed by staining with Sambucus Nigra lectin (SNA) to detect the reduction in sialylation of surface proteins (Figure 7.35 A). Loss of SLC35A1 reduced but did not entirely eliminate surface sugar staining by SNA; however, enabling the separation between WT and SLC35A1 KO cells and FACS sorting to obtain a pure KO cell line (Figure 7.35 A). SLC35A1 KO cells displayed a broader alterations in the expression of NK-related surface molecules, including Galectin-3, HLA-ABC, HLA-E, HLA-DR, TRAILR2, MICAB and B7H3 (Figure 7.35 B).

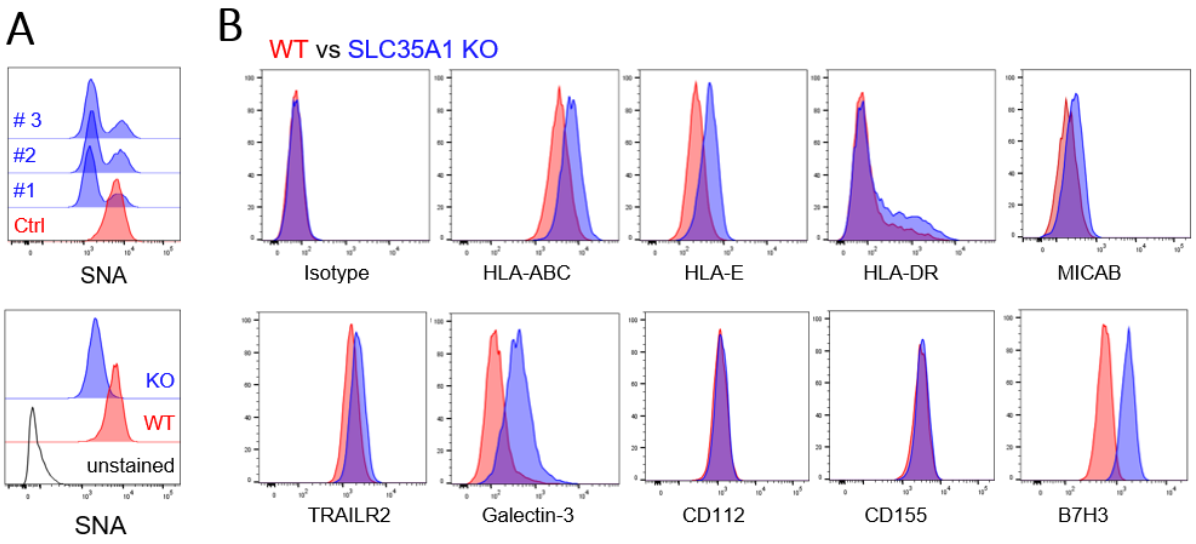

Figure 7.35 Staining of surface NK cell ligands on SLC35A1 KO A375 cells.

A) Histogram showing the staining of surface sugar residues with FITC-conjugated SNA lectin on WT and 3 sgRNA-transfected cells targeting *SLC35A1* gene (upper) and sorted SLC35A1 KO vs WT A375 cells (lower). **B)** Histograms showing the staining of selected surface molecules on WT and SLC35A1 KO A375 cells.

I next assed the resistance of SLC35A1 KO melanoma cells to NK cells. In some experiments, SLC35A1 KO cells did not cause a sufficient reduction in SNA staining and a clear separation of WT and SLC35A1 KO cells. Thus, I included B7H3 staining, which consistently showed a clear separation of WT and SLC35A1 KO cells (Figure 7.36 A). During the 24-hour co-culture, SLC35A1 KO cells exhibited reduced resistance to NK cell killing, particularly at higher E:T ratios (Figure 7.36 B, C). The reduction in the SLC35A1 KO cell population was directly dependent on NK cell cytotoxicity, as pre-treatment with IFNγ or NK/tumor supernatant did not alter the WT/SLC35A1 KO cell ratio (Figure 7.36 D). Given that SLC35A1 KO cells exhibited increased expression of MHC-I and lower sgRNA counts in the B2M KO screen, I investigated the resistance of SLC35A1 KO cells to NK cell killing in the absence of MHC-I (Figure 7.36 E). I transfected B2M sgRNA into SLC35A1 KO A375 cells to generate the SLC35A1/B2M dKO A375 cell line. I then mixed WT, SLC35A1 KO, B2M KO and SLC35A1/B2M dKO cells, allowing the separation of the four melanoma cell lines and a simultaneous co-culture with NK cells (Figure 7.36 F, G). After the 24-h co-culture with NK cells, in the absence of MHC-I, the SLC35A1 KO cell population showed a higher reduction in resistance to NK cells in comparison to SLC35A1 KO cells that express MHC-I (Figure 7.36 H). Together, these data show a successful generation of a SLC35A1 KO cell line, which displayed changes in the cell surface expression of multiple NK cell ligands and a higher sensitivity to NK cell killing particularly in the absence of MHC-I.

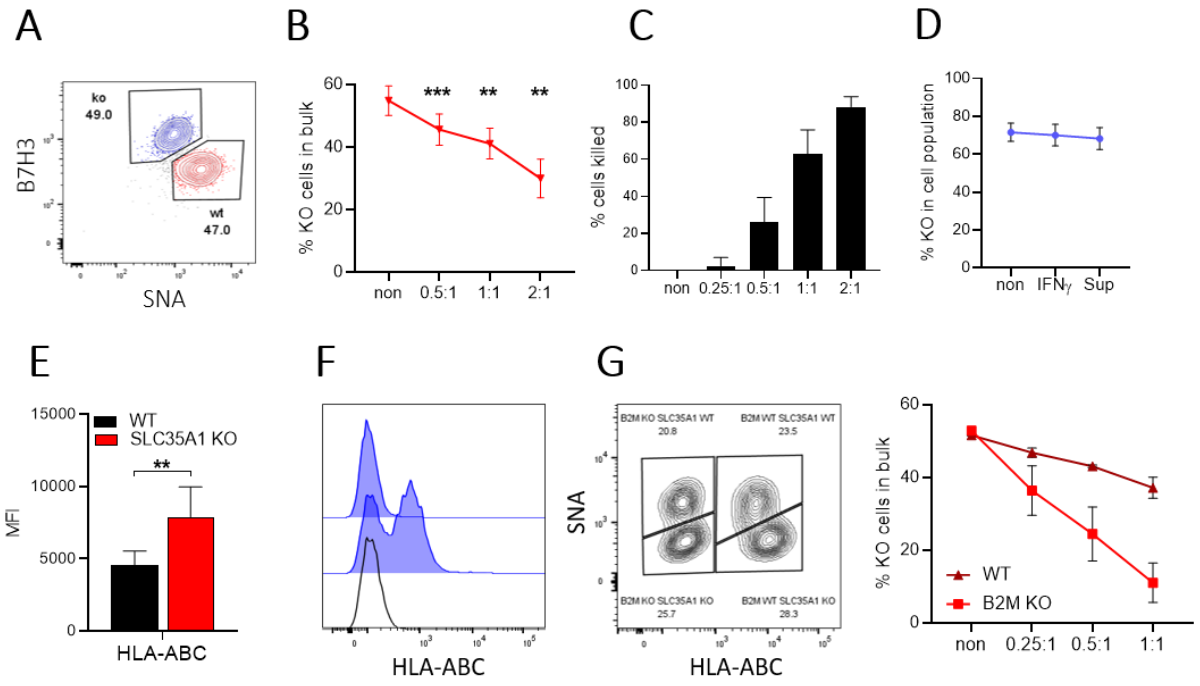

(Figure legend on the next page)

Figure 7.36 Resistance of SLC35A1 KO melanoma cells to NK cell cytotoxicity.

A) Representative contour plot showing the gating of WT and SLC35A1 KO A375 cells based on the SNA and B7H3 staining.**B)** Reduction in SLC35A1 KO cell population after 24-h co-culture of mixed WT:SLC35A1 KO A375 cells (1:1) co-cultured with NK cells at different E:T ratios. n=7 **C)** Overall NK cell killing efficiency of mixed WT:SLC35A1 KO cells at different E:T ratios. **D)** Reduction in the SLC35A1 KO cell population after 12 h treatment of mixed WT:SLC35A1 A375 cells with IFNγ or NK/tumor supernatant. **E)** MFI of the expression of HLA-ABC on WT and SLC35A1 KO A375 cells. n=3 **F)** Histogram showing the expression of HLA-ABC on SLC35A1 KO cells transfected with B2M sgRNA before and after sort. **G)** Contour plot showing the gating of SLC35A1 KO vs WT cells in B2M WT or B2M KO A375 cells. WT, SLC35A1 KO, B2M KO and SLC35A1/B2M dKO were mixed at 1:1:1:1 ratio and co-cultured with NK cells at different E:T ratios (left). Reduction in the SLC35A1 KO cell population after 24-h co-culture with NK cells at different E:T ratios (right). n=2 Statistical analysis was performed by one-way ANOVA (multiple comparisons), p-value **<0.01, ***<0.001.

Sialic acid-binding immunoglobulin-type lectins (Siglecs) are known to interact with sialylated proteins[228]. Siglec-7 is expressed by the majority of NK cells, whereas the expression of Siglec-9 is restricted to a subset of NK cells, with higher expression detected on $NKG2A^-$ NK cells. (Figure 7.37 A, B). Next, I used a recombinant Siglec-7 and Siglec-9 Fc fusion proteins to stain their cognate ligands on melanoma cell lines that could potentially mediate the inhibition of NK cell cytotoxicity. All melanoma cell lines tested displayed high expression of Siglec-7 and Siglec-9 ligands (Figure 7.37 C). According to its inhibitory function, $Siglec\text{-}9^+$ NK cells exhibited lower degranulation regardless of the NKG2A expression against multiple melanoma cell lines (Figure 7.37 D, E). To connect the role of SLC35A1 to Siglec receptors, I stained Siglec-7 and Siglec-9 ligands on SLC35A1 KO cells. The absence of *SLC35A1* in melanoma cells completely abolished the staining with Siglec-7 and Siglec-9 Fc fusion proteins (Figure 7.37 F). Together, these data show that melanoma cells express ligands for Siglec-7 and Siglec-9, an inhibitory receptors expressed on NK cells. Furthermore, the expression of Siglec-9 defines two NK cell subsets, with Siglec-9+ NK cells exhibiting a lower degranulation capacity compared to Siglec-9- NK cells after co-culture with melanoma cells.

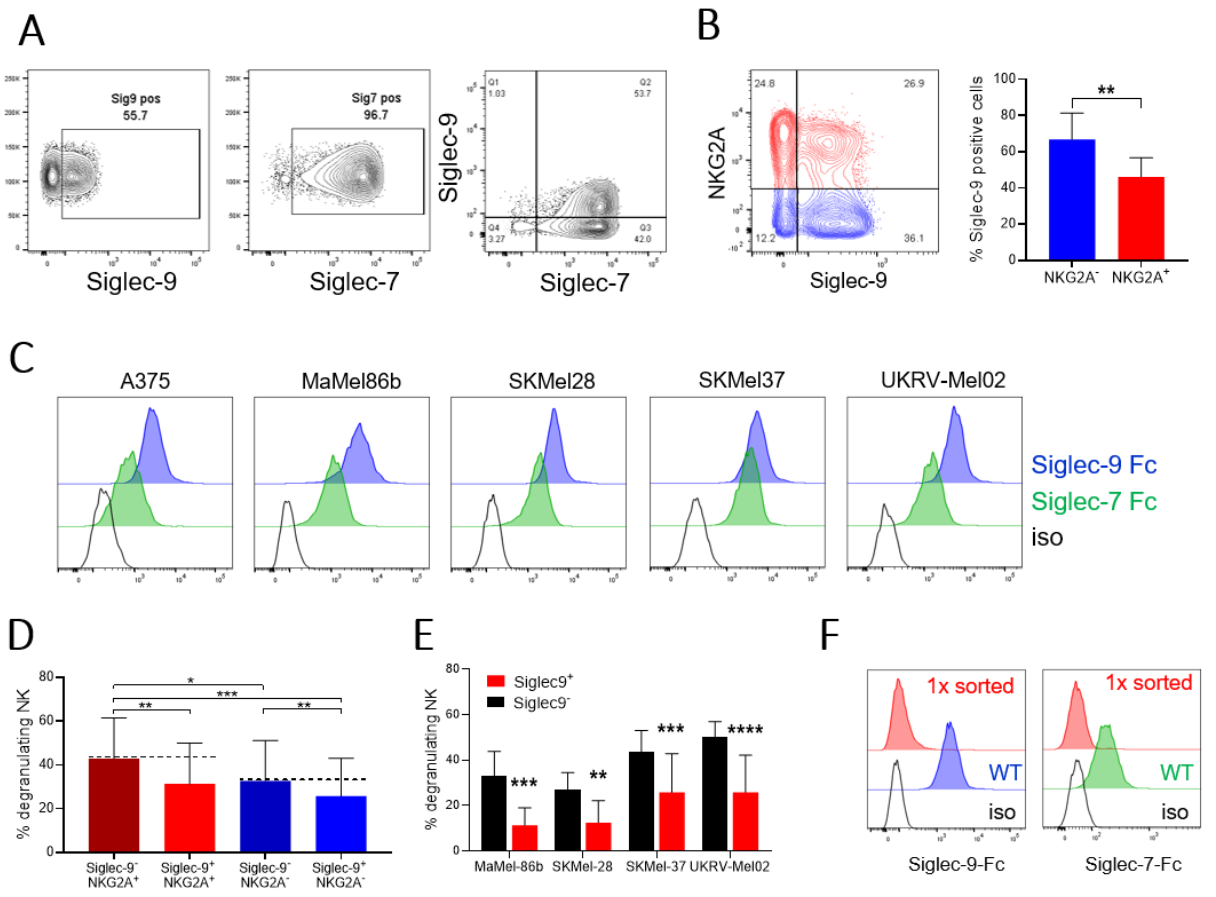

Figure 7.37 The expression of Siglec-7 and -9 receptors and their ligands.

A) Contour plot showing the expression of Siglec-7 and Siglec-9 on 2-d IL-2-activated NK cells. **B)** Contour plot and quantification of the expression of Siglec-9 on NKG2A NK cell subsets. n=10 **C)** Histograms showing the expression Siglec-7 and Siglec-9 ligands on melanoma cell lines stained with Siglec-7 Fc and Siglec-9 Fc fusion proteins. **D)** Degranulation of Siglec-9^{+} and Siglec-9^{-} NK cells on NKG2A NK cell subsets after 4-h co-culture with A375 cells. n=10 **E)** Degranulation of Siglec-9^{+} and Siglec-9^{-} NK cells after 4-h co-culture with other melanoma cell lines. n=3 **D)** Histograms showing the expression of Siglec-7 and Siglec-9 ligands on WT and SLC35A1 KO A375 cells detected by Siglec-7 Fc and Siglec-9 Fc fusion proteins. Statistical analysis was performed by one-way ANOVA (multiple comparisons) test (D) and two-tailed Student's *t* test (B, E), p-value *<0.05, **<0.01, ***<0.001, ****<0.0001.

Next, I tested SLC35A1 KO melanoma cells in a functional assay with NK cells. The loss of *SLC35A1* in melanoma cells specifically increased the degranulation of Siglec-9^{+} NK cells, whereas the degranulation of Siglec-9^{-} NK cells remained unaffected despite the expression of Siglec-7 (Figure 7.38 A, B). Siglec-9^{+} NK cells can be further divided into two subpopulations characterized by either bright Siglec-9 or dim Siglec-9 staining (Figure 7.38 C). Siglec-9^{bright} NK cells, in comparison to dim Siglec-9^{dim} NK cells, exhibited the lowest

degranulation after co-culture with WT melanoma cells. However, this difference was not observed after co-culture with SLC35A1 KO cells, where the degranulation of Siglec-9^{bright} NK cells was comparable to Siglec-9^{-} NK cells (Figure 7.38 C). To exclude the A375-specific role of SLC35A1 in mediating the inhibition of Siglec-9^{+} NK cells, the KO of *SLC35A1* was also generated in SKMel-28 and UKRV-Mel02 cell lines. The loss of SLC35A1 also resulted in reduced SNA lectin staining, absence of Siglec-9 Fc fusion protein staining and increased expression of B7H3 (Figure 7.38 D, E). The degranulation of NK cells in response to SLC35A1 KO cells was overall higher in comparison to WT cells. The loss of SLC35A1 in melanoma cells had the most significant impact on Siglec-9^{+} NK cells; nonetheless, a partial increase in the degranulation of Siglec-9^{-} NK cells was observed after co-culture with SLC35A1 KO UKRV-Mel02 cells (Figure 7.39 F, G). In summary, the deletion of the SLC35A1 gene specifically enhanced the degranulation of Siglec-9^{+} NK cells. Siglec-9^{-} NK cells, despite high expression of Siglec-7, demonstrate low to no changes in response to SLC35A1 KO cells.

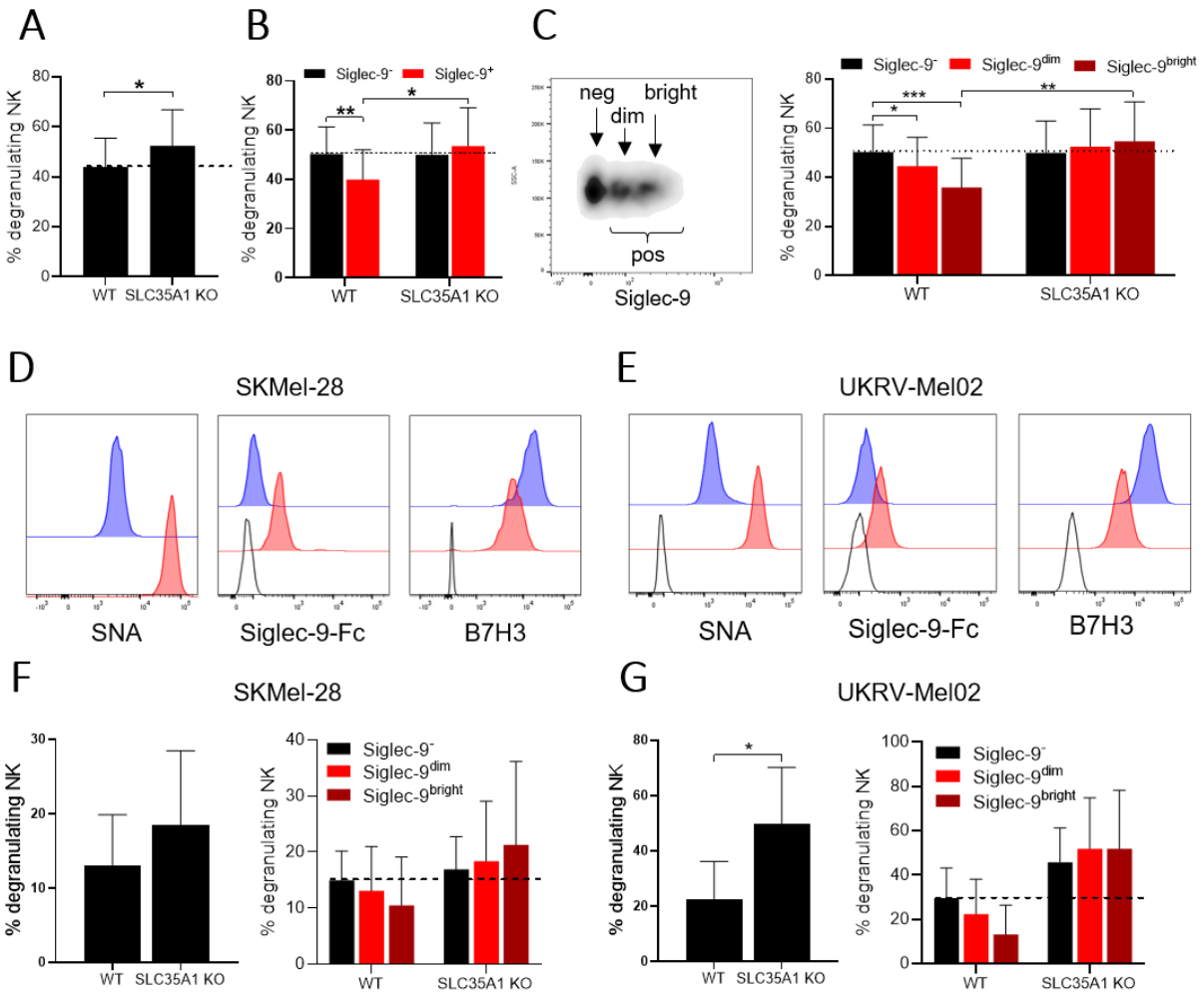

(Figure legend on the next page)

Figure 7.38 Co-culture of SLC35A1 KO melanoma cells with NK cells.

A) Degranulation of NK cells after 4-h co-culture with WT or SLC35A1 KO A375 cells. n=6 **B)** Degranulation of Siglec-9^{+} and Siglec-9^{-} NK cells after 4-h co-culture with WT or SLC35A1 KO A375 cells. n=6 **C)** Representative plot showing Siglec-9^{-}, Siglec-9^{dim} and Siglec-9^{bright} NK cell subsets and a corresponding degranulation after 4-h co-culture with WT or SLC35A1 KO A375 cells. n=6 **D-E)** Sorted WT and SLC35A1 KO D) SKMel-28 or E) UKRV-Mel02 cells stained with SNA, Siglec-9-Fc and B7H3 mAb. **F-G)** Degranulation of NK cells after 4-h co-culture with WT or SLC35A1 KO F) SKMel-28 or G) UKRV-Mel02 cells. The effect is shown on bulk (left) or Siglec-9 NK cell subsets (right). n=3 Statistical analysis was performed by one-way ANOVA (multiple comparisons) test (B, C) and two-tailed Student's *t* test (A, F, G), p-value *<0.05, **<0.01, ***<0.001.

7.2.3 Role of TM9SF3 in melanoma cell resistance to NK cell cytotoxicity

Transmembrane 9 superfamily member 3 (TM9SF3), another candidate with a membrane localization, emerged in the B2M KO GW CRISPR/Cas9 KO screen. The TM9SF family, comprising four members including TM9SF3, is located in the Golgi network and plays a role in tumor invasion[542–544]. Previous studies have shown that members of the TM9SF family also affect the transport of glycosylated proteins to plasma membrane[545,546]. To confirm the involvement of TM9SF3 in the expression of Siglec-9 ligands, I transfected melanoma cells with a sgRNA targeting the TM9SF3 gene. All cells transfected with TM9SF3 sgRNA showed a reduction in staining with the Siglec-9 Fc protein. (Figure 7.39 A). The loss of TM9SF3 did not completely abolish but rather reduced the staining of Siglec-9 ligands. Surface and intracellular staining of WT and TM9SF3 KO melanoma cells with an antibody against the TM9SF3 protein did not reveal differences in TM9SF3 expression, potentially indicating the unspecificity of the polyclonal antibody primarily used for immunohistochemistry (Figure 7.39 B). In contrast to SLC35A1 KO cells, TM9SF3 KO cells did not exhibit increased expression of HLA molecules and other NK cell ligands (Figure 7.39 C). Next, I assessed the expression of NKG2D, NKp30, DNAM-1, Siglec-9 and Siglec-7 ligands by staining with receptor fusion proteins. TM9SF3 KO cells exhibited a dramatic reduction in the staining of Siglec-7, Siglec-9, and NKp30 ligands (Figure 7.39 D). In comparison, SLC35A1 KO cells exhibited abolished staining of Siglec-7 and Siglec-9 ligands, a reduction in NKp30 ligands and increased staining of DNAM-1 ligands (Figure 7.39 D).

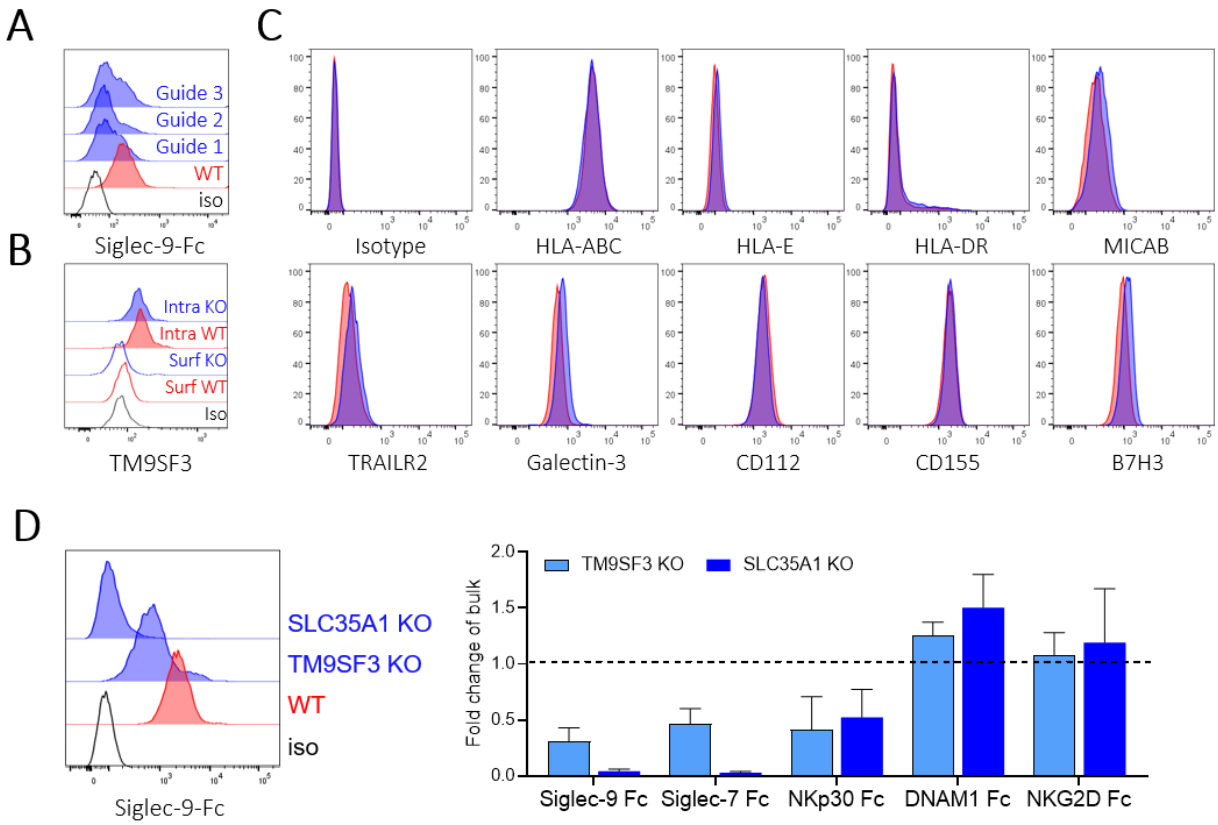

Figure 7.39 Staining of surface NK cell ligands on TM9SF3 KO A375 cells.

A) Histograms showing the staining of WT and 3 TM9SF3 sgRNAs transfected A375 cells with recombinant Siglec-9-Fc fusion protein. **B)** Histograms showing the surface and intracellular staining of WT and TM9SF3 KO A375 cells with polyclonal TM9SF3 Ab. **C)** Histograms showing the surface staining of selected NK cell ligands on WT and TM9SF3 KO cells. **D)** Fold change of the expression of ligands on SLC35A1 KO and TM9SF3 KO A375 cells with Siglec-9, Siglec-7, DNAM-1, NKp30 and NKG2D Fc fusion proteins normalized to the staining of WT A375 cells. n=2-4

Subsequently, I used TM9SF3 KO melanoma cells in functional assays and observed a higher overall degranulation of NK cells after co-culture with TM9SF3 KO cells (Figure 7.40 A). Similar to SLC35A1 KO cells, TM9SF3 KO cells failed to inhibit Siglec-9^{+} NK cells, which exhibited comparable degranulation capacity as Siglec-9^{-} NK cells (Figure 7.40 B, C). In comparison to WT cells, TM9SF3 KO cells also exhibited reduced resistance to NK cell killing during 24-h co-culture (Figure 7.40 D). Taken together, compared to SLC35A1 KO cells, TM9SF3 KO melanoma cells exhibited relatively minor alterations in the expression of surface NK cell ligands but still showed reduced detection of Siglec-9, Siglec-7, and NKp30 ligands. Moreover, the absence of *TM9SF3* in melanoma cells also increased the degranulation of Siglec-9^{+} NK cells and reduced melanoma cell resistance to NK cell cytotoxicity.

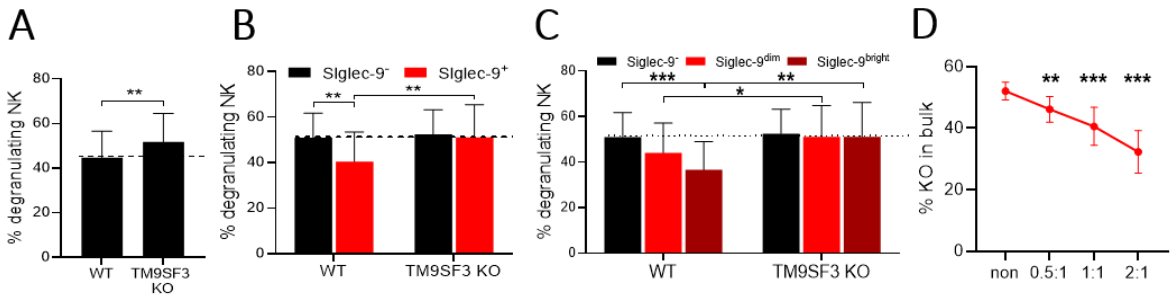

Figure 7.40 Resistance of TM9SF3 KO melanoma cells to NK cell cytotoxicity.

A-C) Degranulation of A) bulk NK cells, B) Siglec-9^{+} and Siglec-9^{-} NK cells and C) Siglec-9^{-}, Siglec-9^{dim} and Siglec-9^{bright} NK cell subsets after 4-h co-culture with WT and TM9SF3 KO A375 cells. n=6 **D)** Reduction in the TM9SF3 KO cell population after 24-h co-culture of mixed WT:TM9SF3 KO A375 cells (1:1) co-cultured with NK cells at different E:T ratios. n=8 Statistical analysis was performed by one-way ANOVA (multiple comparisons) test (B, C, D) and two-tailed Student's *t* test (A), p-value *<0.05, **<0.01, ***<0.001.

7.2.4 Role of Hippo and AHR pathway in melanoma cell resistance to NK cell killing

Besides the IFNγ-dependent MHC-I pathway and sialic acid pathway, which protect melanoma cells from NK cell cytotoxicity, other pathways emerged in both GW CRISPR/Cas9 KO screens. Melanoma cells deficient in the Hippo pathway key signalling transcription factor TAZ (*WWTR1*) showed highly enriched sgRNA counts after screen co-culture with NK cells, while sgRNAs targeting the negative regulators of TAZ (*LATS2*, *NF2*, *YWHAE*, *VGLL4*, *SAV1*) showed highly depleted sgRNA counts (Figure 7.41 A, B). Genes such as *AHR*, *ARNT*, *HSP90AB*, all forming a complex regulating the aryl hydrocarbon receptor (AHR) pathway, also showed highly depleted sgRNA counts (Figure 7.41 A, B). I selected a key component of the Hippo pathway, the transcription factor TAZ, and transfected melanoma cells with sgRNA targeting the *WWTR1* gene. The transfection of WWTR1 sgRNA into melanoma cells induced only a slight reduction in the degranulation of NK cells. During the 24-hour co-culture, WWTR1 sgRNA-transfected cells exhibited a major increase in resistance to NK cell killing (Figure 7.41 C, D). However, since the Hippo pathway's involvement in cell proliferation, WWTR1 was not my primary focus[547]. Next, I validated the involvement of the AHR pathway in melanoma cell resistance to NK cell killing. Melanoma cells transfected with sgRNA targeting the *AHR* gene did not induce higher NK cell degranulation compared to WT cells, but exhibited a reduction in melanoma cell resistance to NK cell killing (Figure 7.41 E, F).

Together, these data show additional mechanisms such as the Hippo and AHR pathways regulating melanoma cell resistance to NK cell cytotoxicity. However, they do not directly alter the degranulation of NK cells; thus, the effect of these pathways may reside in regulating apoptosis, as both pathways induce genes involved in apoptosis regulation.[547–552].

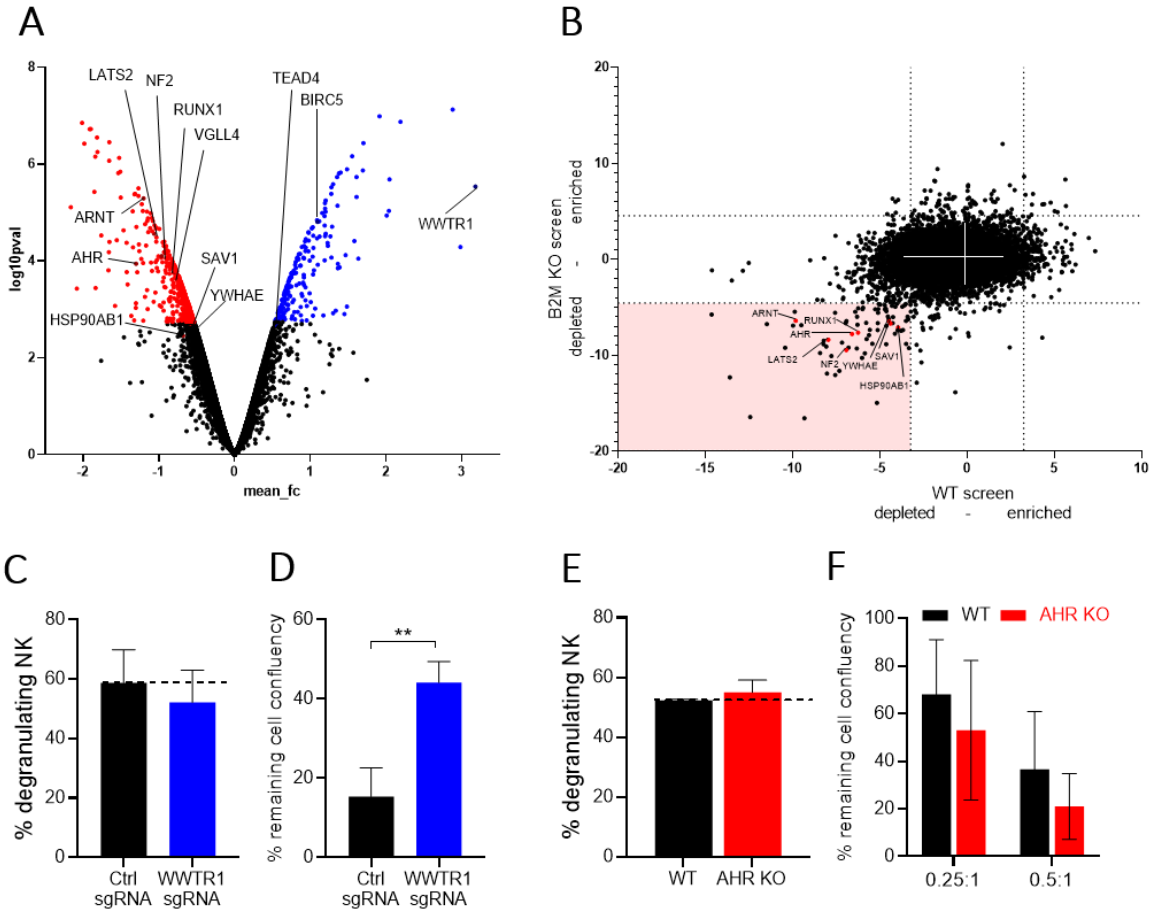

Figure 7.41 Other pathways involved in melanoma cell resistance to NK cell cytotoxicity.
A) Volcano plot showing Hippo and AHR pathway genes highlighted in depleted sgRNAs vs enriched sgRNAs from WT screen dataset. Significant KO cells bellow fdr 0.05 are marked as red (sensitive) and blue (resistant). **B)** Comparison of depleted sgRNAs vs enriched sgRNAs from WT screen (x axis) with B2M KO screen (y axis) without genes that affect cell proliferation highlighting the genes from Hippo and AHR pathway. **C)** Degranulation of NK cells after 4-h co-culture with WWTR1 sgRNA transfected A375 cells. n=3 **D)** Remaining cell confluency of WT vs WWTR1 sgRNA transfected A375 cells after separate 24-h co-culture with NK cells at 0.5:1 E:T ratio. n=5 **E)** Degranulation of NK cells after 4-h co-culture with AHR sgRNA transfected A375 cells. n=2 **F)** Remaining cell confluency of WT vs AHR sgRNA transfected A375 cells after separate 24-h co-culture with NK cells at different E:T ratio. n=3 Statistical analysis was performed by two-tailed Student's *t* test (F), p-value *<0.05, **<0.01, ***<0.001.

8 DISCUSSION

Skin cancer is the most prevalent form of cancer among humans, with the majority of cases being attributed to basal cell carcinoma (BCC) and squamous cell carcinoma (SCC). Of these, 8 out of 10 cases are BCC. Due to low mortality and poor registry, BCC and SCC are not overall included in cancer statistical measures[553]. Melanoma is rare but the most aggressive type of skin cancer due to its resistance and ability to metastasize. This places melanoma as the fifth most common type of cancer. The 5-year relative survival rates for melanoma drop from >99% in localized tumor to 71% in regional tumor to 32% metastatic tumor[461,554]. The introduction of novel therapies such as immune checkpoint blockade into the clinic has revolutionized the treatment of advanced melanoma patients, showing improved overall survival. To this date, anti-CTLA-4, anti-PD-1, anti-PDL-1 and anti-LAG-3 blocking antibodies are the only ones approved by the Food and Drug Administration to treat advanced melanoma[555]. This improvement in treatment resulted in declined mortality rates by about 3-5% per year over the past decade (2011 to 2020)[556]. However, despite the enhanced anti-tumor immune response and prolonged tumor regression observed in many cases with ICB, certain patient subsets fail to respond to current therapy and relapse. Current ICB used in the clinic only unleashes the adaptive anti-tumor response of T cell. Thus, there is a growing demand for novel immune checkpoint targets that not only engage adaptive immunity but the innate immune system as well. NK cells and innate immune cells in general are considered as the first tumor encounters and critical for the initial tumor suppression and development. The absence or defects in NK cell function in murine models shows impaired acute tumor cells rejection, suppressing tumor metastasis and tumor outgrowth[557,558]. In humans, the absence or low NK cell activity is connected to a higher frequency of infections and cancer[559–561]. Therefore, the aim of this study was to utilize the power of GW CRISPR/Cas9 KO screen in order to describe major melanoma resistance mechanisms to NK cells.

8.1 WT GW CRISPR/Cas9 KO resistance screen

Just as ICB revolutionized clinical treatment of cancer patients, CRISPR-Cas9 technology has revolutionized the process of gene inactivation. Using a GW sgRNA library, covering approximately 18,000 human genes, enabled a large-scale loss of gene function in Cas9 expressing melanoma cell line. Subsequent use of this pool of melanoma cell KOs in a functional assay enabled connecting individual genes to their inhibitory or stimulating function in response to NK cells.

8.1.1 NK sensitivity and suitability of melanoma cell lines

One of the key considerations was the selection of a suitable melanoma cell line expressing multiple NK ligands, resulting in high sensitivity to NK cell killing across various assays and time points. I chose the well-studied A375 cell line, a BRAF V600E mutated MHC-I^{+} malignant melanoma cell line, which exhibited moderate sensitivity to NK cells and relatively fast growth (Figure 7.2). Due to the significant clonal variability observed even within a cell line, I conducted clonal selection of Cas9-expressing cells that demonstrated high Cas9 editing efficiency. To maintain variability during the CRISPR/Cas9 KO screen co-culture, I chose 3 A375 single-clone lines that exhibited high Cas9-editting efficiency and similar characteristics to the parental A375 cells. (Figure 7.3-7.4).

8.1.2 Antigen presenting pathway protects melanoma cells from in NK cell cytotoxicity

Classical MHC-I molecules are considered the major inhibitory axis of NK cells due to their role in NK cell education, ensuring the selective targeting of cells with 'missing-self' signal posing a potential threat to the host. Absent or reduced MHC-I expression, commonly observed in cancer or virus-infected cells as an escape mechanism from cytotoxic T cells, leads to NK cell activation and target cell killing. The MHC-I matching is also a significant issue in transplantation since educated NK cells recognize only host-specific HLA alleles. This often results in host vs. graft disease and subsequent rejection of the transplanted organ [562]. Regardless of MHC-I matching, GW CRISPR/Cas9 KO screen co-culture of A375 melanoma cells with primary human NK cells revealed a major inhibitory role of molecules involved in antigen presentation (*TAPBP, SUGT1, B2M, TAP1, TAP2, CALR, DDB1, DCAF15, RFXANK, NLRC5, HLA-E*) as well as IFNγ signalling (*IRF1, IRF2, STAT1*) (Fig.7.5, 8.1). Loss of NK cell activation ligands such as adhesion molecule ICAM-1 and NKp30 ligand B7H6 resulted in the resistance of melanoma cells to NK cell cytotoxicity (Figure 7.5, 7.6). These findings align with other GW CRISPR/Cas9 screens conducted on various tumor types or using NK cell lines as effector cells for selection[526,528,532,563,564]. These shared resistance mechanisms between melanoma and other cancers such as blood or colorectal cancers underscore the significance of these molecules in conferring resistance to NK cells.

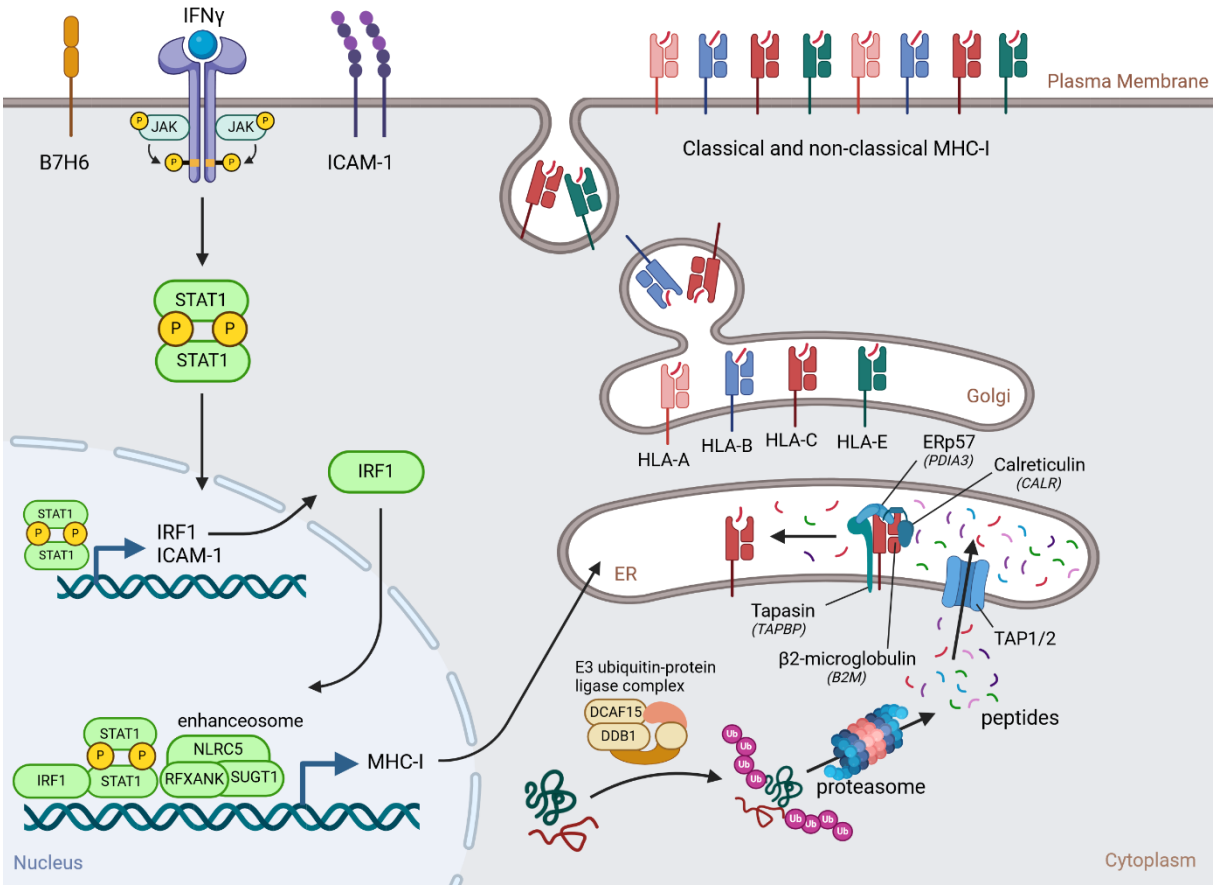

Figure 8.1 Schematic representation of candidates with high changes in sgRNA counts after screen co-culture and their involvement in IFNγ signalling and antigen presenting machinery. Image created using Biorender.

8.1.3 ICAM-1 and B7H6 activates while MHC-I inhibits NK cell cytotoxicity

The comparison of our data with studies involving GW CRISPR/Cas9 KO screen co-cultures with NK cells, as well as the identification of top-scoring candidates known to be involved in NK cell cytotoxicity, indicates successful performance of the screen co-culture. Nevertheless, individual validation of the top-scoring candidates was conducted to confirm the screen results and evaluate the extent of their effect on NK cell cytotoxicity. I confirmed that the absence of ICAM-1 expression on melanoma cells or blocking the interaction of B7H6 with the NKp30 receptor reduced NK cell degranulation (Figure 7.6). PVR or MICAB, which are DNAM-1 or NKG2D ligands, did not score significantly in the GW CRISPR/Cas9 KO screen co-culture, even though blocking these receptors reduced NK cell degranulation against melanoma cells (Figure 7.3). This inconsistency might be explained by the potential shedding of MICAB and CD155 by WT melanoma cells, which could interfere with corresponding activating receptors during longer co-culture, thereby protecting KO melanoma cells from their

preferential killing by NK cells [61,62,355]. Since MICAB and CD155 are not the only ligands for DNAM-1 or NKG2D, other ligands might also compensate for the loss of one ligand, thus masking its effect on the resistance of melanoma cell to NK cell killing.

Inhibitory ligands are particularly appealing targets to explore due to their potential to be blocked by therapeutic agents, which could be utilized in a clinical settings to enhance patients' anti-tumor immune responses. Therefore, I focused on candidates that reduced the resistance of melanoma cells to NK cell killing. I confirmed that inactivation of the *B2M* gene, resulting in total loss of MHC-I, significantly sensitized melanoma cells to NK cell killing in a 24-h co-culture system (Figure 7.7). However, during a shorter 4-h co-culture, only a small differences in the resistance of B2M KO melanoma cells to NK cell killing was observed. During this brief 4-h co-culture, NK cells displayed comparable degranulation against both WT and B2M KO melanoma cells (Figure 7.8). I hypothesized that the differences in the sensitivity of B2M KO cells to NK cells observed during 4-h vs 24-h co-cultures were connected to TME present in longer co-cultures. The fact that the genes involved in IFNγ signalling showed significantly reduced sgRNA counts after the GW screen co-culture prompted me to replicate the effect of the TME in a 4-h co-culture system by pre-treating melanoma cells with supernatant from 24-h NK/tumor co-culture containing IFNγ derived from NK cells. Supernatant as well as recombinant IFNγ-pre-treatment of melanoma cells caused a dramatic reduction in NK cell degranulation, which was fully dependent on the expression of MHC-I, as IFNγ-pre-treated B2M KO melanoma cells failed to inhibit NK cell function (Figure 7.8, 8.2). IFN-γ pre-treatment of melanoma cells resulted in increased expression of HLA-ABC and was potent enough to inhibit ADCC, considered to be one of the most robust NK cell activating signals, as well as contradicting a substantial upregulation of ICAM-1 (Figure 7.9). The importance of IFNγ was further confirmed by neutralizing IFNγ during longer co-culture or by generating IFNγ KO NK cells, which failed to induce melanoma cell resistance and remained efficient in killing MHC-I+ melanoma cells during longer co-cultures (Figure 7.10).

IFNγ is an important cytokine with broad effects not just on melanoma cell surface ligand composition but also on overall immune cell responses. In the context of MHC-I, IFNγ has a negative impact on NK cell function. However, its presence is highly beneficial for cytotoxic T cells that recognize tumors through TCR-MHC-I interactions. This has been confirmed in other GW CRISPR/Cas9 screens that utilized T cells as effector cells, where IFNγ and antigen presentation genes were identified as key molecules facilitating anti-tumor T cell cytotoxicity[565–568]. Additionally, IFNγ not only upregulates classical MHC-I but also non-

classical MHC-I molecules, such as HLA-E, which are not restricted to NK cell education and specific allele recognition by NKG2A or NKG2C receptors[175].

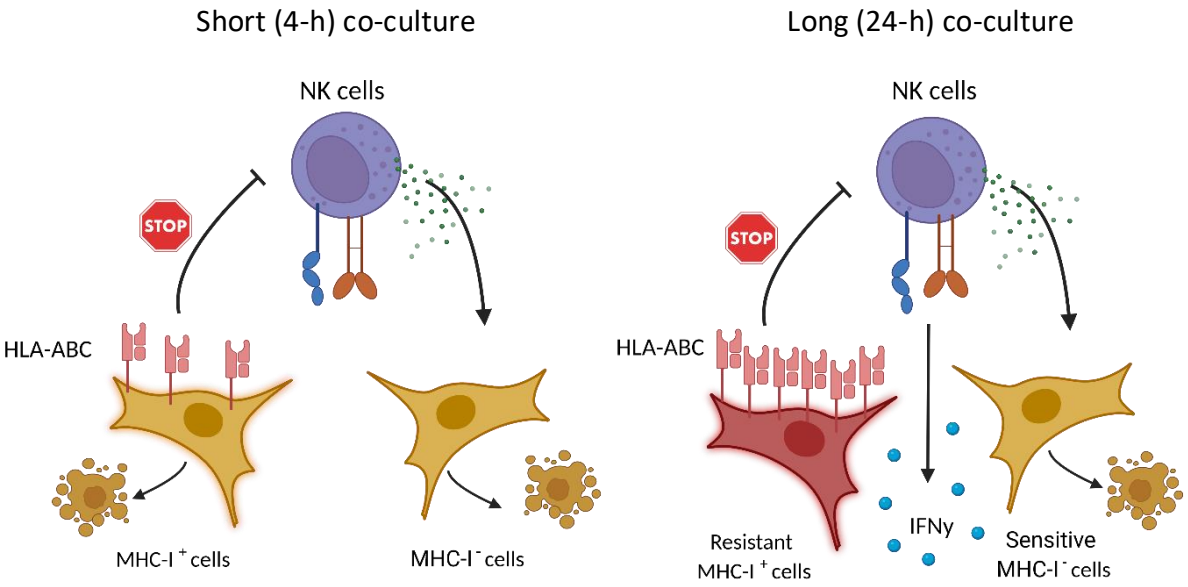

Figure 8.2 Schematic representation of MHC-I$^+$ and MHC-I$^-$ melanoma cell sensitivity to NK cell cytotoxicity during 4-h or 24-h co-culture. Image created using Biorender.

8.1.4 IFNγ induces the expression of HLA-E and inhibits NKG2A$^+$ NK cells

HLA-E, a ligand for inhibitory NKG2A receptor[174,175], is the only MHC-I molecule that significantly scored in my GW CRISPR/Cas9 KO screen co-culture. HLA-E is not expressed at steady state on melanoma cells but is transiently upregulated by IFNγ (Figure 7.12, 7.13). Thus. the inhibitory effect of HLA-E on NK cells is only revealed after IFNγ pre-treatment of melanoma cells (Fig.7.14, 7.15). Since the expression of NKG2A defines two distinct NK cell subsets, the inhibitory effect of HLA-E was only observed on NKG2A$^+$ NK cells (Figure 7.12, 7.14, 7.15). The absence of HLA-E complete restored the degranulation of CD56^{bright} NK cells and nearly complete restoration on NKG2A$^+$ CD56^{dim} NK cells. Besides NKG2A$^+$ NK cells, IFNγ pre-treatment of WT melanoma cells, but not B2M KO cells, also inhibited the degranulation of NKG2A$^-$ NK cells (Figure 7.14, 7.15). IFNγ thus induces changes in the expression of MHC-I on melanoma cells, selectively inhibiting both NKG2A$^+$ and NKG2A$^-$ NK cell subsets through different HLA molecules. These data also align with a GW CRISPR/Cas9 KO screen conducted on the K562 lymphoma cell line co-cultured with NK cells, where IFNγ-induced HLA-E inhibited NK cells via NKG2A and was identified as the sole molecule responsible for IFNγ-mediated resistance of K562 cells to NK cell killing[528].

8.1.5 Classical HLA molecules inhibits KIR$^+$ NK cell cytotoxicity

Since the inhibition of NKG2A$^-$ NK cells degranulation was still present during co-culture with HLA-E KO cells but not B2M KO cells, I focused on individual classical MHC-I molecules. A375 is considered a MHC-I$^+$ cell line due to its high staining of HLA-ABC by the conventional and widely used pan-HLA antibody clone W6/32. However, upon closer examination of individual HLA molecules, it became apparent that only HLA-A molecules are expressed at steady state, while the expression of HLA-B and HLA-C is induced upon exposure to IFNγ. Therefore, the MHC-I positivity determined by antibody clone W6/32 could falsely classify cell line as HLA-ABC$^+$ despite no HLA-B and HLA-C expression (Figure 7.18). To investigate the effect of classical MHC-I on NKG2A- NK cells, I generated melanoma cells deficient in classical HLA molecules. The fact that simultaneous deletion of all classical MHC-I molecules also led to a reduction in the expression of HLA-E[79,178], which requires peptides derived from classical MHC-I for its expression, I avoided the reduction in HLA-E expression by generating HLA-BC dKO melanoma cells that remained the expression of HLA-A unaltered, thus providing signal peptides for HLA-E expression (Figure 7.23). The absence of *HLA-B* and *HLA-C* specifically increased the degranulation of only NKG2A$^-$ NK cell subsets while keeping NKG2A$^+$ NK cells inhibited by HLA-E after IFNγ pre-treatment of melanoma cells.

I focused on KIRs as the major receptors for MHC-I molecules, which in allogeneic settings, should exhibit no inhibition resulting in potent NK cell degranulation due to their inability to recognize non-self HLA alleles on melanoma cells. Regardless, since A375 cells express HLA alleles that are reported to be bound by KIR receptors[168,569], I proceeded to validate the potential of KIRs as receptors for classical MHC-I, and thus mediators of the inhibition of NKG2A- NK cell cytotoxicity. In my experimental system, 2-d IL-2-activated NK cells were used, which still resemble similar proportions of NKG2A NK cell subsets and exhibit predominant expression of KIRs on NKG2A$^-$ NK cells (Figure 7.16, 7.24), as reported before[570]. Expression of KIRs together with NKG2A clearly delineated 4 distinct NK cell subsets that varied in terms of regulation and magnitude of degranulation (Figure 7.24). The absence of *HLA-B* and *HLA-C* on IFNγ-pre-treated melanoma cells specifically increased the degranulation of NKG2A$^-$ KIR$^+$ NK cells, while showing no effect on NKG2A$^+$ KIR$^+$ NK cells. Moreover, the inhibition of NKG2A$^+$ KIR$^-$ NK cells after IFNγ pre-treatment of melanoma cell relied entirely on HLA-E, whereas NKG2A$^+$ KIR$^+$ NK cells still displayed partial inhibition after co-culture with HLA-E KO cells. I further focused on the discrepancy in the NKG2A$^-$ KIR$^+$ NK and NKG2A$^+$ KIR$^+$ NK cell response against HLA BC dKO cells.

I hypothesized, that NKG2A$^+$ KIR$^+$ NK cells originate from NKG2A$^-$ KIR$^+$ NK cells by upregulating NKG2A, which exerts a dominant inhibitory role over the KIRs. I confirmed, that during the course of NK cell expansion, both proliferating KIR$^-$ and KIR$^+$ NKG2A$^-$ NK cell subsets upregulate NKG2A, thereby transitioning to the NKG2A$^+$ NK cell subset (Figure 7.25). Recently, Kaulfuss et al. published similar findings depicting NKG2A as an essential factor for maintaining the expansion NK cells by preventing the activation-induced cell death[571]. The plasticity of NKG2A$^-$ NK cells in transitioning to NKG2A$^+$ NK cells by upregulating NKG2A as a dominant inhibitory receptor explains why NKG2A$^+$ KIR$^+$ NK cells remain highly inhibited after co-culture with HLA-BC KO cells, where the expression of HLA-E remained. I further confirmed that the loss of *HLA-E* in HLA-BC dKO cells unmasked the effect of HLA-BC and further augmented the degranulation of NKG2A$^+$ KIR$^+$ NK cells in comparison to co-culture with single HLA-E KO cells (Figure 7.26, 8.3).

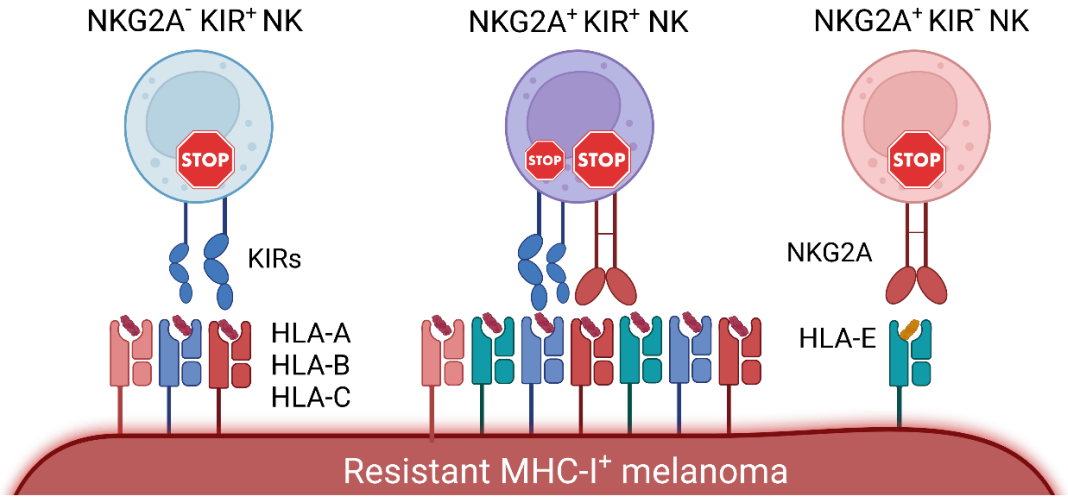

Figure 8.3 Schematic representation of individual HLA alleles inhibiting distinct NK cell subsets defined by NKG2A and KIRs expression. Image created using Biorender.

8.1.6 Monalizumab/lirilumab/DX9 treatment restores NK cell cytotoxicity

The expression of MHC-I or NKG2A and KIRs in cancer patients is crucial for transferring this knowledge into a clinical practise. In tumors, NKG2A is frequently expressed on NK and T cells in various human cancers and is correlated with poor patient outcomes[180,183,572–574]. In addition to elevated NKG2A expression, intratumoral NK cells exhibit a significant decrease in activating receptors and MHC-I receptors such as ILT-2 and KIRs[575]. This, along with other suppressive factors within the TME, may explain why NK cells isolated from tumor tissues exhibit lower cytotoxic potential compared to NK cells from healthy tissue[576]. Contrary to low classical MHC-I expression, which aids in T-cell evasion, HLA-E is

frequently overexpressed in tumors and is associated with poor patient prognosis, potentially contributing to resistance to ICB therapy. [180,574,575,577–582]. Due to the clinical relevance of these molecules, I mimicked the effects of HLA knockouts on NK cell function using therapeutic blocking mAbs. Monalizumab, a NKG2A blocking mAb, enhances the anti-tumor activity of both T and NK cells and is currently undergoing clinical trials. Initial results indicate improved patient responses, particularly when combined with other therapeutic agents[180,537–539]. Lirilumab, a KIR2D blocking mAb, is also being evaluated in clinical trials but has shown limited efficacy in improving patient survival[583–585]. Monalizumab treatment fully restored the degranulation of NKG2A^{+} KIR^{-} NK cells but only partially NKG2A^{+} KIR^{+} NK cells comparably as observed during co-culture with HLA-E KO cells (Figure 7.27). Lirilumab increased degranulation of NKG2A^{-} NK cells to the same level as observed during co-culture with HLA-BC dKO cells (Figure 7.28). As lirilumab does not block all KIRs, I combined it with DX9, a KIR3DL1 blocking mAb, which fully restored the degranulation of NKG2A^{-} KIR^{+} NK cells against IFNγ pre-treated melanoma cells (Figure 7.31). The combined treatment of monalizumab, lirilumab and DX9 almost completely abolished the IFNγ-mediated resistance of melanoma cells to NK cell cytotoxicity. This was evidenced by the nearly complete restoration of the degranulation of all NKG2A/KIR NK cell subsets against IFNγ-pre-treated melanoma cells (Figure 7.29 – 7.31). Lastly, I incorporated 6 other MHC-I+ tumor cell lines of different origin and observed, that IFNγ pre-treatment of all tumor cell lines resulted in the reduction of NK cell degranulation, which was fully restored by combined monalizumab, lirilumab and DX9 treatment (Figure 7.32). Taken together, IFNγ-mediated tumor cell resistance to NK cell cytotoxicity appears to be a shared tumor evasion mechanism across multiple cancer types, which can be potently abolished by combined monalizumab, lirilumab, and DX9 treatment (Figure 8.4).

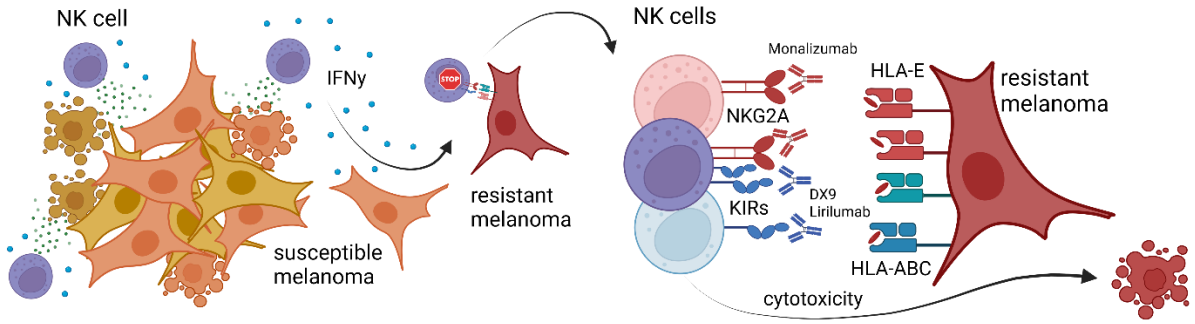

Figure 8.4 Schematic representation IFNγ-mediated resistance of melanoma cells to NK cell cytotoxicity abolished by using NKG2A and KIRs blocking mAbs. Image created using Biorender.

8.1.7 Proposed model

Several studies have shown that NK cells are the major players in the early stages of tumor development and in the elimination of circulating metastases, while the control of the already established or dormant tumors relies primarily on the adaptive immune system, particularly cytotoxic T cellscells[388–392]. In accordance with the current understanding of the roles played by NK and T cells in various stages of tumor development, I propose a model of tumor resistance, where NK cells, upon encountering tumor cells, would not distinguish and would attempt to eliminate tumor cells regardless of their capability to express MHC-I. However, activation of NK cells by tumor cells is often accompanied by high IFNγ production. The presence of IFNγ within the TME would lead to the induction of HLA-E and classical MHC-I expression. This combination of MHC-I inhibits the cytotoxicity of multiple NK cell subsets by engaging with inhibitory NKG2A and KIR receptors, where NKG2A displays the highest impact on the inhibition of NK cell cytotoxicity. Therefore, in this context, NK-produced IFNγ serves as a self-regulating NK cell shutdown mechanism due to the induction of strong tumor cell resistance. This potentially explains why NK cells become less effective in controlling already established tumors where IFNγ is present (Figure 8.5).

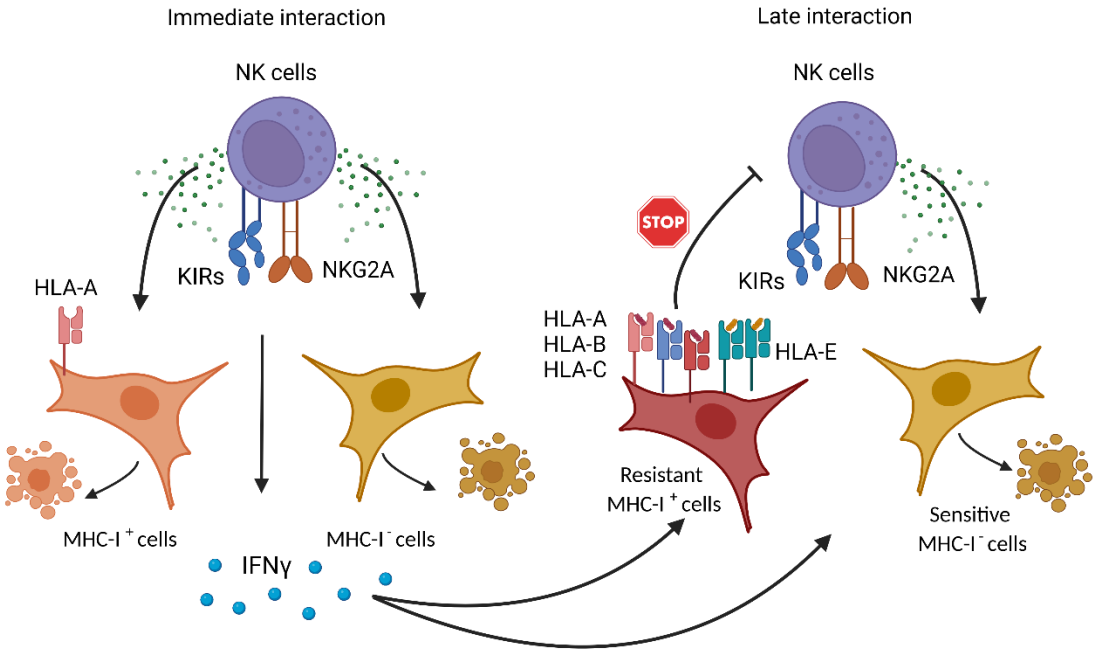

Figure 8.5 Schematic representation of a proposed model of NK cells in the early step of tumor recognition in comparison to a later stage, where melanoma cells acquire resistance to NK cell cytotoxicity by upregulating MHC-I molecules by NK-produced IFNγ. Image created using Biorender.

IFNγ, one of the main NK cell weapons, is depicted here as a shutdown mechanism in regards to NK cells ability to eliminate MHC-I$^+$ tumors. The IFNγ-induced resistance of MHC-I$^+$ melanoma cells to NK cell cytotoxicity aligns with Kelly et al. in vivo study, where NK cells were capable of rejecting only MHC-I deficient tumor cells, while the rejection of MHC-I sufficient tumor cells was mediated by effector T cells[399]. However, this should not imply that NK cells are not important for eliminating MHC-I$^+$ tumors. NK cells are still capable of rejecting MHC-I+ tumor cells that exhibit increased expression of activating ligands such as stress-induced NKG2D ligands[586]. However, the likelihood of tumor escape for MHC-I$^+$ tumor cells is greater due to the potent inhibitory function of MHC-I, which can be abolished by the blockade MHC-I receptors[587].

In general, NK cells and IFNγ are crucial for inducing adaptive immunity and preventing primary tumor development[393,400,588]. Indeed, mice deficient in IFNγ signalling developed tumors more rapidly and with higher frequency than WT mice[29]. IFNγ is important for antigen processing by DC and for mediating T cell response via antigen peptides presented by classical MHC-I induced by NK-derived IFNγ within TME[393,400,588]. The opposing roles of IFNγ and classical MHC-I on NK and T cells allow T cells to sustain tumor surveillance initiated by NK cells, which later become dysfunctional due to upregulated classical MHC-I expression. The transient nature of HLA-C could also suggest a potential evasion mechanism to both NK and T cell. IFNγ induces high expression of HLA-C, which inhibits NK cells; however, the followed downregulation of HLA-C might also facilitate evasion to T-cell mediated recognition via TCR. The role of IFNγ and classical MHC-I for T cell recognition of tumor cells is also reflected in patient datasets, which demonstrate frequent mutations in the IFNγ signalling pathway or in genes associated with antigen presentation pathways[405,466,589,590]. These patient data from established tumors mostly reflect escape mutations that occur after initial evasion of the innate immune system, targeting adaptive T cells. The crucial role of NK cells in the initial recognition of tumor cells was also reflected in an *in vivo* GW CRISPR/Cas9 KO screen, where both NK and T cells were present[591]. The study revealed that MHC-I and IFNγ play significant roles in tumor resistance to the immune system thus reflecting the importance of NK cells over T cells in the early elimination of tumor cells[591].

The question of targeting IFNγ signalling pathway as a potential therapeutic approach is complex due to its opposing effects on NK and T cells concerning the induction of classical MHC-I. Neutralizing IFNγ or targeting IFNGR in context of preventing the expression of HLA-E is less favourable compared to a direct NKG2A receptor blocking by monalizumab, which would keep the beneficial effect of IFNγ on other immune cells while specifically restoring

both innate and adaptive antitumor immune response unleashing NK and T cell anti-tumor function[592]. Direct unleashing of NK cells by KIR2 blockade with lirilumab has failed to fulfill expectations in adding efficacy to anti-PD-1 therapy in head and neck cancer and as a single agent also did not significantly improve patient survival[583–585]. One potential explanation for this low efficacy of lirilumab in patients can be found in my data, where lirilumab might not have been able to restore the function of NKG2A$^+$ KIR$^+$ NK cells due to the presence of the HLA-E/NKG2A inhibitory axis. Thereby, therapeutic use of combined monalizumab, lirilumab and DX9 treatment might be an attractive approach to restore function of multiple NK cell subsets in already established MHC-I$^+$ tumors or as a prevention from disseminating metastases from primary tumor site. In addition to checkpoint inhibitors, adoptive transfer of NK cells equipped by chimeric antigen receptors (CARs) showed evidence of clinical benefits[593]. However, high expansion of these cell products might also result in the upregulation of NKG2A. Therefore, the addition of combined monalizumab, lirilumab and DX9 treatment or genetic depletion of NKG2A and KIRs from CAR NK cells might enhance their responsiveness against resistant tumors in patients.

8.2 B2M KO GW CRISPR/Cas9 KO resistance screen

My initial screen, alongside other GW CRISPR/Cas9 screens, demonstrated the significant role of MHC-I in mediating tumor resistance to NK cell killing[528,532,563,564,591]. Due to its dominant inhibitory role, any genes that influence MHC-I expression on various levels, including cytokine signalling molecules, transcription factors, protein translation and modification, peptide loading machinery genes or genes involved in the transport of MHC-I to plasma membrane would greatly sensitize tumor cells to NK cell killing. To overcome the inhibitory effect of the major MHC-I axis and its associated genes, I repeated GW CRISPR/Cas9 KO screen on the B2M KO melanoma cell line. Genes involved in IFNγ signalling and antigen presentation machinery, which scored highly in the WT screen, did not score in the B2M KO screen. Multiple MHC-I-independent candidates involved in autophagy, AHR and Hippo pathway highly scored in both screens. I decided to focus on candidates that did not score highly in WT screen, but had more potent effect on NK cell killing in B2M KO screen. These genes include sugar-modifying enzymes in the sialylation pathway (*CMAS, GALE, GNE*) as well as channels (*SLC35A1, SLC35A2*) that transport sialic acid into Golgi network, where it is used for peptide sialylation[594] (Figure 7.33, 7.34).

8.2.1 Loss of *SLC35A1* or *TM9SF3* in melanoma cells unleashes the cytotoxicity of Siglec-9$^+$ NK cells

The loss of sialic acid transporter *SLC35A1* in melanoma cells resulted in decreased sugar content displayed on the plasma membrane, as well as increased expression of multiple NK-related molecules (Figure 7.35). The increase in the expression of MHC-I might be the reason why SLC35A1 did not score highly in the WT screen, as the higher MHC-I expression could have masked the loss of *SLC35A1*. I confirmed that SLC35A1 KO melanoma cells showed reduced resisitance to NK cell killing, which was even more pronounced in B2M KO conditions (Figure 7.36). The main receptors for sialylated proteins are Siglecs, which have an inhibitory function and are broadly expressed throughout the immune system. NK cells primarily express Siglec-7 and Siglec-9 receptors, both of which contribute to immune surveillance. Their expression levels are associated with either a dysfunctional or highly active state depending on the type of disease[230,232,240,242,595–599]. All tested melanoma cell lines exhibited high expression of Siglec-7 and Siglec-9 ligands; however, no expression was detected upon deletion of *SLC35A1* (Figure 7.37). Correspondingly, unlike WT cells, SLC35A1 KO cell failed to inhibit Siglec-9$^+$ NK cells, despite high expression of Siglec-7 (Figure 7.38). The effect of SLC35A1 on the Siglec-9+ NK cell subset was also reproduced in two other melanoma cell lines. However, the deletion of *SLC35A1* in UKRV-Mel02 cells also increased the degranulation of Siglec-9$^-$ NK cells, suggesting a potential involvement of other Siglec-7 ligands, which might exhibit different potency specific to tumor cells.

Since the main goal was to identify a novel surface membrane candidate that could potentially be blocked to restore NK cell function, I focused on candidates classified as membrane proteins or predicted as membrane proteins. These criteria would also involve proteins that do not necessarily reside in the plasma membrane, but are part of intracellular membrane structures, such as ER, Golgi apparatus, mitochondria or lysosomes. One of the candidates that emerged is TM9SF3, an understudied member of a four-member family located in the Golgi network and potentially expressed on the cell surface. Its high expression is involved in tumor invasion and is associated with poor patient outcome[542,544]. The loss of TM9SF3 in melanoma cells did not significantly alter the expression of melanoma cell surface molecules to the extent observed in SLC35A1 KO cells. However, a reduction in ligand expression for NKp30, Siglec-7, and Siglec-9 receptors was observed in TM9SF3 KO cells, similar to SLC35A1 KO cells (Figure 7.40). TM9SF3 KO cells showed no inhibition of the degranulation of Siglec-9$^+$ NK cells potentially responsible for a reduced resistance of TM9SF3

KO cells to NK cell killing. Previous studies have shown that members of TM9SF family affects the transport of glycosylated proteins to the plasma membrane[545,546,600]. The similar phenotype of TM9SF3 KO cells to SLC35A1 KO cells might suggest a potential involvement of TM9SF3 in the sialic acid biosynthesis pathway, glycoprotein modifications or in the transport of ligands to the plasma membrane (Figure 8.6). Therefore, Golgi-located TM9SF3 might serve as a checkpoint step controlling glycosylated Siglec ligands and facilitating their transport to the plasma membrane to inhibit NK cell cytotoxicity. Since TM9SF3 KO cells exhibited less broad alterations in the expression of cell surface ligands compared to SLC35A1 KO cells, pharmacological targeting of TM9SF3 with small molecular compounds or inhibitors might represent an attractive strategy to specifically increase cytotoxic function of Siglec-9^{+} NK cells. Recently a Siglec-9 blocking mAb showed improvements in NK cell cytotoxicity *in vitro* and *in vivo*[251]. This suggests that Siglec-9 could be a promising new target worth of further clinical investigation.

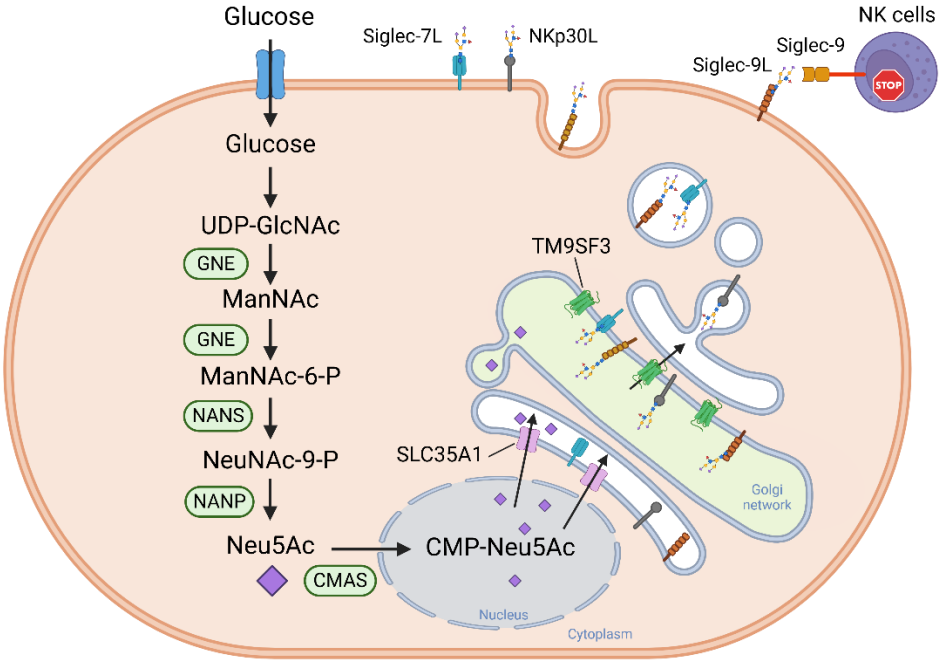

Figure 8.6 Schematic representation of top scoring candidates revealed in B2M KO GW CRISPR/Cas9 KO screen and their involvement in sialic acid biosynthesis pathway and protein glycosylation machinery. Image created using Biorender.

8.2.2 Role of AHR and Hippo pathway in melanoma cell resistance to NK cells

Candidates that significantly scored in both screens are also highly attractive research targets, as they may play a crucial role in anti-tumor function irrespective of tumor MHC-I positivity. Two MHC-I-independent candidate pathways are the AHR pathway (*AHR, ARNT, HSP90AB1*) and the Hippo pathway (*LATS2, NF2, RUNX1, VGLL4, SAV1*) (Figure 7.41). Melanoma cells transfected with sgRNA against the AHR gene showed reduced tumor resistance to NK cell killing but no alterations in NK cell degranulation (Figure 7.41). Multiple candidates that exhibited reduced sgRNA counts in both screens are negative regulators of the key Hippo pathway transcription factor TAZ, which displayed highly enriched sgRNA counts. Cells transfected with sgRNA targeting WWTR1, encoding the TAZ protein, exhibited high resistance to NK cell killing but showed no effect on NK cell degranulation. Despite their effect on tumor cell resistance to NK cell killing, both of these pathways were excluded due to their involvement in cell proliferation and regulation of apoptosis[548,551,552,601–608]. The alterations in the regulation of apoptosis signalling would explain the effect on tumor cell resistance to NK cell cytotoxicity without a direct effect on the degranulation of NK cells. Given the extensive involvement of both these pathways in cell-cell contact inhibition, proliferation and apoptosis, further research holds the potential to unveil mechanisms that could prove beneficial for advancing cancer treatment.

9 CONCLUSION

To address the question of melanoma cell resistance mechanisms to NK cell killing, I successfully performed a GW CRISPR/Cas9 KO screens that revealed multiple candidates protecting melanoma cells from NK cell cytotoxicity. Instead of observing their effect on overall NK cell function, I connected the inhibitory function of each studied candidate to a specific NK cell subset.

I described a crucial role of IFNγ in inducing strong tumor cell resistance to multiple NK cell subsets by different classical and non-classical MHC-I-dependent mechanisms. IFNγ transiently induced expression of HLA-E, which as a single ligand was potent enough to fully inhibit the function of NKG2A^{+} KIR^{-} NK cell subset while only partially NKG2A^{+} KIR^{+} NK cell subset. IFNγ-induced classical MHC-I molecules inhibited the function of NKG2A^{-} KIR^{+} NK cell subset despite mismatched conditions. The inhibitory role these HLA molecules was then synergistically reflected on NKG2A^{+} KIR^{+} NK cell subset, where NKG2A acted as a dominant inhibitory receptor over KIRs inhibitory function. These data were also fully reproduced by using therapeutic blocking antibodies monalizumab and lirilumab in combination with DX9 mAb. The existence of these blocking antibodies and their use in a clinical trials might accelerate their combined use to combat tumor cell resistance and restoring NK cell anti-tumor function in patients.

I investigated the resistance mechanisms of MHC-I-deficient melanoma cells, by performing another GW CRISPR/Cas9 KO screen in a B2M KO cell line, which unmasked less potent candidates otherwise masked by a potent IFNγ/MHC-I inhibitory signal. This screen revealed that melanoma cells deficient in the sialic acid biosynthesis pathway showed higher susceptibility to NK cell cytotoxicity. The function of these two candidates, SLC35A1 and TM9SF3, was again connected to a specific NK cell subset, Siglec-9^{+} NK cells.

Thus, combining these inhibitory axes either by generating NKG2A^{-} KIR^{-} Siglec-9^{-} NK cells for adoptive transfer therapy or the use of therapeutic antibodies blocking these receptors could overcome both IFNγ- as well as sialic acid-mediated resistance of tumor cells to NK cell cytotoxicity.

10 REFERENCES

1. Duan, L. & Mukherjee, E. Janeway's Immunobiology, Ninth Edition. *Yale J Biol Med* **89**, 424–425 (2016).
2. Taylor, P., Botto, M. & Walport, M. The complement system. *Curr Biol* **8**, R259-261 (1998).
3. Li, D. & Wu, M. Pattern recognition receptors in health and diseases. *Sig Transduct Target Ther* **6**, 1–24 (2021).
4. Innate and Adaptive Immunity - Creative Diagnostics. https://www.creative-diagnostics.com/innate-and-adaptive-immunity.htm.
5. Roth, D. B. V(D)J Recombination: Mechanism, Errors, and Fidelity. *Microbiol Spectr* **2**, 10.1128/microbiolspec.MDNA3-0041–2014 (2014).
6. Nemazee, D. Mechanisms of central tolerance for B cells. *Nat Rev Immunol* **17**, 281–294 (2017).
7. Takaba, H. & Takayanagi, H. The Mechanisms of T Cell Selection in the Thymus. *Trends in Immunology* **38**, 805–816 (2017).
8. Mondino, A., Khoruts, A. & Jenkins, M. K. The anatomy of T-cell activation and tolerance. *Proc Natl Acad Sci U S A* **93**, 2245–2252 (1996).
9. Goodnow, C. C., Vinuesa, C. G., Randall, K. L., Mackay, F. & Brink, R. Control systems and decision making for antibody production. *Nat Immunol* **11**, 681–688 (2010).
10. Lanier, L. L., Testi, R., Bindl, J. & Phillips, J. H. Identity of Leu-19 (CD56) leukocyte differentiation antigen and neural cell adhesion molecule. *J Exp Med* **169**, 2233–2238 (1989).
11. Nagler, A., Lanier, L. L., Cwirla, S. & Phillips, J. H. Comparative studies of human FcRIII-positive and negative natural killer cells. *The Journal of Immunology* **143**, 3183–3191 (1989).
12. Lanier, L. L., Ruitenberg, J. J. & Phillips, J. H. Functional and biochemical analysis of CD16 antigen on natural killer cells and granulocytes. *J Immunol* **141**, 3478–3485 (1988).
13. Masson, D. & Tschopp, J. Isolation of a lytic, pore-forming protein (perforin) from cytolytic T-lymphocytes. *J Biol Chem* **260**, 9069–9072 (1985).
14. Liu, C. C., Perussia, B., Cohn, Z. A. & Young, J. D. Identification and characterization of a pore-forming protein of human peripheral blood natural killer cells. *J Exp Med* **164**, 2061–2076 (1986).
15. Masson, D., Nabholz, M., Estrade, C. & Tschopp, J. Granules of cytolytic T-lymphocytes contain two serine esterases. *EMBO J* **5**, 1595–1600 (1986).
16. Prager, I. *et al.* NK cells switch from granzyme B to death receptor–mediated cytotoxicity during serial killing. *Journal of Experimental Medicine* **216**, 2113–2127 (2019).
17. Orange, J. S. *et al.* The mature activating natural killer cell immunologic synapse is formed in distinct stages. *Proceedings of the National Academy of Sciences* **100**, 14151–14156 (2003).
18. Li, Y. & Orange, J. S. Degranulation enhances presynaptic membrane packing, which protects NK cells from perforin-mediated autolysis. *PLoS Biol* **19**, e3001328 (2021).
19. Lopez, J. A. *et al.* Rapid and Unidirectional Perforin Pore Delivery at the Cytotoxic Immune Synapse. *The Journal of Immunology* **191**, 2328–2334 (2013).
20. Chaudhary, P. M. *et al.* Death Receptor 5, a New Member of the TNFR Family, and DR4 Induce FADD-Dependent Apoptosis and Activate the NF-κB Pathway. *Immunity* **7**, 821–830 (1997).
21. Walczak, H. *et al.* TRAIL-R2: a novel apoptosis-mediating receptor for TRAIL. *The EMBO Journal* **16**, 5386–5397 (1997).

22. MacFarlane, M. *et al*. Identification and Molecular Cloning of Two Novel Receptors for the Cytotoxic Ligand TRAIL *. *Journal of Biological Chemistry* **272**, 25417–25420 (1997).
23. Medema, J. P. *et al.* FLICE is activated by association with the CD95 death-inducing signaling complex (DISC). *The EMBO Journal* **16**, 2794–2804 (1997).
24. Rouvier, E., Luciani, M. F. & Golstein, P. Fas involvement in Ca(2+)-independent T cell-mediated cytotoxicity. *Journal of Experimental Medicine* **177**, 195–200 (1993).
25. Zamai, L. *et al.* Natural Killer (NK) Cell–mediated Cytotoxicity: Differential Use of TRAIL and Fas Ligand by Immature and Mature Primary Human NK Cells. *J Exp Med* **188**, 2375–2380 (1998).
26. Prager, I. & Watzl, C. Mechanisms of natural killer cell-mediated cellular cytotoxicity. *Journal of Leukocyte Biology* **105**, 1319–1329 (2019).
27. Kurosawa, S. *et al*. Early-appearing tumour-infiltrating natural killer cells play a crucial role in the generation of anti-tumour T lymphocytes. *Immunology* **85**, 338 (1995).
28. Maraskovsky, E., Chen, W. F. & Shortman, K. IL-2 and IFN-gamma are two necessary lymphokines in the development of cytolytic T cells. *The Journal of Immunology* **143**, 1210–1214 (1989).
29. Kaplan, D. H. *et al*. Demonstration of an interferon γ-dependent tumor surveillance system in immunocompetent mice. *Proceedings of the National Academy of Sciences* **95**, 7556–7561 (1998).
30. Wendel, M., Galani, I. E., Suri-Payer, E. & Cerwenka, A. Natural Killer Cell Accumulation in Tumors Is Dependent on IFN-γ and CXCR3 Ligands. *Cancer Research* **68**, 8437–8445 (2008).
31. Zhao, Y.-H. *et al.* Anti-proliferation effects of interferon-gamma on gastric cancer cells. *Asian Pac J Cancer Prev* **14**, 5513–5518 (2013).
32. Homann, L. *et al.* IFN-γ and TNF Induce Senescence and a Distinct Senescence-Associated Secretory Phenotype in Melanoma. *Cells* **11**, 1514 (2022).
33. Woznicki, J. A. *et al.* TNF-α synergises with IFN-γ to induce caspase-8-JAK1/2-STAT1-dependent death of intestinal epithelial cells. *Cell Death Dis* **12**, 1–15 (2021).
34. De Saint Jean, M., Brignole, F., Feldmann, G., Goguel, A. & Baudouin, C. Interferon-gamma induces apoptosis and expression of inflammation-related proteins in Chang conjunctival cells. *Invest Ophthalmol Vis Sci* **40**, 2199–2212 (1999).
35. Zhou, F. Molecular Mechanisms of IFN-γ to Up-Regulate MHC Class I Antigen Processing and Presentation. *International Reviews of Immunology* **28**, 239–260 (2009).
36. Mimura, K. *et al.* PD-L1 expression is mainly regulated by interferon gamma associated with JAK-STAT pathway in gastric cancer. *Cancer Sci* **109**, 43–53 (2018).
37. Vivier, E., Tomasello, E., Baratin, M., Walzer, T. & Ugolini, S. Functions of natural killer cells. *Nat Immunol* **9**, 503–510 (2008).
38. Yu, J., Freud, A. G. & Caligiuri, M. A. Location and cellular stages of natural killer cell development. *Trends in Immunology* **34**, 573–582 (2013).
39. Abel, A. M., Yang, C., Thakar, M. S. & Malarkannan, S. Natural Killer Cells: Development, Maturation, and Clinical Utilization. *Frontiers in Immunology* **9**, (2018).
40. Scoville, S. D., Freud, A. G. & Caligiuri, M. A. Modeling Human Natural Killer Cell Development in the Era of Innate Lymphoid Cells. *Frontiers in Immunology* **8**, (2017).
41. Poli, A. *et al.* CD56bright natural killer (NK) cells: an important NK cell subset. *Immunology* **126**, 458–465 (2009).
42. Perussia, B., Starr, S., Abraham, S., Fanning, V. & Trinchieri, G. Human natural killer cells analyzed by B73.1, a monoclonal antibody blocking Fc receptor functions. I. Characterization of the lymphocyte subset reactive with B73.1. *The Journal of Immunology* **130**, 2133–2141 (1983).

43. Lanier, L. L., Le, A. M., Phillips, J. H., Warner, N. L. & Babcock, G. F. Subpopulations of human natural killer cells defined by expression of the Leu-7 (HNK-1) and Leu-11 (NK-15) antigens. *The Journal of Immunology* **131**, 1789–1796 (1983).
44. Hibbs, M. L. *et al.* Mechanisms for Regulating Expression of Membrane Isoforms of FcγRIII (CD16). *Science* **246**, 1608–1611 (1989).
45. Lanier, L. L., Yu, G. & Phillips, J. H. Co-association of CD3ζ with a receptor (CD16) for IgG Fc on human natural killer cells. *Nature* **342**, 803–805 (1989).
46. Merkt, W., Lorenz, H.-M. & Watzl, C. Rituximab induces phenotypical and functional changes of NK cells in a non-malignant experimental setting. *Arthritis Res Ther* **18**, 206 (2016).
47. Enqvist, M. *et al.* Systemic and Intra-Nodal Activation of NK Cells After Rituximab Monotherapy for Follicular Lymphoma. *Front Immunol* **10**, 2085 (2019).
48. Lanier, L. L. NK cell recognition. *Annu Rev Immunol* **23**, 225–274 (2005).
49. Balzasch, B. M. & Cerwenka, A. Microenvironmental signals shaping NK-cell reactivity in cancer. *European Journal of Immunology* **n/a**, 2250103.
50. Bauer, S. *et al.* Activation of NK Cells and T Cells by NKG2D, a Receptor for Stress-Inducible MICA | Science. *Science (New York, N.Y.)* **285**, 727–9 (1999).
51. Nausch, N. & Cerwenka, A. NKG2D ligands in tumor immunity. *Oncogene* **27**, 5944–5958 (2008).
52. Wu, J. *et al.* An activating immunoreceptor complex formed by NKG2D and DAP10. *Science* **285**, 730–732 (1999).
53. Cosman, D. *et al.* ULBPs, Novel MHC Class I–Related Molecules, Bind to CMV Glycoprotein UL16 and Stimulate NK Cytotoxicity through the NKG2D Receptor. *Immunity* **14**, 123–133 (2001).
54. Jan Chalupny, N., Sutherland, C. L., Lawrence, W. A., Rein-Weston, A. & Cosman, D. ULBP4 is a novel ligand for human NKG2D. *Biochemical and Biophysical Research Communications* **305**, 129–135 (2003).
55. Gasser, S., Orsulic, S., Brown, E. J. & Raulet, D. H. The DNA damage pathway regulates innate immune system ligands for the NKG2D receptor. *Nature* **436**, 1186–1190 (2005).
56. Raulet, D. H., Gasser, S., Gowen, B. G., Deng, W. & Jung, H. Regulation of Ligands for the NKG2D Activating Receptor. *Annual Review of Immunology* **31**, 413–441 (2013).
57. Oppenheim, D. E. *et al.* Sustained localized expression of ligand for the activating NKG2D receptor impairs natural cytotoxicity in vivo and reduces tumor immunosurveillance. *Nat Immunol* **6**, 928–937 (2005).
58. Champsaur, M. *et al.* Intact NKG2D-Independent Function of NK Cells Chronically Stimulated with the NKG2D Ligand Rae-1. *The Journal of Immunology* **185**, 157–165 (2010).
59. Groh, V., Wu, J., Yee, C. & Spies, T. Tumour-derived soluble MIC ligands impair expression of NKG2D and T-cell activation. *Nature* **419**, 734–738 (2002).
60. Salih, H. R., Rammensee, H.-G. & Steinle, A. Cutting Edge: Down-Regulation of MICA on Human Tumors by Proteolytic Shedding. *The Journal of Immunology* **169**, 4098–4102 (2002).
61. Song, H., Kim, J., Cosman, D. & Choi, I. Soluble ULBP suppresses natural killer cell activity via down-regulating NKG2D expression. *Cellular Immunology* **239**, 22–30 (2006).
62. Ashiru, O. *et al.* Natural Killer Cell Cytotoxicity Is Suppressed by Exposure to the Human NKG2D Ligand MICA*008 That Is Shed by Tumor Cells in Exosomes. *Cancer Research* **70**, 481–489 (2010).

63. Boutet, P. *et al.* Cutting Edge: The Metalloproteinase ADAM17/TNF-α-Converting Enzyme Regulates Proteolytic Shedding of the MHC Class I-Related Chain B Protein1. *The Journal of Immunology* **182**, 49–53 (2009).
64. Ferrari de Andrade, L. *et al.* Antibody-mediated inhibition of MICA and MICB shedding promotes NK cell-driven tumor immunity. *Science* **359**, 1537–1542 (2018).
65. de Andrade, L. F. *et al.* Inhibition of MICA and MICB Shedding Elicits NK cell–mediated Immunity against Tumors Resistant to Cytotoxic T cells. *Cancer Immunol Res* **8**, 769–780 (2020).
66. Arai, J. *et al*. Enzymatic inhibition of MICA sheddase ADAM17 by lomofungin in hepatocellular carcinoma cells. *Int J Cancer* **143**, 2575–2583 (2018).
67. Kohga, K. *et al*. Anticancer chemotherapy inhibits MHC class I-related chain a ectodomain shedding by downregulating ADAM10 expression in hepatocellular carcinoma. *Cancer Res* **69**, 8050–8057 (2009).
68. Liu, G., Atteridge, C. L., Wang, X., Lundgren, A. D. & Wu, J. D. Cutting Edge: The Membrane Type Matrix Metalloproteinase MMP14 Mediates Constitutive Shedding of MHC Class I Chain-Related Molecule A Independent of A Disintegrin and Metalloproteinases. *The Journal of Immunology* **184**, 3346–3350 (2010).
69. Salih, H. R. *et al*. Determination of Soluble MICA in Serum as a Novel Marker for Tumor Stage and Metastasis. *Blood* **104**, 1344 (2004).
70. Arreygue-Garcia, N. A. *et al.* Augmented serum level of major histocompatibility complex class I-related chain A (MICA) protein and reduced NKG2D expression on NK and T cells in patients with cervical cancer and precursor lesions. *BMC Cancer* **8**, 16 (2008).
71. Holdenrieder, S. *et al.* Soluble MICB in malignant diseases: analysis of diagnostic significance and correlation with soluble MICA. *Cancer Immunol Immunother* **55**, 1584–1589 (2006).
72. Schwinn, N. *et al.* Interferon-gamma down-regulates NKG2D ligand expression and impairs the NKG2D-mediated cytolysis of MHC class I-deficient melanoma by natural killer cells. *Int J Cancer* **124**, 1594–1604 (2009).
73. Lazetic, S., Chang, C., Houchins, J. P., Lanier, L. L. & Phillips, J. H. Human natural killer cell receptors involved in MHC class I recognition are disulfide-linked heterodimers of CD94 and NKG2 subunits. *The Journal of Immunology* **157**, 4741–4745 (1996).
74. Brooks, A. G., Posch, P. E., Scorzelli, C. J., Borrego, F. & Coligan, J. E. NKG2A Complexed with CD94 Defines a Novel Inhibitory Natural Killer Cell Receptor. *Journal of Experimental Medicine* **185**, 795–800 (1997).
75. Vance, R. E., Jamieson, A. M. & Raulet, D. H. Recognition of the Class Ib Molecule Qa-1b by Putative Activating Receptors Cd94/Nkg2c and Cd94/Nkg2e on Mouse Natural Killer Cells. *Journal of Experimental Medicine* **190**, 1801–1812 (1999).
76. Lanier, L. L., Corliss, B., Wu, J. & Phillips, J. H. Association of DAP12 with Activating CD94/NKG2C NK Cell Receptors. *Immunity* **8**, 693–701 (1998).
77. Gumá, M. *et al.* Expansion of CD94/NKG2C+ NK cells in response to human cytomegalovirus-infected fibroblasts. *Blood* **107**, 3624–3631 (2006).
78. Gumá, M. *et al.* Imprint of human cytomegalovirus infection on the NK cell receptor repertoire. *Blood* **104**, 3664–3671 (2004).
79. Lee, N., Goodlett, D. R., Ishitani, A., Marquardt, H. & Geraghty, D. E. HLA-E surface expression depends on binding of TAP-dependent peptides derived from certain HLA class I signal sequences. *J Immunol* **160**, 4951–4960 (1998).
80. Nattermann, J. *et al*. HIV-1 infection leads to increased HLA-E expression resulting in impaired function of natural killer cells. *Antivir Ther* **10**, 95–107 (2005).

81. Ulbrecht, M. *et al.* Cutting Edge: The Human Cytomegalovirus UL40 Gene Product Contains a Ligand for HLA-E and Prevents NK Cell-Mediated Lysis1. *The Journal of Immunology* **164**, 5019–5022 (2000).
82. Tomasec, P. *et al.* Surface Expression of HLA-E, an Inhibitor of Natural Killer Cells, Enhanced by Human Cytomegalovirus gpUL40. *Science* **287**, 1031–1033 (2000).
83. Jørgensen, P. B., Livbjerg, A. H., Hansen, H. J., Petersen, T. & Höllsberg, P. Epstein-Barr virus peptide presented by HLA-E is predominantly recognized by CD8(bright) cells in multiple sclerosis patients. *PLoS One* **7**, e46120 (2012).
84. Pessino, A. *et al.* Molecular cloning of NKp46: a novel member of the immunoglobulin superfamily involved in triggering of natural cytotoxicity. *J Exp Med* **188**, 953–960 (1998).
85. Sivori, S. *et al.* p46, a Novel Natural Killer Cell–specific Surface Molecule That Mediates Cell Activation. *Journal of Experimental Medicine* **186**, 1129–1136 (1997).
86. Cantoni, C. *et al.* NKp44, a triggering receptor involved in tumor cell lysis by activated human natural killer cells, is a novel member of the immunoglobulin superfamily. *J Exp Med* **189**, 787–796 (1999).
87. Vitale, M. *et al.* NKp44, a Novel Triggering Surface Molecule Specifically Expressed by Activated Natural Killer Cells, Is Involved in Non–Major Histocompatibility Complex–restricted Tumor Cell Lysis. *Journal of Experimental Medicine* **187**, 2065–2072 (1998).
88. Pende, D. *et al.* Identification and Molecular Characterization of Nkp30, a Novel Triggering Receptor Involved in Natural Cytotoxicity Mediated by Human Natural Killer Cells. *Journal of Experimental Medicine* **190**, 1505–1516 (1999).
89. Barrow, A. D., Martin, C. J. & Colonna, M. The Natural Cytotoxicity Receptors in Health and Disease. *Frontiers in Immunology* **10**, (2019).
90. Sivori, S. *et al.* NKp46 is the major triggering receptor involved in the natural cytotoxicity of fresh or cultured human NK cells. Correlation between surface density of NKp46 and natural cytotoxicity against autologous, allogeneic or xenogeneic target cells. *European Journal of Immunology* **29**, 1656–1666 (1999).
91. Mandelboim, O. *et al.* Recognition of haemagglutinins on virus-infected cells by NKp46 activates lysis by human NK cells. *Nature* **409**, 1055–1060 (2001).
92. Garg, A. *et al.* Vimentin expressed on Mycobacterium tuberculosis-infected human monocytes is involved in binding to the NKp46 receptor. *J Immunol* **177**, 6192–6198 (2006).
93. Moretta, A., Biassoni, R., Bottino, C., Mingari, M. C. & Moretta, L. Natural cytotoxicity receptors that trigger human NK-cell-mediated cytolysis. *Immunology Today* **21**, 228–234 (2000).
94. Cagnano, E. *et al.* Expression of Ligands to NKp46 in Benign and Malignant Melanocytes. *Journal of Investigative Dermatology* **128**, 972–979 (2008).
95. Narni-Mancinelli, E. *et al.* Complement factor P is a ligand for the natural killer cell–activating receptor NKp46. *Science Immunology* **2**, eaam9628 (2017).
96. Gur, C. *et al.* Recognition and killing of human and murine pancreatic beta cells by the NK receptor NKp46. *J Immunol* **187**, 3096–3103 (2011).
97. Mattiola, I. *et al.* Priming of Human Resting NK Cells by Autologous M1 Macrophages via the Engagement of IL-1β, IFN-β, and IL-15 Pathways. *The Journal of Immunology* **195**, 2818–2828 (2015).
98. Campbell, K. S., Yusa, S., Kikuchi-Maki, A. & Catina, T. L. NKp44 Triggers NK Cell Activation through DAP12 Association That Is Not Influenced by a Putative Cytoplasmic Inhibitory Sequence 1. *The Journal of Immunology* **172**, 899–906 (2004).

99. Fuchs, A., Cella, M., Kondo, T. & Colonna, M. Paradoxic inhibition of human natural interferon-producing cells by the activating receptor NKp44. *Blood* **106**, 2076–2082 (2005).
100. Ho, J. W. *et al.* H5-Type Influenza Virus Hemagglutinin Is Functionally Recognized by the Natural Killer-Activating Receptor NKp44. *Journal of Virology* **82**, 2028–2032 (2008).
101. Arnon, T. I. *et al.* Recognition of viral hemagglutinins by NKp44 but not by NKp30. *European Journal of Immunology* **31**, 2680–2689 (2001).
102. McQuaid, S. *et al.* Haemagglutinin-neuraminidase from HPIV3 mediates human NK regulation of T cell proliferation via NKp44 and NKp46. *Journal of General Virology* **99**, 763–767.
103. Jarahian, M. *et al.* Activation of Natural Killer Cells by Newcastle Disease Virus Hemagglutinin-Neuraminidase. *Journal of Virology* **83**, 8108–8121 (2009).
104. Hershkovitz, O. *et al.* NKp44 Receptor Mediates Interaction of the Envelope Glycoproteins from the West Nile and Dengue Viruses with NK Cells1. *The Journal of Immunology* **183**, 2610–2621 (2009).
105. Hecht, M.-L. *et al.* Natural Cytotoxicity Receptors NKp30, NKp44 and NKp46 Bind to Different Heparan Sulfate/Heparin Sequences. *J. Proteome Res.* **8**, 712–720 (2009).
106. Hershkovitz, O. *et al.* Characterization of the Recognition of Tumor Cells by the Natural Cytotoxicity Receptor, NKp44. *Biochemistry* **46**, 7426–7436 (2007).
107. Gaggero, S. *et al.* Nidogen-1 is a novel extracellular ligand for the NKp44 activating receptor. *OncoImmunology* **7**, e1470730 (2018).
108. Barrow, A. D. *et al.* Natural Killer Cells Control Tumor Growth by Sensing a Growth Factor. *Cell* **172**, 534-548.e19 (2018).
109. Horton, N. C., Mathew, S. O. & Mathew, P. A. Novel Interaction between Proliferating Cell Nuclear Antigen and HLA I on the Surface of Tumor Cells Inhibits NK Cell Function through NKp44. *PLOS ONE* **8**, e59552 (2013).
110. Stoimenov, I. & Helleday, T. PCNA on the crossroad of cancer. *Biochemical Society Transactions* **37**, 605–613 (2009).
111. Rosental, B., Hadad, U., Brusilovsky, M., Campbell, K. S. & Porgador, A. A novel mechanism for cancer cells to evade immune attack by NK cells. *OncoImmunology* **1**, 572–574 (2012).
112. Shemesh, A. *et al.* NKp44-Derived Peptide Binds Proliferating Cell Nuclear Antigen and Mediates Tumor Cell Death. *Frontiers in Immunology* **9**, (2018).
113. Textor, S. *et al.* The proto-oncogene Myc drives expression of the NK cell-activating NKp30 ligand B7-H6 in tumor cells. *OncoImmunology* **5**, e1116674 (2016).
114. Matta, J. *et al.* Induction of B7-H6, a ligand for the natural killer cell–activating receptor NKp30, in inflammatory conditions. *Blood* **122**, 394–404 (2013).
115. Brandt, C. S. *et al.* The B7 family member B7-H6 is a tumor cell ligand for the activating natural killer cell receptor NKp30 in humans. *Journal of Experimental Medicine* **206**, 1495–1503 (2009).
116. Obiedat, A. *et al.* The integrated stress response promotes B7H6 expression. *J Mol Med (Berl)* **98**, 135–148 (2020).
117. Schlecker, E. *et al.* Metalloprotease-Mediated Tumor Cell Shedding of B7-H6, the Ligand of the Natural Killer Cell–Activating Receptor NKp30. *Cancer Research* **74**, 3429–3440 (2014).
118. Fiegler, N. *et al.* Downregulation of the activating NKp30 ligand B7-H6 by HDAC inhibitors impairs tumor cell recognition by NK cells. *Blood* **122**, 684–693 (2013).

119. Pogge von Strandmann, E. *et al.* Human Leukocyte Antigen-B-Associated Transcript 3 Is Released from Tumor Cells and Engages the NKp30 Receptor on Natural Killer Cells. *Immunity* **27**, 965–974 (2007).
120. Ponath, V. *et al.* Secreted Ligands of the NK Cell Receptor NKp30: B7-H6 Is in Contrast to BAG6 Only Marginally Released via Extracellular Vesicles. *Int J Mol Sci* **22**, 2189 (2021).
121. Wang, W. *et al.* Tumor-released Galectin-3, a Soluble Inhibitory Ligand of Human NKp30, Plays an Important Role in Tumor Escape from NK Cell Attack. *Journal of Biological Chemistry* **289**, 33311–33319 (2014).
122. Farhad, M., Rolig, A. S. & Redmond, W. L. The role of Galectin-3 in modulating tumor growth and immunosuppression within the tumor microenvironment. *OncoImmunology* **7**, e1434467 (2018).
123. Mathew, P. A. *et al.* Cloning and characterization of the 2B4 gene encoding a molecule associated with non-MHC-restricted killing mediated by activated natural killer cells and T cells. *The Journal of Immunology* **151**, 5328–5337 (1993).
124. Latchman, Y., McKay, P. F. & Reiser, H. Cutting Edge: Identification of the 2B4 Molecule as a Counter-Receptor for CD481. *The Journal of Immunology* **161**, 5809–5812 (1998).
125. Vaidya, S. V. *et al.* Targeted Disruption of the 2B4 Gene in Mice Reveals an In Vivo Role of 2B4 (CD244) in the Rejection of B16 Melanoma Cells1. *The Journal of Immunology* **174**, 800–807 (2005).
126. Messmer, B., Eissmann, P., Stark, S. & Watzl, C. CD48 stimulation by 2B4 (CD244)-expressing targets activates human NK cells. *J Immunol* **176**, 4646–4650 (2006).
127. Zhang, Z. *et al.* DNAM-1 controls NK cell activation via an ITT-like motif. *J Exp Med* **212**, 2165–2182 (2015).
128. Bottino, C. *et al.* Identification of PVR (CD155) and Nectin-2 (CD112) as Cell Surface Ligands for the Human DNAM-1 (CD226) Activating Molecule. *Journal of Experimental Medicine* **198**, 557–567 (2003).
129. Tahara-Hanaoka, S. *et al.* Functional characterization of DNAM-1 (CD226) interaction with its ligands PVR (CD155) and nectin-2 (PRR-2/CD112). *International Immunology* **16**, 533–538 (2004).
130. Masson, D. *et al.* Overexpression of the CD155 gene in human colorectal carcinoma. *Gut* **49**, 236–240 (2001).
131. El-Sherbiny, Y. M. *et al.* The Requirement for DNAM-1, NKG2D, and NKp46 in the Natural Killer Cell-Mediated Killing of Myeloma Cells. *Cancer Research* **67**, 8444–8449 (2007).
132. Pende, D. *et al.* Analysis of the receptor-ligand interactions in the natural killer–mediated lysis of freshly isolated myeloid or lymphoblastic leukemias: evidence for the involvement of the Poliovirus receptor (CD155) and Nectin-2 (CD112). *Blood* **105**, 2066–2073 (2005).
133. Castriconi, R. *et al.* Natural Killer Cell-Mediated Killing of Freshly Isolated Neuroblastoma Cells: Critical Role of DNAX Accessory Molecule-1–Poliovirus Receptor Interaction. *Cancer Research* **64**, 9180–9184 (2004).
134. Carlsten, M. *et al.* DNAX Accessory Molecule-1 Mediated Recognition of Freshly Isolated Ovarian Carcinoma by Resting Natural Killer Cells. *Cancer Research* **67**, 1317–1325 (2007).
135. Tahara-Hanaoka, S. *et al.* Tumor rejection by the poliovirus receptor family ligands of the DNAM-1 (CD226) receptor. *Blood* **107**, 1491–1496 (2006).
136. Stanietsky, N. *et al.* The interaction of TIGIT with PVR and PVRL2 inhibits human NK cell cytotoxicity. *Proceedings of the National Academy of Sciences* **106**, 17858–17863 (2009).

137. Zhang, Q. *et al.* Blockade of the checkpoint receptor TIGIT prevents NK cell exhaustion and elicits potent anti-tumor immunity. *Nat Immunol* **19**, 723–732 (2018).
138. Maas, R. J. *et al.* TIGIT blockade enhances functionality of peritoneal NK cells with altered expression of DNAM-1/TIGIT/CD96 checkpoint molecules in ovarian cancer. *OncoImmunology* **9**, 1843247 (2020).
139. Fuchs, A., Cella, M., Giurisato, E., Shaw, A. S. & Colonna, M. Cutting edge: CD96 (tactile) promotes NK cell-target cell adhesion by interacting with the poliovirus receptor (CD155). *J Immunol* **172**, 3994–3998 (2004).
140. Chan, C. J. *et al.* The receptors CD96 and CD226 oppose each other in the regulation of natural killer cell functions. *Nat Immunol* **15**, 431–438 (2014).
141. Roman Aguilera, A. *et al.* CD96 targeted antibodies need not block CD96-CD155 interactions to promote NK cell anti-metastatic activity. *OncoImmunology* **7**, e1424677 (2018).
142. Chiang, E. Y. & Mellman, I. TIGIT-CD226-PVR axis: advancing immune checkpoint blockade for cancer immunotherapy. *J Immunother Cancer* **10**, e004711 (2022).
143. Shibuya, K. *et al*. CD226 (DNAM-1) Is Involved in Lymphocyte Function–associated Antigen 1 Costimulatory Signal for Naive T Cell Differentiation and Proliferation. *Journal of Experimental Medicine* **198**, 1829–1839 (2003).
144. Shibuya, K. *et al*. Physical and Functional Association of LFA-1 with DNAM-1 Adhesion Molecule. *Immunity* **11**, 615–623 (1999).
145. Wee, H., Oh, H.-M., Jo, J.-H. & Jun, C.-D. ICAM-1/LFA-1 interaction contributes to the induction of endothelial cell-cell separation: implication for enhanced leukocyte diapedesis. *Exp Mol Med* **41**, 341–348 (2009).
146. Gorina, R., Lyck, R., Vestweber, D. & Engelhardt, B. β2 Integrin–Mediated Crawling on Endothelial ICAM-1 and ICAM-2 Is a Prerequisite for Transcellular Neutrophil Diapedesis across the Inflamed Blood–Brain Barrier. *The Journal of Immunology* **192**, 324–337 (2014).
147. Figenschau, S. L. *et al*. ICAM1 expression is induced by proinflammatory cytokines and associated with TLS formation in aggressive breast cancer subtypes. *Sci Rep* **8**, 11720 (2018).
148. Roland, C. L., Harken, A. H., Sarr, M. G. & Barnett, C. C. ICAM-1 expression determines malignant potential of cancer. *Surgery* **141**, 705–707 (2007).
149. Giavazzi, R. *et al.* Soluble intercellular adhesion molecule 1 is released by human melanoma cells and is associated with tumor growth in nude mice. *Cancer Res* **52**, 2628–2630 (1992).
150. Chong, A. S., Boussy, I. A., Jiang, X. L., Lamas, M. & Graf, L. H. CD54/ICAM-1 is a costimulator of NK cell-mediated cytotoxicity. *Cell Immunol* **157**, 92–105 (1994).
151. Naganuma, H. *et al.* Increased susceptibility of ifn-γ-treated neuroblastoma cells to lysis by lymphokine-activated killer cells: Participation of ICAM-1 induction on target cells. *International Journal of Cancer* **47**, 527–532 (1991).
152. Wang, R., Jaw, J. J., Stutzman, N. C., Zou, Z. & Sun, P. D. Natural killer cell-produced IFN-γ and TNF-α induce target cell cytolysis through up-regulation of ICAM-1. *Journal of Leukocyte Biology* **91**, 299–309 (2012).
153. Gross, C. C., Brzostowski, J. A., Liu, D. & Long, E. O. Tethering of intercellular adhesion molecule on target cells is required for LFA-1-dependent NK cell adhesion and granule polarization. *J Immunol* **185**, 2918–2926 (2010).
154. Barber, D. F., Faure, M. & Long, E. O. LFA-1 contributes an early signal for NK cell cytotoxicity. *J Immunol* **173**, 3653–3659 (2004).

155. Bryceson, Y. T., Ljunggren, H.-G. & Long, E. O. Minimal requirement for induction of natural cytotoxicity and intersection of activation signals by inhibitory receptors. *Blood* **114**, 2657–2666 (2009).
156. Natural Killer Cell Receptors: Human Target Cell – NK Cell Ligand-Receptor Interactions. *www.rndsystems.com* https://www.rndsystems.com/pathways/natural-killer-cell-receptors-human-target-cell-nk-cell-ligand-receptor-interactions-pathway.
157. Morvan, M. G. & Lanier, L. L. NK cells and cancer: you can teach innate cells new tricks. *Nat Rev Cancer* **16**, 7–19 (2016).
158. He, Y. & Tian, Z. NK cell education via nonclassical MHC and non-MHC ligands. *Cell Mol Immunol* **14**, 321–330 (2017).
159. HLA Nomenclature @ hla.alleles.org. https://hla.alleles.org/nomenclature/index.html.
160. Matsumura, M., Fremont, D. H., Peterson, P. A. & Wilson, Ian A. Emerging Principles for the Recognition of Peptide Antigens by MHC Class I Molecules. *Science* **257**, 927–934 (1992).
161. Jones, E. Y. MHC class I and class II structures. *Current Opinion in Immunology* **9**, 75–79 (1997).
162. Hoeffel, G. *et al.* Antigen Crosspresentation by Human Plasmacytoid Dendritic Cells. *Immunity* **27**, 481–492 (2007).
163. Ortmann, B. *et al.* A Critical Role for Tapasin in the Assembly and Function of Multimeric MHC Class I-TAP Complexes. *Science* **277**, 1306–1309 (1997).
164. Sadasivan, B., Lehner, P. J., Ortmann, B., Spies, T. & Cresswell, P. Roles for Calreticulin and a Novel Glycoprotein, Tapasin, in the Interaction of MHC Class I Molecules with TAP. *Immunity* **5**, 103–114 (1996).
165. Silva, M. B. da, Cunha, F. F. da, Terra, F. F. & Camara, N. O. S. Old game, new players: Linking classical theories to new trends in transplant immunology. *World Journal of Transplantation* **7**, 1–25 (2017).
166. Burshtyn, D. N., Yang, W., Yi, T. & Long, E. O. A novel phosphotyrosine motif with a critical amino acid at position -2 for the SH2 domain-mediated activation of the tyrosine phosphatase SHP-1. *J Biol Chem* **272**, 13066–13072 (1997).
167. Cassidy, S. A., Cheent, K. S. & Khakoo, S. I. Effects of Peptide on NK cell-mediated MHC I recognition. *Front Immunol* **5**, 133 (2014).
168. Epling-Burnette, P. K., Wei, S. & Djeu, J. Y. Chapter Seven - Signalling events in natural killer cells. in *Natural Killer Cells* (eds. Lotze, M. T. & Thomson, A. W.) 95–112 (Academic Press, San Diego, 2010). doi:10.1016/B978-0-12-370454-2.00007-7.
169. Rajagopalan, S. & Long, E. O. A human histocompatibility leukocyte antigen (HLA)-G-specific receptor expressed on all natural killer cells. *J Exp Med* **189**, 1093–1100 (1999).
170. Lanier, L. L., Corliss, B. & Phillips, J. H. Arousal and inhibition of human NK cells. *Immunological Reviews* **155**, 145–154 (1997).
171. Fittje, P. *et al.* HIV-1 Nef-mediated downregulation of CD155 results in viral restriction by KIR2DL5+ NK cells. *PLOS Pathogens* **18**, e1010572 (2022).
172. Ren, X. *et al.* Blockade of the immunosuppressive KIR2DL5/PVR pathway elicits potent human NK cell–mediated antitumor immunity. *J Clin Invest* **132**, (2022).
173. Pende, D. *et al.* Killer Ig-Like Receptors (KIRs): Their Role in NK Cell Modulation and Developments Leading to Their Clinical Exploitation. *Frontiers in Immunology* **10**, (2019).
174. Lee, N. *et al.* HLA-E is a major ligand for the natural killer inhibitory receptor CD94/NKG2A. *Proceedings of the National Academy of Sciences* **95**, 5199–5204 (1998).
175. Braud, V. M. *et al.* HLA-E binds to natural killer cell receptors CD94/NKG2A, B and C. *Nature* **391**, 795–799 (1998).

176. Zhang, X., Feng, J., Chen, S., Yang, H. & Dong, Z. Synergized regulation of NK cell education by NKG2A and specific Ly49 family members. *Nat Commun* **10**, 5010 (2019).
177. Gustafson, K. S. & Ginder, G. D. Interferon-gamma induction of the human leukocyte antigen-E gene is mediated through binding of a complex containing STAT1alpha to a distinct interferon-gamma-responsive element. *J Biol Chem* **271**, 20035–20046 (1996).
178. Braud, V., Yvonne Jones, E. & McMichael, A. The human major histocompatibility complex class Ib molecule HLA-E binds signal sequence-derived peptides with primary anchor residues at positions 2 and 9. *European Journal of Immunology* **27**, 1164–1169 (1997).
179. van Hall, T. *et al*. Monalizumab: inhibiting the novel immune checkpoint NKG2A. *J Immunother Cancer* **7**, 263 (2019).
180. André, P. *et al.* Anti-NKG2A mAb Is a Checkpoint Inhibitor that Promotes Anti-tumor Immunity by Unleashing Both T and NK Cells. *Cell* **175**, 1731-1743.e13 (2018).
181. Membranome. https://membranome.org/proteins?search=tm9sf3.
182. Katz, H. R. Inhibition of Inflammatory Responses by Leukocyte Ig-Like Receptors. in *Advances in Immunology* vol. 91 251–272 (Academic Press, 2006).
183. Mamessier, E. *et al.* Human breast cancer cells enhance self tolerance by promoting evasion from NK cell antitumor immunity. *J Clin Invest* **121**, 3609–3622 (2011).
184. Shiroishi, M. *et al*. Human inhibitory receptors Ig-like transcript 2 (ILT2) and ILT4 compete with CD8 for MHC class I binding and bind preferentially to HLA-G. *Proceedings of the National Academy of Sciences* **100**, 8856–8861 (2003).
185. Lepin, E. J. M. *et al.* Functional characterization of HLA-F and binding of HLA-F tetramers to ILT2 and ILT4 receptors. *European Journal of Immunology* **30**, 3552–3561 (2000).
186. Baía, D. *et al.* Interaction of the LILRB1 inhibitory receptor with HLA class Ia dimers. *European Journal of Immunology* **46**, 1681–1690 (2016).
187. Chapman, T. L., Heikema, A. P. & Bjorkman, P. J. The Inhibitory Receptor LIR-1 Uses a Common Binding Interaction to Recognize Class I MHC Molecules and the Viral Homolog UL18. *Immunity* **11**, 603–613 (1999).
188. Favier, B., LeMaoult, J., Lesport, E. & Carosella, E. D. ILT2/HLA-G interaction impairs NK-cell functions through the inhibition of the late but not the early events of the NK-cell activating synapse. *The FASEB Journal* **24**, 689–699 (2010).
189. Chen, H. *et al.* Antagonistic anti-LILRB1 monoclonal antibody regulates antitumor functions of natural killer cells. *J Immunother Cancer* **8**, e000515 (2020).
190. Roberti, M. P. *et al*. Overexpression of CD85j in TNBC patients inhibits Cetuximab-mediated NK-cell ADCC but can be restored with CD85j functional blockade. *European Journal of Immunology* **45**, 1560–1569 (2015).
191. Colonna, M. *et al.* Cutting Edge: Human Myelomonocytic Cells Express an Inhibitory Receptor for Classical and Nonclassical MHC Class I Molecules1. *The Journal of Immunology* **160**, 3096–3100 (1998).
192. Li, D. *et al*. Ig-Like Transcript 4 Inhibits Lipid Antigen Presentation through Direct CD1d Interaction1. *The Journal of Immunology* **182**, 1033–1040 (2009).
193. Zheng, J. *et al.* Inhibitory receptors bind ANGPTLs and support blood stem cells and leukaemia development. *Nature* **485**, 656–660 (2012).
194. Kim, T. *et al.* Human LilrB2 Is a β-Amyloid Receptor and Its Murine Homolog PirB Regulates Synaptic Plasticity in an Alzheimer's Model. *Science* **341**, 1399–1404 (2013).
195. Zhang, Z. *et al*. The Leukocyte Immunoglobulin-Like Receptor Family Member LILRB5 Binds to HLA-Class I Heavy Chains. *PLOS ONE* **10**, e0129063 (2015).

196. Borges, L., Hsu, M. L., Fanger, N., Kubin, M. & Cosman, D. A family of human lymphoid and myeloid Ig-like receptors, some of which bind to MHC class I molecules. *The Journal of Immunology* **159**, 5192–5196 (1997).
197. Yu, X. *et al.* The surface protein TIGIT suppresses T cell activation by promoting the generation of mature immunoregulatory dendritic cells. *Nat Immunol* **10**, 48–57 (2009).
198. Reches, A. *et al.* Nectin4 is a novel TIGIT ligand which combines checkpoint inhibition and tumor specificity. *J Immunother Cancer* **8**, e000266 (2020).
199. Stanietsky, N. *et al.* The interaction of TIGIT with PVR and PVRL2 inhibits human NK cell cytotoxicity. *Proc Natl Acad Sci U S A* **106**, 17858–17863 (2009).
200. Chauvin, J.-M. *et al.* TIGIT and PD-1 impair tumor antigen–specific $CD8^+$ T cells in melanoma patients. *J Clin Invest* **125**, 2046–2058 (2015).
201. Lozano, E., Dominguez-Villar, M., Kuchroo, V. & Hafler, D. A. The TIGIT/CD226 Axis Regulates Human T Cell Function. *The Journal of Immunology* **188**, 3869–3875 (2012).
202. Ziegler, A. E. *et al.* The co-inhibitory receptor TIGIT regulates NK cell function and is upregulated in human intrahepatic CD56bright NK cells. *Front Immunol* **14**, 1117320 (2023).
203. Lee, W. J. *et al.* Expression of lymphocyte-activating gene 3 and T-cell immunoreceptor with immunoglobulin and ITIM domains in cutaneous melanoma and their correlation with programmed cell death 1 expression in tumor-infiltrating lymphocytes. *Journal of the American Academy of Dermatology* **81**, 219–227 (2019).
204. Zhou, X.-M. *et al.* Intrinsic Expression of Immune Checkpoint Molecule TIGIT Could Help Tumor Growth in vivo by Suppressing the Function of NK and CD8+ T Cells. *Frontiers in Immunology* **9**, (2018).
205. Minnie, S. A. *et al.* Myeloma escape after stem cell transplantation is a consequence of T-cell exhaustion and is prevented by TIGIT blockade. *Blood* **132**, 1675–1688 (2018).
206. Dixon, K. O. *et al.* Functional Anti-TIGIT Antibodies Regulate Development of Autoimmunity and Antitumor Immunity. *The Journal of Immunology* **200**, 3000–3007 (2018).
207. Hung, A. L. *et al.* TIGIT and PD-1 dual checkpoint blockade enhances antitumor immunity and survival in GBM. *OncoImmunology* **7**, e1466769 (2018).
208. Xu, F. *et al.* Blockade of CD112R and TIGIT signaling sensitizes human natural killer cell functions. *Cancer Immunol Immunother* **66**, 1367–1375 (2017).
209. Zhu, Y. *et al.* Identification of CD112R as a novel checkpoint for human T cells. *Journal of Experimental Medicine* **213**, 167–176 (2016).
210. Liu, J. *et al.* Crystal Structure of Cell Adhesion Molecule Nectin-2/CD112 and Its Binding to Immune Receptor DNAM-1/CD226. *The Journal of Immunology* **188**, 5511–5520 (2012).
211. Li, Y. *et al.* Blockade of checkpoint receptor PVRIG unleashes anti-tumor immunity of NK cells in murine and human solid tumors. *J Hematol Oncol* **14**, 100 (2021).
212. McLane, L. M., Abdel-Hakeem, M. S. & Wherry, E. J. CD8 T Cell Exhaustion During Chronic Viral Infection and Cancer. *Annual Review of Immunology* **37**, 457–495 (2019).
213. Sanchez-Correa, B. *et al.* DNAM-1 and the TIGIT/PVRIG/TACTILE Axis: Novel Immune Checkpoints for Natural Killer Cell-Based Cancer Immunotherapy. *Cancers* **11**, 877 (2019).
214. Murter, B. *et al.* Mouse PVRIG Has CD8+ T Cell–Specific Coinhibitory Functions and Dampens Antitumor Immunity. *Cancer Immunology Research* **7**, 244–256 (2019).
215. Whelan, S. *et al.* PVRIG and PVRL2 Are Induced in Cancer and Inhibit CD8+ T-cell Function. *Cancer Immunology Research* **7**, 257–268 (2019).
216. Seth, S. *et al.* The murine pan T cell marker CD96 is an adhesion receptor for CD155 and nectin-1. *Biochemical and Biophysical Research Communications* **364**, 959–965 (2007).

217. Holmes, V. M. *et al.* Interaction between nectin-1 and the human natural killer cell receptor CD96. *PLoS One* **14**, e0212443 (2019).
218. Ouyang, Q. *et al.* Age-associated accumulation of CMV-specific CD8+ T cells expressing the inhibitory killer cell lectin-like receptor G1 (KLRG1). *Experimental Gerontology* **38**, 911–920 (2003).
219. Voehringer, D., Koschella, M. & Pircher, H. Lack of proliferative capacity of human effector and memory T cells expressing killer cell lectinlike receptor G1 (KLRG1). *Blood* **100**, 3698–3702 (2002).
220. Lopez-Vergès, S. *et al.* CD57 defines a functionally distinct population of mature NK cells in the human CD56dimCD16+ NK-cell subset. *Blood* **116**, 3865–3874 (2010).
221. Ito, M. *et al.* Killer cell lectin-like receptor G1 binds three members of the classical cadherin family to inhibit NK cell cytotoxicity. *Journal of Experimental Medicine* **203**, 289–295 (2006).
222. Müller-Durovic, B. *et al.* Killer Cell Lectin-like Receptor G1 (KLRG1) inhibits NK cell function through activation of AMP-activated Protein Kinase. *J Immunol* **197**, 2891–2899 (2016).
223. Huntington, N. D. *et al.* NK Cell Maturation and Peripheral Homeostasis Is Associated with KLRG1 Up-Regulation1. *The Journal of Immunology* **178**, 4764–4770 (2007).
224. Wang, J. M. *et al.* KLRG1 Negatively Regulates Natural Killer Cell Functions through the Akt Pathway in Individuals with Chronic Hepatitis C Virus Infection. *Journal of Virology* **87**, 11626–11636 (2013).
225. Gheldof, A. & Berx, G. Cadherins and epithelial-to-mesenchymal transition. *Prog Mol Biol Transl Sci* **116**, 317–336 (2013).
226. Na, T.-Y., Schecterson, L., Mendonsa, A. M. & Gumbiner, B. M. The functional activity of E-cadherin controls tumor cell metastasis at multiple steps. *Proc Natl Acad Sci U S A* **117**, 5931–5937 (2020).
227. Pillai, S., Netravali, I. A., Cariappa, A. & Mattoo, H. Siglecs and Immune Regulation. *Annu Rev Immunol* **30**, 357–392 (2012).
228. Von Gunten, S. & Bochner, B. S. Basic and Clinical Immunology of Siglecs. *Annals of the New York Academy of Sciences* **1143**, 61–82 (2008).
229. Hakomori, S. Tumor Malignancy Defined by Aberrant Glycosylation and Sphingo(glyco)lipid Metabolism1. *Cancer Research* **56**, 5309–5318 (1996).
230. Jandus, C. *et al.* Interactions between Siglec-7/9 receptors and ligands influence NK cell–dependent tumor immunosurveillance. *J Clin Invest* **124**, 1810–1820 (2014).
231. MUNDAY, J. *et al.* Identification, characterization and leucocyte expression of Siglec-10, a novel human sialic acid-binding receptor. *Biochemical Journal* **355**, 489–497 (2001).
232. Nicoll, G. *et al.* Identification and Characterization of a Novel Siglec, Siglec-7, Expressed by Human Natural Killer Cells and Monocytes *. *Journal of Biological Chemistry* **274**, 34089–34095 (1999).
233. Zhang, J. Q., Nicoll, G., Jones, C. & Crocker, P. R. Siglec-9, a Novel Sialic Acid Binding Member of the Immunoglobulin Superfamily Expressed Broadly on Human Blood Leukocytes *. *Journal of Biological Chemistry* **275**, 22121–22126 (2000).
234. Chen, G.-Y., Tang, J., Zheng, P. & Liu, Y. CD24 and Siglec-10 Selectively Repress Tissue Damage–Induced Immune Responses. *Science* **323**, 1722–1725 (2009).
235. Zhang, P. *et al.* Siglec-10 is associated with survival and natural killer cell dysfunction in hepatocellular carcinoma. *J Surg Res* **194**, 107–113 (2015).
236. Bandala-Sanchez, E. *et al.* T cell regulation mediated by interaction of soluble CD52 with the inhibitory receptor Siglec-10. *Nat Immunol* **14**, 741–748 (2013).
237. Kivi, E. *et al.* Human Siglec-10 can bind to vascular adhesion protein-1 and serves as its substrate. *Blood* **114**, 5385–5392 (2009).

238. Alphey, M. S., Attrill, H., Crocker, P. R. & Aalten, D. M. F. van. High Resolution Crystal Structures of Siglec-7: INSIGHTS INTO LIGAND SPECIFICITY IN THE SIGLEC FAMILY *. *Journal of Biological Chemistry* **278**, 3372–3377 (2003).
239. Zheng, Y. *et al.* The Roles of Siglec7 and Siglec9 on Natural Killer Cells in Virus Infection and Tumour Progression. *J Immunol Res* **2020**, 6243819 (2020).
240. Shao, J.-Y. *et al.* Siglec-7 Defines a Highly Functional Natural Killer Cell Subset and Inhibits Cell-Mediated Activities. *Scand J Immunol* **84**, 182–190 (2016).
241. Wisnovsky, S. *et al.* Genome-wide CRISPR screens reveal a specific ligand for the glycan-binding immune checkpoint receptor Siglec-7. *Proceedings of the National Academy of Sciences* **118**, e2015024118 (2021).
242. Belisle, J. A. *et al.* Identification of Siglec-9 as the receptor for MUC16 on human NK cells, B cells, and monocytes. *Mol Cancer* **9**, 118 (2010).
243. Ohta, M. *et al.* Immunomodulation of monocyte-derived dendritic cells through ligation of tumor-produced mucins to Siglec-9. *Biochemical and Biophysical Research Communications* **402**, 663–669 (2010).
244. Tanida, S. *et al.* Binding of the Sialic Acid-binding Lectin, Siglec-9, to the Membrane Mucin, MUC1, Induces Recruitment of β-Catenin and Subsequent Cell Growth. *Journal of Biological Chemistry* **288**, 31842–31852 (2013).
245. Brossart, P. *et al.* The Epithelial Tumor Antigen MUC1 Is Expressed in Hematological Malignancies and Is Recognized by MUC1-specific Cytotoxic T-Lymphocytes1. *Cancer Research* **61**, 6846–6850 (2001).
246. Beatson, R. *et al.* The mucin MUC1 modulates the tumor immunological microenvironment through engagement of the lectin Siglec-9. *Nat Immunol* **17**, 1273–1281 (2016).
247. Haridas, D. *et al.* MUC16: molecular analysis and its functional implications in benign and malignant conditions. *The FASEB Journal* **28**, 4183–4199 (2014).
248. Jing, X., Liang, H., Hao, C., Yang, X. & Cui, X. Overexpression of MUC1 predicts poor prognosis in patients with breast cancer. *Oncol Rep* **41**, 801–810 (2019).
249. Läubli, H. *et al.* Lectin Galactoside-binding Soluble 3 Binding Protein (LGALS3BP) Is a Tumor-associated Immunomodulatory Ligand for CD33-related Siglecs *. *Journal of Biological Chemistry* **289**, 33481–33491 (2014).
250. Ibarlucea-Benitez, I., Weitzenfeld, P., Smith, P. & Ravetch, J. V. Siglecs-7/9 function as inhibitory immune checkpoints in vivo and can be targeted to enhance therapeutic antitumor immunity. *Proceedings of the National Academy of Sciences* **118**, e2107424118 (2021).
251. Choi, H. *et al.* Development of Siglec-9 Blocking Antibody to Enhance Anti-Tumor Immunity. *Frontiers in Oncology* **11**, (2021).
252. Triebel, F. *et al.* LAG-3, a novel lymphocyte activation gene closely related to CD4. *J Exp Med* **171**, 1393–1405 (1990).
253. Huard, B., Tournier, M., Hercend, T., Triebel, F. & Faure, F. Lymphocyte-activation gene 3/major histocompatibility complex class II interaction modulates the antigenic response of CD4+ T lymphocytes. *European Journal of Immunology* **24**, 3216–3221 (1994).
254. Xu, F. *et al.* LSECtin Expressed on Melanoma Cells Promotes Tumor Progression by Inhibiting Antitumor T-cell Responses. *Cancer Research* **74**, 3418–3428 (2014).
255. Wang, J. *et al.* Fibrinogen-like Protein 1 Is a Major Immune Inhibitory Ligand of LAG-3. *Cell* **176**, 334-347.e12 (2019).
256. Kouo, T. *et al.* Galectin-3 Shapes Antitumor Immune Responses by Suppressing CD8+ T Cells via LAG-3 and Inhibiting Expansion of Plasmacytoid Dendritic Cells. *Cancer Immunology Research* **3**, 412–423 (2015).

257. Huard, B., Tournier, M. & Triebel, F. LAG-3 does not define a specific mode of natural killing in human. *Immunology Letters* **61**, 109–112 (1998).
258. Sordo-Bahamonde, C. *et al.* LAG-3 Blockade with Relatlimab (BMS-986016) Restores Anti-Leukemic Responses in Chronic Lymphocytic Leukemia. *Cancers* **13**, 2112 (2021).
259. Merino, A. *et al.* Chronic stimulation drives human NK cell dysfunction and epigenetic reprograming. *J Clin Invest* **129**, 3770–3785 (2019).
260. Huo, J.-L., Wang, Y.-T., Fu, W.-J., Lu, N. & Liu, Z.-S. The promising immune checkpoint LAG-3 in cancer immunotherapy: from basic research to clinical application. *Frontiers in Immunology* **13**, (2022).
261. Kim, S. K. & Cho, S. W. The Evasion Mechanisms of Cancer Immunity and Drug Intervention in the Tumor Microenvironment. *Frontiers in Pharmacology* **13**, (2022).
262. Baym, M. *et al.* Spatiotemporal microbial evolution on antibiotic landscapes. *Science (New York, N.Y.)* **353**, 1147 (2016).
263. Nandan, D. & Reiner, N. E. TGF-beta attenuates the class II transactivator and reveals an accessory pathway of IFN-gamma action. *The Journal of Immunology* **158**, 1095–1101 (1997).
264. Geissmann, F. *et al.* TGF-β1 Prevents the Noncognate Maturation of Human Dendritic Langerhans Cells1. *The Journal of Immunology* **162**, 4567–4575 (1999).
265. Castriconi, R. *et al.* Transforming growth factor β1 inhibits expression of NKp30 and NKG2D receptors: Consequences for the NK-mediated killing of dendritic cells. *Proceedings of the National Academy of Sciences* **100**, 4120–4125 (2003).
266. Donatelli, S. S. *et al.* TGF-β–inducible microRNA-183 silences tumor-associated natural killer cells. *Proceedings of the National Academy of Sciences* **111**, 4203–4208 (2014).
267. Budhu, S. *et al.* Blockade of surface-bound TGF-β on regulatory T cells abrogates suppression of effector T cell function in the tumor microenvironment. *Science Signaling* **10**, eaak9702 (2017).
268. Brabletz, T. *et al.* Transforming Growth Factor β and Cyclosporin A Inhibit the Inducible Activity of the Interleukin-2 Gene in T Cells Through a Noncanonical Octamer-Binding Site. *Molecular and Cellular Biology* **13**, 1155–1162 (1993).
269. Thomas, D. A. & Massagué, J. TGF-β directly targets cytotoxic T cell functions during tumor evasion of immune surveillance. *Cancer Cell* **8**, 369–380 (2005).
270. Mulé, J. J., Schwarz, S. L., Roberts, A. B., Sporn, M. B. & Rosenberg, S. A. Transforming growth factor-beta inhibits the in vitro generation of lymphokine-activated killer cells and cytotoxic T cells. *Cancer Immunol Immunother* **26**, 95–100 (1988).
271. Smyth, M. J., Strobl, S. L., Young, H. A., Ortaldo, J. R. & Ochoa, A. C. Regulation of lymphokine-activated killer activity and pore-forming protein gene expression in human peripheral blood CD8+ T lymphocytes. Inhibition by transforming growth factor-beta. *The Journal of Immunology* **146**, 3289–3297 (1991).
272. Ahuja, S. S., Paliogianni, F., Yamada, H., Balow, J. E. & Boumpas, D. T. Effect of transforming growth factor-beta on early and late activation events in human T cells. *The Journal of Immunology* **150**, 3109–3118 (1993).
273. Kehrl, J. H. *et al.* Production of transforming growth factor beta by human T lymphocytes and its potential role in the regulation of T cell growth. *Journal of Experimental Medicine* **163**, 1037–1050 (1986).
274. Gorelik, L. & Flavell, R. A. Immune-mediated eradication of tumors through the blockade of transforming growth factor-β signaling in T cells. *Nat Med* **7**, 1118–1122 (2001).
275. Itakura, E. *et al.* IL-10 expression by primary tumor cells correlates with melanoma progression from radial to vertical growth phase and development of metastatic competence. *Mod Pathol* **24**, 801–809 (2011).

276. Chen, Q., Daniel, V., Maher, D. W. & Hersey, P. Production of IL-10 by melanoma cells: Examination of its role in immunosuppression mediated by melanoma. *International Journal of Cancer* **56**, 755–760 (1994).
277. Yssel, H. *et al.* IL-10 is produced by subsets of human CD4+ T cell clones and peripheral blood T cells. *The Journal of Immunology* **149**, 2378–2384 (1992).
278. Fiorentino, D. F., Bond, M. W. & Mosmann, T. R. Two types of mouse T helper cell. IV. Th2 clones secrete a factor that inhibits cytokine production by Th1 clones. *Journal of Experimental Medicine* **170**, 2081–2095 (1989).
279. Moore, K. W., de Waal Malefyt, R., Coffman, R. L. & O'Garra, A. Interleukin-10 and the Interleukin-10 Receptor. *Annual Review of Immunology* **19**, 683–765 (2001).
280. Hsu, P. *et al.* IL-10 Potentiates Differentiation of Human Induced Regulatory T Cells via STAT3 and Foxo1. *The Journal of Immunology* **195**, 3665–3674 (2015).
281. Chaudhry, A. *et al.* Interleukin-10 Signaling in Regulatory T Cells Is Required for Suppression of Th17 Cell-Mediated Inflammation. *Immunity* **34**, 566–578 (2011).
282. Chen, W. *et al.* Conversion of Peripheral CD4+CD25− Naive T Cells to CD4+CD25+ Regulatory T Cells by TGF-β Induction of Transcription Factor Foxp3. *J Exp Med* **198**, 1875–1886 (2003).
283. Motz, G. T. *et al.* Tumor endothelium FasL establishes a selective immune barrier promoting tolerance in tumors. *Nat Med* **20**, 607–615 (2014).
284. Huang, Y. *et al.* Vascular normalizing doses of antiangiogenic treatment reprogram the immunosuppressive tumor microenvironment and enhance immunotherapy. *Proceedings of the National Academy of Sciences* **109**, 17561–17566 (2012).
285. Shrimali, R. K. *et al.* Antiangiogenic agents can increase lymphocyte infiltration into tumor and enhance the effectiveness of adoptive immunotherapy of cancer. *Cancer Res* **70**, 6171–6180 (2010).
286. Gabrilovich, D. I. *et al.* Production of vascular endothelial growth factor by human tumors inhibits the functional maturation of dendritic cells. *Nat Med* **2**, 1096–1103 (1996).
287. Smith, R. J. Modulation of phagocytosis by and lysosomal enzyme secretion from guinea-pig neutrophils: effect of nonsteroid anti-inflammatory agents and prostaglindins. *J Pharmacol Exp Ther* **200**, 647–657 (1977).
288. Sá-Nunes, A. *et al.* Prostaglandin E2 Is a Major Inhibitor of Dendritic Cell Maturation and Function in Ixodes scapularis Saliva1. *The Journal of Immunology* **179**, 1497–1505 (2007).
289. Specht, C., Bexten, S., Kölsch, E. & Pauels, H.-G. Prostaglandins, but not tumor-derived IL-10, shut down concomitant tumor-specific CTL responses during murine plasmacytoma progression. *International Journal of Cancer* **91**, 705–712 (2001).
290. Betz, M. & Fox, B. S. Prostaglandin E2 inhibits production of Th1 lymphokines but not of Th2 lymphokines. *The Journal of Immunology* **146**, 108–113 (1991).
291. Obermajer, N., Muthuswamy, R., Lesnock, J., Edwards, R. P. & Kalinski, P. Positive feedback between PGE2 and COX2 redirects the differentiation of human dendritic cells toward stable myeloid-derived suppressor cells. *Blood* **118**, 5498–5505 (2011).
292. Kaliński, P., Hilkens, C. M., Snijders, A., Snijdewint, F. G. & Kapsenberg, M. L. IL-12-deficient dendritic cells, generated in the presence of prostaglandin E2, promote type 2 cytokine production in maturing human naive T helper cells. *The Journal of Immunology* **159**, 28–35 (1997).
293. Serezani, C. H. *et al.* Prostaglandin E2 Suppresses Bacterial Killing in Alveolar Macrophages by Inhibiting NADPH Oxidase. *Am J Respir Cell Mol Biol* **37**, 562–570 (2007).

294. Aronoff, D. M., Canetti, C. & Peters-Golden, M. Prostaglandin E2 Inhibits Alveolar Macrophage Phagocytosis through an E-Prostanoid 2 Receptor-Mediated Increase in Intracellular Cyclic AMP12. *The Journal of Immunology* **173**, 559–565 (2004).
295. Walker, W. & Rotondo, D. Prostaglandin E2 is a potent regulator of interleukin-12- and interleukin-18-induced natural killer cell interferon-γ synthesis. *Immunology* **111**, 298–305 (2004).
296. Goto, T., Herberman, R. B., Maluish, A. & Strong, D. M. Cyclic AMP as a mediator of prostaglandin E-induced suppression of human natural killer cell activity. *The Journal of Immunology* **130**, 1350–1355 (1983).
297. Uyttenhove, C. *et al.* Evidence for a tumoral immune resistance mechanism based on tryptophan degradation by indoleamine 2,3-dioxygenase. *Nat Med* **9**, 1269–1274 (2003).
298. Baban, B. *et al.* IDO activates regulatory T cells and blocks their conversion into TH17-like T cells. *J Immunol* **183**, 2475–2483 (2009).
299. Mezrich, J. D. *et al.* An Interaction between Kynurenine and the Aryl Hydrocarbon Receptor Can Generate Regulatory T Cells. *The Journal of Immunology* **185**, 3190–3198 (2010).
300. Holmgaard, R. B. *et al*. Tumor-expressed IDO recruits and activates MDSCs in a Treg-dependent manner. *Cell Rep* **13**, 412–424 (2015).
301. Kerkvliet, N. I., Shepherd, D. M. & Baecher-Steppan, L. T Lymphocytes Are Direct, Aryl Hydrocarbon Receptor (AhR)-Dependent Targets of 2,3,7,8-Tetrachlorodibenzo-p-dioxin (TCDD): AhR Expression in Both CD4+ and CD8+ T Cells Is Necessary for Full Suppression of a Cytotoxic T Lymphocyte Response by TCDD. *Toxicology and Applied Pharmacology* **185**, 146–152 (2002).
302. Moreno-Nieves, U. Y., Mundy, D. C., Shin, J. H., Tam, K. & Sunwoo, J. B. The aryl hydrocarbon receptor modulates the function of human CD56bright NK cells. *European Journal of Immunology* **48**, 771–776 (2018).
303. Belladonna, M. L. *et al.* Kynurenine Pathway Enzymes in Dendritic Cells Initiate Tolerogenesis in the Absence of Functional IDO1. *The Journal of Immunology* **177**, 130–137 (2006).
304. Chiesa, M. D. *et al*. The tryptophan catabolite l-kynurenine inhibits the surface expression of NKp46- and NKG2D-activating receptors and regulates NK-cell function. *Blood* **108**, 4118–4125 (2006).
305. Munn, D. H. *et al.* Potential Regulatory Function of Human Dendritic Cells Expressing Indoleamine 2,3-Dioxygenase. *Science* **297**, 1867–1870 (2002).
306. Opitz, C. A. *et al*. An endogenous tumour-promoting ligand of the human aryl hydrocarbon receptor. *Nature* **478**, 197–203 (2011).
307. Platten, M. *et al.* Treatment of Autoimmune Neuroinflammation with a Synthetic Tryptophan Metabolite. *Science* **310**, 850–855 (2005).
308. Gandhi, R. *et al.* Activation of the aryl hydrocarbon receptor induces human type 1 regulatory T cell-like and Foxp3(+) regulatory T cells. *Nat Immunol* **11**, 846–853 (2010).
309. Parodi, M. *et al*. Hypoxia Modifies the Transcriptome of Human NK Cells, Modulates Their Immunoregulatory Profile, and Influences NK Cell Subset Migration. *Front Immunol* **9**, 2358 (2018).
310. Krzywinska, E. *et al.* Loss of HIF-1α in natural killer cells inhibits tumour growth by stimulating non-productive angiogenesis. *Nat Commun* **8**, 1597 (2017).
311. Saragovi, A. *et al*. Systemic hypoxia inhibits T cell response by limiting mitobiogenesis via matrix substrate-level phosphorylation arrest. *Elife* **9**, e56612 (2020).
312. Ni, J. *et al.* Single-Cell RNA Sequencing of Tumor-Infiltrating NK Cells Reveals that Inhibition of Transcription Factor HIF-1α Unleashes NK Cell Activity. *Immunity* **52**, 1075-1087.e8 (2020).

313. Jayaprakash, P. *et al.* Targeted hypoxia reduction restores T cell infiltration and sensitizes prostate cancer to immunotherapy. *J Clin Invest* **128**, 5137–5149 (2018).
314. Ino, Y. *et al.* Immune cell infiltration as an indicator of the immune microenvironment of pancreatic cancer. *Br J Cancer* **108**, 914–923 (2013).
315. Yusa, T. *et al.* Survival impact of immune cells infiltrating peritumoral area of hepatocellular carcinoma. *Cancer Sci* **113**, 4048–4058 (2022).
316. Bonanni, V., Antonangeli, F., Santoni, A. & Bernardini, G. Targeting of CXCR3 improves anti-myeloma efficacy of adoptively transferred activated natural killer cells. *Journal for ImmunoTherapy of Cancer* **7**, 290 (2019).
317. Karin, N. CXCR3 Ligands in Cancer and Autoimmunity, Chemoattraction of Effector T Cells, and Beyond. *Frontiers in Immunology* **11**, (2020).
318. Bayati, F. *et al.* The Therapeutic Potential of Regulatory T Cells: Challenges and Opportunities. *Frontiers in Immunology* **11**, (2021).
319. Trzonkowski, P., Szmit, E., Myśliwska, J., Dobyszuk, A. & Myśliwski, A. CD4+CD25+ T regulatory cells inhibit cytotoxic activity of T CD8+ and NK lymphocytes in the direct cell-to-cell interaction. *Clinical Immunology* **112**, 258–267 (2004).
320. Ghiringhelli, F. *et al.* CD4+CD25+ regulatory T cells inhibit natural killer cell functions in a transforming growth factor-beta-dependent manner. *J Exp Med* **202**, 1075–1085 (2005).
321. Rodríguez, P. C. & Ochoa, A. C. Arginine regulation by myeloid derived suppressor cells and tolerance in cancer: mechanisms and therapeutic perspectives. *Immunological Reviews* **222**, 180–191 (2008).
322. Rodriguez, P. C. *et al.* Regulation of T Cell Receptor CD3ζ Chain Expression byl-Arginine *. *Journal of Biological Chemistry* **277**, 21123–21129 (2002).
323. Gabrilovich, D. I. & Nagaraj, S. Myeloid-derived suppressor cells as regulators of the immune system. *Nat Rev Immunol* **9**, 162–174 (2009).
324. Kusmartsev, S., Nefedova, Y., Yoder, D. & Gabrilovich, D. I. Antigen-Specific Inhibition of CD8+ T Cell Response by Immature Myeloid Cells in Cancer Is Mediated by Reactive Oxygen Species1. *The Journal of Immunology* **172**, 989–999 (2004).
325. Huang, B. *et al.* Gr-1+CD115+ Immature Myeloid Suppressor Cells Mediate the Development of Tumor-Induced T Regulatory Cells and T-Cell Anergy in Tumor-Bearing Host. *Cancer Research* **66**, 1123–1131 (2006).
326. Galani, I. E. *et al.* Regulatory T cells control macrophage accumulation and activation in lymphoma. *International Journal of Cancer* **127**, 1131–1140 (2010).
327. He, Z. & Zhang, S. Tumor-Associated Macrophages and Their Functional Transformation in the Hypoxic Tumor Microenvironment. *Front Immunol* **12**, 741305 (2021).
328. Tripathi, C. *et al.* Macrophages are recruited to hypoxic tumor areas and acquire a Pro-Angiogenic M2-Polarized phenotype via hypoxic cancer cell derived cytokines Oncostatin M and Eotaxin. *Oncotarget* **5**, 5350–5368 (2014).
329. Wang, H.-W. & Joyce, J. A. Alternative activation of tumor-associated macrophages by IL-4. *Cell Cycle* **9**, 4824–4835 (2010).
330. Zhang, F. *et al.* TGF-β induces M2-like macrophage polarization via SNAIL-mediated suppression of a pro-inflammatory phenotype. *Oncotarget* **7**, 52294–52306 (2016).
331. Pyonteck, S. M. *et al.* CSF-1R inhibition alters macrophage polarization and blocks glioma progression. *Nat Med* **19**, 1264–1272 (2013).
332. Wheeler, K. C. *et al.* VEGF may contribute to macrophage recruitment and M2 polarization in the decidua. *PLOS ONE* **13**, e0191040 (2018).
333. Pekarek, L. A., Starr, B. A., Toledano, A. Y. & Schreiber, H. Inhibition of tumor growth by elimination of granulocytes. *Journal of Experimental Medicine* **181**, 435–440 (1995).

334. Sparmann, A. & Bar-Sagi, D. Ras-induced interleukin-8 expression plays a critical role in tumor growth and angiogenesis. *Cancer Cell* **6**, 447–458 (2004).
335. Tazawa, H. *et al.* Infiltration of Neutrophils Is Required for Acquisition of Metastatic Phenotype of Benign Murine Fibrosarcoma Cells: Implication of Inflammation-Associated Carcinogenesis and Tumor Progression. *The American Journal of Pathology* **163**, 2221–2232 (2003).
336. Keane, M. P., Belperio, J. A., Xue, Y. Y., Burdick, M. D. & Strieter, R. M. Depletion of CXCR2 Inhibits Tumor Growth and Angiogenesis in a Murine Model of Lung Cancer1. *The Journal of Immunology* **172**, 2853–2860 (2004).
337. Andzinski, L. *et al.* Type I IFNs induce anti-tumor polarization of tumor associated neutrophils in mice and human. *International Journal of Cancer* **138**, 1982–1993 (2016).
338. Fridlender, Z. G. *et al.* Polarization of Tumor-Associated Neutrophil Phenotype by TGF-β: "N1" versus "N2" TAN. *Cancer Cell* **16**, 183–194 (2009).
339. Mishalian, I. *et al.* Tumor-associated neutrophils (TAN) develop pro-tumorigenic properties during tumor progression. *Cancer Immunol Immunother* **62**, 1745–1756 (2013).
340. Kwantwi, L. B. *et al.* Tumor-associated neutrophils activated by tumor-derived CCL20 (C-C motif chemokine ligand 20) promote T cell immunosuppression via programmed death-ligand 1 (PD-L1) in breast cancer. *Bioengineered* **12**, 6996–7006.
341. Zhou, S.-L. *et al.* Tumor-Associated Neutrophils Recruit Macrophages and T-Regulatory Cells to Promote Progression of Hepatocellular Carcinoma and Resistance to Sorafenib. *Gastroenterology* **150**, 1646-1658.e17 (2016).
342. Waldhauer, I. & Steinle, A. Proteolytic Release of Soluble UL16-Binding Protein 2 from Tumor Cells. *Cancer Research* **66**, 2520–2526 (2006).
343. Waldhauer, I. *et al.* Tumor-associated MICA is shed by ADAM proteases. *Cancer Res* **68**, 6368–6376 (2008).
344. Chitadze, G. *et al.* Shedding of endogenous MHC class I-related chain molecules A and B from different human tumor entities: heterogeneous involvement of the 'a disintegrin and metalloproteases' 10 and 17. *Int J Cancer* **133**, 1557–1566 (2013).
345. Sun, D., Wang, X., Zhang, H., Deng, L. & Zhang, Y. MMP9 mediates MICA shedding in human osteosarcomas. *Cell Biol Int* **35**, 569–574 (2011).
346. Qizhi, L. *et al.* Tumor-Derived Soluble MICA Obstructs the NKG2D Pathway to Restrain NK Cytotoxicity. *Aging and disease* **11**, 118–128 (2020).
347. Klöß, S. *et al.* Increased sMICA and TGFβ1 levels in HNSCC patients impair NKG2D-dependent functionality of activated NK cells. *Oncoimmunology* **4**, e1055993 (2015).
348. Ou, Z.-L. *et al.* Hypoxia-induced shedding of MICA and HIF1A-mediated immune escape of pancreatic cancer cells from NK cells: role of circ_0000977/miR-153 axis. *RNA Biol* **16**, 1592–1603 (2019).
349. Zingoni, A. *et al.* Genotoxic Stress Induces Senescence-Associated ADAM10-Dependent Release of NKG2D MIC Ligands in Multiple Myeloma Cells. *J Immunol* **195**, 736–748 (2015).
350. Li, J.-J. *et al.* Prognostic value of soluble MICA levels in the serum of patients with advanced hepatocellular carcinoma. *Chin J Cancer* **32**, 141–148 (2013).
351. Rebmann, V. *et al.* Soluble MICA as an independent prognostic factor for the overall survival and progression-free survival of multiple myeloma patients. *Clinical Immunology* **123**, 114–120 (2007).
352. Kegasawa, T. *et al.* Soluble UL16-binding protein 2 is associated with a poor prognosis in pancreatic cancer patients. *Biochemical and Biophysical Research Communications* **517**, 84–88 (2019).

353. Arai, J. *et al.* Leukotriene receptor antagonists enhance HCC treatment efficacy by inhibiting ADAMs and suppressing MICA shedding. *Cancer Immunol Immunother* **70**, 203–213 (2021).
354. Reiners, K. S. *et al.* Soluble ligands for NK cell receptors promote evasion of chronic lymphocytic leukemia cells from NK cell anti-tumor activity. *Blood* **121**, 3658–3665 (2013).
355. Okumura, G. *et al.* Tumor-derived soluble CD155 inhibits DNAM-1-mediated antitumor activity of natural killer cells. *J Exp Med* **217**, 1 (2020).
356. Iguchi-Manaka, A. *et al.* Increased Soluble CD155 in the Serum of Cancer Patients. *PLOS ONE* **11**, e0152982 (2016).
357. Iguchi-Manaka, A. *et al.* High expression of soluble CD155 in estrogen receptor-negative breast cancer. *Breast Cancer* **27**, 92–99 (2020).
358. Liu, Z. *et al.* Tumor necroptosis-mediated shedding of cell surface proteins promotes metastasis of breast cancer by suppressing anti-tumor immunity. *Breast Cancer Research* **25**, 10 (2023).
359. Gründemann, C. *et al.* Cutting Edge: Identification of E-Cadherin as a Ligand for the Murine Killer Cell Lectin-Like Receptor G11. *The Journal of Immunology* **176**, 1311–1315 (2006).
360. Puppo, F., Contini, P., Ghio, M. & Indiveri, F. Soluble HLA class I molecules/CD8 ligation trigger apoptosis of CD8+ cells by Fas/Fas-ligand interaction. *ScientificWorldJournal* **2**, 421–423 (2002).
361. Contini, P. *et al.* Soluble HLA-A,-B,-C and -G molecules induce apoptosis in T and NK CD8+ cells and inhibit cytotoxic T cell activity through CD8 ligation. *Eur J Immunol* **33**, 125–134 (2003).
362. Contini, P. *et al.* Apoptosis of antigen-specific T lymphocytes upon the engagement of CD8 by soluble HLA class I molecules is Fas ligand/Fas mediated: evidence for the involvement of p56lck, calcium calmodulin kinase II, and Calcium-independent protein kinase C signaling pathways and for NF-kappaB and NF-AT nuclear translocation. *J Immunol* **175**, 7244–7254 (2005).
363. Derré, L. *et al.* Expression and release of HLA-E by melanoma cells and melanocytes: potential impact on the response of cytotoxic effector cells. *J Immunol* **177**, 3100–3107 (2006).
364. Natali, P. G. *et al.* Distribution of Human Class I (HLA-A,B,C) Histocompatibility Antigens in Normal and Malignant Tissues of Nonlymphoid Origin1. *Cancer Research* **44**, 4679–4687 (1984).
365. Garrido, F. MHC/HLA Class I Loss in Cancer Cells. in *MHC Class-I Loss and Cancer Immune Escape* (ed. Garrido, F.) 15–78 (Springer International Publishing, Cham, 2019). doi:10.1007/978-3-030-17864-2_2.
366. Garrido, A. *et al.* Influence of class I H-2 gene expression on local tumor growth. Description of a model obtained from clones derived from a solid BALB/c tumor. *Exp Clin Immunogenet* **3**, 98–110 (1986).
367. Montesion, M. *et al.* Somatic HLA Class I Loss Is a Widespread Mechanism of Immune Evasion Which Refines the Use of Tumor Mutational Burden as a Biomarker of Checkpoint Inhibitor Response. *Cancer Discovery* **11**, 282–292 (2021).
368. Sheyhidin, I., Hasim, A., Zheng, F. & Ma, H. Epigenetic changes within the promoter regions of antigen processing machinery family genes in Kazakh primary esophageal squamous cell carcinoma. *Asian Pac J Cancer Prev* **15**, 10299–10306 (2014).
369. Chang, C.-C. *et al.* Multiple Structural and Epigenetic Defects in the Human Leukocyte Antigen Class I Antigen Presentation Pathway in a Recurrent Metastatic Melanoma Following Immunotherapy *. *Journal of Biological Chemistry* **290**, 26562–26575 (2015).

370. Hasim, A. *et al.* Post-Transcriptional and Epigenetic Regulation of Antigen Processing Machinery (APM) Components and HLA-I in Cervical Cancers from Uighur Women. *PLOS ONE* **7**, e44952 (2012).
371. Hanalioglu, D. *et al.* A novel mutation in TAP1 gene leading to MHC class I deficiency: Report of two cases and review of the literature. *Clinical Immunology* **178**, 74–78 (2017).
372. Yoshihama, S. *et al.* NLRC5/MHC class I transactivator is a target for immune evasion in cancer. *Proceedings of the National Academy of Sciences* **113**, 5999–6004 (2016).
373. Burr, M. L. *et al.* An Evolutionarily Conserved Function of Polycomb Silences the MHC Class I Antigen Presentation Pathway and Enables Immune Evasion in Cancer. *Cancer Cell* **36**, 385-401.e8 (2019).
374. Ozcan, M., Janikovits, J., von Knebel Doeberitz, M. & Kloor, M. Complex pattern of immune evasion in MSI colorectal cancer. *OncoImmunology* **7**, e1445453 (2018).
375. Kriegsman, B. A. *et al.* Frequent Loss of IRF2 in Cancers Leads to Immune Evasion through Decreased MHC Class I Antigen Presentation and Increased PD-L1 Expression. *The Journal of Immunology* **203**, 1999–2010 (2019).
376. Lazaridou, M.-F. *et al.* Identification of microRNAs Targeting the Transporter Associated with Antigen Processing TAP1 in Melanoma. *Journal of Clinical Medicine* **9**, 2690 (2020).
377. Colangelo, T. *et al.* Proteomic screening identifies calreticulin as a miR-27a direct target repressing MHC class I cell surface exposure in colorectal cancer. *Cell Death Dis* **7**, e2120–e2120 (2016).
378. Mari, L. *et al.* microRNA 125a Regulates MHC-I Expression on Esophageal Adenocarcinoma Cells, Associated With Suppression of Antitumor Immune Response and Poor Outcomes of Patients. *Gastroenterology* **155**, 784–798 (2018).
379. Yan, Y., Liang, Z., Du, Q., Yang, M. & Geller, D. A. MicroRNA-23a downregulates the expression of interferon regulatory factor-1 in hepatocellular carcinoma cells. *Oncology Reports* **36**, 633–640 (2016).
380. Garrido, F., Romero, I., Aptsiauri, N. & Garcia-Lora, A. M. Generation of MHC class I diversity in primary tumors and selection of the malignant phenotype. *International Journal of Cancer* **138**, 271–280 (2016).
381. Carretero, R. *et al.* Analysis of HLA class I expression in progressing and regressing metastatic melanoma lesions after immunotherapy. *Immunogenetics* **60**, 439–447 (2008).
382. del Campo, A. B. *et al.* Immune escape of cancer cells with beta2-microglobulin loss over the course of metastatic melanoma. *International Journal of Cancer* **134**, 102–113 (2014).
383. Shklovskaya, E. *et al.* Tumor MHC Expression Guides First-Line Immunotherapy Selection in Melanoma. *Cancers* **12**, 3374 (2020).
384. Le Maux Chansac, B. *et al.* NK cells infiltrating a MHC class I-deficient lung adenocarcinoma display impaired cytotoxic activity toward autologous tumor cells associated with altered NK cell-triggering receptors. *J Immunol* **175**, 5790–5798 (2005).
385. Ardolino, M. *et al.* Cytokine therapy reverses NK cell anergy in MHC-deficient tumors. *J Clin Invest* **124**, 4781–4794 (2014).
386. de Kruijf, E. M. *et al.* HLA-E and HLA-G Expression in Classical HLA Class I-Negative Tumors Is of Prognostic Value for Clinical Outcome of Early Breast Cancer Patients. *The Journal of Immunology* **185**, 7452–7459 (2010).
387. Wagner, S. N., Rebmann, V., Willers, C. P., Grosse-Wilde, H. & Goos, M. Expression analysis of classic and non-classic HLA molecules before interferon alfa-2b treatment of melanoma. *The Lancet* **356**, 220–221 (2000).
388. Koebel, C. M. *et al.* Adaptive immunity maintains occult cancer in an equilibrium state. *Nature* **450**, 903–907 (2007).

389. Ichise, H. *et al.* Functional visualization of NK cell-mediated killing of metastatic single tumor cells. *eLife* **11**, e76269 (2022).
390. Lo, H. C. *et al.* Resistance to natural killer cell immunosurveillance confers a selective advantage to polyclonal metastasis. *Nat Cancer* **1**, 709–722 (2020).
391. Hanna, N. & Fidler, I. J. Role of natural killer cells in the destruction of circulating tumor emboli. *J Natl Cancer Inst* **65**, 801–809 (1980).
392. Barlozzari, T., Reynolds, C. W. & Herberman, R. B. In vivo role of natural killer cells: involvement of large granular lymphocytes in the clearance of tumor cells in anti-asialo GM1-treated rats. *J Immunol* **131**, 1024–1027 (1983).
393. Nguyen-Pham, T.-N. *et al.* Optimal culture conditions for the generation of natural killer cell-induced dendritic cells for cancer immunotherapy. *Cell Mol Immunol* **9**, 45–53 (2012).
394. Liu, C. *et al.* Plasmacytoid dendritic cells induce NK cell-dependent, tumor antigen-specific T cell cross-priming and tumor regression in mice. *J Clin Invest* **118**, 1165–1175 (2008).
395. Srivastava, R. M. *et al.* Cetuximab-Activated Natural Killer and Dendritic Cells Collaborate to Trigger Tumor Antigen–Specific T-cell Immunity in Head and Neck Cancer Patients. *Clinical Cancer Research* **19**, 1858–1872 (2013).
396. Adam, C. *et al.* DC-NK cell cross talk as a novel CD4+ T-cell–independent pathway for antitumor CTL induction. *Blood* **106**, 338–344 (2005).
397. Mocikat, R. *et al.* Natural Killer Cells Activated by MHC Class ILow Targets Prime Dendritic Cells to Induce Protective CD8 T Cell Responses. *Immunity* **19**, 561–569 (2003).
398. Lindsay, R. S. *et al.* NK cells reduce anergic T cell development in early-stage tumors by promoting myeloid cell maturation. *Frontiers in Oncology* **12**, (2022).
399. Kelly, J. M. *et al.* Induction of tumor-specific T cell memory by NK cell–mediated tumor rejection. *Nat Immunol* **3**, 83–90 (2002).
400. Shankaran, V. *et al.* IFNgamma and lymphocytes prevent primary tumour development and shape tumour immunogenicity. *Nature* **410**, 1107–1111 (2001).
401. Romero, I. *et al.* T Lymphocytes Restrain Spontaneous Metastases in Permanent Dormancy. *Cancer Research* **74**, 1958–1968 (2014).
402. Garrido, C. *et al.* Immunotherapy eradicates metastases with reversible defects in MHC class I expression. *Cancer Immunol Immunother* **60**, 1257–1268 (2011).
403. Slotta-Huspenina, J. *et al.* MHC I Expression Predicts Response to Checkpoint Inhibitors in Metastatic Urothelial Carcinoma but Lacks Prognostic Value in Localized Disease. *Bladder Cancer* **8**, 269–276 (2022).
404. Gettinger, S. *et al.* Impaired HLA Class I Antigen Processing and Presentation as a Mechanism of Acquired Resistance to Immune Checkpoint Inhibitors in Lung Cancer. *Cancer Discovery* **7**, 1420–1435 (2017).
405. Zaretsky, J. M. *et al.* Mutations Associated with Acquired Resistance to PD-1 Blockade in Melanoma. *New England Journal of Medicine* **375**, 819–829 (2016).
406. Gu, S. S. *et al.* Therapeutically increasing MHC-I expression potentiates immune checkpoint blockade. *Cancer Discov* **11**, 1524–1541 (2021).
407. Prager, M. D., Ludden, C. M., Mandy, W. J., Allison, J. P. & Kitto, G. B. Brief Communication: Endotoxin-Stimulated Immune Response to Modified Lymphoma Cells2. *JNCI: Journal of the National Cancer Institute* **54**, 773–775 (1975).
408. Leach, D. R., Krummel, M. F. & Allison, J. P. Enhancement of Antitumor Immunity by CTLA-4 Blockade. *Science* **271**, 1734–1736 (1996).
409. Krummel, M. F. & Allison, J. P. CD28 and CTLA-4 have opposing effects on the response of T cells to stimulation. *Journal of Experimental Medicine* **182**, 459–465 (1995).

410. Linsley, P. S. *et al.* CTLA-4 is a second receptor for the B cell activation antigen B7. *Journal of Experimental Medicine* **174**, 561–569 (1991).
411. Li, J., Yang, Y., Inoue, H., Mori, M. & Akiyoshi, T. The expression of costimulatory molecules CD80 and CD86 in human carcinoma cell lines: its regulation by interferon gamma and interleukin-10. *Cancer Immunol Immunother* **43**, 213–219 (1996).
412. Fellner, C. Ipilimumab (Yervoy) Prolongs Survival In Advanced Melanoma. *P T* **37**, 503–530 (2012).
413. Hodi, F. S. *et al.* Improved Survival with Ipilimumab in Patients with Metastatic Melanoma. *N Engl J Med* **363**, 711–723 (2010).
414. Dalle, S. *et al.* Long-term real-world experience with ipilimumab and non-ipilimumab therapies in advanced melanoma: the IMAGE study. *BMC Cancer* **21**, 642 (2021).
415. Cabel, L. *et al.* Long-term complete remission with ipilimumab in metastatic castrate-resistant prostate cancer: case report of two patients. *J Immunother Cancer* **5**, 31 (2017).
416. Fizazi, K. *et al.* Final Analysis of the Ipilimumab Versus Placebo Following Radiotherapy Phase III Trial in Postdocetaxel Metastatic Castration-resistant Prostate Cancer Identifies an Excess of Long-term Survivors. *Eur Urol* **78**, 822–830 (2020).
417. Loi, S. *et al.* Neoadjuvant ipilimumab and nivolumab in combination with paclitaxel following anthracycline-based chemotherapy in patients with treatment resistant early-stage triple-negative breast cancer (TNBC): A single-arm phase 2 trial. *JCO* **40**, 602–602 (2022).
418. Agata, Y. *et al*. Expression of the PD-1 antigen on the surface of stimulated mouse T and B lymphocytes. *International Immunology* **8**, 765–772 (1996).
419. Ishida, Y., Agata, Y., Shibahara, K. & Honjo, T. Induced expression of PD-1, a novel member of the immunoglobulin gene superfamily, upon programmed cell death. *The EMBO Journal* **11**, 3887–3895 (1992).
420. Freeman, G. J. *et al.* Engagement of the PD-1 immunoinhibitory receptor by a novel B7 family member leads to negative regulation of lymphocyte activation. *J Exp Med* **192**, 1027–1034 (2000).
421. Latchman, Y. *et al.* PD-L2 is a second ligand for PD-1 and inhibits T cell activation. *Nat Immunol* **2**, 261–268 (2001).
422. Iwai, Y. *et al.* Involvement of PD-L1 on tumor cells in the escape from host immune system and tumor immunotherapy by PD-L1 blockade. *Proceedings of the National Academy of Sciences* **99**, 12293–12297 (2002).
423. Inozume, T. *et al.* Selection of CD8+PD-1+ lymphocytes in fresh human melanomas enriches for tumor-reactive T-cells. *J Immunother* **33**, 956–964 (2010).
424. Beldi-Ferchiou, A. *et al.* PD-1 mediates functional exhaustion of activated NK cells in patients with Kaposi sarcoma. *Oncotarget* **7**, 72961–72977 (2016).
425. Gros, A. *et al.* PD-1 identifies the patient-specific $CD8^+$ tumor-reactive repertoire infiltrating human tumors. *J Clin Invest* **124**, 2246–2259 (2014).
426. Niu, C. *et al.* PD-1-positive Natural Killer Cells have a weaker antitumor function than that of PD-1-negative Natural Killer Cells in Lung Cancer. *Int J Med Sci* **17**, 1964–1973 (2020).
427. Liu, Y. *et al.* Increased expression of programmed cell death protein 1 on NK cells inhibits NK-cell-mediated anti-tumor function and indicates poor prognosis in digestive cancers. *Oncogene* **36**, 6143–6153 (2017).
428. Sponaas, A.-M. *et al.* PD1 is expressed on exhausted T cells as well as virus specific memory CD8+ T cells in the bone marrow of myeloma patients. *Oncotarget* **9**, 32024–32035 (2018).

429. Chan, T. S. Y. *et al.* Low-dose pembrolizumab and nivolumab were efficacious and safe in relapsed and refractory classical Hodgkin lymphoma: Experience in a resource-constrained setting. *Hematol Oncol* **38**, 726–736 (2020).
430. Yau, T. *et al.* Nivolumab versus sorafenib in advanced hepatocellular carcinoma (CheckMate 459): a randomised, multicentre, open-label, phase 3 trial. *The Lancet Oncology* **23**, 77–90 (2022).
431. Motzer, R. J. *et al.* Nivolumab versus Everolimus in Advanced Renal-Cell Carcinoma. *New England Journal of Medicine* **373**, 1803–1813 (2015).
432. Topalian, S. L. *et al.* Survival, Durable Tumor Remission, and Long-Term Safety in Patients With Advanced Melanoma Receiving Nivolumab. *J Clin Oncol* **32**, 1020–1030 (2014).
433. Brahmer, J. *et al.* Nivolumab versus Docetaxel in Advanced Squamous-Cell Non-Small-Cell Lung Cancer. *N Engl J Med* **373**, 123–135 (2015).
434. Daher, S. *et al.* Nivolumab in Non-Small Cell Lung Cancer: Real World Long-Term Survival Results and Blood-Based Efficacy Biomarkers. *Frontiers in Oncology* **11**, (2021).
435. Qin, S. *et al.* Pembrolizumab Versus Placebo as Second-Line Therapy in Patients From Asia With Advanced Hepatocellular Carcinoma: A Randomized, Double-Blind, Phase III Trial. *JCO* **41**, 1434–1443 (2023).
436. Zhang, Q., Huo, G., Zhang, H. & Song, Y. Efficacy of pembrolizumab for advanced/metastatic melanoma: a meta-analysis. *Open Med (Wars)* **15**, 447–456 (2020).
437. de Azevedo, S. J. *et al.* First-line atezolizumab monotherapy in patients with advanced BRAFV600 wild-type melanoma. *Pigment Cell Melanoma Res* **34**, 973–977 (2021).
438. Herbst, R. S. *et al.* Atezolizumab for First-Line Treatment of PD-L1–Selected Patients with NSCLC. *New England Journal of Medicine* **383**, 1328–1339 (2020).
439. Korman, A. J., Garrett-Thomson, S. C. & Lonberg, N. The foundations of immune checkpoint blockade and the ipilimumab approval decennial. *Nat Rev Drug Discov* **21**, 509–528 (2022).
440. Motzer, R. J. *et al.* Nivolumab plus Ipilimumab versus Sunitinib in Advanced Renal-Cell Carcinoma. *New England Journal of Medicine* **378**, 1277–1290 (2018).
441. Hellmann, M. D. *et al.* Nivolumab plus Ipilimumab in Lung Cancer with a High Tumor Mutational Burden. *New England Journal of Medicine* **378**, 2093–2104 (2018).
442. Hodi, F. S. *et al.* Nivolumab plus ipilimumab or nivolumab alone versus ipilimumab alone in advanced melanoma (CheckMate 067): 4-year outcomes of a multicentre, randomised, phase 3 trial. *The Lancet Oncology* **19**, 1480–1492 (2018).
443. Curran, M. A., Montalvo, W., Yagita, H. & Allison, J. P. PD-1 and CTLA-4 combination blockade expands infiltrating T cells and reduces regulatory T and myeloid cells within B16 melanoma tumors. *Proceedings of the National Academy of Sciences* **107**, 4275–4280 (2010).
444. Larkin, J. *et al.* Five-Year Survival with Combined Nivolumab and Ipilimumab in Advanced Melanoma. *N Engl J Med* **381**, 1535–1546 (2019).
445. The Nobel Prize in Physiology or Medicine 2018. *NobelPrize.org* https://www.nobelprize.org/prizes/medicine/2018/summary/.
446. Opdualag Approved to Treat Advanced Melanoma - NCI. https://www.cancer.gov/news-events/cancer-currents-blog/2022/fda-opdualag-melanoma-lag-3 (2022).
447. Tawbi, H. A. *et al.* Relatlimab and Nivolumab versus Nivolumab in Untreated Advanced Melanoma. *New England Journal of Medicine* **386**, 24–34 (2022).
448. Schöffski, P. *et al.* Phase I/II study of the LAG-3 inhibitor ieramilimab (LAG525) ± anti-PD-1 spartalizumab (PDR001) in patients with advanced malignancies. *J Immunother Cancer* **10**, e003776 (2022).

449. Niu, J. *et al.* First-in-human phase 1 study of the anti-TIGIT antibody vibostolimab as monotherapy or with pembrolizumab for advanced solid tumors, including non-small-cell lung cancer☆. *Ann Oncol* **33**, 169–180 (2022).
450. Curigliano, G. *et al.* Phase I/Ib Clinical Trial of Sabatolimab, an Anti-TIM-3 Antibody, Alone and in Combination with Spartalizumab, an Anti-PD-1 Antibody, in Advanced Solid Tumors. *Clin Cancer Res* **27**, 3620–3629 (2021).
451. Soularue, E. *et al.* Enterocolitis due to immune checkpoint inhibitors: a systematic review. *Gut* **67**, 2056–2067 (2018).
452. Gordon, R. Skin Cancer: An Overview of Epidemiology and Risk Factors. *Seminars in Oncology Nursing* **29**, 160–169 (2013).
453. Skin cancer - Symptoms and causes. *Mayo Clinic* https://www.mayoclinic.org/diseases-conditions/skin-cancer/symptoms-causes/syc-20377605.
454. Non-melanoma skin cancer statistics. *Cancer Research UK* https://www.cancerresearchuk.org/health-professional/cancer-statistics/statistics-by-cancer-type/non-melanoma-skin-cancer (2018).
455. McCormack, C. J., Kelly, J. W. & Dorevitch, A. P. Differences in Age and Body Site Distribution of the Histological Subtypes of Basal Cell Carcinoma: A Possible Indicator of Differing Causes. *Archives of Dermatology* **133**, 593–596 (1997).
456. Madan, V., Lear, J. T. & Szeimies, R.-M. Non-melanoma skin cancer. *The Lancet* **375**, 673–685 (2010).
457. Cancer Facts & Figures 2023| American Cancer Society. https://www.cancer.org/research/cancer-facts-statistics/all-cancer-facts-figures/2023-cancer-facts-figures.html.
458. Parkin, D. M., Mesher, D. & Sasieni, P. 13. Cancers attributable to solar (ultraviolet) radiation exposure in the UK in 2010. *Br J Cancer* **105**, S66–S69 (2011).
459. Pfahlberg, A., Kölmel, K. F., Gefeller, O., & Febim Study Group. Timing of excessive ultraviolet radiation and melanoma: epidemiology does not support the existence of a critical period of high susceptibility to solar ultraviolet radiation- induced melanoma. *Br J Dermatol* **144**, 471–475 (2001).
460. Lew, R. A., Sober, A. J., Cook, N., Marvell, R. & Fitzpatrick, T. B. Sun exposure habits in patients with cutaneous melanoma: a case control study. *J Dermatol Surg Oncol* **9**, 981–986 (1983).
461. Melanoma Survival Rates | Melanoma Survival Statistics. https://www.cancer.org/cancer/types/melanoma-skin-cancer/detection-diagnosis-staging/survival-rates-for-melanoma-skin-cancer-by-stage.html.
462. Hersey, P., Edwards, A., Honeyman, M. & McCarthy, W. H. Low natural-killer-cell activity in familial melanoma patients and their relatives. *Br J Cancer* **40**, 113–122 (1979).
463. Hersey, P., Edwards, A. & McCarthy, W. H. Tumour-related changes in natural killer cell activity in melanoma patients. Influence of stage of disease, tumour thickness and age of patients. *International Journal of Cancer* **25**, 187–194 (1980).
464. Seaman, W. E., Sleisenger, M., Eriksson, E. & Koo, G. C. Depletion of natural killer cells in mice by monoclonal antibody to NK-1.1. Reduction in host defense against malignancy without loss of cellular or humoral immunity. *The Journal of Immunology* **138**, 4539–4544 (1987).
465. Krebs, P. *et al.* NK cell–mediated killing of target cells triggers robust antigen-specific T cell–mediated and humoral responses. *Blood* **113**, 6593–6602 (2009).
466. Gao, J. *et al.* Loss of IFN-γ pathway genes in tumor cells as a mechanism of resistance to anti-CTLA-4 therapy. *Cell* **167**, 397-404.e9 (2016).

467. Morgado, S. *et al.* NK Cell Recognition and Killing of Melanoma Cells Is Controlled by Multiple Activating Receptor-Ligand Interactions. *Journal of Innate Immunity* **3**, 365–373 (2011).
468. Collins, K. A. & White, W. L. Intercellular adhesion molecule 1 (ICAM-1) and bcl-2 are differentially expressed in early evolving malignant melanoma. *Am J Dermatopathol* **17**, 429–438 (1995).
469. Natali, P. G. *et al.* Clinical Significance of αvβ3 Integrin and Intercellular Adhesion Molecule-1 Expression in Cutaneous Malignant Melanoma Lesions1. *Cancer Research* **57**, 1554–1560 (1997).
470. Lakshmikanth, T. *et al.* NCRs and DNAM-1 mediate NK cell recognition and lysis of human and mouse melanoma cell lines in vitro and in vivo. *J Clin Invest* **119**, 1251–1263 (2009).
471. Casado, J. G. *et al.* Expression of adhesion molecules and ligands for activating and costimulatory receptors involved in cell-mediated cytotoxicity in a large panel of human melanoma cell lines. *Cancer Immunol Immunother* **58**, 1517–1526 (2009).
472. Pietra, G. *et al.* Melanoma Cells Inhibit Natural Killer Cell Function by Modulating the Expression of Activating Receptors and Cytolytic Activity. *Cancer Research* **72**, 1407–1415 (2012).
473. Kolasińska, E., Przybyło, M., Janik, M. & Lityńska, A. Towards understanding the role of sialylation in melanoma progression. *Acta Biochim Pol* **63**, 533–541 (2016).
474. Passaniti, A. & Hart, G. W. Cell surface sialylation and tumor metastasis. Metastatic potential of B16 melanoma variants correlates with their relative numbers of specific penultimate oligosaccharide structures. *J Biol Chem* **263**, 7591–7603 (1988).
475. Haas, Q. *et al.* Siglec-9 Regulates an Effector Memory CD8+ T-cell Subset That Congregates in the Melanoma Tumor Microenvironment. *Cancer Immunol Res* **7**, 707–718 (2019).
476. Porgador, A., Mandelboim, O., Restifo, N. P. & Strominger, J. L. Natural killer cell lines kill autologous β2-microglobulin-deficient melanoma cells: Implications for cancer immunotherapy. *Proceedings of the National Academy of Sciences* **94**, 13140–13145 (1997).
477. Mendez, R. *et al.* HLA and melanoma: multiple alterations in HLA class I and II expression in human melanoma cell lines from ESTDAB cell bank. *Cancer Immunol Immunother* **58**, 1507–1515 (2009).
478. Balsamo, M. *et al.* Melanoma cells become resistant to NK-cell-mediated killing when exposed to NK-cell numbers compatible with NK-cell infiltration in the tumor. *Eur J Immunol* **42**, 1833–1842 (2012).
479. Mirjacic Martinovic, K. M. *et al.* Decreased expression of NKG2D, NKp46, DNAM-1 receptors, and intracellular perforin and STAT-1 effector molecules in NK cells and their dim and bright subsets in metastatic melanoma patients. *Melanoma Research* **24**, 295 (2014).
480. Barry, K. C. *et al.* A natural killer–dendritic cell axis defines checkpoint therapy–responsive tumor microenvironments. *Nat Med* **24**, 1178–1191 (2018).
481. Treatment of Melanoma by Stage. https://www.cancer.org/cancer/types/melanoma-skin-cancer/treating/by-stage.html.
482. De Luca, R., Meraviglia, S., Blasi, L., Maiorana, A. & Cicero, G. Nivolumab in metastatic melanoma: good efficacy and tolerability in elderly patients. *Curr Oncol* **27**, e75–e80 (2020).
483. Olson, D. J. *et al.* Pembrolizumab Plus Ipilimumab Following Anti-PD-1/L1 Failure in Melanoma. *JCO* **39**, 2647–2655 (2021).

484. Robert, C. *et al.* Pembrolizumab versus Ipilimumab in Advanced Melanoma. *New England Journal of Medicine* **372**, 2521–2532 (2015).
485. Chapman, P. B. *et al.* Improved survival with vemurafenib in melanoma with BRAF V600E mutation. *N Engl J Med* **364**, 2507–2516 (2011).
486. Vu, H. L. & Aplin, A. E. Targeting Mutant NRAS Signaling Pathways in Melanoma. *Pharmacol Res* **107**, 111–116 (2016).
487. Ascierto, P. A. *et al.* MEK162 for patients with advanced melanoma harbouring NRAS or Val600 BRAF mutations: a non-randomised, open-label phase 2 study. *The Lancet Oncology* **14**, 249–256 (2013).
488. Hayes, T. K. *et al.* A Functional Landscape of Resistance to MEK1/2 and CDK4/6 Inhibition in NRAS-Mutant Melanoma. *Cancer Research* **79**, 2352–2366 (2019).
489. Posch, C. *et al.* MEK/CDK4,6 co-targeting is effective in a subset of NRAS, BRAF and 'wild type' melanomas. *Oncotarget* **9**, 34990–34995 (2018).
490. Woodman, S. E. *et al.* Activity of dasatinib against L576P KIT mutant melanoma: molecular, cellular, and clinical correlates. *Mol Cancer Ther* **8**, 2079–2085 (2009).
491. Guo, J. *et al.* Efficacy and safety of nilotinib in patients with KIT-mutated metastatic or inoperable melanoma: final results from the global, single-arm, phase II TEAM trial. *Ann Oncol* **28**, 1380–1387 (2017).
492. Wei, X. *et al.* Efficacy Evaluation of Imatinib for the Treatment of Melanoma: Evidence From a Retrospective Study. *Oncol Res* **27**, 495–501 (2019).
493. Saint-Jean, M. *et al.* Chemotherapy efficacy after first-line immunotherapy in 18 advanced melanoma patients. *Medicine (Baltimore)* **99**, e21329 (2020).
494. Neelapu, S. S. *et al.* Axicabtagene Ciloleucel CAR T-Cell Therapy in Refractory Large B-Cell Lymphoma. *New England Journal of Medicine* **377**, 2531–2544 (2017).
495. Maude, S. L. *et al.* Chimeric Antigen Receptor T Cells for Sustained Remissions in Leukemia. *New England Journal of Medicine* **371**, 1507–1517 (2014).
496. Zhou, W. *et al.* Injectable and photocurable CAR-T cell formulation enhances the anti-tumor activity to melanoma in mice. *Biomaterials* **291**, 121872 (2022).
497. Louis, C. U. *et al.* Antitumor activity and long-term fate of chimeric antigen receptor–positive T cells in patients with neuroblastoma. *Blood* **118**, 6050–6056 (2011).
498. Shah, P. D. *et al.* Phase I trial of autologous cMET-directed CAR-t cells administered intravenously in patients with melanoma & breast carcinoma. *JCO* **38**, 10035–10035 (2020).
499. Fire, A. *et al.* Potent and specific genetic interference by double-stranded RNA in Caenorhabditis elegans. *Nature* **391**, 806–811 (1998).
500. Zamore, P. D., Tuschl, T., Sharp, P. A. & Bartel, D. P. RNAi: double-stranded RNA directs the ATP-dependent cleavage of mRNA at 21 to 23 nucleotide intervals. *Cell* **101**, 25–33 (2000).
501. Tuschl, T., Zamore, P. D., Lehmann, R., Bartel, D. P. & Sharp, P. A. Targeted mRNA degradation by double-stranded RNA in vitro. *Genes Dev* **13**, 3191–3197 (1999).
502. Elbashir, S. M. *et al.* Duplexes of 21-nucleotide RNAs mediate RNA interference in cultured mammalian cells. *Nature* **411**, 494–498 (2001).
503. Novina, C. D. *et al.* siRNA-directed inhibition of HIV-1 infection. *Nat Med* **8**, 681–686 (2002).
504. McMANUS, M. T., Petersen, C. P., Haines, B. B., Chen, J. & Sharp, P. A. Gene silencing using micro-RNA designed hairpins. *RNA* **8**, 842–850 (2002).
505. STEWART, S. A. *et al.* Lentivirus-delivered stable gene silencing by RNAi in primary cells. *RNA* **9**, 493–501 (2003).
506. McManus, M. T. & Sharp, P. A. Gene silencing in mammals by small interfering RNAs. *Nat Rev Genet* **3**, 737–747 (2002).

507. Paddison, P. J. *et al.* A resource for large-scale RNA-interference-based screens in mammals. *Nature* **428**, 427–431 (2004).
508. Martin, S. *et al.* A genome-wide siRNA screen identifies a druggable host pathway essential for the Ebola virus life cycle. *Genome Medicine* **10**, 58 (2018).
509. Díaz-Martínez, L. A. *et al.* Genome-wide siRNA screen reveals coupling between mitotic apoptosis and adaptation. *The EMBO Journal* **33**, 1960–1976 (2014).
510. Müller, M. *et al.* High content genome-wide siRNA screen to investigate the coordination of cell size and RNA production. *Sci Data* **8**, 162 (2021).
511. Brusilovsky, M. *et al.* Genome-wide siRNA screen reveals a new cellular partner of NK cell receptor KIR2DL4: heparan sulfate directly modulates KIR2DL4-mediated responses. *J Immunol* **191**, 5256–5267 (2013).
512. Luo, J. *et al.* A genome-wide RNAi screen identifies multiple synthetic lethal interactions with the Ras oncogene. *Cell* **137**, 835–848 (2009).
513. Khandelwal, N. *et al.* A high-throughput RNAi screen for detection of immune-checkpoint molecules that mediate tumor resistance to cytotoxic T lymphocytes. *EMBO Mol Med* **7**, 450–463 (2015).
514. Yasunaga, A. *et al.* Genome-Wide RNAi Screen Identifies Broadly-Acting Host Factors That Inhibit Arbovirus Infection. *PLOS Pathogens* **10**, e1003914 (2014).
515. Hu, G. *et al.* A genome-wide RNAi screen identifies a new transcriptional module required for self-renewal. *Genes Dev* **23**, 837–848 (2009).
516. Bobbin, M. L., Burnett, J. C. & Rossi, J. J. RNA interference approaches for treatment of HIV-1 infection. *Genome Med* **7**, 50 (2015).
517. Cas9 Protein | OriGene. https://www.origene.com/products/gene-expression/crispr-cas9/cas9-protein.
518. Ishino, Y., Shinagawa, H., Makino, K., Amemura, M. & Nakata, A. Nucleotide sequence of the iap gene, responsible for alkaline phosphatase isozyme conversion in Escherichia coli, and identification of the gene product. *Journal of Bacteriology* **169**, 5429–5433 (1987).
519. Mojica, F. J., Ferrer, C., Juez, G. & Rodríguez-Valera, F. Long stretches of short tandem repeats are present in the largest replicons of the Archaea Haloferax mediterranei and Haloferax volcanii and could be involved in replicon partitioning. *Mol Microbiol* **17**, 85–93 (1995).
520. Makarova, K. S., Grishin, N. V., Shabalina, S. A., Wolf, Y. I. & Koonin, E. V. A putative RNA-interference-based immune system in prokaryotes: computational analysis of the predicted enzymatic machinery, functional analogies with eukaryotic RNAi, and hypothetical mechanisms of action. *Biol Direct* **1**, 7 (2006).
521. Jinek, M. *et al.* A Programmable Dual-RNA–Guided DNA Endonuclease in Adaptive Bacterial Immunity. *Science* **337**, 816–821 (2012).
522. Evers, B. *et al.* CRISPR knockout screening outperforms shRNA and CRISPRi in identifying essential genes. *Nat Biotechnol* **34**, 631–633 (2016).
523. Shalem, O. *et al.* Genome-Scale CRISPR-Cas9 Knockout Screening in Human Cells. *Science* **343**, 84–87 (2014).
524. Konermann, S. *et al.* Genome-scale transcriptional activation by an engineered CRISPR-Cas9 complex. *Nature* **517**, 583–588 (2015).
525. Cheng, A. W. *et al.* Multiplexed activation of endogenous genes by CRISPR-on, an RNA-guided transcriptional activator system. *Cell Res* **23**, 1163–1171 (2013).
526. Chiba, M. *et al.* Genome-wide CRISPR screens identify CD48 defining susceptibility to NK cytotoxicity in peripheral T-cell lymphomas. *Blood* **140**, 1951–1963 (2022).
527. Shifrut, E. *et al.* Genome-wide CRISPR Screens in Primary Human T Cells Reveal Key Regulators of Immune Function. *Cell* **175**, 1958-1971.e15 (2018).

528. Zhuang, X., Veltri, D. P. & Long, E. O. Genome-Wide CRISPR Screen Reveals Cancer Cell Resistance to NK Cells Induced by NK-Derived IFN-γ. *Front Immunol* **10**, 2879 (2019).
529. de Groot, R., Lüthi, J., Lindsay, H., Holtackers, R. & Pelkmans, L. Large-scale image-based profiling of single-cell phenotypes in arrayed CRISPR-Cas9 gene perturbation screens. *Molecular Systems Biology* **14**, e8064 (2018).
530. Dufva, O. *et al.* Integrated drug profiling and CRISPR screening identify essential pathways for CAR T-cell cytotoxicity. *Blood* **135**, 597–609 (2020).
531. Dersh, D. *et al.* Genome-wide Screens Identify Lineage- and Tumor-Specific Genes Modulating MHC-I- and MHC-II-Restricted Immunosurveillance of Human Lymphomas. *Immunity* **54**, 116-131.e10 (2021).
532. Sheffer, M. *et al.* Genome-scale screens identify factors regulating tumor cell responses to natural killer cells. *Nat Genet* **53**, 1196–1206 (2021).
533. Wang, D. *et al.* CRISPR Screening of CAR T Cells and Cancer Stem Cells Reveals Critical Dependencies for Cell-Based Therapies. *Cancer Discovery* **11**, 1192–1211 (2021).
534. Henkel, L., Rauscher, B., Schmitt, B., Winter, J. & Boutros, M. Genome-scale CRISPR screening at high sensitivity with an empirically designed sgRNA library. *BMC Biology* **18**, 174 (2020).
535. Li, W. *et al.* MAGeCK enables robust identification of essential genes from genome-scale CRISPR/Cas9 knockout screens. *Genome Biology* **15**, 554 (2014).
536. Brandt, C. S. *et al.* The B7 family member B7-H6 is a tumor cell ligand for the activating natural killer cell receptor NKp30 in humans. *Journal of Experimental Medicine* **206**, 1495–1503 (2009).
537. Home | ClinicalTrials.gov. https://clinicaltrials.gov/.
538. Fayette, J. *et al.* Results of a phase II study evaluating monalizumab in combination with cetuximab in previously treated recurrent or metastatic squamous cell carcinoma of the head and neck (R/M SCCHN). *Annals of Oncology* **29**, viii374 (2018).
539. Colevas, D. A. *et al.* 123MO Monalizumab, cetuximab and durvalumab in first-line treatment of recurrent or metastatic squamous cell carcinoma of the head and neck (R/M SCCHN): A phase II trial. *Annals of Oncology* **32**, S1432 (2021).
540. Zhao, W., Chen, T.-L. L., Vertel, B. M. & Colley, K. J. The CMP-sialic acid transporter is localized in the medial-trans Golgi and possesses two specific endoplasmic reticulum export motifs in its carboxyl-terminal cytoplasmic tail. *J Biol Chem* **281**, 31106–31118 (2006).
541. Perdicchio, M. *et al.* Tumor sialylation impedes T cell mediated anti-tumor responses while promoting tumor associated-regulatory T cells. *Oncotarget* **7**, 8771–8782 (2016).
542. Oo, H. Z. *et al.* Identification of Novel Transmembrane Proteins in Scirrhous-Type Gastric Cancer by the Escherichia coli Ampicillin Secretion Trap (CAST) Method: TM9SF3 Participates in Tumor Invasion and Serves as a Prognostic Factor. *PAT* **81**, 138–148 (2014).
543. Liu, Q. *et al. Cancer-Associated Adipocytes Release FUCA2 to Promote Aggressive Phenotype in Triple-Negative Breast Cancer*. https://www.researchsquare.com/article/rs-617083/v1 (2021) doi:10.21203/rs.3.rs-617083/v1.
544. Au, C. E. *et al.* Expression, sorting, and segregation of Golgi proteins during germ cell differentiation in the testis. *MBoC* **26**, 4015–4032 (2015).
545. Perrin, J. *et al.* The Nonaspanins TM9SF2 and TM9SF4 Regulate the Plasma Membrane Localization and Signalling Activity of the Peptidoglycan Recognition Protein PGRP-LC in Drosophila. *JIN* **7**, 37–46 (2015).

546. Yamaji, T. *et al.* A CRISPR Screen Identifies LAPTM4A and TM9SF Proteins as Glycolipid-Regulating Factors. *iScience* **11**, 409–424 (2019).
547. Lei, Q.-Y. *et al.* TAZ Promotes Cell Proliferation and Epithelial-Mesenchymal Transition and Is Inhibited by the Hippo Pathway. *Molecular and Cellular Biology* **28**, 2426–2436 (2008).
548. Bekki, K. *et al.* The aryl hydrocarbon receptor (AhR) mediates resistance to apoptosis induced in breast cancer cells. *Pesticide Biochemistry and Physiology* **120**, 5–13 (2015).
549. Huang, Y. *et al.* Aryl Hydrocarbon Receptor Regulates Apoptosis and Inflammation in a Murine Model of Experimental Autoimmune Uveitis. *Frontiers in Immunology* **9**, (2018).
550. Marlowe, J. L. *et al.* The Aryl Hydrocarbon Receptor Binds to E2F1 and Inhibits E2F1-induced Apoptosis. *MBoC* **19**, 3263–3271 (2008).
551. García-Gutiérrez, L., Fallahi, E., Aboud, N., Quinn, N. & Matallanas, D. Interaction of LATS1 with SMAC links the MST2/Hippo pathway with apoptosis in an IAP-dependent manner. *Cell Death Dis* **13**, 1–15 (2022).
552. Reuven, N., Adler, J., Meltser, V. & Shaul, Y. The Hippo pathway kinase Lats2 prevents DNA damage-induced apoptosis through inhibition of the tyrosine kinase c-Abl. *Cell Death Differ* **20**, 1330–1340 (2013).
553. Basal & Squamous Cell Skin Cancer Statistics. https://www.cancer.org/cancer/types/basal-and-squamous-cell-skin-cancer/about/key-statistics.html.
554. Siegel, R. L., Miller, K. D., Wagle, N. S. & Jemal, A. Cancer statistics, 2023. *CA: A Cancer Journal for Clinicians* **73**, 17–48 (2023).
555. Drugs Approved for Melanoma - NCI. https://www.cancer.gov/about-cancer/treatment/drugs/melanoma (2011).
556. Melanoma Skin Cancer Statistics. https://www.cancer.org/cancer/types/melanoma-skin-cancer/about/key-statistics.html.
557. Kim, S., Iizuka, K., Aguila, H. L., Weissman, I. L. & Yokoyama, W. M. In vivo natural killer cell activities revealed by natural killer cell-deficient mice. *Proc Natl Acad Sci U S A* **97**, 2731–2736 (2000).
558. Sathe, P. *et al.* Innate immunodeficiency following genetic ablation of Mcl1 in natural killer cells. *Nat Commun* **5**, 4539 (2014).
559. Imai, K., Matsuyama, S., Miyake, S., Suga, K. & Nakachi, K. Natural cytotoxic activity of peripheral-blood lymphocytes and cancer incidence: an 11-year follow-up study of a general population. *Lancet* **356**, 1795–1799 (2000).
560. Orange, J. S. Human natural killer cell deficiencies and susceptibility to infection. *Microbes and Infection* **4**, 1545–1558 (2002).
561. Biron, C. A., Byron, K. S. & Sullivan, J. L. Severe herpesvirus infections in an adolescent without natural killer cells. *N Engl J Med* **320**, 1731–1735 (1989).
562. Elliott, J. M. & Yokoyama, W. M. Unifying concepts of MHC-dependent natural killer cell education. *Trends in Immunology* **32**, 364–372 (2011).
563. Pech, M. F. *et al.* Systematic identification of cancer cell vulnerabilities to natural killer cell-mediated immune surveillance. *eLife* **8**, e47362 (2019).
564. Dufva, O. *et al.* Single-cell functional genomics reveals determinants of sensitivity and resistance to natural killer cells in blood cancers. *Immunity* **56**, 2816-2835.e13 (2023).
565. Patel, S. J. *et al.* Identification of essential genes for cancer immunotherapy. *Nature* **548**, 537–542 (2017).
566. Han, P. *et al.* Genome-Wide CRISPR Screening Identifies JAK1 Deficiency as a Mechanism of T-Cell Resistance. *Frontiers in Immunology* **10**, (2019).
567. Sucker, A. *et al.* Acquired IFNγ resistance impairs anti-tumor immunity and gives rise to T-cell-resistant melanoma lesions. *Nat Commun* **8**, 15440 (2017).

568. Freeman, A. J. *et al.* Natural Killer Cells Suppress T Cell-Associated Tumor Immune Evasion. *Cell Reports* **28**, 2784-2794.e5 (2019).
569. Boegel, S., Löwer, M., Bukur, T., Sahin, U. & Castle, J. C. A catalog of HLA type, HLA expression, and neo-epitope candidates in human cancer cell lines. *Oncoimmunology* **3**, e954893 (2014).
570. Björkström, N. K. *et al.* Expression patterns of NKG2A, KIR, and CD57 define a process of CD56dim NK-cell differentiation uncoupled from NK-cell education. *Blood* **116**, 3853–3864 (2010).
571. Kaulfuss, M. *et al.* The NK cell checkpoint NKG2A maintains expansion capacity of human NK cells. *Scientific Reports* **13**, (2023).
572. Sheu, B.-C. *et al.* Up-regulation of inhibitory natural killer receptors CD94/NKG2A with suppressed intracellular perforin expression of tumor-infiltrating CD8+ T lymphocytes in human cervical carcinoma. *Cancer Res* **65**, 2921–2929 (2005).
573. Katou, F. *et al.* Differing phenotypes between intraepithelial and stromal lymphocytes in early-stage tongue cancer. *Cancer Res* **67**, 11195–11201 (2007).
574. Sun, C. *et al.* High NKG2A expression contributes to NK cell exhaustion and predicts a poor prognosis of patients with liver cancer. *Oncoimmunology* **6**, e1264562 (2017).
575. Platonova, S. *et al.* Profound Coordinated Alterations of Intratumoral NK Cell Phenotype and Function in Lung Carcinoma. *Cancer Research* **71**, 5412–5422 (2011).
576. Carrega, P. *et al.* Natural killer cells infiltrating human nonsmall-cell lung cancer are enriched in CD56 bright CD16(-) cells and display an impaired capability to kill tumor cells. *Cancer* **112**, 863–875 (2008).
577. Talebian Yazdi, M. *et al.* The positive prognostic effect of stromal CD8+ tumor-infiltrating T cells is restrained by the expression of HLA-E in non-small cell lung carcinoma. *Oncotarget* **7**, 3477–3488 (2016).
578. Lagana, A. *et al.* Increased HLA-E Expression Correlates with Early Relapse in Multiple Myeloma. *Blood* **132**, 59 (2018).
579. Gooden, M. *et al.* HLA-E expression by gynecological cancers restrains tumor-infiltrating CD8+ T lymphocytes. *Proceedings of the National Academy of Sciences* **108**, 10656–10661 (2011).
580. Zhang, X. *et al.* Qa-1b Modulates Resistance to Anti–PD-1 Immune Checkpoint Blockade in Tumors with Defects in Antigen Processing. *Molecular Cancer Research* **19**, 1076–1084 (2021).
581. Zhen, Z.-J., Ling, J.-Y., Cai, Y., Luo, W.-B. & He, Y.-J. Impact of HLA-E gene polymorphism on HLA-E expression in tumor cells and prognosis in patients with stage III colorectal cancer. *Med Oncol* **30**, 482 (2013).
582. Ducoin, K. *et al.* Targeting NKG2A to boost anti-tumor CD8 T-cell responses in human colorectal cancer. *Oncoimmunology* **11**, 2046931 (2022).
583. Hanna, G. J. *et al.* Neoadjuvant and Adjuvant Nivolumab and Lirilumab in Patients with Recurrent, Resectable Squamous Cell Carcinoma of the Head and Neck. *Clin Cancer Res* **28**, 468–478 (2022).
584. Vey, N. *et al.* Randomized Phase 2 Trial of Lirilumab (anti-KIR monoclonal antibody, mAb) As Maintenance Treatment in Elderly Patients (pts) with Acute Myeloid Leukemia (AML): Results of the Effikir Trial. *Blood* **130**, 889 (2017).
585. Vey, N. *et al.* A phase 1 study of lirilumab (antibody against killer immunoglobulin-like receptor antibody KIR2D; IPH2102) in patients with solid tumors and hematologic malignancies. *Oncotarget* **9**, 17675–17688 (2018).
586. Cerwenka, A., Baron, J. L. & Lanier, L. L. Ectopic expression of retinoic acid early inducible-1 gene (RAE-1) permits natural killer cell-mediated rejection of a MHC class I-bearing tumor in vivo. *Proc Natl Acad Sci U S A* **98**, 11521–11526 (2001).

587. Koh, C. Y. *et al.* Augmentation of antitumor effects by NK cell inhibitory receptor blockade in vitro and in vivo. *Blood* **97**, 3132–3137 (2001).
588. Martín-Fontecha, A. *et al.* Induced recruitment of NK cells to lymph nodes provides IFN-gamma for T(H)1 priming. *Nat Immunol* **5**, 1260–1265 (2004).
589. Sucker, A. *et al.* Genetic evolution of T-cell resistance in the course of melanoma progression. *Clin Cancer Res* **20**, 6593–6604 (2014).
590. Shin, D. S. *et al.* Primary Resistance to PD-1 Blockade Mediated by JAK1/2 Mutations. *Cancer Discov* **7**, 188–201 (2017).
591. Dubrot, J. *et al.* In vivo CRISPR screens reveal the landscape of immune evasion pathways across cancer. *Nat Immunol* **23**, 1495–1506 (2022).
592. Galot, R. *et al.* A phase II study of monalizumab in patients with recurrent/metastatic squamous cell carcinoma of the head and neck: The I1 cohort of the EORTC-HNCG-1559 UPSTREAM trial. *European Journal of Cancer* **158**, 17–26 (2021).
593. Zhang, L., Meng, Y., Feng, X. & Han, Z. CAR-NK cells for cancer immunotherapy: from bench to bedside. *Biomarker Research* **10**, 12 (2022).
594. Song, Z. Roles of the nucleotide sugar transporters (SLC35 family) in health and disease. *Molecular Aspects of Medicine* **34**, 590–600 (2013).
595. Brunetta, E. *et al.* The decreased expression of Siglec-7 represents an early marker of dysfunctional natural killer–cell subsets associated with high levels of HIV-1 viremia. *Blood* **114**, 3822–3830 (2009).
596. Varchetta, S. *et al.* Lack of Siglec-7 expression identifies a dysfunctional natural killer cell subset associated with liver inflammation and fibrosis in chronic HCV infection. *Gut* **65**, 1998–2006 (2016).
597. Zhao, D. *et al.* Decreased Siglec-9 Expression on Natural Killer Cell Subset Associated With Persistent HBV Replication. *Frontiers in Immunology* **9**, (2018).
598. Yang, L. *et al.* Siglec-7 is an indicator of natural killer cell function in acute myeloid leukemia. *International Immunopharmacology* **99**, 107965 (2021).
599. Tao, L. *et al.* Reduced Siglec-7 expression on NK cells predicts NK cell dysfunction in primary hepatocellular carcinoma. *Clinical and Exp. Immunology* **201**, 161–170 (2020).
600. Paolillo, R. *et al.* Human TM9SF4 Is a New Gene Down-Regulated by Hypoxia and Involved in Cell Adhesion of Leukemic Cells. *PLOS ONE* **10**, e0126968 (2015).
601. Zhao, B. *et al.* Cell detachment activates the Hippo pathway via cytoskeleton reorganization to induce anoikis. *Genes Dev* **26**, 54–68 (2012).
602. Zhang, X. *et al.* The Hippo pathway transcriptional co-activator, YAP, is an ovarian cancer oncogene. *Oncogene* **30**, 2810–2822 (2011).
603. Heallen, T. *et al.* Hippo pathway inhibits Wnt signaling to restrain cardiomyocyte proliferation and heart size. *Science* **332**, 458–461 (2011).
604. Dietrich, C. & Kaina, B. The aryl hydrocarbon receptor (AhR) in the regulation of cell–cell contact and tumor growth. *Carcinogenesis* **31**, 1319–1328 (2010).
605. Vondrácek, J. *et al.* Aryl hydrocarbon receptor-activating polychlorinated biphenyls and their hydroxylated metabolites induce cell proliferation in contact-inhibited rat liver epithelial cells. *Toxicol Sci* **83**, 53–63 (2005).
606. Hébert, C. D., Cao, Q. L. & Birnbaum, L. S. Inhibition of high-density growth arrest in human squamous carcinoma cells by 2,3,7,8-tetrachlorodibenzo-p-dioxin (TCDD). *Carcinogenesis* **11**, 1335–1342 (1990).
607. Milstone, L. M. & LaVigne, J. F. 2,3,7,8-Tetrachlorodibenzo-p-dioxin induces hyperplasia in confluent cultures of human keratinocytes. *J Invest Dermatol* **82**, 532–534 (1984).
608. Tschöp, K. *et al.* A kinase shRNA screen links LATS2 and the pRB tumor suppressor. *Genes Dev* **25**, 814–830 (2011).

11 ABBREVIATIONS

ADCC	-	Antibody-Dependent Cellular Cytotoxicity
AHR	-	Aryl Hydrocarbon Receptor
ANOVA	-	Analysis Of Variance
APC	-	Antigen-Presenting Cell
B2M	-	B2-Microglobulin
BCC	-	Basal Cell Carcinoma
BCR	-	B Cell Receptor
Cas9	-	CRISPR Associated Protein 9
CAR	-	Chimeric Antigen Receptor
CD	-	Cluster Of Differentiation
CRISPR	-	Clustered Regularly Interspaced Short Palindromic Repeats
CTV	-	Cell Trace Violet
Ctrl	-	Control
d	-	Day/days
DAMPs	-	Damage Associated Molecular Patterns
DC	-	Dendritic Cell
dKO	-	Double Knockout
DMEM	-	Dulbecco's Modified Eagle Medium
DMSO	-	Dimethylsulfoxide
DNA	-	Deoxyribonucleic Acid
DNAM-1	-	DNAX Accessory Molecule-1
E:T	-	Effector to Target
EGFP	-	*Enhanced Green Fluorescent Protein*
EGFR	-	Epidermal Growth Factor Receptor
FACS	-	Fluorescence-Activated Cell Sorting
FBS	-	Fetal Bovine Serum
FCS	-	Fetal Calf Serum
fdr	-	Fold Discovery Rate
FITC	-	Fluorescein Isothiocyanate
FSC/SSC	-	forward/side scatter
gDNA	-	Genomic Deoxyribonucleic Acid
GFP	-	*Green Fluorescent Protein*
GW	-	Genome Wide
h	-	Hour/hours
hIgG1	-	Human Immunoglobulin 1
HLA	-	Human Leukocyte Antigens
ICAM1	-	Intercellular Adhesion Molecule 1
IFNGR1	-	Interferon Gamma Receptor 1
IFNγ	-	Interferon Gamma
IgG	-	Immunoglobulin
IL-2	-	Interleukin-2
ILC	-	Innate Lymphoid Cell
ILT	-	Ig-Like Transcript
iso	-	Isotype
ITAM	-	Immunoreceptor Tyrosine-Based Activation Motif
ITIM	-	Immunoreceptor Tyrosine-Based Inhibitory Motif
LFA-1	-	Lymphocyte Function-Associated Antigen 1
Liri	-	Lirilumab

KIR	-	Killer-Cell Immunoglobulin-Like Receptor
KEGG	-	Kyoto Encyclopedia Of Genes And Genomes
KO	-	Knockout
mg	-	Milligram
MHC	-	Major Histocompatibility Complex
MIC-A	-	MHC Class I Polypeptide-Related Sequence A
MIC-B	-	MHC Class I Polypeptide-Related Sequence B
mIgG1	-	Mouse Immunoglobulin 1
min	-	Minute/minutes
ml	-	Millilitre
Mona	-	Monalizumab
NCR	-	Natural Cytotoxicity Receptor
NK	-	Natural Killer
NKG2A	-	Natural Killer Group 2, Member A
NKG2C	-	Natural Killer Group 2, Member C
NKG2D	-	Natural Killer Group 2, Member D
Nt	-	nucleotide
PAMP	-	Pathogen-Associated Molecular Pattern
PBMCs	-	Peripheral Blood Mononuclear Cells
PBS	-	Phosphate Buffered Saline
PD-L1	-	Programmed Cell Death 1 Ligand 1
RNP	-	Ribonucleoprotein
RPMI	-	*Roswell Park Memorial Institute*
sgRNA	-	Single Guide Ribonucleic Acid
Siglec	-	Sialic Acid-Binding Immunoglobulin-Like Lectins
SLC35A1	-	Solute Carrier Family 35 Member A1
SNA	-	Sambucus Nigra Lectin
STAT	-	Signal Transducers And Activators Of Transcription
sup	-	Supernatant
TAP	-	Transporter Associated With Antigen-Processing
Targ	-	Target
TCR	-	T Cell Receptor
TIGIT	-	T Cell Immunoreceptor With Ig And ITIM Domains
TILs	-	Tumor Infiltrating Lyphocytes
tKO	-	Triple Knockout
TLR	-	Toll-Like Receptor
TM9SF3	-	Transmembrane 9 Superfamily Member 3
TNFα	-	Tumor Necrosis Factor-Alpha
TRAIL	-	TNF-Related Apoptosis Inducing Ligand
U	-	Unit
ug	-	Microgram
untr	-	Untreated
WT	-	Wild Type
WWTR1	-	WW Domain Containing Transcription Regulator 1

12 ACKNOWLEDGEMENT

First, I would like to thank **Prof. Adelheid Cerwenka** for providing me with the opportunity to pursue my PhD in her lab. Her support, coupled with the freedom and independence she granted me, had a significant impact on shaping my scientific development. I am particularly thankful for the support and numerous discussions, especially during the last years of my PhD. These interactions helped narrow my initially chaotic and broad focus, eventually resulting in a manuscript and thesis with a clear and coherent story.

Next, I would like to extend my thanks to **Prof. Michael Boutros**, my first examiner of my thesis and member of TAC, who provided me with his CRISPR library crucial for my thesis project. I highly appreciate the contributions of **Prof. Viktor Umansky**, who accepted being a member of my defence committee and who consistently challenged me during TAC meetings and offered valuable insights and questions. I also want to thank **Dr. Christiane Opitz**, who kindly agreed being the fourth member of my defence examination committee.

I would like to thank **Dr. Ana Stojanovic**, whose vast expertise and opinions I often sought. She was always helpful whenever I jumped in her office for a 4 min chat, seeking clarification on my data or assistance with ideas that had just come to mind. Special thanks goes to **Dr. Silvina Romero Suárez** for correcting my initial (and admittedly very bad) draft of the paper and for being part of many enjoyable social events, creating lasting memories. I also express my gratitude to **Dr. Indra Shaltiël** for correcting parts of my thesis. I extend my thanks to **Dr. Jens Pahl**, my only postdoc supervisor, who was consistently available for discussions about my data. Special thanks goes to **Stefanie Uhlig** for always finding time to sort my extensive repertoire of knockout cell lines or setting up the sorter for me. A major thank you goes to **Sina Schwalm**, our guardian angel, protecting us from the evil of German bureaucracy. Her effort to help and take some of the burden from our shoulders was truly remarkable.

The biggest thanks, of course, goes to the PhD students with whom I shared my troubles - my family here. I believe that when I am 80 years old, lying on a hospital bed with a terminal stage of dementia, and my grandkids come to visit me, asking about some PhD, that I apparently did, but cannot recall, the name **Irene Garaces Lázavo** will float into my degrading mind. My orphanage PhD sister, the only reason I survived this crazy and long journey. I could dedicate two pages for you just to thank you for being here during my PhD and how big impact you had on me, and it still won't be enough. I think you know even though I never expressed it enough. When our supervisor left to industry and left his children stranded without guidance to find their

way, you became my supervisor to talk to. The failures and troubles we went through together is something I will never forget. Your resilience, putting on a smile while crying inside, never and never giving up, no matter how hard and bad things went, and watching you scientifically grow into such a smart and hard-working scientist was the main thing that motivated me to keep pushing. I will forever remember the time we had in and outside of Tridomus, late experiments with beers and pizza and just the amount of laugh we had in our PhD office. Often you were the only thing I looked forward to when I had no energy to go to the lab or continue. Forever grateful for you. Next member of the core PhD office gang, **Sophia Papasomething**, the crazy planning and perfectionist German lab manager. I want to thank you for your organizing skills, the willingness and care for others. Thank you for being so supportive when the life kicked me down, you and Irenita were my safe place to talk to, someone to hug and cry in front. Next, **Mingeuuum Jeong**, the first person to share office in the early mornings, when everyone else was still sleeping. Thank you for our conversations about science, but also deep talks about life and troubles that come with living. Next thanks go to our senior PhD **Jia Xiang See** and the last member of the PhD office gang. A hardworking scientist and a great, easy to be drunk company during our social events in Eichbaum, office and our trip in Florida. **Francesco Babysteps**, our drama queen and permanently stressed child to take care of. Your childish jokes, sometimes non-existing problems, but also a real problems that just doesn't seem real to be happening, just made my day. You were a great company, a pain in the ass, but also a great person to talk to. When I was down, your childish you changed to a therapeutic professional with whom I could discuss my private problems and have deep talks about life and relationships. Next, I want to thank **Bianca Balzasch**, a good friend and a top boulder colleague with whom I could also discuss my problems and clear my head during our climbing sessions. Next, I want to thank **Andi von Kries**, our CrossFit master. Thank you for saving my time by sharing your isolated NK cells with me and but also statistical or bioinformatics knowledge. **Helen Stark**, "my student" who doesn't need my supervision at all, thank you for your company, help with organizational stuff in the lab and translating my summary on late Friday evening into German, a language I truly hate. I also want to thank our insect expert **Sebastiano Giorgeta** and excellent cake baker **Jana Götz** for being part of my PhD journey. I am deeply grateful to **Samuel Oldman** for his valuable assistance in refining my sentences and reducing the amount of grammatical mistakes in this thesis. Lastly, I want to thank our **cemetery** for having beautiful paths in nature with squirrels running around, and **Eichbaum** for having discount prices for schnitzel and burgers that made our pub stays more affordable.

I would be killed if I don’t thank to my girlfriend **Miruš**, who convinced me not to bury my scientific potential in Czechia, but to pursue my PhD abroad. Therefore, logically, all my achievements must be automatically attributed to her. Thank you for your support and for guiding me out of the imposter syndrome loop I frequently found myself in. I also want to express my gratitude to my **family** for always supporting me and not pressuring me about not having children yet.